Durham E-Theses

Intracellular Responsive Lanthanide Probes

SMITH, DAVID,GEOFFREY

How to cite:

Use policy

Department of Chemistry

Intracellular Responsive Lanthanide Probes

David G. Smith

A thesis submitted for the degree of Doctor of Philosophy

February 2012

Abstract

The use of lanthanide complexes for the detection of biologically relevant species such as anions, pH and metal ions has grown significantly over the past decade. Such probes offer significant advantages over conventional probes; sharp narrow emission lines encode detailed spectral information and allow ratiometric analysis, and their luminescence is long-lived allowing selective spectral acquisition. Many lanthanide-based probes operate in aqueous media, but few have been applied to intracellular measurements.

The introductory chapter considers the design of lanthanide based probes for cellular applications. The fundamentals of lanthanide emission are discussed, and how the ligand structure needs to be carefully constructed to maximise emission efficiency. Reported bicarbonate- and pH-responsive probes, both lanthanide based and non-lanthanide based, are reviewed, leading to a set of proposed novel probe structures.

The synthesis of these probes with further reasoning behind their design is described in chapter two. The chapter concludes with an overview of the complexes in terms of their emission spectral form, hydration number, HPLC and mass spectrometry properties.

Chapter three presents work on bicarbonate-responsive probes. Through a series of spectral titrations, affinity constants for a range of anions were assessed. A high selectivity for bicarbonate was observed over other oxy-anions, and in the presence of protein. The complexes exhibited a mitochondrial localisation profile, and the europium luminescence intensity was modulated reversibly in response to pCO_2. The terbium analogues showed negligible change under such conditions, and thus a europium to terbium emission intensity ratio could be used to calibrate pCO_2. This principle was also applied to the analysis of bicarbonate levels in simulated biological fluid, and in a serum sample.

Several pH-responsive complexes are described in chapter four. Key aspects of pH-probe design were highlighted in early examples, leading to the final set of probes based on reversible sulphonamide ligation. Spectral titrations were performed to assess pKa values, and the use of europium to terbium emission intensity ratios was again found to offer a convenient method for assessing pH. Unprecedented changes in CPL were found in response to pH in these systems, and g_{em} values could be used to report upon pH. The complexes were observed to exhibit a lysosomal distribution.

Finally, chapter five contains experimental procedures for each compound synthesised, as well as general experimental procedures.

Both sets of complexes described in this thesis show great promise for use as well-defined intracellular probes of bicarbonate or pH.

Declaration

The research described herein was undertaken at the Department of Chemistry, Durham University between October 2008 and December 2011. All of the work is my own; no part of it has previously been submitted for a degree at this, or any other, university

Statement of Copyright

Acknowledgements

I would like to thank all of the following, without their contributions the work presented in this thesis would not have been possible:

My supervisor, Professor David Parker, whose wisdom, inspiration, creativity and patience has been greatly valued. I have been lucky to learn a lot over the past three years, and have gained a lot of knowledge regarding scientific research and far more. I hope that I can take this forward with me.

Thank you to the excellent Durham Analytical Service teams. Dr Alan Kenwright, Dr Ian McKeag and Dr Catherine Hefferman for NMR spectroscopy, Dr Jackie Mosely and Dr Mike Jones for mass spectrometry and Dr Ellie Hurst for HPLC.

Dr. Robert Pal, for help with time-gated detection measurements and confocal microscopy. Dr. Rosalind Rickaby, at the department of Earth Sciecnes, Oxford University, for providing the samples of marine algae along with helpful advice. Dr. Bob Peacock, at the University of Glasgow, for assistance with CPL measurements. Prof. Gary Wong, for acting as an excellent host in Hong-Kong, and allowing many of the variable CO_2 experiments to be performed at Hong-Kong City University.

All the members of CG27, past and present, for providing a stimulating and happy environment in which to work. Thank you to you all, whether it be for offering friendly advice, a starting precursor or your time in assisting with measurements. Most importantly, great friendships have made my time in Durham very enjoyable, and I would particularly like to mention James, Rachel, Pete, Kirsten, Brad, Liz, Elena, Kanthi and Robek. Additionally to Anurag, Steve, Brian, Nick, Ben, Craig, Filip, Neil, Alex, Katie, Martina and many others throughout the department.

A very special thanks to Mum, Dad and my family for their continued love and support, and for the opportunity to achieve so much.

FOR MUM AND DAD

& IN MEMORY OF MY GRAN

Abbreviations

A	absorbance
AGP	alpha acid glycoprotein
ATP	adenosine 5'-triphosphate
ATX	azathioxanthone group
BOC_2O	di-*tert*-butyl dicarbonate
BODIPY	boron-dipyrromethene
BP	band pass
BPS	bathophenanthroline disulfonate
CBZ	carboxybenzyl
CCCP	carbonyl cyanide *m*-chlorophenyl hydrazine
CCD	charge couplet device
CHO	chinese hamster ovary
CPL	circularly polarized luminescence
CT	charge transfer
Cyclen	1,4,7,10-tetraazacyclododecane
d	doublet
dd	doublet of doublets
DCM	dichloromethane
DIPEA	diisopropylethylamine
DMEM	Dulbeccos modified eagle media
DMF	dimethylformamide
DMSO	dimethylsulfoxide
DOTA	1,4,7,10-tetraazacyclododecane-1,4,7,10-tetraacetic acid
EDC	1-ehtyl-3-[3-dimethylaminopropyl]carbodiimide hydrochloride
ESMS-	electrospray mass spectrometry using negative ion mode
ESMS+	electrospray mass spectrometry using positive ion mode
FBS	foetal bovine serum
EtOAc	ethyl acetate
FITC	fluorescein isothiocyanate
HPLC	high performance liquid chromatography
HRMS	high-resolution mass spectrometry
HSA	human serum albumim
ISC	inter-system crossing
Ln	lanthanide
LP	long pass

MeOH	methanol
MS	mass spectrometry
MSN	mesoporous silica nanoparticles
MTT	3-(4,5-dimethylthiazol-2-yl)-2,5-diphenyltetrazolium bromide
NBS	*N*-bromosuccinimide
NCS	newborn calf serum
NHS	*N*-hydroxysuccinimide
NMR	nuclear magnetic resonance
PBS	phosphate buffered saline
PMT	photomultiplier tube
PPA	polyphosphoric acid
q	quartet
s	singlet
t	triplet
THF	tetrahydrofuran
TFA	trifluoroacetic acid
TLC	thin layer chromatography
TPP	triphenylphosphonium

Scientific Abbreviations

A   absorbance

μ   micro

λ   wavelength

Φ   quantum yield

τ_r natural radiative lifetime

τ_{ab} angle between the two vectors (CPL)

ε   molar extinction coefficient

D_{ab} dipole strength (CPL)

g_{em} emission dissymmetry factor

P_{ab} electronic transition (CPL)

R_{ab} rotatory strength (CPL)

K_{sv}^{-1} Stern-Volmer constant

S_1 singlet excited state

T_1 triplet excited state

1 Introduction

This review chapter starts with an introduction to the lanthanides, paying particular attention to europium and terbium, and discusses their characteristic luminescence properties. It considers the rational design of responsive lanthanide probes, considering the structural features they possess, and through examples from the literature, the various methods through which their luminescence output can be modulated. Aspects of the cellular uptake, localisation, and toxicity of such complexes are reviewed. The mitochondria and lysosomes are introduced, and methods of selectively targeting them. Finally, after a short discussion of non-lanthanide optical pH- and bicarbonate-responsive probes, previous work on their lanthanide analogues is overviewed, discussing the basis and providing the aims for the work presented in this thesis.

1.1   Lanthanides

The lanthanoids are generally referred to as the elements of lanthanum and the *f*-block series from cerium to lutetium. In nature, they are found almost exclusively in their trivalent oxidation state, and are known as the lanthanides. Their unique luminescent properties have facilitated their use in a wide range of applications and are increasingly finding use as bio-probes.[3]

1.1.1   Luminescence properties of the lanthanides

Luminescence spectra of the lanthanides are characterised by sharp peaks. The wavelength is largely independent of their local coordination environment, but the fine structure and relative intensities are highly sensitive. The luminescence arises from *f-f* transitions, so all the lanthanides are luminescent with the exception of lanthanum and lutetium, which have no unpaired *f* electrons. These $4f$ electrons are shielded by full $5p$ and $5s/6s$ sub-shells which inhibits the participation of $4f$ electrons in chemical bonding. This leads to a negligible interaction with ligand orbitals; the ligand-field splitting is small (~ 100 cm^{-1}).[4] This explains the observation that upon complexation or change in coordination environment, there is neither a broadening nor a shift in the wavelength of emission.

As the $4f$ electrons are not available for bonding they have little influence on the stereochemistry adopted by ligands. Instead, geometry is ruled largely by steric repulsion of the ligands, and coordination numbers of 8-9 are usually preferred.

The *f-f* transitions are parity forbidden, this has two main consequences. It leads to long luminescent lifetimes, of the order of μs (for Yb, Nd) to ms (Eu, Tb). This is advantageous as it

allows the use of time-gated data acquisition (Fig. 1). This is particularly useful in biological systems to circumvent the large amount of relatively short lived fluorescence which may be observed from proteins and other biomolecules. Applying a short time delay between the excitation pulse and data acquisition allows the selective detection of lanthanide luminescence. Time-gated measurements increase sensitivity, and lead to improved signal-to-noise and signal-to-background ratios. These forbidden transitions also give rise to very low extinction coefficients (<1 M^{-1} cm^{-1})[5] so optical irradiation is insufficient to directly populate the excited state. High intensity lasers can be used to directly populate europium (457 nm, $^7F_0 \rightarrow {}^5D_2$) and terbium (488 nm, $^7F_6 \rightarrow {}^5D_4$) excited states.[6] However, in practice they seldom used and the process of sensitised emission is employed (Section 1.3.3).[7]
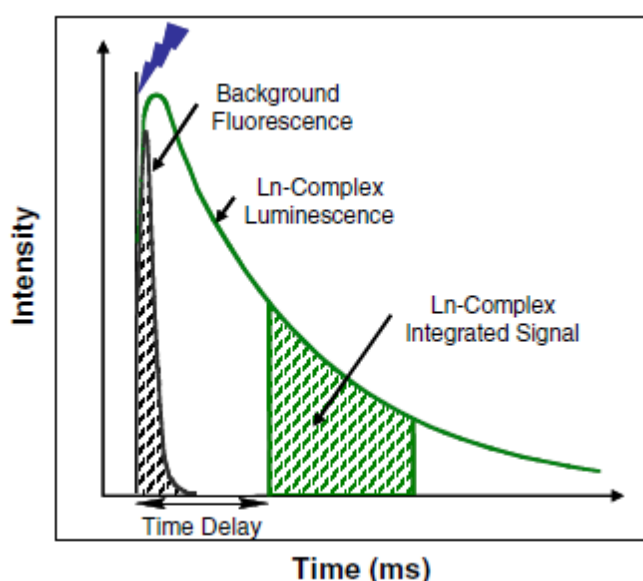
Fig. 1: The principle of time-gated detection.[1]

Although every Ln(III) ion is luminescent (except La, Lu), to be useful as an optical probe there is a requirement for a sufficient energy gap between the ground and first excited states in order to maximise luminescence over non-radiative processes. A small energy gap facilitates undesired non-radiative processes such as coupling to solvent vibrational modes.[7, 8] Europium, gadolinium and terbium have suitably large energy gaps (12,300, 32,200 and 14,800 cm^{-1} respectively), however gadolinium emits in the UV range making it unsuitable for biological applications. This leaves both europium and terbium as lanthanides suitable to be used in optical probes.

1.1.2 Emission of europium and terbium

Europium emits in the red region of the spectrum, terbium in the green (Fig. 2). The emissive state of the Eu(III) ion is $^5D_0$, and there exists a number of transitions from this state leading to

the bands observed. The strongest transitions are $^5D_0 \rightarrow {}^7F_1$ and $^5D_0 \rightarrow {}^7F_2$. The $\Delta J = 2$ manifold is 'electric-dipole allowed', and is hypersensitive to the local coordination environment. Its intensity is enhanced in high symmetry and by the presence of polarisable donor groups such as carbonate or serine. The $\Delta J = 1$ manifold is magnetic-dipole allowed and displays less change in intensity as a function of the coordination environment.[9] This forms the basis for ratiometric analysis, whereby the $\Delta J = 1$ manifold is used as an internal calibration, allowing the ratio of the $\Delta J = 2 / \Delta J = 1$ to determine the concentration of a given analyte.
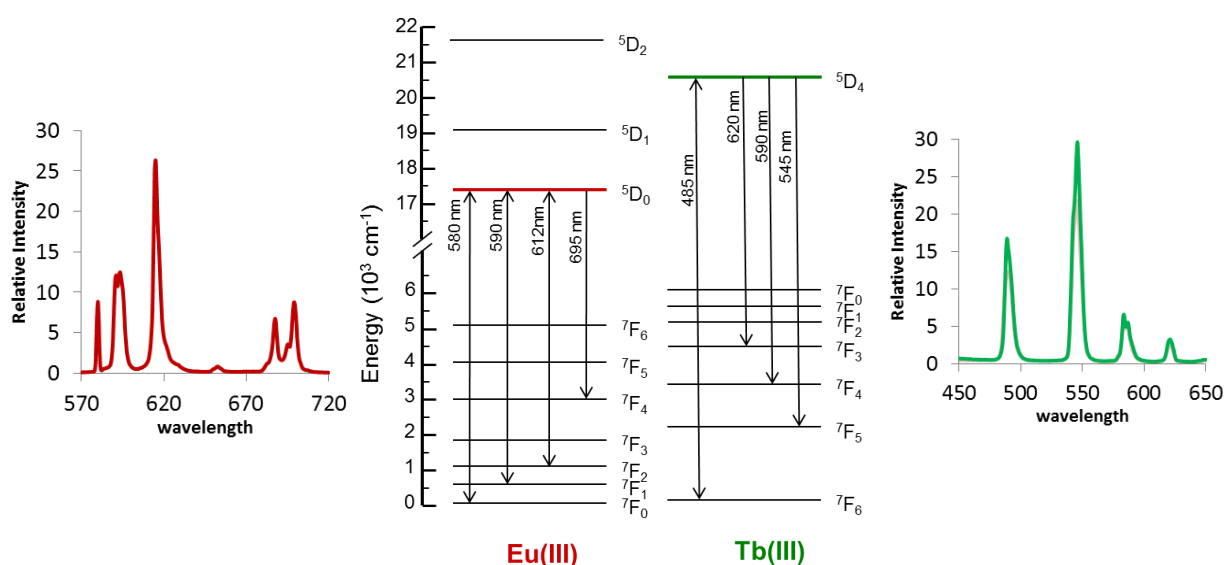
Fig. 2: Partial energy level diagram and typical emission spectra for Eu(III) (left) and Tb(III) (right).

The Tb(III) emissive state is $^5D_4$, and the four main emission bands are commonly observed arising from decay to the ^7F_J ($J = 3\text{-}6$) ground states. The $^5D_4 \rightarrow {}^7F_5$ transition, centred usually at 545 nm is the most intense. There are further bands centred at ~650 nm and ~690 nm but these are usually extremely weak and of no use in analysis.

The $^5D_0$ emissive state of europium is non-degenerate, therefore europium spectra are easier to interpret.[10] The $\Delta J = 0$ band in europium spectra is a direct indicator of the number of distinct europium coordination sites. For the $\Delta J = 1$ manifold, two bands indicate a C_n symmetric complex while the presence of three bands indicates a complex with less symmetry. There are many transitions within each of the terbium bands and so little information on local symmetry can be gleaned from these.

Table 1: Transitions from the emissive states of Eu(III) and Tb(III).[11]

Transition		Spectral region (nm)	Relative intensity	Comments
Terbium				
$^5D_4$	$\rightarrow^7F_6$	485-500	Medium-strong	Moderate sensitivity to ligand environment
	$\rightarrow^7F_5$	540-555	Strongest	Best probe transition
	$\rightarrow^7F_4$	580-595	Medium	Moderate sensitivity to ligand environment
	$\rightarrow^7F_3$	615-625	Medium-weak	Some structure under high resolution
	$\rightarrow^7F_2$	645-655	Weak	Too weak to be of use
Europium				
$^5D_0$	$\rightarrow^7F_0$	578-580	Weak	Non-degenerate, appears as a single sharp line
	$\rightarrow^7F_1$	585-600	Strong	Sharp and structured under high resolution; up to 3 transitions observed
	$\rightarrow^7F_2$	610-630	Strong	Exhibits hypersensitivity to ligand environment
	$\rightarrow^7F_3$	645-660	Very weak	Always very weak
	$\rightarrow^7F_4$	680-705	Medium	Intensity and structure very sensitive to ligand environment

1.1.3   Sensitised emission

Sensitised emission is required due to the very low molar extinction coefficients of the lanthanides.[12] A simplified Jablonski diagram best illustrates the desired pathway to lanthanide luminescence (Fig. 3). Unwanted competitive deactivating pathways will be described in Section 1.2. The initial step is absorption of a photon which excites the sensitiser to a vibrationally excited level, S_n. Non-radiative decay quickly brings this to the lowest vibrational energy level of S_1. Intersystem crossing to the T_1 manifold of the sensitiser can then occur. The rate of intersystem crossing is particularly effective in lanthanide complexes as the heavy atom
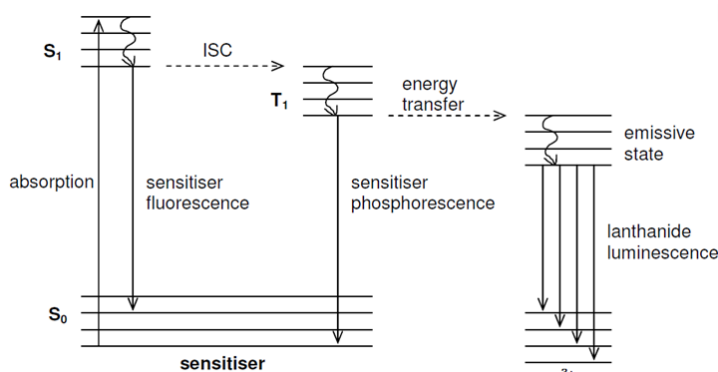
Fig. 3: A simplified Jablonski diagram representing sensitised lanthanide emission.

effect leads to a significant amount of spin-orbit coupling.[13]   Non-radiative decay follows to the lowest excited T_1 level. From the T_1 manifold, energy transfer to the lanthanide excited state is desired.[14] Non-radiative decay again brings this to the lowest excited emissive level. Finally, from the lanthanide excited state, emission occurs in the form of lanthanide luminescence.

The luminescence quantum yield is defined as the number of photons emitted as lanthanide luminescence per photon absorbed by the sensitiser.[15] The overall quantum yield is maximised by optimising the pathway outlined above. This is achieved through both careful consideration of ligand design (Section 1.3) and by minimising competitive deactivating processes (Section 1.2). The process of sensitised emission is additionally advantageous as it leads to a large Stokes' shift, and thus allows a greater resolution of incident light from emitted luminescence.[16]

1.1.4 Circularly polarised luminescence

Circularly polarised luminescence (CPL) spectroscopy is based upon the differential emission of left- and right-handed circularly polarised light, and is a direct probe of the chirality of the excited emissive state.[17, 18] It can be considered as the emission analogue of circular dichroism spectroscopy. Lanthanide complexes are particularly suitable for CPL spectroscopy as they exhibit relatively large g_{em} values, often in the range 0.1 – 0.4.[19]   This is associated with magnetic-dipole allowed transitions that exhibit relatively large rotatory strength to dipole ratios.[20]

The rotatory strength of a given transition is related to the magnitude and sign of the CPL associated with that transition. The dipole strength is influential in determining the intensity of the total luminescence. The ratio of the rotatory strength (R_{ab}) to dipole strength (D_{ab}) thus gives an indication of the magnitude of the luminescence dissymmetry factor associated with a given transition.[21]

$$g_{em} = \frac{4R_{ab}}{|D_{ab}|} \qquad \textit{[Eq. 1]}$$

The rotatory and dipole strengths relate to the size and relative orientation of the corresponding electronic and magnetic transition dipole moments. Hence, if the electronic and magnetic transition moments of a given transition are orthogonal, the rotatory strength will be zero, and no CPL is observed. The relationship between the luminescence dissymmetry factor and the electronic and transition dipole moments is given by *[Eq. 2]* where M_{ab} is the magnetic transition dipole of the transition between states a and b, P_{ab} is the electronic transition associated with this transition and τ_{ab} is the angle between the two vectors.

$$g_{em} \sim \frac{4|M_{ab}\cos\tau_{ab}|}{|P_{ab}|} \qquad \textbf{[Eq. 2]}$$

The angle between the magnetic and electronic dipole transition moment vectors, τ_{AB}, will also influence the magnitude of g_{em}. For 8-coordinate complexes, or the analogous 9-coordinate complex in which one face is capped, the CPL is predicted to exhibit a sin4θ dependence, where θ is the twist angle about the principle axis.[19] Hence, at 45° there will be no CPL, and the maximum CPL is observed when this angle is 22.5°. The fact that this angle is determined by the local helicity at the lanthanide centre partially accounts for the sensitivity of CPL spectra of lanthanide complexes to complex coordination geometry and stereochemistry, and intermolecular interactions with chiral analytes.[6]

Experimentally, the measured parameter is $\Delta I(\lambda)$, from which the emission dissymmetry factors, $g_{em}(\lambda)$ can be calculated using **[Eq. 3-4]**.[18]

$$\Delta I(\lambda) = I_L(\lambda) - I_R(\lambda) \qquad \textbf{[Eq. 3]}$$
$$g_{em}(\lambda) = 2\Delta I(\lambda) / I(\lambda) \qquad \textbf{[Eq. 4]}$$
$$I(\lambda) = I_L(\lambda) + I_R(\lambda) \qquad \textbf{[Eq. 5]}$$

For europium spectra, the $\Delta J = 0$ transition gives no CPL, as this transition is not magnetic-dipole allowed. There can be no mixing of the $^5D_0$ and $^7F_0$ states due to the axial crystal field term, accounting for the electric dipole intensity of the transition, being of odd parity. The largest g_{em} values are associated with magnetic dipole allowed transitions that have weak electronic dipole character.[19] For europium this is invariably observed with the $\Delta J = 1$ transition, reflecting the predominantly magnetic dipole characteristics of this transition, compared to the predominantly electric dipole characteristic of the other higher energy europium bands.[19] As such, the best probes of CPL and larger g_{em} values are usually associated with the $\Delta J = 1$ transition, even though ΔI may be larger for the $\Delta J = 2$ manifold.

For terbium spectra, where the strongest emission usually arises to the $^7F_5$ band, the largest g_{em} values are found both with the $^5D_4$ to $^7F_5$ and $^5D_4$ to $^7F_3$ transitions, as these are calculated to have most magnetic dipole character.

CPL spectra of europium complexes are the easiest to interpret, due to the non-degeneracy of the emissive $^5D_0$ state outlined in Section 1.1.2. However, if sensitivity is an issue, it may be the terbium analogue which proves most useful due to their higher quantum yield.

1.2   Luminescence deactivation pathways

Considering the mechanistic pathway for sensitised lanthanide emission, there are three excited states that may be perturbed, each of which leads to a reduction of the overall lanthanide luminescence quantum yield. Fig. 4 summarises potentially deactivating pathways, occurring from the sensitiser singlet state (^{1}sens-Ln), sensitiser triplet state (^{3}sens-Ln) and excited lanthanide state (sens-*Ln), each of which may serve to reduce the observed lanthanide luminescence.   To maximise the quantum yield it is necessary to have a fast rate of intersystem crossing and energy transfer, particularly with respect to the rates of these deactivating processes.
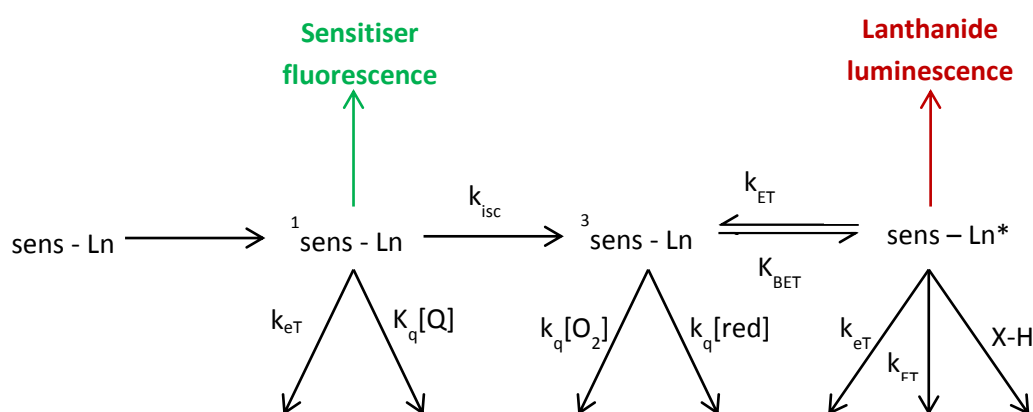
Fig. 4: Deactivating pathways following excitation of the sensitiser (k_{ET} is the rate constant for electron transfer; k_{eT} is the rate constant for energy transfer).

In addition to the processes shown above in Fig. 4, other factors are capable of affecting the intensity of the signal. Perhaps most relevant in a biological context is the unwanted co-excitation of biomolecules. Proteins can strongly absorb light with wavelengths around 280 nm, with a decreasing efficiency up to around 340 nm, mainly due to the presence of tryptophan, tyrosine and cysteine amino acid residues. If this corresponds to the absorption of the sensitiser, then protein absorption will be competitive and it will be necessary to use higher intensity incident irradiation in order to achieve the same luminescence output. This may be potentially damaging to the fluorophore or cell. Additionally, the fluorescence output from proteins or small molecules such as biotin (λ_{max} = 620 nm) may interfere with the output from the probe molecule.

1.2.1   Quenching of the sensitiser singlet state

Both the singlet and triplet excited states of the sensitiser can be quenched. The singlet excited state can be quenched by electron or charge transfer processes that can occur intra- or inter-molecularly.[13] For example, collisional interaction with halide anions such as iodide can

deactivate this state. Modest degrees of quenching of the chromophore singlet excited state via charge transfer interactions between electron rich residues in a protein and the chromophore excited state have also been reported.[22] Furthermore, the chromophore could undergo a reversible reaction such as protonation, or binding of a metal ion, which may change the energy level of this singlet state. This can be used advantageously however, as selecting an appropriate excitation wavelength may lead to pH dependent luminescence.[23]

1.2.2 Quenching of the sensitiser triplet state

The triplet excited state of the sensitiser is susceptible to quenching by molecular oxygen.[23] This again has been proven advantageous in the design of O_2 responsive sensors. The deactivation processes lead to relaxation of the sensitiser to the ground state and the formation of singlet oxygen. Localisation of such terbium probes in cells and the subsequent singlet oxygen formation can be used to induce regioselective cell death.[24] Other deactivating pathways from this state include back-intersystem crossing to the singlet excited state. However, this can be avoided by designing a complex with a singlet-triplet energy gap of more than 2000 cm^{-1}, in order to create a significant thermal barrier that prevents this process from occurring at room temperature.[20]

The intermediate chromophore triplet state can be quenched by electron rich species such as ascorbate and urate by electron or charge transfer processes.[25] Urate and ascorbate can quench via exciplex formation between the electron-poor sensitising chromophore and the electron-rich reductant.[25] Terbium is more sensitive to this mechanism of quenching than europium as exciplex formation creates a broad band of lower energy than the sensitiser T_1 state, to which reversible energy transfer occurs more efficiently for Tb compared to Eu systems.[26-28] Complexes which are susceptible to these quenching mechanisms may therefore be difficult to observe by microscopy *in cellulo*, although may be strongly emissive *in vitro* where such species may not be present.

1.2.3 Quenching of the lanthanide excited state

The lanthanide excited state is prone to deactivation through vibrational energy transfer by energy matched X-H oscillators (X = O, N, C), resulting in a decrease in both luminescence intensity and lifetime.[29] This is most significant for water bound solvent molecules or bound amino or amide NH groups from the ligand. These quenching mechanisms can be minimised by utilising octa-or nona-dentate ligands, which limit the number of bound water molecules.

Quenching of the lanthanide excited state may also occur by transfer of energy to acceptor groups with closely matching energy. This is the principle exploited in FRET applications; the acceptor must be close in space (within about 9 nm) and the energy overlap must be sufficient.[30]

In aqueous solution, quenching by directly coordinated water molecules is often the major process. Quenching can be attributed to weak coupling between *f*-electronic states of the europium and terbium ions and the third and fourth vibrational overtones of bound O-H oscillators respectively (Fig. 5). Europium complexes are more sensitive than terbium due to coupling to the lower O-H overtone. The O-D oscillators resonate at a lower energy than the corresponding O-H equivalent, and it has been established that quenching is significantly reduced in D_2O as the Franck-Condon overlap factor with the metal emissive state is less favourable.[31] The vibrational stretching frequencies of amine NH bonds (3,300 cm^{-1}) are similar in energy to the OH group (3,400 cm^{-1}) so can also quench the emissive state; again, this is less pronounced for terbium. It is possible to estimate the solution hydration state for a given complex from measurements of the rate constants for depopulation of the lanthanide excited state in D_2O and H_2O.[29, 32, 33]
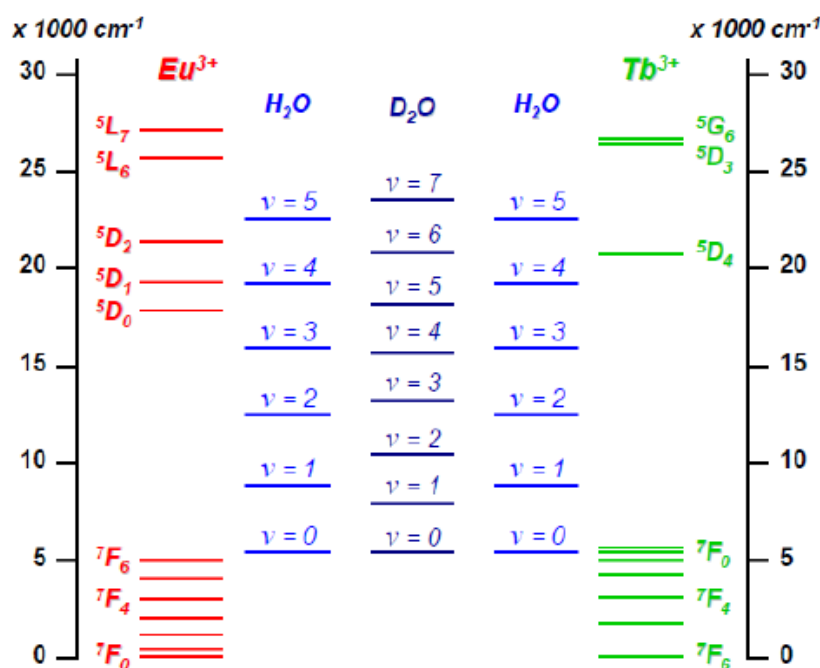
Fig. 5: Energy level diagram of Eu(III), Tb(III), compared to idealised vibrational energy levels of O-H and O-D oscillators.

1.3   The design of responsive lanthanide probes

As discussed in Sections 1.1.1 and 1.1.2, europium and terbium are arguably the two best suited lanthanides for use in responsive lanthanide probes. The ligand framework is often based on the 12-N-4 macrocycle, cyclen, which is used extensively in medicinal inorganic chemistry.

Ligands based on cyclen are able to form stable metal complexes with a range of transition metal and lanthanide ions and have found extensive use in medical imaging and radiotherapy. Substitution of the four ring nitrogens can take place with the heterocyclic sensitising unit, and then either two or three carboxylate, phosphinate or amide arms, each of which is capable of interacting with the central lanthanide ion (Fig. 6). A separate pH responsive unit can be incorporated at the final ring nitrogen position, to generate an effective pH-responsive probe.
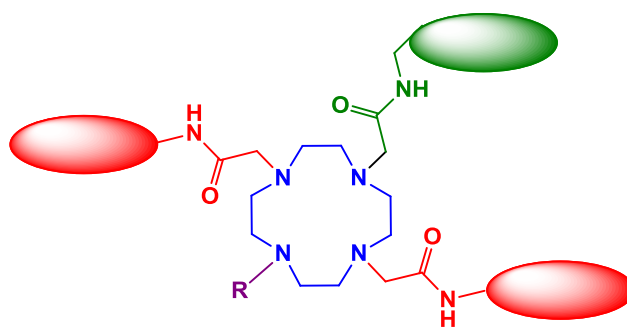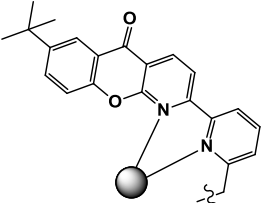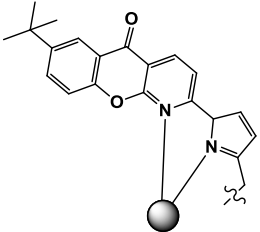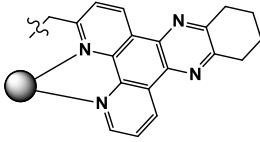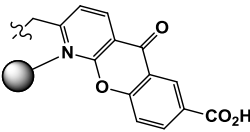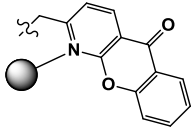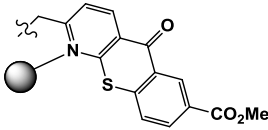
Fig. 6: Representation of the general structure of a ligand for a responsive lanthanide probe. The core cyclen structure (blue) is appended with a sensitising chromophore (green) and pendant arms (red). The substituent on the fourth cyclen nitrogen, R, (purple) may be hydrogen, a third pendant arm, or a pH sensing moiety.

1.3.1 The chromophore

A number of spectroscopic requirements exist that a chromophore for Eu(III) and Tb(III) sensitisation should fulfill. Primarily, it should possess a high molar absorption coefficient at an appropriate excitation wavelength. The singlet state should ideally lie below 29,000 cm^{-1}, giving an excitation wavelength of above 340 nm thereby minimising unwanted co-excitation of biologically active molecules; the high extinction coefficient should be associated with light absorption in this range. A small singlet-triplet energy gap of < 7,000 cm^{-1} is required to allow an efficient rate of intersystem crossing to populate the triplet state, minimising the time spent in the singlet state thus limiting the potential for unwanted depopulation of this state by ligand fluorescence.[20] The triplet excited state should lie at least 2,000 cm^{-1} above the lanthanide excited state in order to give a fast rate of energy transfer and allow efficient population of this lanthanide excited state.[20] A smaller energy difference would lead to a decreased lifetime and emission due to thermally activated back energy transfer. To enhance the rate of intramolecular energy transfer the sensitiser should be close in space to the lanthanide centre.[34] This is most readily achieved by allowing at least one point of direct coordination. This can also help inhibit the possibility of quenching by electron transfer by shielding the lanthanide centre.

Examples of suitable chromophores include azathioxanthones,[35] azaxanthones,[35] acridones,[36, 37] m-terphenyls,[38] phenanthroline derivatives,[39] pyrene[40] and tetraazatriphenylenes.[28] The properties of some of the sensitisers used in complexes discussed in this introduction are highlighted in Table 2.

Table 2: Chromophores used for the sensitisation of lanthanide emission. Quantum yields and lifetimes refer to the corresponding DO3A complex analogues.

	λ_{max}	ε / cm^{-1}	E_T / cm^{-1}	ϕ_{Eu}	τ_{Eu}	ϕ_{Tb}	τ_{Tb}
	356 nm	10,100	20,950	14%	1.00 ms		

Pyrazoyl-1-azaxanthone

	λ_{max}	ε / cm^{-1}	E_T / cm^{-1}	ϕ_{Eu}	τ_{Eu}	ϕ_{Tb}	τ_{Tb}
	345 nm	10,100	23,450	1.2%	0.70 ms		
	347 nm	8,300	23,800	18%	1.05	40%	1.56 ms
	336 nm	6,900	24,800	6.9%	0.57	24%	1.82 ms
	336 nm	5,700	24,900	8%	0.60	12%	1.89 ms
	375 nm	5,300	23,800	2.2%	0.51		

Triazophthalazine
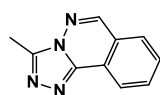
	λ_{max}	ε / cm^{-1}	E_T / cm^{-1}	ϕ_{Eu}			
	304 nm	2,400	23,600	62%			

1,10-Phenanthroline
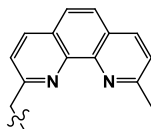
	λ_{max}	ε / cm^{-1}	E_T / cm^{-1}	ϕ_{Eu}	τ_{Eu}	ϕ_{Tb}	τ_{Tb}
	278 nm	14,760	22,100	21%	0.24	11%	0.31 ms
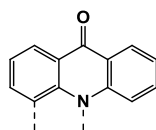
	λ_{max}	ε / cm^{-1}	E_T / cm^{-1}	ϕ_{Eu}	τ_{Eu}
	410 nm	5,300	21,050	5%	0.37

The azathioxanthone chromophore fulfills some of these criteria. The absorption wavelength lies in the range of 370 – 380 nm with a small singlet-triplet energy gap, typically around 3,500 cm^{-1}. Possessing a triplet energy of 23,500 ± 500 cm^{-1}, they are well suited to sensitising europium emission but lie at the very limit (at room temperature) for terbium sensitisation. Degassing the solution leads to an improvement for terbium emission.[35] This is consistent with back energy transfer from the lanthanide excited state to the aryl triplet state, reported when the triplet to terbium excited state energy level gap is under 2,500 cm^{-1}.

Azaxanthones arguably offer an improvement.[35] They have a fast rate of intersystem crossing with <4% ligand-based fluorescence observed. It is possible to introduce alkyl and carboxy groups onto the 7-position without perturbing the triplet energy or enhancing the tendency to fluoresce and introduction of these groups potentially allows conjugation to biomolecules. They are equally suited to terbium sensitisation as to europium, giving them the edge over azathioxanthones.

1.3.2   Ligand selection and consideration of the metal ion coordination geometry

The ligand needs to form a complex that is both kinetically and thermodynamically stable to find use in responsive cellular probes. This aspect is addressed by using an appropriately functionalised cyclen derived ligand.

Water molecules within the inner coordination sphere will lead to a reduction in emission intensity and lifetime as discussed in Section 1.2.3. It is therefore necessary to keep this number to a minimum and as such, hepta- or octadentate ligands are preferred, leaving just one or two

bound water molecules. These are nonetheless essential, as responsive probes require vacant coordination sites to allow for anion ligation or pH dependent binding to the metal centre.

Anion affinity is enhanced when there is direct ligation to a charged metal centre. The affinity of a lanthanide complex towards a given anion may be controlled by varying the ligand steric demand and the overall charge of the ligand and its resulting complex. For example, inclusion of a sterically demanding pyridyl-bound 2-azaxanthone moiety in structure [Eu·**L¹²**]³⁺ favours citrate chelation but inhibits bicarbonate binding.[41, 42] The inclusion of sterically bulky pendant arms may inhibit anion binding by increasing steric demand at the metal centre.
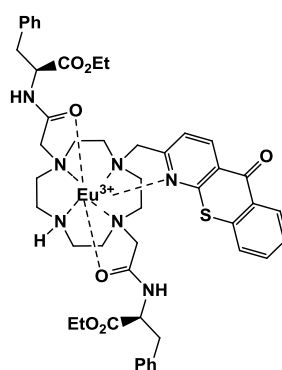
[Eu·**L¹²**]³⁺

It is the nature and polarisability of the group occupying the position on or close to the principle axis which determines the magnitude of B_0^2, which controls the degree of splitting in the $\Delta J = 1$ manifold and intensity of the $\Delta J = 2$ band, in addition to the dipolar NMR shift. Crucially, replacement of the donor group which occupies the axial position will result in significant changes or modulation in the emission spectrum. Only small changes in spectral form were observed when [Eu·**L¹⁴**]³⁺ was titrated with various anions (bicarbonate, citrate, lactate, phosphate).[2] Consideration of emission lifetimes were consistent with a ternary product with
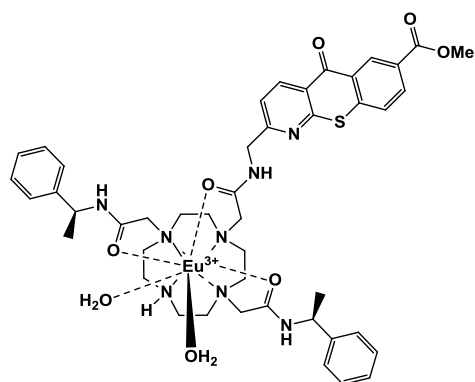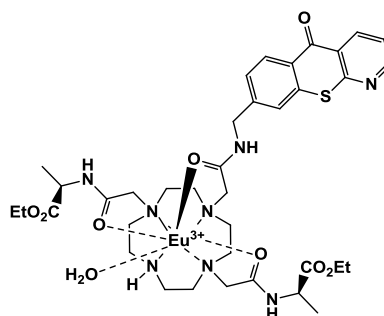
[Eu·**L¹³**]³⁺   [Eu·**L¹⁴**]³⁺

no bound waters, indicating that binding of the anion was indeed taking place. With [Eu·**L¹³**]³⁺, significant spectral changes were observed upon addition of the same anions at the same typical extracellular concentrations.[2] This contrasting behaviour can be rationalised in terms of the nature of the coordination polyhedron and the axial donor. In [Eu·**L¹⁴**]³⁺, the benzylic amide oxygen has been suggested to occupy the capping position in both the di-aqua and anion ternary adduct, with anion addition taking place at two positions in the plane of the square antiprism. In contrast, a capping water molecule becomes displaced by anion chelation in the case of [Eu·**L¹³**]³⁺.

1.3.3 Chirality of lanthanide complexes

Chiral complexes may adopt a Δ or Λ configuration where the NCCO torsion angle is +30° or -30° respectively, with the four ring NCCN torsion angles being either δ or λ, corresponding to +60° or -60° respectively. These can be graphically represented by considering the simple DOTA framework (Fig. 7 and Fig. 8).
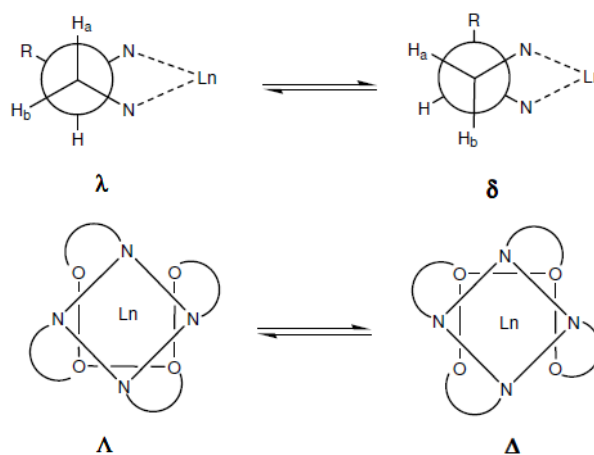
Fig. 7: Representation of the torsion angles involved in cyclen complexes.

These four stereoisomers are related as two enantiomeric pairs. Arm rotation can be inhibited by introducing chiral centres into the pendant arms. The Δ- λλλλ and Λ- δδδδ isomers adopt a monocapped square antiprismatic geometry and interconversion between these diastereomeric conformations in solution occurs through cooperative ring inversion followed by rearrangement of the coordination polyhedron (Fig. 8).[43]
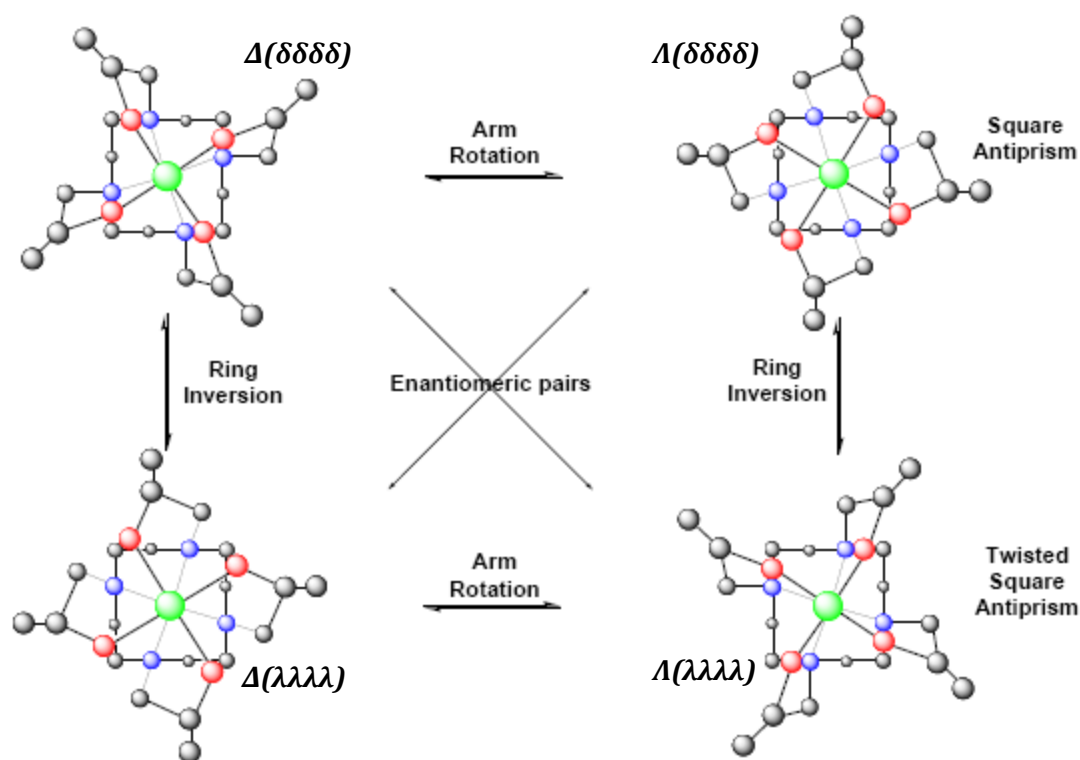
Fig. 8: Representation of the four possible stereoisomers of [LnDOTA]⁻.

1.4 Responsive lanthanide probes

Responsive lanthanide probes exhibit a change in their emission profile, circularly polarised luminescence or lifetime upon interaction with the analyte of interest. For use as responsive probes for cellular imaging it is imperative that they are water soluble and fully functional in aqueous solution. The following two subsections detail classes of signalling and consider different approaches to modulating the form of the lanthanide emission.

1.4.1 Signalling methods

Fluorescent or luminescent responsive probes can report an event in three main ways (Fig. 9). First, they may exhibit an increase or decrease in the emission intensity of a peak in response to an analyte, or much better, by modulation of the intensity ratio of a pair of emission bands. The former method has severe limitations. In order for it to provide quantitative information, the precise concentration of the probe also needs to be known. Therefore, this method is more suited to define qualitative trends, except for simple cases where it may be possible to assess complex concentration accurately. Ratiometric analysis is independent of probe concentration, so can be used to give quantitative results in complex systems such as live cell imaging where the precise probe concentration is unknown. A third, but lesser used approach, utilises the probes radiative lifetime as the reporter. This parameter is also

concentration independent but the method suffers from potential dynamic quenching processes, which can also reduce the observed lifetime (Section 1.2).
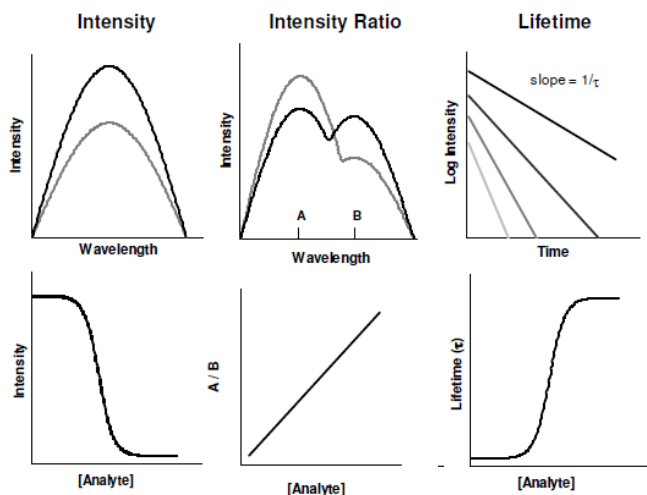
Fig. 9: Three idealised methods of signalling a binding event using responsive probes

1.4.2   Ratiometric probes

Ratiometric probes can be constructed by the coupling of two separate reporters.[44, 45] Measuring the dynamic emission response of one reporter and calibrating against a second whose emission is invariant with respect to the analyte leads to a ratiometric response.[46] This may require two differing sets of excitation and emission wavelengths limiting temporal resolution, and if the two reporters are not covalently linked they may exhibit a non-homogenous distribution, so any data obtained may be inaccurate.[47] Alternatively, the process of resonance energy transfer can be used if the excited state of the first reporter group is coupled to that of the second probe.[48] A responsive output will be obtained if interaction with an analyte interferes with this process. Use of this method may be limited if the probes have differing susceptibilities to photobleaching or quenching mechanisms.

Responsive europium and terbium complexes potentially offer an attractive solution to these problems by performing ratiometric analysis on pairs of emission wavelengths or bands. For example, a ratiometric analysis has been defined by monitoring the change in the ratio of the $\Delta J = 2$ band, which is hypersensitive to the ligand environment against the relative insensitive $\Delta J = 1$ band upon anion binding. The chromophore is the same in each case, so that only one excitation wavelength is required.

It is also possible to perform ratiometric analysis using the europium and terbium analogues of a common ligand in tandem. The first report detailing this method involved an assay for measuring uric acid.[27] Urate binding selectively quenched the terbium excited state of $[Ln \cdot L^{15}]^{3-}$ by electron transfer from the urate anion, and a ratio of the europium emission at 616 nm to the terbium emission at 546 nm allowed a calibration of the urate concentration. Europium and terbium complexes of the same ligand exhibit the same degree of solubility and localisation profile and so do not experience the potential limitations of a non-homogenous localisation, compared to other dual probes. Additionally, a single excitation wavelength is required.

$[Ln \cdot L^{15}]^{3-}$
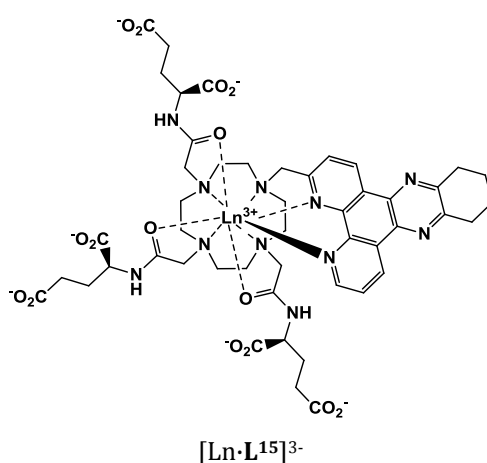
1.4.3 Approaches to modulating the emission

Most responsive lanthanide probes work on the basis of one of four principles:[1]

1) the analyte binds directly to the lanthanide centre, displacing one or more bound water molecules, thus modulating the intensity and /or form of spectral luminescence;

2) the analyte binds to the chromophore, altering the energy transfer process to the lanthanide;

3) the analyte causes the chromophore to move closer to, or bind directly to the lanthanide, causing an enhancement of emission intensity;

4) the analyte otherwise causes a change in the inner-sphere hydration number.

A relatively simple approach to this fourth method of responsive probe involves a displacement assay to monitor Fe(II). The europium emission of $[Eu \cdot L^{16}]^{3+}$ is switched off following addition of the Fe(II) ion through displacement of the BPS sensitiser, which has a high affinity for Fe(II).[49] The number of coordinated water molecules increases from zero to two. Although the probe responds selectively to Fe(II) ions and works in a buffered aqueous solution

at physiological pH, the output is not ratiometric as it relies simply upon a switching off of emission as the sensitising unit is removed. This limits its use in any cellular systems as it is not possible to accurately know the probe concentration.

$[Eu \cdot L^{16}]^{3+}$
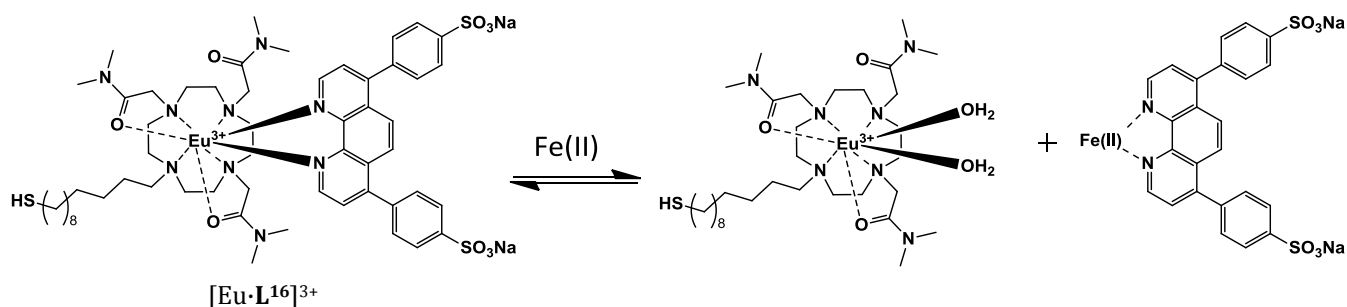
A further example of a probe capable of sensing biologically relevant cations under mimicked physiological conditions is the europium based zinc-selective sensor, $[Eu \cdot L^{17}]$.[50] The probe is based upon a DO3A framework, incorporating a chromophoric bis-picolyl unit for binding zinc. Upon zinc chelation the probe undergoes a conformational change, and the number of coordinated water molecules switches from zero to two. With overall quenching, presumably due to the increased solvation at the europium centre deactivating the lanthanide excited state, the form as well as intensity of europium emission spectra changes, particularly in the ligand sensitive $\Delta J = 4$ band. This allows a ratiometric analysis.

$[Eu \cdot L^{17}]$
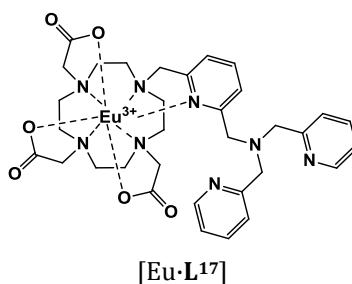
The third example mentioned above related to modulation of the sensitiser-lanthanide distance. As the quantum yield of lanthanide luminescence is highly dependent upon this, it can be used as the basis for modulating emission. The highly selective potassium sensor, $[Tb \cdot L^{18}]$, works in this way.[51] An azaxanthone sensitiser is linked via a lariat ether to a phenyl moiety. In the absence of potassium, the flexibility of the arm keeps the sensitiser far away from the terbium ion, and Tb(III) luminescence is very weak. Upon potassium binding, a cation-π interaction with the arene brings the azaxanthone into close proximity to the terbium ion, allowing efficient sensitisation. This leads to a 26-fold increase in luminescence intensity. The

major limitations of this work relate to its applicability in aqueous media and the inability to perform a ratiometric analysis.

[Tb·**L¹⁸**]   [Eu·**L¹⁹**]
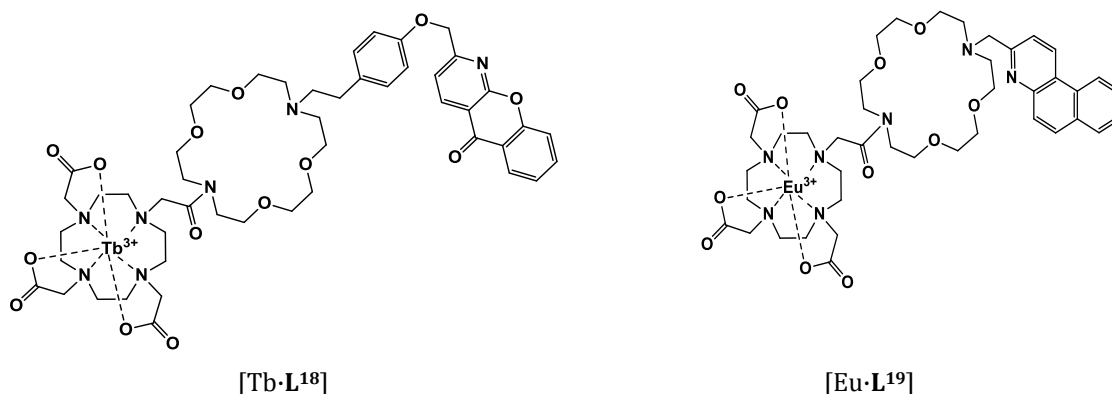
An improved potassium probe, [Eu·**L¹⁹**] using a phenanthridine-based antenna has subsequently been reported, involving ratiometric analysis.[51] Effectively using time-gated detection, a binding affinity of 0.33(4) µM was calculated, which is well suited to the clinically relevant range of 0-10mM. This probe relies upon coordination of the phenanthridine nitrogen to potassium, which modifies the excited state energy levels of the antenna. This in turn affects the excitation spectral profile, allowing a ratiometric quantification of potassium concentration.

Two terbium lanthanide systems, [Tb·**L²⁰**] and [Tb·**L²¹**], have been reported for the time-gated detection of H_2O_2 in living systems.[52] A chemoselective H_2O_2-mediated oxidation of a boronate protected probe with H_2O_2 uncages a pendant aniline or phenol antenna which is better able to

[Tb·**L²⁰**]

[Tb·**L²¹**]

-31-
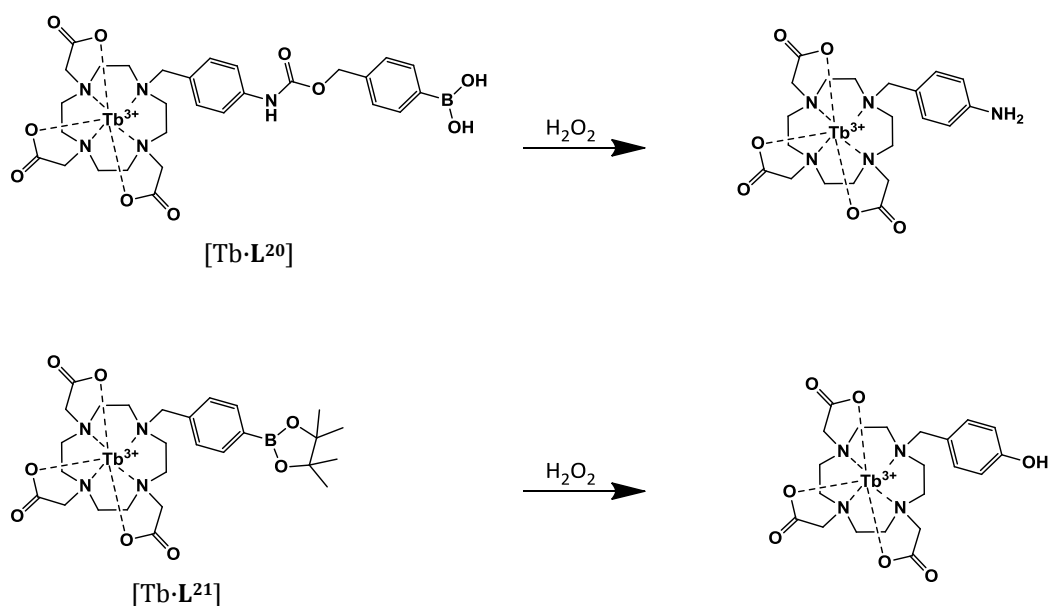
sensitise terbium emission. In the absence of H_2O_2, the boronate-capped aromatic is electron withdrawing and a poor sensitiser. Reaction with H_2O_2 generates an electron rich phenol or aniline. The enhanced sensitisation leads to a 6-fold increase in luminescence intensity *in vitro*. The probe demonstrated a high selectivity for H_2O_2 over other biologically relevant reactive oxygen species such as superoxide or nitric oxide. Further, the probe was able to detect elevated levels of H_2O_2 production in live RAW 264.7 macrophages during an oxidative immune response using time gated spectroscopy, taking advantage of the long-lived lanthanide luminescence. This example does offer considerable room for improvement; in particular longer wavelength excitation is desirable. Additionally, in order to obtain quantifiable data, the kinetics of the boronate oxidation reaction need to be established as well as the local probe concentration. These limitations further highlight the need to develop probes which are ratiometric in their response.

Approaches based upon direct analyte binding to the metal centre, and analyte binding to the chromophore will be discussed in detail in Section 1.9, focusing on bicarbonate and pH responsive systems.

1.5   Uptake mechanism, subcellular localisation and toxicity

It is necessary to have a good understanding of the mechanism by which the probes enter the cells in order to influence the design of novel complexes.[53] Additionally, an understanding of features that exert an influence on the subcellular localisation, and factors to avoid cellular toxicity should also be considered.

1.5.1 Uptake mechanism of lanthanide complexes

There are a number of classes of uptake mechanism by which substances are able to enter into cells.[54] Passive transport does not require energy input, the driving force is the movement of molecules down a concentration gradient. In contrast, active transport requires the input of
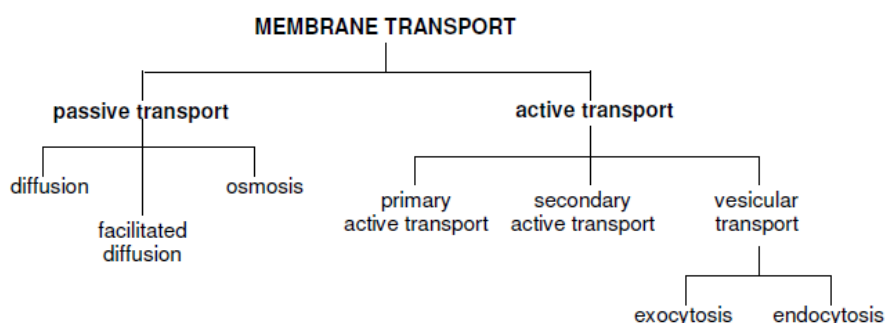
Fig. 10: Classes of uptake mechanism

energy. Primary active transport involves specific membrane-bound channels to transport species. Secondary active transport requires the use of an ion gradient, established by the simultaneous transport of a second species. The third class of active transport is vesicular in nature and can be further sub-divided into two classes.[55] Endocytosis and exocytosis[56] are essentially the reverse of one another, moving substances into, and out of a cell respectively.

For lanthanide complexes entering a cell, endocytosis is the class of interest, and this may occur via a number of different mechanisms (Fig. 11). Phagocytosis involves the transport of large (>0.5 μm) multimolecular particles such as dead cells, bacteria and viruses.[57] Pinocytosis involves the uptake of extracellular fluid along with any particles this contains, again this can occur via a number of different methods. Clathrin-mediated endocytosis is arguably the best
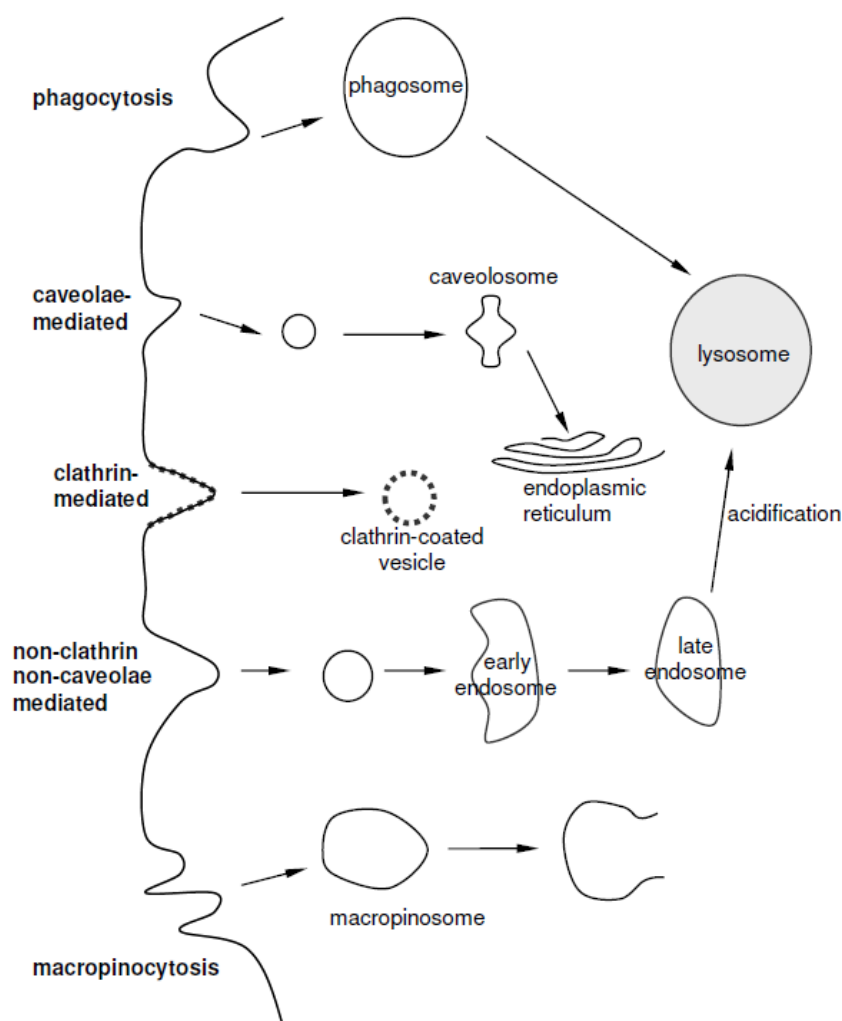
Fig. 11: Endocytotic uptake mechanisms.

understood mechanism, this is the principal process for the internalisation of proteins, membrane-localised receptors and ion-channels. Another mechanism involves carveolae.[58] These are flask shaped invaginations of the cell membrane that are able to internalise by a process termed potocytosis.[59] Lastly, macropinocytosis is a non-specific mechanism where ligand-binding to a receptor is not required, unlike the two methods mentioned above.[60] In macropinocytosis, vesicles are formed via the ruffling of the membrane in response to cell surface simulation.

The method of entry for related series of lanthanide complexes has been reported.[61] Evidence for an energy dependent, active-uptake method was established; at 4 °C, uptake of the complexes was greatly reduced compared to 37 °C.[62] This correlated with other work which had shown that molecules in the region of 1 kDa, similar to the lanthanide complexes, are greatly hindered in movement by passive diffusion.[63]

To determine the specific mode of endocytosis, cells were treated with a variety of drug molecules to selectively block or enhance different uptake pathways (Fig. 12). This revealed that macropinocytosis was the mechanism via which the lanthanide complexes entered cells.[64] This is reasonable, as it is unlikely to be a receptor mediated process, given the broad range of complexes with differing geometries, charge and lipophilicities that have been observed to enter cells.
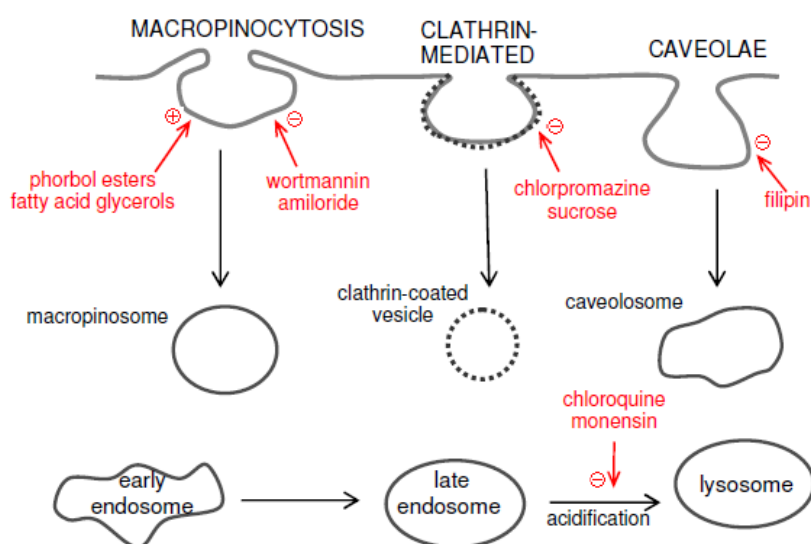
Fig. 12: Inhibition pathways for various uptake mechanisms.

One final observation that is relevant at his point is the time dependent nature of uptake of the complexes. The cellular uptake of complexes based on [Eu·**L**^{22}]$^{3+}$ incorporating an

azaxanthone chromophore was studied as a function of time. It was shown that substitution at the 7-position greatly influenced the rate of uptake. The carboxymethyl derivative showed a very fast rate of uptake, clearly visible after just 2 minutes. In comparison, the corresponding carboxylate only showed localisation after one hour.[22]
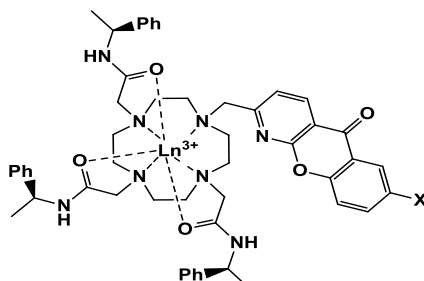
[Eu·**L**[22]][3+]

1.5.2   Subcellular localisation of lanthanide complexes

Out of the range of complexes from Durham, subcellular localisation can be classified into four categories: localisation to the lysosomes; localisation to the mitochondria with subsequent trafficking to the lysosomes (Fig. 13);[2] simultaneous localisation to the lysosomes and mitochondria;[65] and nucleolar localisation.[66] Nucleolar localisation appears to be due to increased membrane permeability induced by necrotic conditions or administration of very high
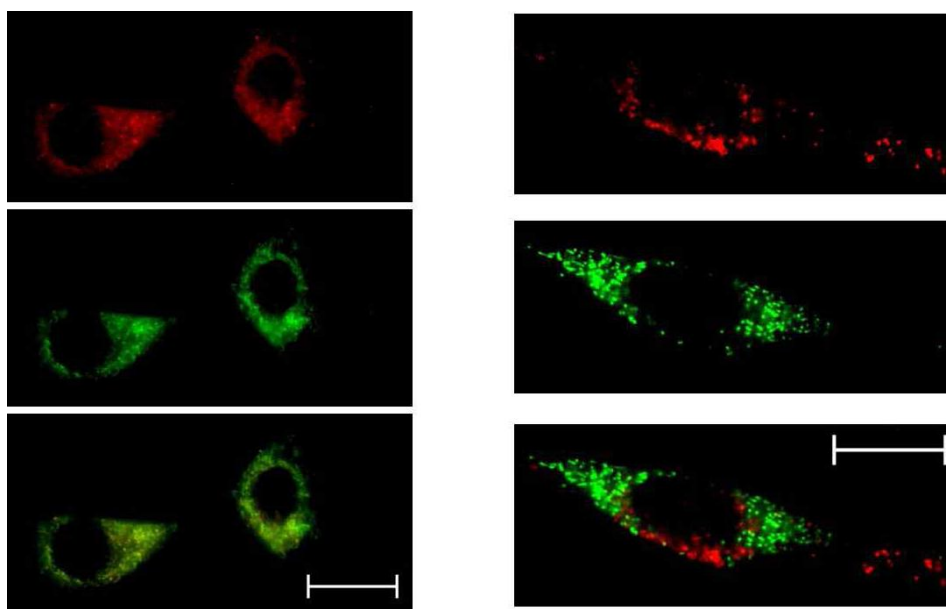
Fig. 13: Epifluorescence microscopy images for [Eu·**L**[13]][3+]: 50 μM complex, 4 h incubation (left set of images); 50 μM complex, 24 h incubation (right set of images). Images reveal a mitochondrial localisation profile after 4 h and a profile consistent with migration of the complex from the mitochondria to the perinuclear endosomes/lysosomes after 24 h. Upper images: Eu(III) complex; centre images: Mitotracker GreenTM; lower images: merged image (scale bars 20 microns).[2]

concentrations of the complex itself, and is discussed briefly in the following section. Mitochondrial and lysosomal distributions are briefly discussed in Sections 1.6.2 and 1.6.4 respectively.

1.5.3 Toxicity of lanthanide complexes

In general, all the complexes studied at Durham have been shown to have low toxicity at the concentrations used in microscopy experiments. Complex toxicity is generally assessed through the MTT assay, which is a colourimetric assay based on the reduction potential of the mitochondrial reductase enzymes.[67] It is discussed in detail in Section 1.23. It is essential that the probes do not interfere with cellular functions. The few reported probes which have exhibited some significant toxicity can be rationalised in terms of their structure, and avoided in future designs.[68] The complexes which localised to the mitochondria did not appear to perturb the MMP, in line with being non-toxic.[2] It is relevant to assess the toxicity at the organelle to which the probes is localising, as this is where the toxic effects are most likely to be observed.

R = CH$_2$CH$_2$CH$_2$CO$_2^-$
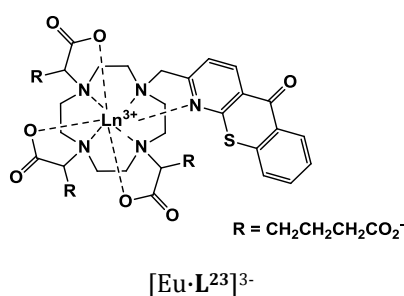
[Eu·**L^{23}**]$^{3-}$

Certain complexes were initially reported to exhibit a nucleolar distribution, but this result was found to be concentration dependent. At lower complex concentrations of [Eu·**L^{23}**]$^{3-}$, for example, a lysosomal distribution was often observed. It appears that the nucleolar distribution may be associated with a loss of cell viability, possibly caused by using excessive concentrations of the complex.[69] Deliberate permeabilisation of the membrane was also shown to induce this localisation pattern, as loss of membrane integrity is one of the first events of necrosis.[64] This rationale also may be invoked to explain cellular distribution results reported by others e.g. the lanthanide complexes of Barton.[70]

1.6 Cellular organelles

1.6.1 Mitochondria

Mitochondria are found in eukaryotic cells where their key function is the production of energy through oxidative phosphorylation. They serve additional functions including

intracellular Ca^{2+} homeostasis,[71] and play a key role in apoptosis.[72] Mitochondrial dysfunction is believed to be an important factor in a number of diseases. Presently, the exact function of the mitochondria and the possible processes of disease are only partially understood. Through careful and considerate design of probes that target the mitochondria and report on a certain biomolecule or process, a deeper understanding of the mechanisms and regulation process can be gained.

1.6.2 Targeting the mitochondria

The simplest probes which target the mitochondria are cell permeable fluorescent dyes such as rhodamine 123[73] (**24**) and tetramethylrosamine (**25**).[74] They serve simply as a stain, highlighting the localisation of the mitochondria within the cell, but do not report upon any activity or function. Further, they are not retained within the mitochondria when the cells are washed.

24

24
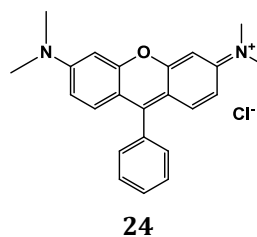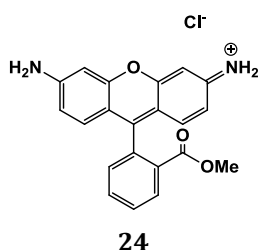
The commercially available MitoTracker probes such as MitoTracker Green FM, (**26**), offer many advantages over these. For example, it is significantly more photostable and gives a brighter, more selective signal at lower concentrations. They enter the cell by passive diffusion across the plasma membrane, accumulating within the cell regardless of the mitochondrial

26
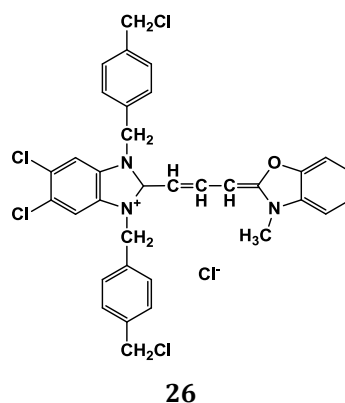
membrane potential. They contain a mildly thiol-reactive chloromethyl moiety which appears to be responsible for keeping the probe within the mitochondria. The MitoTracker series still offer no probe of function but are an effective marker of localisation.

Derivitisation of boronic acids with the lipophilic triphenylphosphonium (TPP) cation results in accumulation of the compounds within the mitochondria. TPP is able to pass rapidly through biological membranes, resulting in a several-hundred-fold accumulation within the mitochondria *in vivo*.[75] By covalently attaching bioactive functionalities to the TPP cation, these probes can then also be delivered. This has been put to particular use in a mass spectrometry ratiometric probe for hydrogen peroxide, **27**.[76] TPP additionally helps facilitate the sensitive detection by mass spectrometry.[77]

27
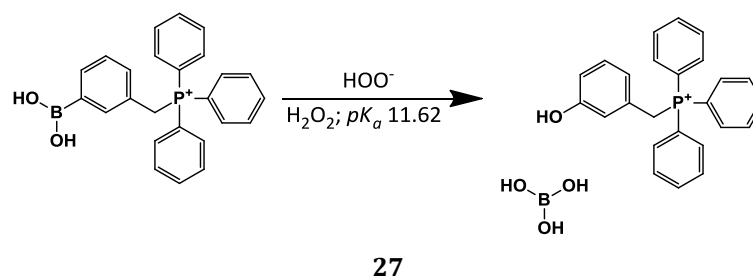
A strong relationship has been established between the structure of the chromophore and its mode of linkage to cyclen and observed cellular localisation profile. The azaxanthone moiety incorporated into some lanthanide complexes has also been shown to dictate a mitochondrial localisation. The europium complex, [Eu·L13]3+, belongs to a small class of complexes that show a mitochondrial distribution at time-points of 5 min to 12 h with subsequent trafficking to the

[Eu·**L28**]3+

[Eu·**L29**]3+

[Eu·**L13**]3+
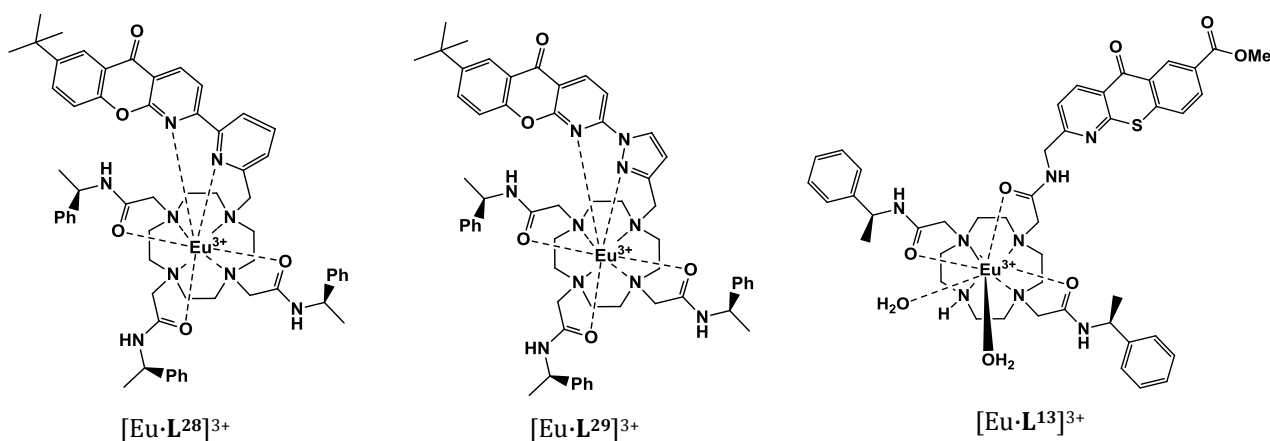
lysosomes at extended time points.[2] This accords with the absence of toxicity observed for these complexes. [Eu·**L²⁸**]³⁺ and [Eu·**L²⁹**]³⁺ exhibit a simultaneous mitochondrial and lysosomal distribution, and so are probably of less use as selective cellular probes.[65]

1.6.3 Lysosomes

The lysosomes are acidic compartments within cells, containing a number of hydrolytic enzymes which break down unwanted waste. The interior of a lysosome has a pH of around 4.5 – 6.0, contrasting with a cytosolic pH of around 7.2. The lower pH maintains ideal conditions for these hydrolytic enzymes to work.[78]

1.6.4 Targeting the lysosomes

Complementary to the MitoTracker series of probes, are the LysoTracker and LysoSensor series. LysoTracker probes exist as subcellular stains, whilst the LysoSensor probes are responsive probes that function as acidic organelle selective pH indicators. With a high selectivity for acidic organelles, they localise well to the lysosomes and effective labeling occurs at nanomolar concentrations. They consist of a fluorophore linked to a weak base, which is partially protonated at neutral pH and can freely permeate organelles. Once within the lysosomes, the weak base is protonated, leading to retention of the probe within the organelle. The protonation of LysoSensor Green DND-189, **30,** suppresses the fluorescence quenching of the dye caused by photoinduced electron transfer quenching of the S_1 excited state by the morpholine nitrogen lone pair. This results in an increase in fluorescence intensity. Some LysoSensor probes are dual emission probes, allowing ratiometric imaging. A potential drawback with this set of probes is that they may localise in membranes. If so, this would only allow qualitative and semi-quantitative comparisons of organelle pH. Additionally, although the probes are taken up within seconds into live cells, the probes can induce an alkalising effect, therefore it is not recommended to dose for longer than 5 minutes. These are significant issues, and as such there is a need for a reliable, non-perturbing probe of lysosomal pH.
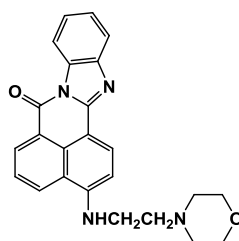
30

A number of lanthanide based probes that preferentially localise to the lysosomes have been reported. Out of the ~80 emissive lanthanide complexes characterized in Durham over the past few years, over 80% have been shown to exhibit an endosomal/lysosomal distribution.[68] This appears to be the default localisation for complexes. Complexes containing azaxanthone chromophores commonly exhibit this localisation profile. A crucial linkage mode involves a methylene group.

1.6.5 Measuring lysosomal pH

There exists a certain amount of controversy regarding measurements of lysosomal pH. A hypothesis has been promulgated that increased levels of ceramide in cystic fibrosis models result from defective lysosomal acidification, and is linked to mutation of the cystic fibrosis trans-membrane conductance regulator protein.[79] This was subsequently refuted when different pH probes were used.[80] These required deliberate cellular permeabilisation to enable lysosomal localisation of the probe. This exemplifies the need for an improved, reliable ratiometric pH probe that targets the lysosomes without perturbing membrane permeability or cellular homeostasis.

Organellar pH can be affected by several mechanisms, including the activities of H^+-pump and H^+-leak pathways, buffer capacity, membrane potential and cytoplasmic ionic content. Elevated lysosomal pH has been noted in several lysosomal storage diseases.[81] There are over fifty of these hereditary metabolic disorders that cause defects in lysosomal function. Most commonly, mutations occur in the lysosomal hydrolase enzymes that degrade various cellular macromolecules. [82] It has been found that lysosomes in some tumour cells have a lower pH than normal lysosomes, while other tumour cells have been found to contain lysosomes with higher pH.[83, 84] The defective pH regulation of the lysosomes of human breast cancer cells,[85] and the elevated lysosomal pH in neural ceroid lipofuscinoses are further examples.[86]

1.7   Bicarbonate

1.7.1 Physiological role of bicarbonate

Bicarbonate fulfills many roles in biological systems. It is a substrate in photosynthesis, it helps maintain the pH of biological fluids and it is generated during cellular respiration from carbon dioxide.[87] Glycolysis, and the citric acid cycle take place within the matrix of the mitochondria, and produce mitochondrial carbon dioxide, which is rapidly converted to bicarbonate by the action of carbonic anhydrase enzymes. A challenge is to monitor the real-time changes in these concentrations, and bicarbonate-selective optical probes potentially offer

a solution. They could offer an insight into signaling mechanisms that regulate, or are regulated by these changes in concentration.

It has been shown that changes in bicarbonate concentration stimulate adenyl cyclase activity, the enzyme responsible for production of cyclic-AMP. It has been suggested that soluble adenyl cyclase is a regulator of oxidative phosphorylation of mitochondrial enzymes, allowing respiration to keep pace with changes in nutritional availability. If the reducing equivalents produced by the Kreb's cycle are not efficiently used, then reactive oxygen species levels may increase causing oxidative damage.[88]

1.7.2 Bicarbonate levels in serum

Accurate measurement of serum bicarbonate levels is critical in assessing metabolic acidosis, abnormally increased hydrogen ion concentration. Low serum bicarbonate concentrations in a dialysis patient with end-stage renal disease, almost always indicates metabolic acidosis.[89] There are concerns regarding the accuracy when such measurements are made due to effects of blood collection techniques, shipping concerns, effects of analysis time and the impact of assay methodology.[90] At present, there are two distinct assays for determining bicarbonate levels based on either enzymatic methods or ion-selective electrodes. There is some discrepancy between the values reported by each technique. This underscores the need for a cellular probe or method to detect bicarbonate concentrations.

1.7.3 Competing anionic species in biological samples

There exist a number of anions that will be present in varying concentration in biological systems which can compete with bicarbonate for binding to the metal centre. Oxy-anions such as citrate, lactate or phosphate have all been shown to bind to lanthanide complexes. Citrate for example, has been shown to bind very strongly to triply positively charged lanthanide complexes on account of its own triple negative charge. In extracellular fluid, for example, some typical concentrations are listed below (Table 3):

Table 3: Typical extracellular concentrations of some common anions.

Anion	Concentration / mM
bicarbonate	25
lactate	2.3
citrate	0.13
phosphate	0.9
chloride	120

Control of the steric demand at the metal centre, and both overall and peripheral charge on the complex should enable a degree of control towards the competitive binding. The affinities towards bicarbonate, citrate, phosphate and lactate for a number of complexes reported in the literature are summarised below, Fig. 14.
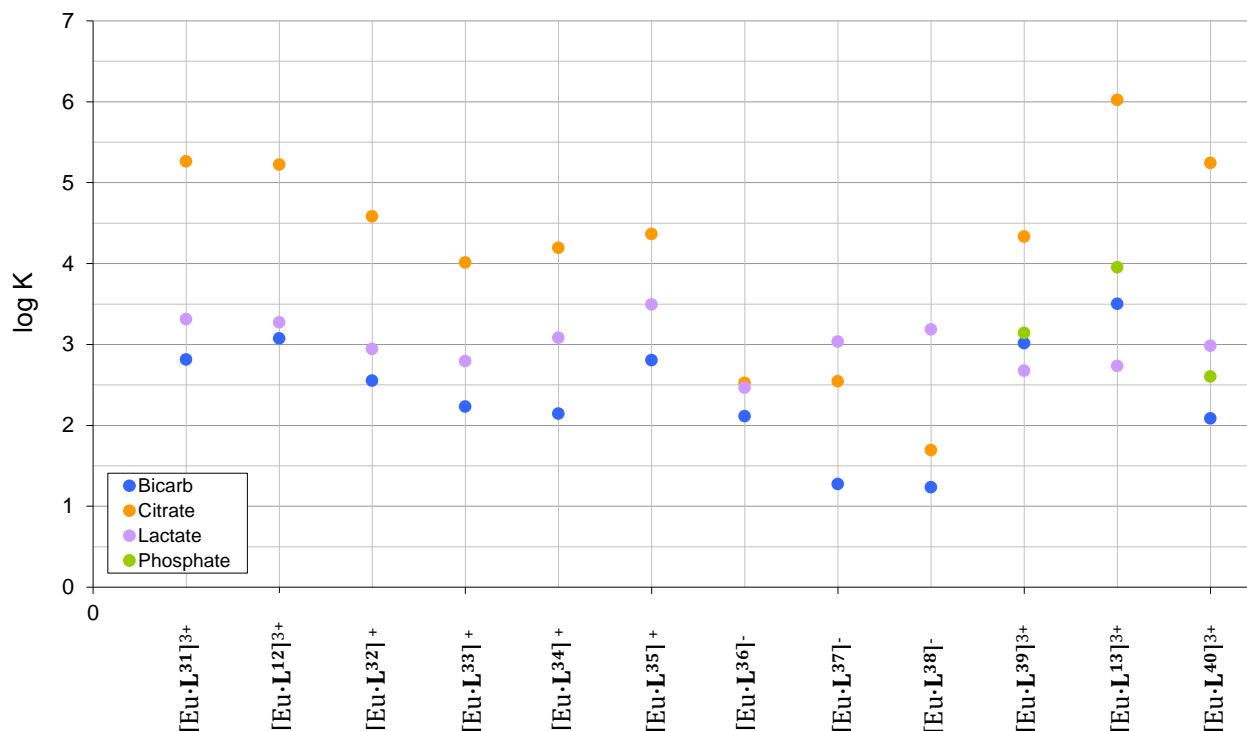
Fig. 14: Binding affinities for a range of complexes towards anions
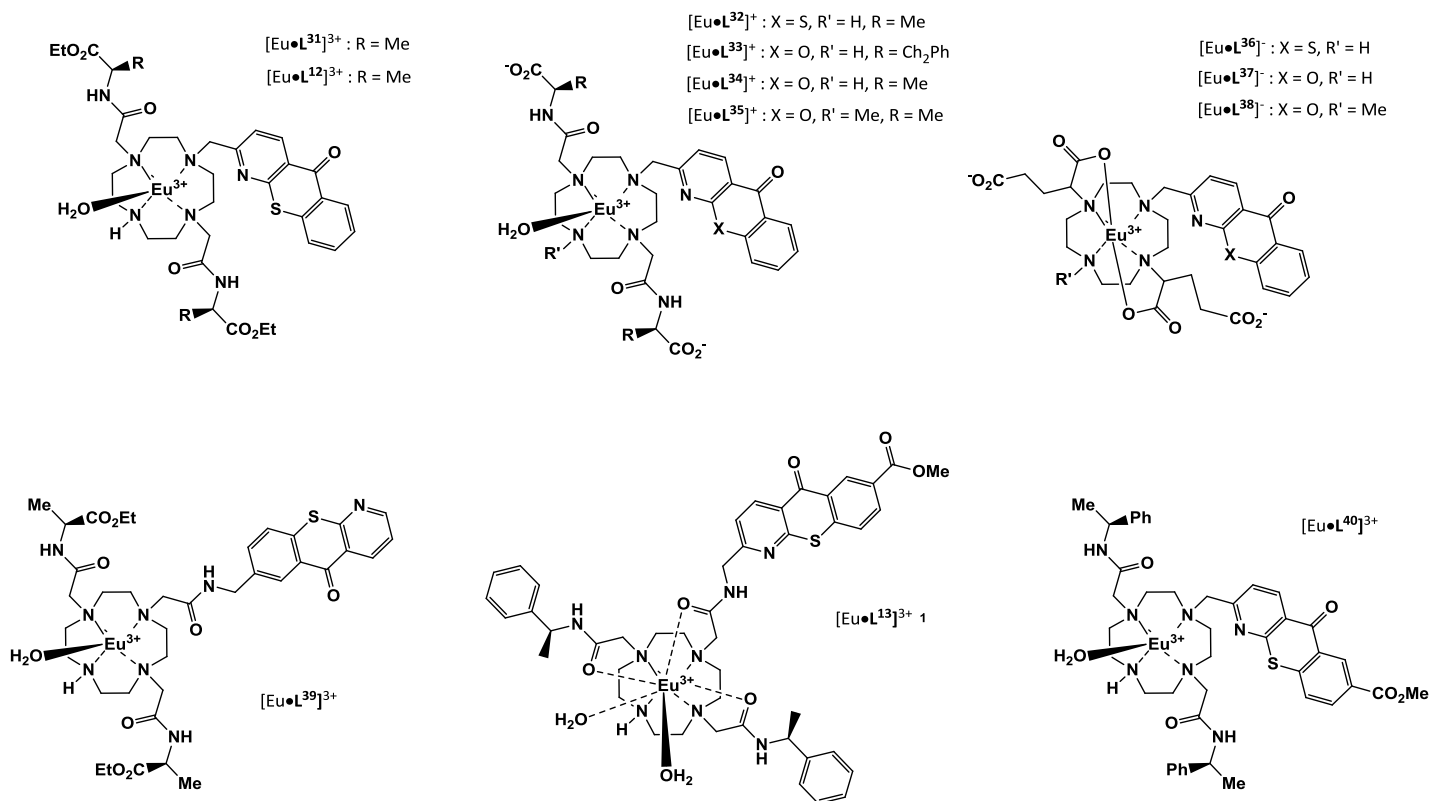
1.7.4 Bicarbonate in marine systems

Calcifying algae are responsible for the bulk of global $CaCO_3$ production with coccolithophorid phytoplankton accounting for a half of oceanic calcium carbonate production.[91] These coccolithophores, such as *Emiliania huxleyi*, extrude elegant calcium carbonate crystalline structures termed coccoliths. Dissolved bicarbonate is the main carbon source for calcification. Ocean pH levels are currently 8.1 but are predicted to drop as atmospheric CO_2 levels rise.[92, 93] Oceanic carbonate levels are predicted to drop as ocean acidity increases, perturbing the saturation state for calcium carbonate.[94]

Calcium carbonate formation occurs in intracellular vesicles to which both Ca^{2+} and HCO_3^- need to be transported. These routes and mechanisms for transport are currently unknown.[95] No direct measurement of local bicarbonate concentrations is possible, as a selective bicarbonate probe is not available. Estimates are made based upon putative local pH and estimated total inorganic carbon levels, with the assumption that the intracellular maximum is 2 mM, the same as that in seawater. These pH measurements stem from a small number of studies using pH responsive fluorophore probes.[92, 96] The estimated values fell in the range 7-8 with two distinct environments observed, with ~50% apparently in vesicles at pH 8 and ~ 50% at pH 7. The development of both bicarbonate and pH responsive probes which are able to enter coccolithophores, therefore, may lead to a better understanding of these processes.

1.8 Reported optical probes for bicarbonate and pH

There are numerous techniques for the selective detection of anions, or the determination of pH. For example, optical spectroscopy, NMR spectrometry, MRI spectrometry and mass spectrometry are all techniques with which it is possible to design responsive probes. Luminescent lanthanide complexes represent just one subset of optical probes. It is appropriate to consider reported responsive fluorescent probes, and some of the examples recently developed for bicarbonate and pH will now be discussed.

1.8.1 Bicarbonate sensing

Synthetic anion sensors are usually engineered to have differing size/geometric properties that are complementary to the target anion.[97] Usually this is achieved using positively charged receptors with appropriately positioned hydrogen bond donors or acceptors.[98] Most synthetic receptors utilise an anion recognition group with a covalently attached chromophore or fluorophore. Hydrogen bonding interactions are particularly effective for anions in non-aqueous solvents. Amides,[99] ureas[100] and thioureas[101] have been successfully utilised in this respect. There exist very few examples of receptors for the bicarbonate anion. As an example probe **41**,

based on the carboxylurea unit, showed selectivity for acetate as well as bicarbonate but only functioned in DMSO, containing 0.5% water.[102] The major challenge lies in creating anion-specific probes which are effective in water.

41

42
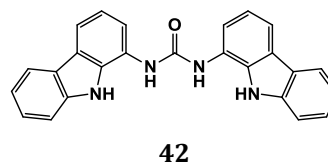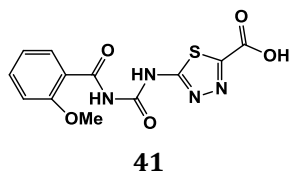
Anion recognition is of great relevance in biological chemistry, yet most reported anion sensors work only in non-aqueous solvents. This is perhaps not surprising given the large free energies of hydration which anions possess [ΔG_{hyd} (HCO_3^- -335 kJ mol^{-1}, $H_2PO_4^-$ -465 kJ mol^{-1}], and that their speciation is often pH dependent. These features combine to make it difficult to create selective synthetic receptors for a given anion.

Fluorescent organic nanoparticales, based on **42**, provides a rare example of an anion sensor which operates in water.[103] They showed good water solubility and exhibited specificity for bicarbonate over other anions. They function as a turn-off sensor, with a linear decrease in emission intensity with increasing bicarbonate concentration in the range 10 μM to 1 mM. This prevents any application in biology, as bicarbonate concentrations are typically an order of magnitude greater.

1.8.2 Lysosomal pH

An example of an intramolecular charge transfer fluorescent probe for lysosomal pH has been reported.[104] The thiazole, **43** was constructed involving a conjugating ethylene bridge between a benzathiazole and a pyridine group to form a D-π-A fluorophore in which the pyridine group is used as the H$^+$ binding moiety. The probe exhibited excellent switching over the relevant pH range for lysosomes with an emission enhancement of 22-fold over the range 3 to 6, with a pKa of 4.22, closely matching to that expected for acidic organelles. The probe was selective for H$^+$

43
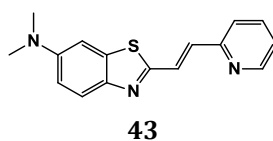
over a range of other biologically relevant cations. An advantage of this probe over other fluorescent pH responsive probes was an improved, larger, Stokes shift. The small Stokes shift of many fluorescent probes limits their applicability due to excitation interference. The location of the probe inside macrophage cells was observed by confocal microscopy, but the punctuated fluorescence also appeared associated with the nucleus and cell membrane. It is likely that selectivity for the lysosomes is a problem and no quantitative data was given.

A successful example, utilising a ratiometric approach, involved mesoporous silica nanoparticles (MSNs) doped with acid sensitive rhodamine-lactam and fluorescein isothiocyanate (FITC) (**44**).[105] Under single wavelength excitation, rhodamine emission increased with increasing pH whilst fluorescein emission decreased. This probe showed greater sensitivity than previous fluorescein based probes, attributed to the inverse pH responses shown by the two components. The pH-responsive range of 3.5 – 6 overlapped well with that expected for lysosomes. The MSNs are readily internalised into cells by endocytosis, and this probe accumulated in the lysosomes. Flow cytometry was successfully used to monitor pH changes in the lysosomes of cells.

44
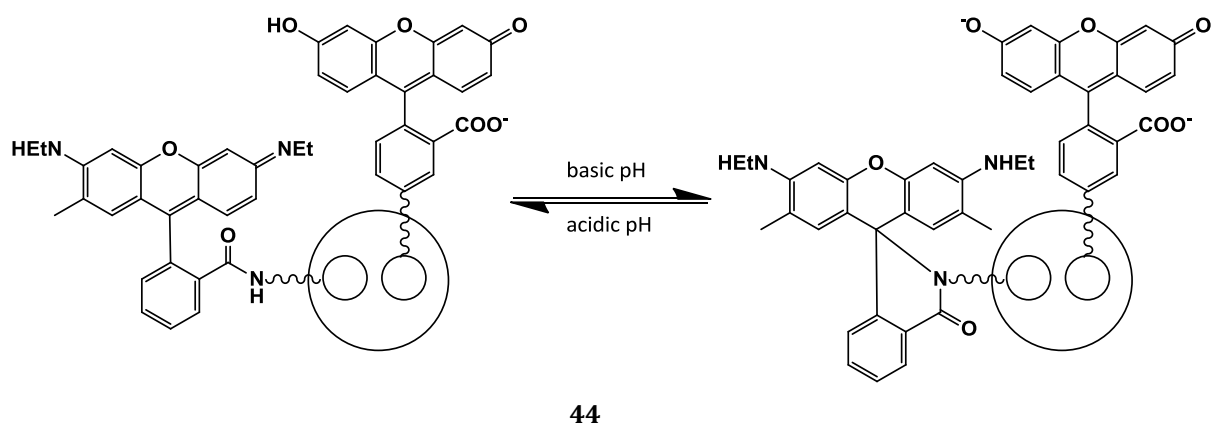
Many BODIPY based probes have also been studied.[106] A series based on **45** with tunable pK_a are non-fluorescent at neutral pH and highly fluorescent at a pH below ~4.[107] The probes were

45
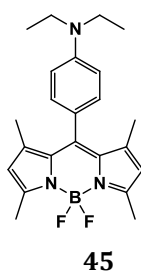
shown to selectively label the lysosomes, and upon treatment of cells with chloroquine, known to induce an increase in lysosomal pH, the fluorescence signal decreased by ~80% accordingly. Although it is useful to be able to easily tune affinity through simple structural modification, these probes again highlight a drawback with organic based fluorophores in that their broad featureless emission does often not allow for ratiometric imaging, so that intracellular pH calibration is difficult.

1.9 Reported responsive lanthanide probes for bicarbonate and lysosomal pH

1.9.1 Bicarbonate responsive lanthanide probes

Anion binding to responsive lanthanide probes works on the principle of reversible binding of an anion to a charged metal centre. This can be signaled by a change in the lanthanide emission spectral form, circular polarisation or lifetime following displacement of one or two coordinated water molecules. A series of emissive europium complexes has been reported in which their anion affinity and cellular localisation is described.[2] Those which showed sensitivity towards anion binding typically contained a water molecule in the axial position (Section 1.3.2). Binding of each anion gave rise to unique characteristics in the corresponding emission spectra.

The measured affinity constant for [Eu·**L13**]$^{3+}$ was highest for citrate, and at their common extracellular concentrations, citrate competes with bicarbonate for europium coordination.[2] This highlights the issue, and potential problem of selectivity towards bicarbonate. In a triply positively charged complex such as this, electrostatics may favour triply charged citrate anions over singly or doubly charged anions such as bicarbonate or carbonate, respectively. Addition of protein caused a 10-fold reduction in emission intensity, and lifetimes measurements were consistent with displacement of one bound water molecule.

Bicarbonate binding to a europium complex has also been signaled by modulation of circularly polarised luminescence (CPL).[108] Significant changes in the circular polarisation of the $\Delta J = 2$ and $\Delta J = 1$ bands accompanied reversible bicarbonate binding for a series of europium probes, associated with a change in local helicity at the metal centre. Upon bicarbonate binding, a reduction in the CPL intensity and alteration of the twist angle was observed. A titration of g_{em}, at a fixed wavelength, as a function of added bicarbonate revealed a similar variation to that observed for the emission intensity ratio change.

1.9.2   pH responsive lanthanide probes

Several pH responsive europium and terbium complexes have been synthesised and studied over the last decade. Early systems such as [Eu·**L⁴⁶**]³⁺ operated on the basis that the first excited states of aromatic fluorophores may be quenched by photoinduced electron transfer from oxidisable groups such as amines. Protonation of the amine, or binding of the amine to a metal will inhibit this leading to a large increase in fluorescence intensity.[109] If the fluorophore in question acts as the sensitiser to lanthanide emission, this will lead to an increase in the quantum yield. It is possible to control the pH range over which this switch operates by varying the basicity of the amine. This is readily achieved by structural modification.

[Eu·**L⁴⁶**]³⁺   [Ln·**L⁴⁷**]
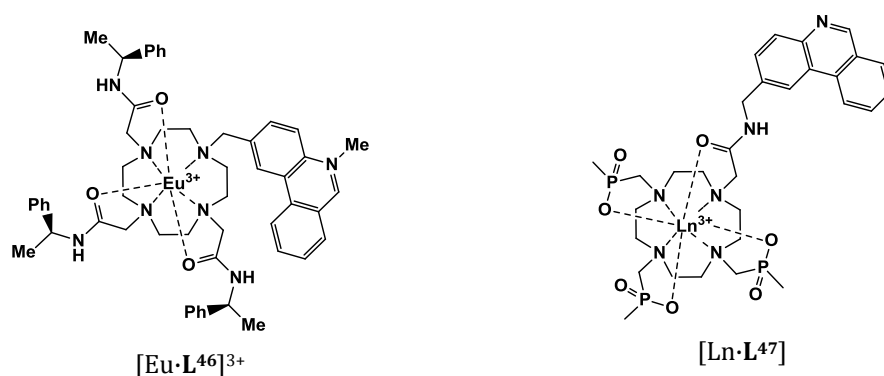
Protonation of the phenanthridine in the europium complex [Ln·**L⁴⁷**] led to a strong increase in luminescence through this process.[110]   The complex showed an on-off emission by perturbation of the singlet excited state of the sensitiser. In contrast, the terbium analogue showed a quenching of emission upon protonation, as the efficiency of back energy transfer to the sensitiser triplet state greatly increases due to a lowering of the triplet energy level.[111] This also affected the lifetime of emission. Excitation spectroscopy was used enabling a ratiometric output to be obtained.[112]

Dansyl[113] and quinolyl[114] sensitising groups have also been incorporated into lanthanide complexes in order to achieve pH sensitive emission. Protonation of the dimethylamino group on the naphthyl ring of the dansyl group (below pH ~5) in [Eu·**L⁴⁸**]³⁻ favours population of the triplet state at 20,600 cm⁻¹, promoting europium emission. With the quinolyl complex, [Eu·**L⁴⁹**] protonation increases the efficiency of energy transfer to the lanthanide leading to a large enhancement of emission intensity. The drawbacks with each probe are the large amounts of ligand fluorescence, an unsuitable excitation wavelength and a lack of sensitivity.

[Eu·**L⁴⁸**]³⁻   [Eu·**L⁴⁹**]
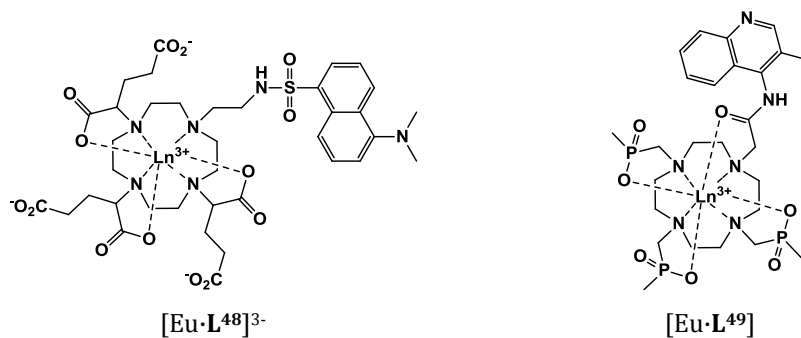
More recently, an improved class of single-component lanthanide pH probes has been developed, based on a change in hydration state at the lanthanide centre involving sulfonamide ligation.[115]   Deprotonation of the sulfonamide enables direct coordination to the metal centre, causing a change in the intensity and lifetime of lanthanide emission upon displacement (Fig. 15).
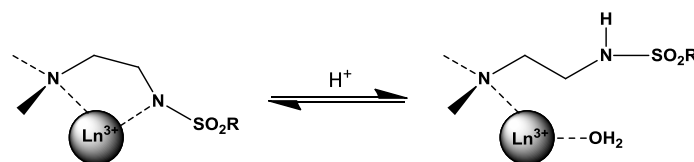
Fig. 15: Representation of the mode of action of pH-dependent sulfonamide ligation.

The first examples of these probes were developed around ten years ago.[115] It was shown that the pKa of the sulfonamide binding could be tuned by variation of the *para*-aryl substituent. These initial probes, such as [Eu·**L⁵⁰**], were excited via the aryl sulfonamide. This is not ideal however, as upon binding the chromophore is brought closer to the lanthanide, enhancing the efficiency of the energy transfer process, leading to increased emission intensity. With two processes contributing, ratiometric analysis is not feasible, as the distance of the sensitising moiety from the lanthanide centre is also pH dependent. Anionic arms were added in order to suppress interference from endogenous anions or protein. When glutarate arms were used, a

[Eu·**L⁵⁰**]

-48-
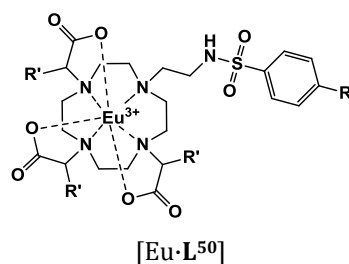
third distinct europium emission spectral form was observed, arising from competitive carboxylate binding forming a 7-membered chelate. This can be suppressed, by extending the alkyl chain length, or increasing electron density on the sulfonamide nitrogen, such as in the *p*–OMe phenyl analogue.

More recently, europium complexes have been synthesised containing a methyl sulfonamide moiety, and a separate heterocyclic sensitising chromophore unit which remains constantly bound to the metal centre.[66, 69] This allowed accurate ratiometric analysis to be performed upon excitation of [Eu·**L51**]+ at 380 nm. The emission intensity ratio at 680 nm / 587 nm was measured and there was an 80% change over the pH range 4.5 – 8 associated with reversible sulfonamide binding. The distinct appearance of a sharp band at 680 nm at pH 8 was ascribed to sulfonamide nitrogen ligation, and has been observed in related systems. The problems with the previous sulfonamide probes were obviated as there is no aryl moiety on the sulfonamide and the binding of the sensitiser throughout pH switching does not change. The complex did exhibit some sensitivity to anions and proteins but a calibration was still possible in human serum. The calibration curve could be constructed giving a protonation constant of 7.2 in the intracellular medium.

[Eu·**L51**]+
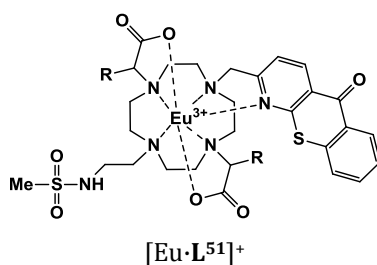
1.10 Objective - Requirements for a pH or bicarbonate responsive lanthanide probe

The aim of this project was to design and synthesise a new class of pH and bicarbonate responsive probes. The compounds must meet a number of criteria:

1) The probe must be water soluble and fully functional in aqueous solution to allow use as a cellular probe.

2) The probe must be sensitive to the analyte over the appropriate biological concentration range for that particular organelle;

    a. For the mitochondrially localising bicarbonate probes, the bicarbonate concentration is in the region of 10 – 40 mM

    b. Lysosomal pH is in the range 4.5 – 6, so the pKa of this probe should lie approximately in the middle of this range

3) The observed spectral change over this range should be sufficient to allow ratiometric analysis to be performed. Ideally this would occur using a pair of emission bands, or alternatively examining the emission arising from the europium versus terbium analogues of a common ligand.

4) The change in the ratio of these bands should also be significant, to increase the accuracy of any measurements made.

5) The probe should resist quenching, either by endogenous proteins or electron rich species.

6) The probe must exhibit a selective and well defined localisation, either mitochondrial or lysosomal.

7) The binding should be fully reversible.

8) The probe should be both thermodynamically and kinetically stable.

9) The probe should be non-toxic (at least in the order of magnitude that the probe will be administered to cells), there is a need to probe normal cellular behavior and function, and not the behavior of a stressed or dying cell induced by the application of the probes themselves.

10) The probe must be selective for the desired analyte. For example, there will be many other anions present and selectivity for bicarbonate is required against a competing background of these. The same applies for pH, it should resist interference from endogenous anions and protein.

11) The probe should, ideally, be highly luminescent.

The following chapter details the synthetic aspects of these complexes and the reasoning behind their design. The subsequent chapters detail the results from the mitochondrial bicarbonate probes and lysosomal pH probes.

2 Synthetic Aspects and Photophysical Characterisation

2.1 Synthesis of the bicarbonate responsive probes

2.1.1 The starting point

The responsive europium complex [Eu·**L¹³**]³⁺, was published in 2008. It showed a large spectral change in its emission profile in response to bicarbonate (or citrate) allowing ratiometric analysis. It is non-toxic to cells and exhibited an unprecedented localisation to the mitochondria.
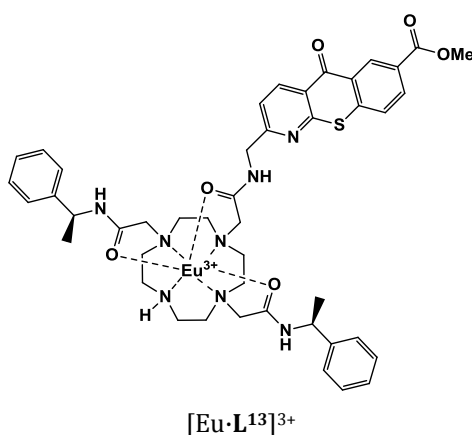
[Eu·**L¹³**]³⁺

Preliminary work studying the azaxanthone analogue of [Eu·**L¹³**]³⁺, [Eu·**L¹**]³⁺, incubated in HeLa cells under a varying atmospheric CO_2 concentration, revealed a decrease in emission intensity as the level of atmospheric CO_2 decreased, and hence mitochondrial bicarbonate concentration was reduced.[116] It was thought that within the mitochondrial environment, the complex existed as carbonate adducts but also with a significant proportion of a citrate bound species. Notwithstanding the carbonate/citrate selectivity issues, the results suggest the probe could find use as a responsive probe for bicarbonate (or citrate) within the mitochondria.

It was proposed, therefore, to design a new ligand, taking the attractive features of this probe and increasing the selectivity towards bicarbonate whilst maintaining the mitochondrial localisation profile. This localisation would hopefully be achieved by retaining the sensitising

azaxanthone unit with the amide linkage to the cyclen. It was decided to switch the azathioxanthone for an azaxanthone, as this would additionally allow the terbium analogues to be synthesised and minimise concomitant fluorescence from the ligand. To increase the selectivity for bicarbonate against other anions, particularly citrate, it was decided this may most readily be achieved by varying the overall charge and/or size of the complex, through structural modification of the pendant arms. A range of related complexes was therefore proposed, with differing geometric constraints, where it was possible to easily vary the overall complex charge from +3, to -2.

$Ln = Eu, Tb$

$[Eu \bullet L^2]^{3+}$ $R = CO_2Et$, $R' = OMe$
$[Eu \bullet L^3]$ $R = CO_2^-$, $R' = O^-$

$Ln = Eu, Tb$

$[Eu \bullet L^4]^{3+}$ $R = CO_2Et$, $R' = OMe$
$[Eu \bullet L^5]^{2-}$ $R = CO_2^-$, $R' = O^-$
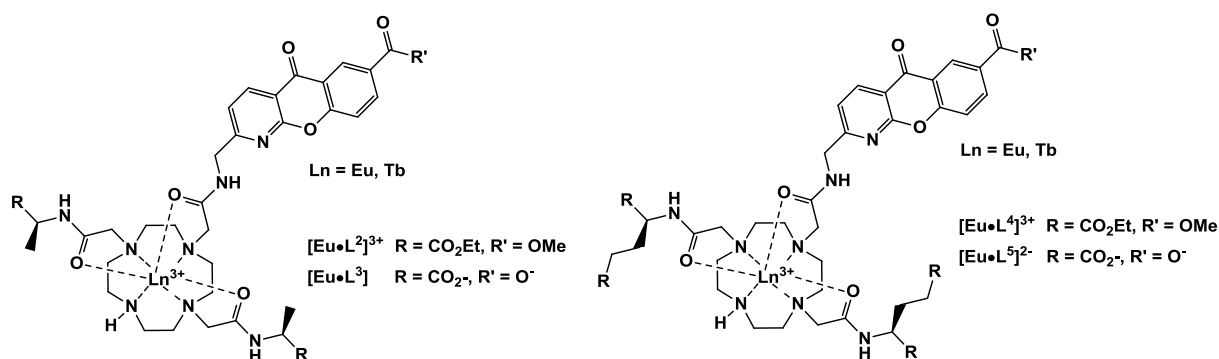
The series of complexes, $[Ln \cdot L^{2-5}]$ embrace a range of europium and terbium complexes with ligands containing an amide linked azaxanthone unit and pendant arms derived from alanine or glutamic acid amino acid residues. This allows some variation of steric demand at the metal centre, and hydrolysis of the ethyl ester groups leads to the variation in complex charge. The original ligand, L^1, was also re-synthesised with an azaxanthone sensitiser, to enable the terbium complex to be synthesised.

$[Eu \cdot L^1]^{3+}$
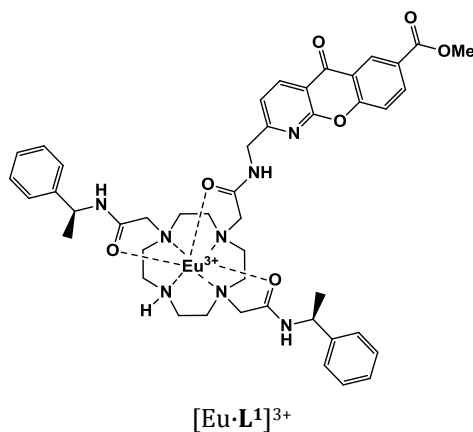
2.1.2 Overall strategy

The synthesis of **L¹** has been reported, and initially involved synthesising the amino-azaxanthone intermediate in five steps. The pendant arms were separately synthesised, before using them to di-alkylate the precursor cyclen-di-CBZ. Deprotection of the two CBZ protecting groups, followed by mono-BOC protection and then alkylation of the last remaining cyclen NH with ethyl bromoacetate. This could then be deprotected using lithium hydroxide to allow coupling with the amino-azaxanthone. BOC deprotection with TFA, and finally complexation gave the europium complex, the overall process is outlined in Scheme 1.
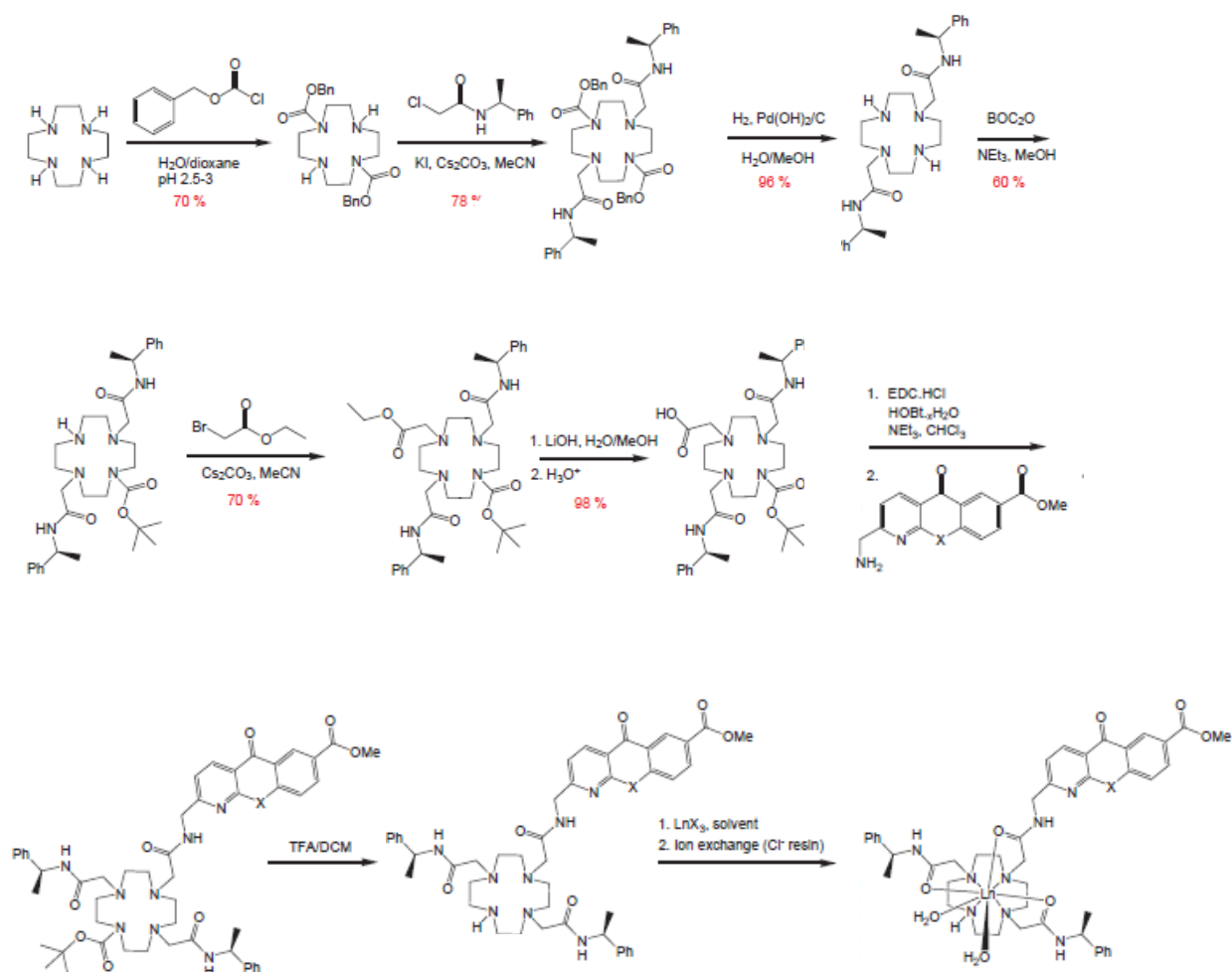
This exact strategy could not be replicated for the synthesis of [Ln·**L²⁻⁵**], as the lithium hydroxide hydrolysis step would remove all the alkyl esters present, including those on the pendant arms and chromophore. Modifications to the scheme were made to avoid this step, and the synthetic route used to prepare [Ln·**L²⁻⁵**] is described below. This new route was then used as the preferred method when synthesising **L¹**. In essence, it involves a similar principle of creating the azaxanthone moiety in one strand, whilst simultaneously building up the

macrocyclic framework with the pendant arms during a series of protection steps, selective mono-alkylations and deprotections, before metal complexation of the final ligand.

2.1.3 Synthesis of the chromophore

The synthesis of 2-aminomethylazaxanthone, **57**, has previously been reported.[2] This method was followed with a slight deviation from the original route when synthesising the mono-brominated derivative. In summary, methyl-4-hydroxybenzoate was deprotonated with sodium methoxide and coupled with 2-chloro-6-methylnicotinic acid in the melt at 155 °C. Electrophilic cyclisation of the product of this reaction, **52**, with PPA yielded 7-methoxycarbonyl-2-methyl-1-azaxanthone, **53**. This step gave the lowest yield (45%) during the stage of chromophore synthesis, largely due to the unavoidable, partial hydrolysis of the methyl ester group during the work-up. This proved difficult to extract from the inorganic phosphate salts produced, due to the challenging solubility properties. It was possible to recover some of this hydrolysed side-product material and increase the final yield by lowering the pH of the work-up to ~pH 2, and then extracting the hydrolysed azaxanthone-carboxylic acid with DCM. This could be re-esterified using methanolic HCl to yield the desired product, **53**.

Previously, the selective mono-bromination step had been the lowest yielding step, being obtained in just 14% yield, due to formation of the di-brominated side-product during the benzylic bromination step.[2] Difficulties were also encountered in separation of the desired product by column chromatography. Initially the same route was followed, but it became clear that it was never possible to obtain greater than a ~35% conversion to the desired mono species at any point, and the resulting chromatographic purification was difficult as each of the three products ran close together, leading to isolated yields of no more than 15 - 20%. Methodology has been established whereby this dibrominated side product can be converted back to the mono-brominated and/or non-brominated precursors using diethyl phosphite.[117] Through refinement of this process by careful control of reaction temperature and reducing the reaction time and number of equivalents of phosphite and base, it became possible to selectively obtain the desired mono-brominated product, with no formation of the original non-brominated precursor. Additionally, it was relatively easy to deliberately and selectively di-brominate from **53**, by using 2.5 equivalents of NBS, driving this dibromination to completion. These reactions were easily monitored by ^{1}H-NMR spectroscopy, observing the aromatic proton at the 3-position, which resonates at 8.6 ppm, 8.7 ppm and 8.8 ppm in the non-, mono- and di-brominated species respectively. No evidence of the tri-brominated species was ever observed, presumably due to steric inhibition. Given the difficulty in separation by column chromatography between the three species, this two-step process became the preferred method,

with an overall yield of 69% for the two steps, a significant improvement and a much simpler purification process.
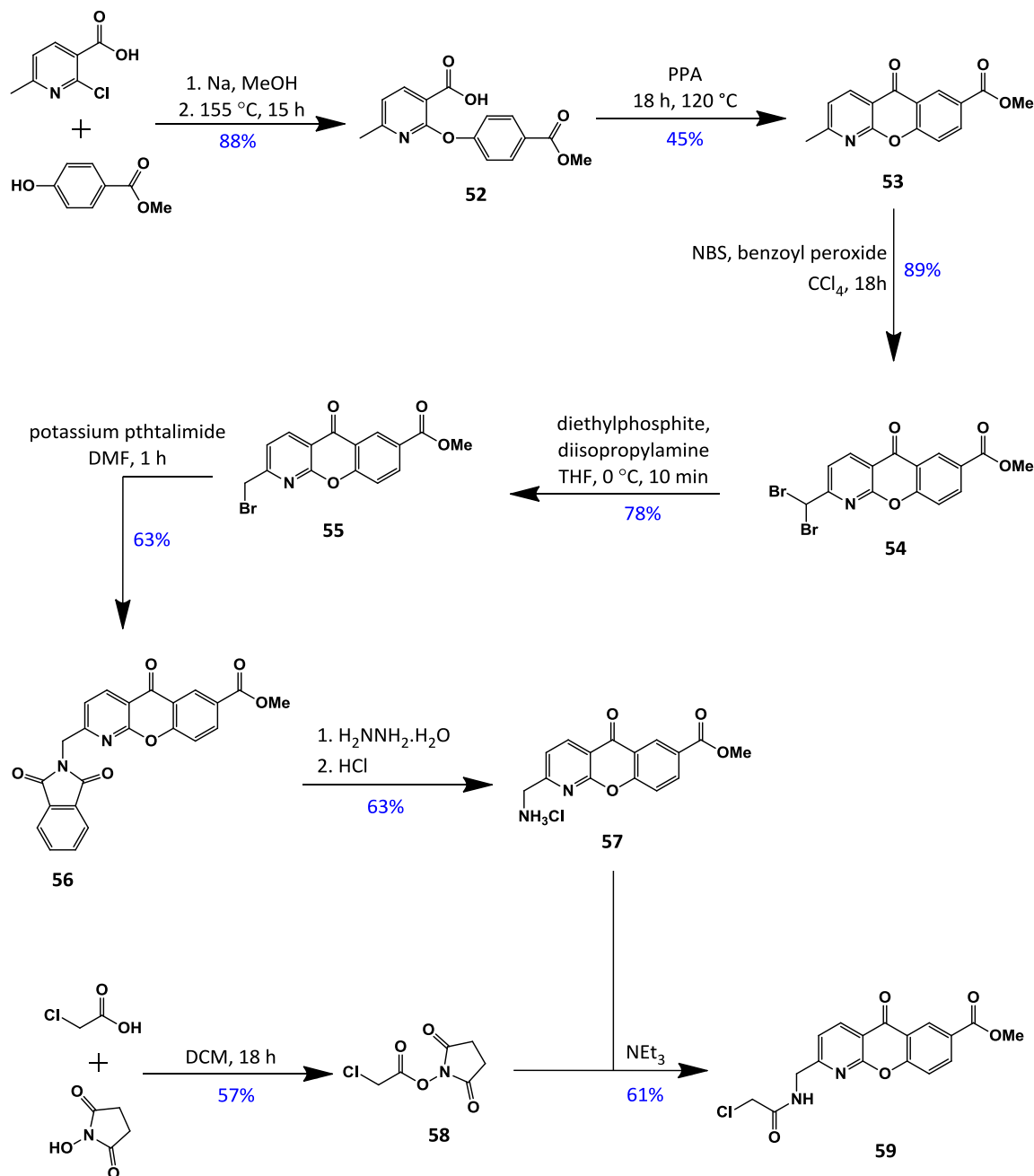

Scheme 2: Synthesis of the azaxanthone chloroamide, **59**.

The following two steps accessing the 2-aminomethylazaxanthone, **57**, derivative followed literature procedures, first using potassium phthalimide in a Gabriel reaction, followed by cleavage with methanolic hydrazine to yield the amino product after work-up.[118]

Previously, it was at this stage that the azaxanthone was coupled with the macrocyclic framework. However, given that this reaction was not applicable for this novel series of probes, the final stage was to couple with the NHS activated ester of chloroacetic acid, **58**, itself easily made in one step, to yield the final azaxanthone product, **59**. It was important that the activated ester was used in high purity for this reaction to proceed cleanly. It was possible to purify this final compound by successive washing with saturated bicarbonate solution, followed by water.

2.1.4 Synthesis of the macrocyclic framework

The ligand macrocyclic framework is built up over a series of protection selective alkylation and deprotection steps. This process starts with cyclen, and its selective *N*-alkylation at the 1,7-positions under pH control using benzyl chloroformate (Scheme **3**).[119]
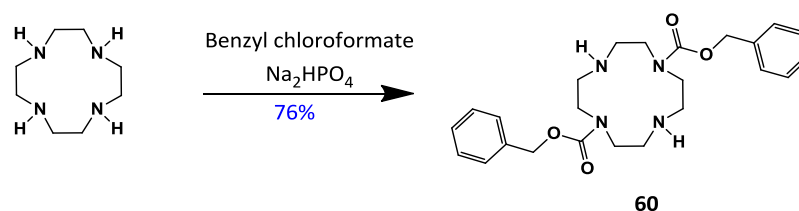
Scheme 3: Synthesis of Di-CBZ cyclen, **60**.

The chiral pendent arms are easily made (Scheme **4**). The glutamic acid arms were commercially available as their ethyl ester hydrochloride salts. For the alanine based pendent arms, formation of the ethyl ester, **61**, was achieved by refluxing in ethanol after dry HCl, generated *in situ* by dropping concentrated sulphuric acid onto NaCl, had been passed through to saturate the solution. Alkylation with bromacetyl bromide yields the chiral pendent arm, **62**.
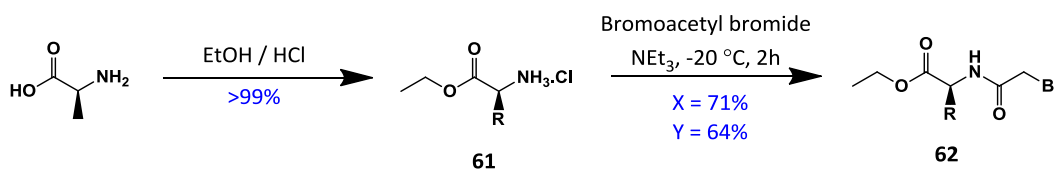
Scheme 4: Synthesis of the ligands, **L¹** and **L²**.

The introduction of the two desired chiral pendant arms into the macrocycle was undertaken by *N*-alkylation of di-CBZ cyclen, **60**, in acetonitrile in the presence of potassium carbonate. The CBZ protecting-groups were subsequently removed by hydrogenation using a palladium

hydroxide on carbon catalyst. Initially, it was hoped to selectively mono-alkylate the intermediate **66** (**67** or **68**) with the α-chloroamide azaxanthone, **59**. However, the formation of the tetra-substituted product could not be avoided and this occurred to a significant extent as deduced by ¹H-NMR spectroscopy and ESMS product analysis. Given that the amide-azaxanthone took a number of steps to synthesise and the amounts were quite precious, a
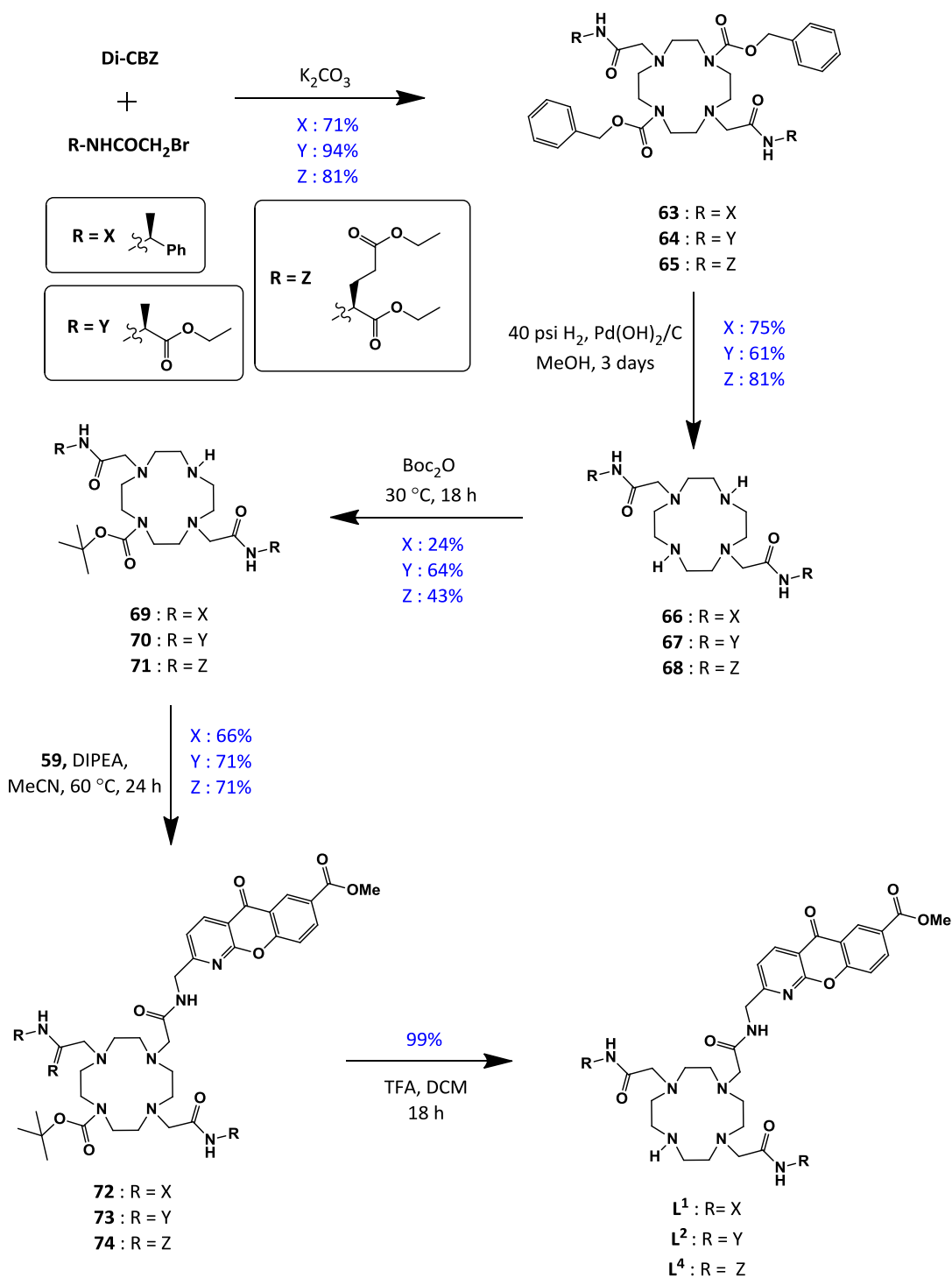
Scheme 4: Synthesis of the ligands, **L¹**, **L²**, and **L³**.

secondary route was undertaken that was considered to be more efficient with respect to this material. This involved mono-protection of one of the cyclen secondary amine position in **66**, **67** or **68** with BOC_2O. Again, the formation of the tetra-substituted product with two BOC groups could not be avoided. However, separation of the desired product by column chromatography was achieved allowing isolation of the desired mono-protected species. This route was additionally more economical, because the unwanted tetra-substituted side-product could be recycled back into the trans pendant arm compound through BOC deprotection using TFA in a near quantitative yield. After obtaining the desired mono-BOC protected species **69**, **70** and **71**, alkylation with the α-chloroamide-azaxanthone could be undertaken. The most efficient reaction conditions found involve using DIPEA as the base, in acetonitrile at 60 °C overnight. Column chromatography of the reaction mixture on silica gel was required to purify this product, Finally, deprotection of the BOC protecting-group with TFA afforded the final ligand in a quantitative yield.

This route (Schemes **2** and **4**) was different to that previously used, driven by the need to avoid the lithium hydroxide deprotection step. It is relevant to point out that the new route offers an improvement in terms of yields and ease of synthesis. In particular, the overall yield to the amino-azaxanthone was increased from 1.0% to 11%; arguably, this is the limiting process in the total synthesis.

2.1.5 Formation of the lanthanide(III) complexes

The complexation of the neutral ligands, **L¹**, **L²** and **L⁴** was carried out by refluxing in acetonitrile with the triflate salt of the given lanthanide ion. It is possible to monitor the extent of complexation relatively easy, particularly with these azaxanthone chromophores, by observing the increase in intensity of the characteristic lanthanide emission by luminescence spectroscopy. Initially, there is a large broad emission centred at ~450 nm corresponding to ligand fluorescence but the relative intensity decreases as the lanthanide spectral intensity grows. At completion, the fluorescence from the ligand is negligible for the azaxanthone derivatives, with an intense emission from the lanthanide complex, confirming that the complexation is complete.

The complexes then need to be purified. Excess lanthanide salts can be removed by increasing the pH of the solution to 10 with concentrated KOH solution, at which point the lanthanide salts precipitate as $Ln(OH)_3$. Care needs to be taken to avoid increasing the pH too far above this as this can result in decomplexation of the lanthanide from the macrocycle. The solution was then filtered to remove the precipitate and the pH of the solution adjusted back to

neutral, and lastly lyophilised. Finally, the complexes were converted to their chloride salts, using anion exchange resin to enhance their water solubility.

In some cases, this pH adjustment to remove excess lanthanide was performed using ammonium hydroxide and reacidifying with acetic acid. This avoids the formation of potassium chloride salts as the products of neutralisation are volatile, and will be removed when lyophilising.

The related complexes, [Ln·L³] and [Ln·L⁵]²⁻, have zero or two negative charges. For these, it was first necessary to hydrolyse the ester groups in each ligand. This was most readily achieved using 0.1 M KOD, adding a small amount of MeOD to initially solubilise the ligand. The deuterated solvent allows monitoring of the extent of the reaction by ^{1}H-NMR spectroscopy. Once complete hydrolysis of the ethyl esters, and the methyl ester of the azaxanthone chromophore was confirmed, the pH was adjusted back to neutral, and the solution passed through a cation exchange resin.

With these anionic ligands, complexes were formed in aqueous solution using lanthanide acetate salts. The pH of the solution was adjusted to around 5.5 to facilitate efficient complexation. Once complete, the excess lanthanide salt was removed by pH adjustment.

2.2 The design and synthesis of pH-responsive emissive probes

2.2.1 Introduction

Previous work has shown that pH responsive lanthanide complexes can be synthesised which are non-toxic, cell-permeable and give a ratiometric output in response to pH through modulation of emission spectral form.[66] However, none has satisfied both the requirement of showing an unambiguous lysosomal localisation, coupled with an appropriate pKa for pH-responsive within this cellular compartment.

The aim was to develop a pH responsive lanthanide complex that would target the lysosomes selectively, having a pKa of around 5, to operate effectively over the lysosomal pH range. Several complexes were proposed and the reasoning behind the design of each one is outlined below. The synthetic details for each of these complexes follows. In practice, the performance of each complex was analysed sequentially, i.e. before the next synthesis was proposed, based on the previous set of results.
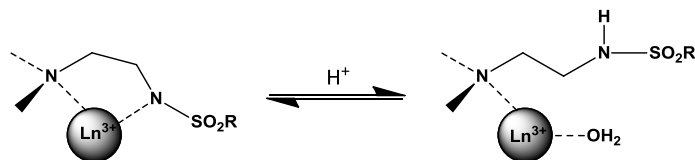
Fig. 16: Representation of sulfonamide pH dependent ligation.

2.2.2 Probes involving sulfonamide ligation

The complex [Eu·**L⁹**]³⁺ is based on a disubstituted-phenylmethylamide ligand and incorporates a dpqC chromophore. The related complex containing three of these pendant arms has been shown to exhibit a lysosomal distribution.[26, 61] It was postulated that replacement of the amide pendant arm *trans* to the dpqC chromophore by a pH sensing moiety might not alter this localisation profile, and would allow pH sensing. This hypothesis was based on the knowledge that it is the nature of the sensitising group, rather than the structure of the pendant arms, which most readily dictates the localisation.[22] The *para*-methoxy sulfonamide pH arm was selected as it had been shown to be suitable for pH-dependent ligation to europium complexes.[115] It offers a pK$_a$ in the range 5.5 to 6.0.


[Eu·**L⁹**]³⁺   [Eu·**L¹⁰**]⁺
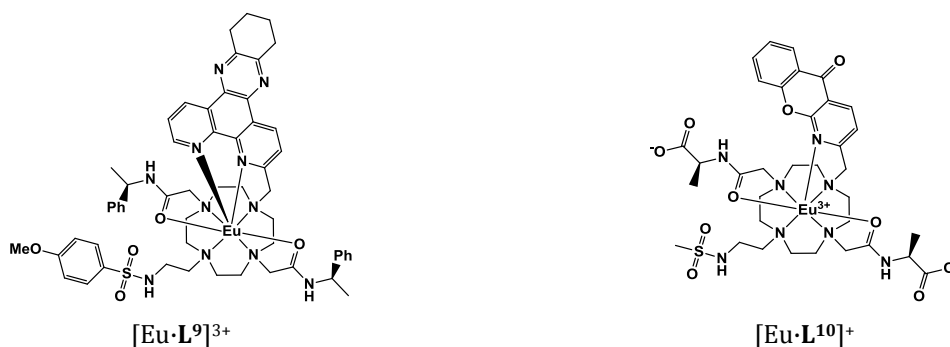
The complex [Eu·**L¹⁰**]³⁺, closely resembles a set of pH probes which have recently been shown to be cell permeable, and exhibit a pH dependent ratiometric output over the range pH 6 - 7, albeit with some interference from endogenous anions and protein.[66, 69] Modifications were suggested to make the complex more amenable to lysosomal pH sensing. Firstly, switching to an azaxanthone instead of an azathioxanthone would minimise concomitant ligand fluorescence and potentially allow both europium and terbium analogues to be synthesised. Secondly, the use of alanine based pendant arms allows the overall charge of the complex to be easily varied through ester hydrolysis, and so allow a greater control, minimising interference from competing anionic species by varying charge repulsion on encounter.

2.2.3 Probes involving reversible carboxylate ligation

The rationale behind the design of the complex [Eu·**L**[11]][3-] is quite different from the above two systems. It uses a different class of pendent arm to provide the pH response, and the chromophore is a non-coordinating azathioxanthone.

[Eu·**L**[11]][3-]
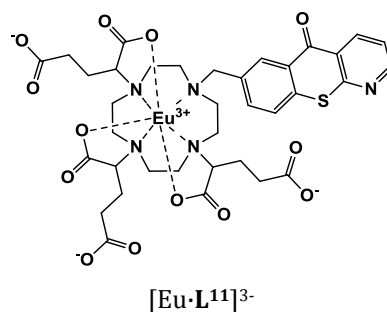
In previous probes, glutarate arms have been introduced in conjunction with a sulfonamide to reduce interference from anions and protein.[66] The desired pH response in these complexes originates from reversible sulfonamide binding. In this instance however, the glutarate arms can also compete with sulfonamide ligation, forming a stable 7-membered chelate with the metal centre.
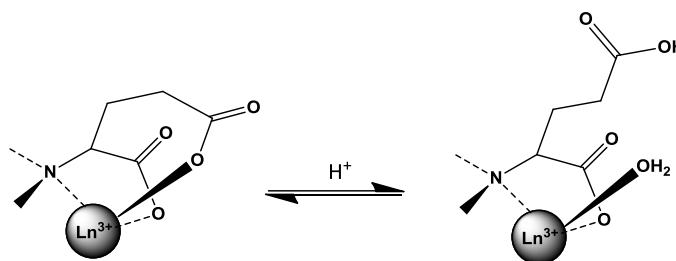
Fig. 17: Representation of the effect of carboxylate binding to the lanthanide centre.

It is anticipated that a complex including three of these arms, without any other arms capable of pH dependent binding will benefit from the anionic protecting properties they have, and utilise the pH depending binding of the carboxylate group only to generate a ratiometric change in the europium emission spectrum. In addition, glutaric acid, possessing a terminal carboxylate pKa of 4.4, should be well suited to assessing lysosomal pH in the desired range.

The second difference with this probe concerns the sensitising unit. This azathioxanthone is non-coordinating with the linkage to the macrocycle occurring through the 7-position, rather than the 2-position as in every previous example in this chapter. The reasoning for this feature

is to avoid potential problems with distance dependent energy transfer. If the chromophore unit were directly bound to the lanthanide centre as in 9 and 10, it is possible that ligation of the pH dependent arm could increase steric demand at the metal centre and cause the pyridine nitrogen in the chromophore to be displaced, i.e. becoming unbound. This would lead to two processes contributing to any change in the emission profile; first, a change in the coordination sphere due to ligation of the pH arm and second, a change in coordination due to removal of the sensitising unit with a corresponding decrease in the efficiency of the energy transfer step.[115] By using a chromophore which is not bound, the lanthanide-chromophore distance should remain constant and not contribute to changes in the intensity of the emission spectrum associated with binding by the pH dependent moiety.

2.2.4 Probes based on a pH dependence of competitive bicarbonate and sulfonamide binding

The final approach was to use the bicarbonate probes e.g. [Ln·L^{1-5}], discussed in the previous section as a starting point. The probe on which these are based showed a lysosomal localisation at extended time-points post incubation, i.e. around 12 – 24 h.

[Ln·L^{6-8}]$^{3+}$
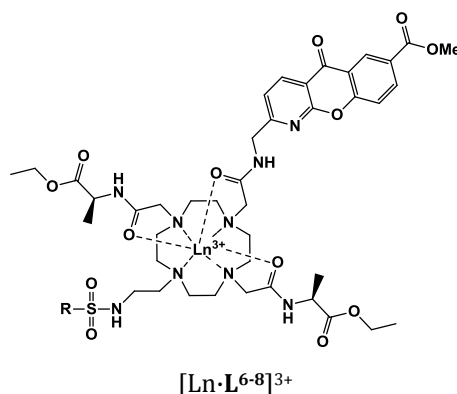
It was hypothesised that, if a pH dependent sulfonamide was incorporated onto the remaining free cyclen NH, bicarbonate binding would compete with sulfonamide binding giving a pH-dependent emissive response over an extended pH range.[120] This structural change would obviously need not to perturb the localisation profile in order to work. Variation of the sulfonamide substituent would also allow the charge density on the nitrogen to be varied, allowing tuning of the pH range over which the probe could operate.

2.2.5 Synthesis of the pH responsive series of probes

For the synthesis of [Eu·L^9]$^{3+}$, the *trans*-phenylmethylamide dpqC framework had previously been synthesised and was available. It was only necessary to alkylate with the sulfonamide. The general procedure for introducing the sulfonamide binding moiety involves the *in situ* formation of an *N*-sulfonylaziridine, and its subsequent ring opening reaction with the secondary amine of the cyclen ring. Potassium carbonate was used as the base, and the product was purified by column chromatography on silica gel. Complexation of the final ligand was achieved using europium triflate .


[Eu·L^9]$^{3+}$
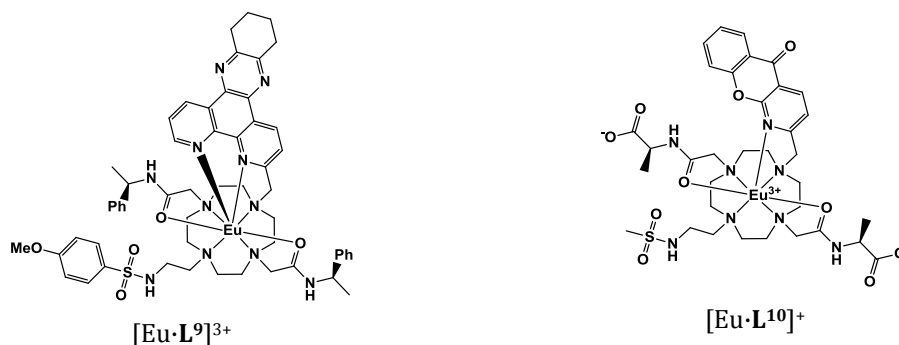
[Eu·L^{10}]$^+$

The synthesis of [Eu·L^{10}]$^{3+}$ followed a similar procedure. The trisubstituted, *trans*-alanine azaxanthone had already been synthesised. All that was required was to alkylate the remaining secondary amine site with the sulfonamide, using the previous procedure, followed by lanthanide ion complexation. These reactions proceeded in good yield.

The synthesis of the complex [Eu·L^{11}]$^{3-}$ required a different approach as it is not based on a *trans*-amide system, and its synthesis does not proceed through the trans-di-CBZ intermediate. Two synthetic routes towards the final complex were considered, and each was attempted. First, monoalkylation of cyclen with the bromomethyl chromophore was carried out followed by trialkylation with the glutarate arm (Scheme **5**). In the alternative route (Scheme **6**), trialklylation was carried out first followed by alkylation of the fourth remaining cyclen NH with the bromomethyl chromophore.

Thus, in the first route (Scheme **4**), cyclen was trialkylated with (*S*)-2-bromopentanedioic acid 5-benzyl ester 1-*tert*-butyl ester. This reaction produced reasonably significant quantities of the di- and tetra-substituted side products and so column chromatography was required to separate the desired tri-substituted product. The final cyclen NH position was alkylated with the bromomethyl chromophore in the presence of potassium carbonate. Deprotection of the glutarate arms then took place in two steps. Firstly, the benzyl groups were removed using lithium hydroxide. Hydrogenation could not be used in this instance as the sulphur in the
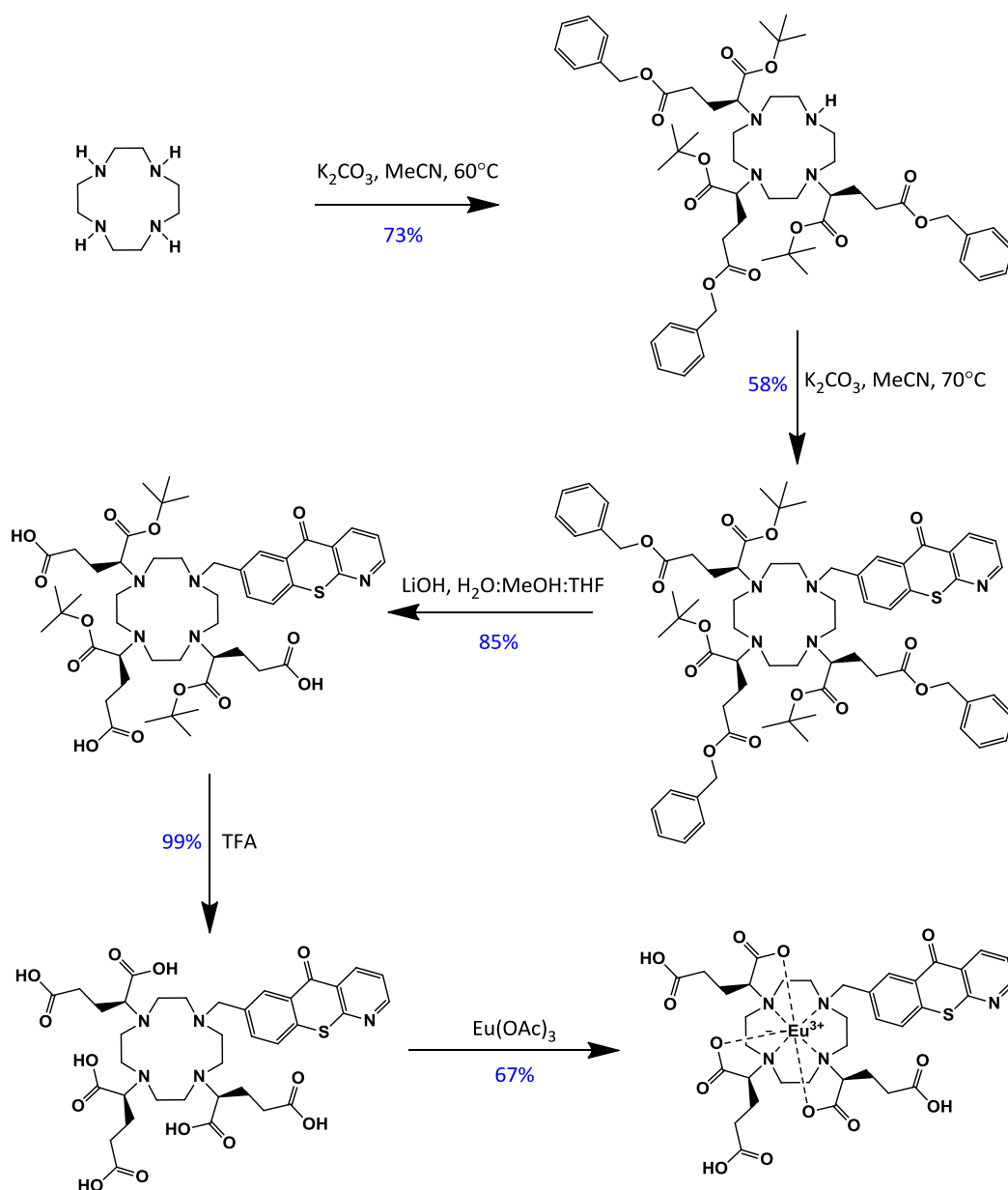
Scheme 4: The synthetic route towards [Eu·**L**[11]][3-] via the first route.

chromophore interfered with the palladium catalyst. After the benzyl groups were removed the BOC groups could be removed using TFA. Complexation of the ligand with europium acetate afforded the final complex after the standard work up procedures.

The azathioxanthone was initially monoalkylated with cyclen, using 10 equivalents of cyclen. Sodium bicarbonate was used as the base offering slightly milder conditions than the potassium carbonate usually used in these alkylations. Excess cyclen was recovered by washing with water. This mono-alkylated product was alkylated in order to introduce the pendant arms. (*S*)-2-Bromopentanedioic dimethyl ester was used this time and this had two advantages. First, it could be deprotected in a single step using lithium hydroxide, and second, the dimethyl ester is a

cheaper starting product than the benzyl-*tert* butyl ester precursor. This route resulted in the desired ligand which was complexed with europium as before.
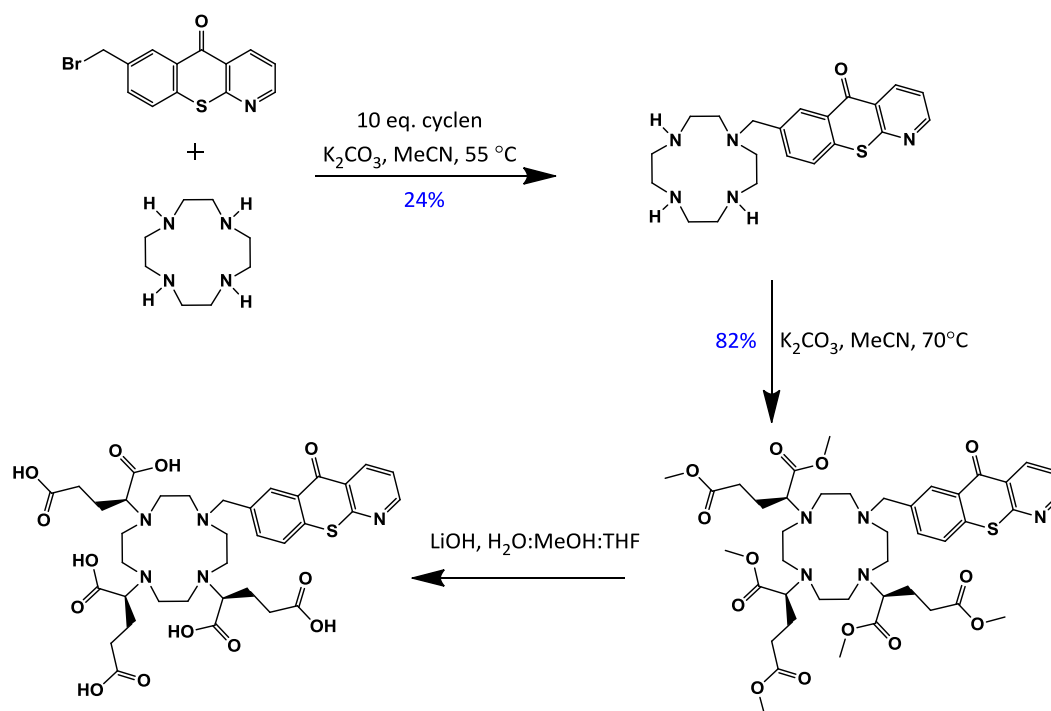

Scheme 5: The synthetic route towards [Eu·**L**[11]][3-] via the second, more efficient, route.

Finally, the series based on bicarbonate probes were made. Taking the final ligand from the bicarbonate synthesis steps, alkylation with the desired sulfonamide precursor in the presence of potassium carbonate, followed by complexation, gave the final complexes. Three different sulfonamides were made, to cover a range of pH values.

2.3   Photophysical characterisation of the bicarbonate probes

2.3.1   Emission spectral analysis

The full emission spectrum of [Ln·**L**[2]][3+], is shown in Fig. 18. The very fast rate of intersystem crossing observed for these azaxanthone systems is highlighted by the negligible amount of ligand fluorescence observed over the region 400 – 550 nm. The form of the emission spectrum is very similar to that observed previously with structurally related europium complexes of tri-amide ligands.[2]
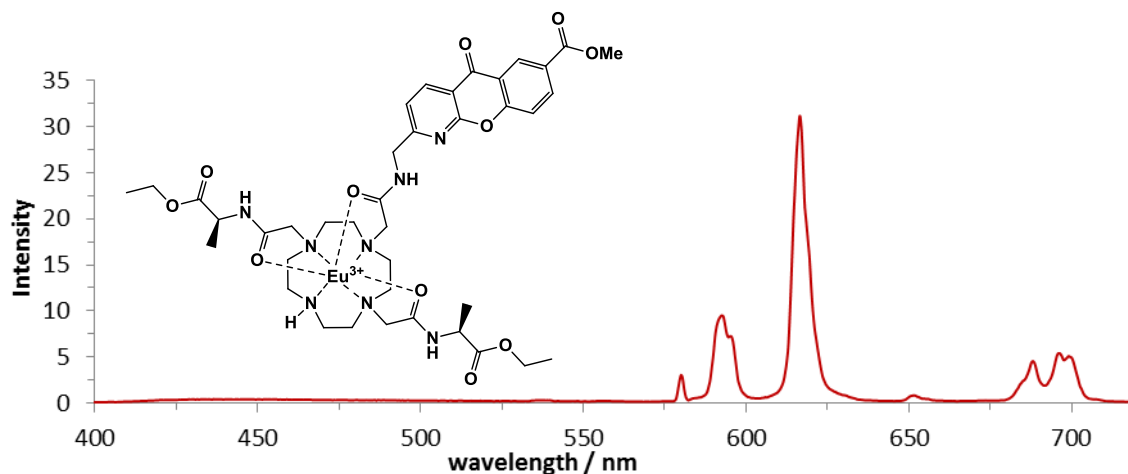
Fig. 18: Full emission spectrum of $[Ln·L^2]^{3+}$ (H_2O, pH 5.5, 25 μM complex, 298 K, λ_{ex} = 332 nm).

At 579 nm, a rather weak $\Delta J = 0$ transition was observed and the magnetic-dipole allowed $\Delta J = 1$ manifold around 590-595 nm appeared as two closely spaced emission bands. The hypersensitive $\Delta J = 2$ manifold was centred at 616 nm and appeared as one intense transition, while the $\Delta J = 3$ and $\Delta J = 4$ (680-710 nm) transitions were of lower intensity.

Unsurprisingly, the form and splitting patterns of the emission spectra for the series $[Ln·L^{1-4}]$ were similar, as only the periphery of the ligand structure has changed. The immediate metal coordination environment which determines the form of the spectrum is identical in each case. There are slight differences in emission intensity, most notably, a reduction by a factor of around two in the overall emission intensity for $[Ln·L^3]$ and $[Ln·L^5]^{3-}$. These are the two complexes which are not positively charged. Each spectrum was recorded at pH 5.5 after bubbling argon through the solution to ensure that the concentration of dissolved bicarbonate was minimised.
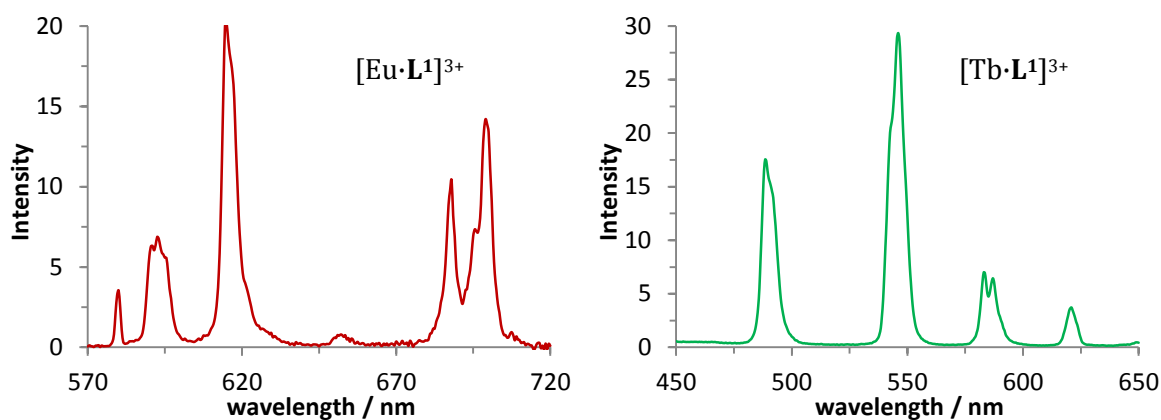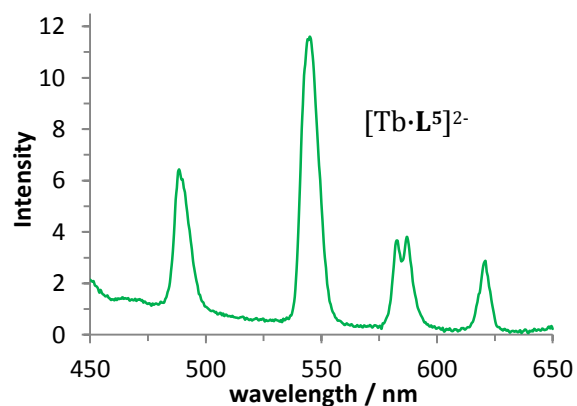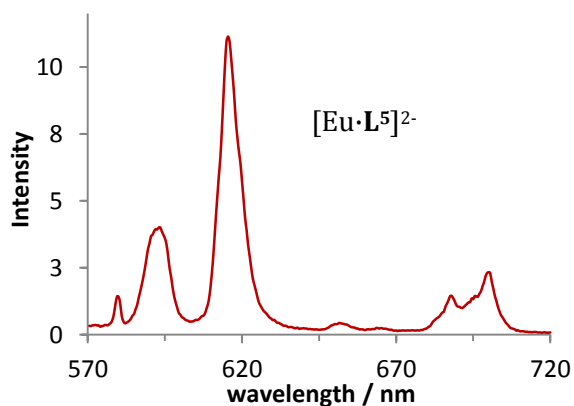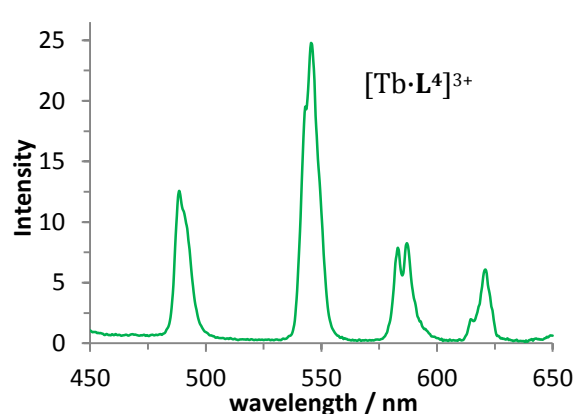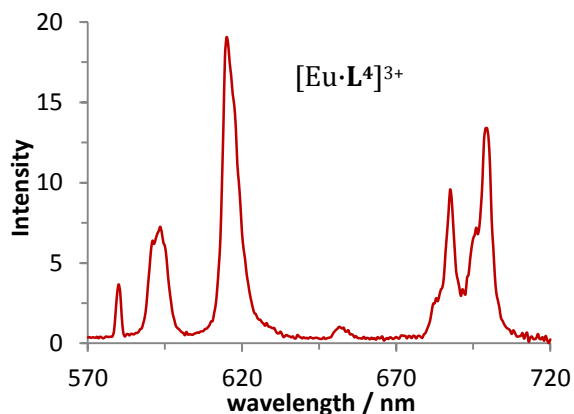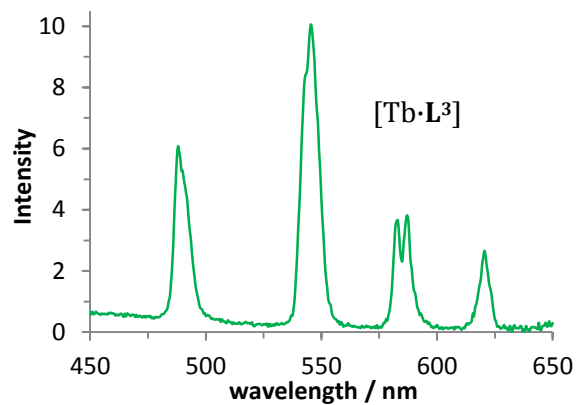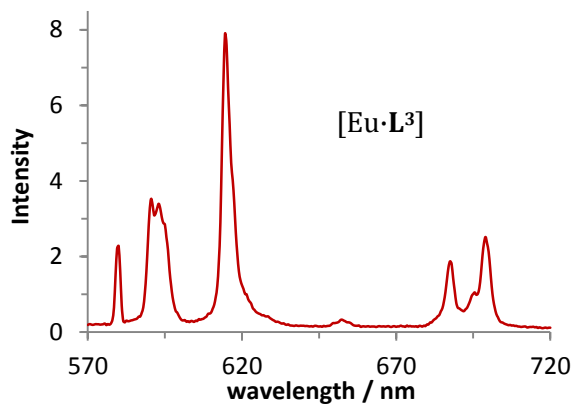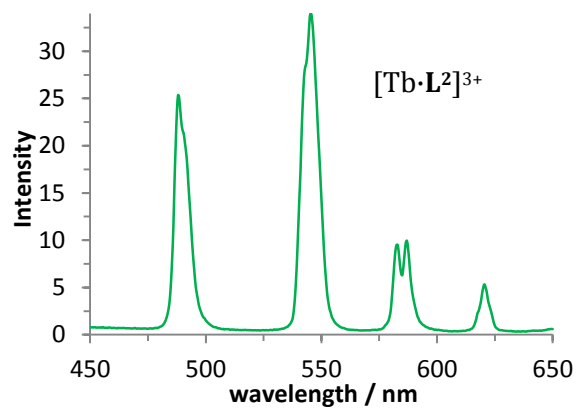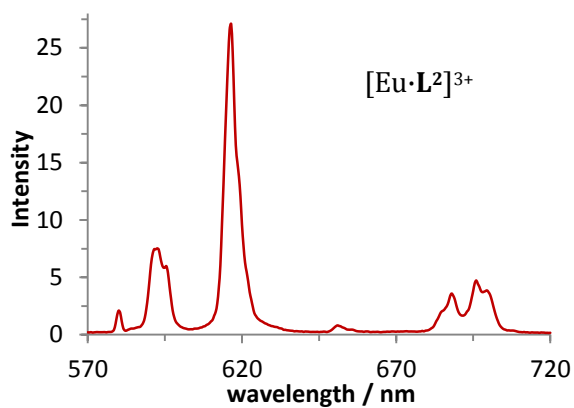
2.3.2 Estimation of the complex hydration state, *q*

The decay of the intensity of the europium emission at 616 nm in H_2O and D_2O is shown in Fig. 19. Each profile was taken using the same concentration of complex. It can be observed that in D_2O a more intense emission was apparent that decays more slowly. These effects result from the less efficient energy transfer from the $^5D_0$ excited state to D_2O oscillators. By plotting the natural logarithm of the emission intensity vs. time, the reciprocal of the gradient gives the radiative decay constant, *k*.
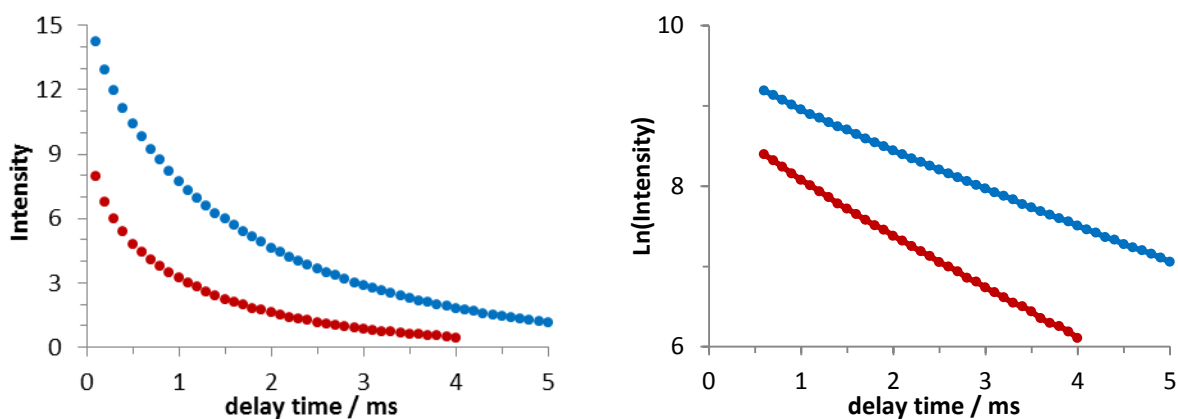
Fig. 19: Representative excited state decay profiles for lanthanide emission as a function of delay time in D_2O (blue) and H_2O (red). The reciprocal of the gradient of ln(intensity) vs. delay time gives the radiative decay constant.

The *q* value of a complex is a measure of the inner sphere hydration number, and indicates the number of water molecules directly bound to the metal centre in the solution state. To calculate this value, the excited state lifetime was first measured in H_2O. Following lyophilisation, the complex was re-dissolved in D_2O, and left overnight to allow exchange of bound H_2O to D_2O. The complex was again lyophilised, and re-dissolved in fresh D_2O, and the excited state lifetime was measured again. Due to the differences in the rates of energy transfer to H_2O and D_2O oscillators, the hydration state can be calculated according to the following equations, *[Eq. 6]* and *[Eq. 7]*, where the terms 0.25 and 0.06 reflect the quenching effect of unbound water molecules and *n* is the number of coordinated secondary amide groups, reflecting the quenching effect of the proximate NH oscillators.[32, 33]

$$q'_{Eu} = 1.2\left(\Delta k - 0.25 - 0.075n\right)$$

[Eq. 6]

$$q'_{Tb} = 5\left(\Delta k - 0.06 - 0.01n\right)$$

[Eq. 7]

Table 4: Rate constants, k, (± 10%) and lifetimes (τ), observing radiative decay of the lanthanide excited state (at 616 nm for Eu(III), 545 nm for Tb(III)) (295 K, 50 μM complex) and derived hydration numbers, q (± 20%).

Complex	k_{H2O} / ms^{-1}	τ / ms	k_{D2O} / ms^{-1}	τ / ms	q
[Eu·**L¹**]³⁺	3.85	0.26	1.56	0.64	2.2
[Tb·**L¹**]³⁺	0.87	1.15	0.40	2.50	2.1
[Eu·**L²**]³⁺	3.85	0.26	1.73	0.58	2.0
[Tb·**L²**]³⁺	0.90	1.11	0.41	2.44	2.2
[Eu·**L³**]	3.86	0.26	1.48	0.68	2.3
[Tb·**L³**]	0.90	1.11	0.39	2.56	2.3
[Eu·**L⁴**]³⁺	2.08	0.48	0.88	1.14	0.9
[Tb·**L⁴**]³⁺	0.81	1.24	0.51	1.96	1.0
[Eu·**L⁵**]²⁻	2.69	0.37	1.33	0.75	1.1
[Tb·**L⁵**]²⁻	0.82	1.21	0.42	2.39	1.5

For [Eu·**L¹⁻³**], a *q* value of two was obtained. There exists no difference in *q* value for the europium and terbium complexes of the same ligand. Thus, in the solution state, two water molecules are bound to the metal centre. Hence the lanthanide ion is nine-coordinate, with binding to the seven nitrogen and oxygen donors of the heptadentate ligand. For [Eu·**L⁴,⁵**] the *q* value is one, indicating just a single bound water molecule. Accordingly, the excited state lifetime for this complex is longer than for [Eu·**L¹**], as there is less quenching from the energy matched OH oscillators with just a single bound water. This reduced hydration number presumably results from an increase in the steric demand at the metal centre, by virtue of the presence of the more bulky glutamic acid based pendant arms.

2.3.3 HPLC analysis of lanthanide complexes

All complexes were examined by reverse phase HPLC analysis to establish homogeneity. This analysis was also used to ensure that complexation of the ligand by the metal was complete. It also offers a useful check that hydrolysis has gone to completion, particularly when it is necessary to hydrolyse 3 or 5 esters per ligand. The retention times are slightly different for each potential semi-hydrolysed product and GC-MS was used to assign peaks when required. The hydrophobic side chains on the column aid separation of relatively hydrophobic complex species. Hence, the hydrolysed complexes, which are more hydrophilic eluted at shorter retention times (eg. compare [Eu·**L²**]³⁺ at 9.4 minutes and [Eu·**L³**] at 8.8 min. (Table 5)

Table 5: HPLC retention times of Ln(III) complexes (295 K, see experimental section for details). The terbium analogues gave very similar retention times.

Complex	retention time (min)
[Eu·L^1]$^{3+}$	10.0
[Eu·L^2]$^{3+}$	9.4
[Eu·L^3]	8.8
[Eu·L^4]$^{3+}$	10.3
[Eu·L^5]$^{2-}$	8.6

2.3.4 Mass spectrometry analysis of the lanthanide complexes

Mass spectrometry data was used to characterise each lanthanide complex and confirm that complexation has taken place. In contrast to terbium which exists only as ^{159}Tb, europium has a characteristic isotope profile. A comparison of the observed profile to the calculated isotopic distribution of each complex was found to be in good agreement, indicating complexation had occurred. A representative example is shown in Fig. 20. This data is for [Eu·L^6]$^{3+}$, the pH responsive methyl sulfonamide complex. The sulfonamide is deprotonated and bound to the metal, so a doubly charged complex at half mass is observed.
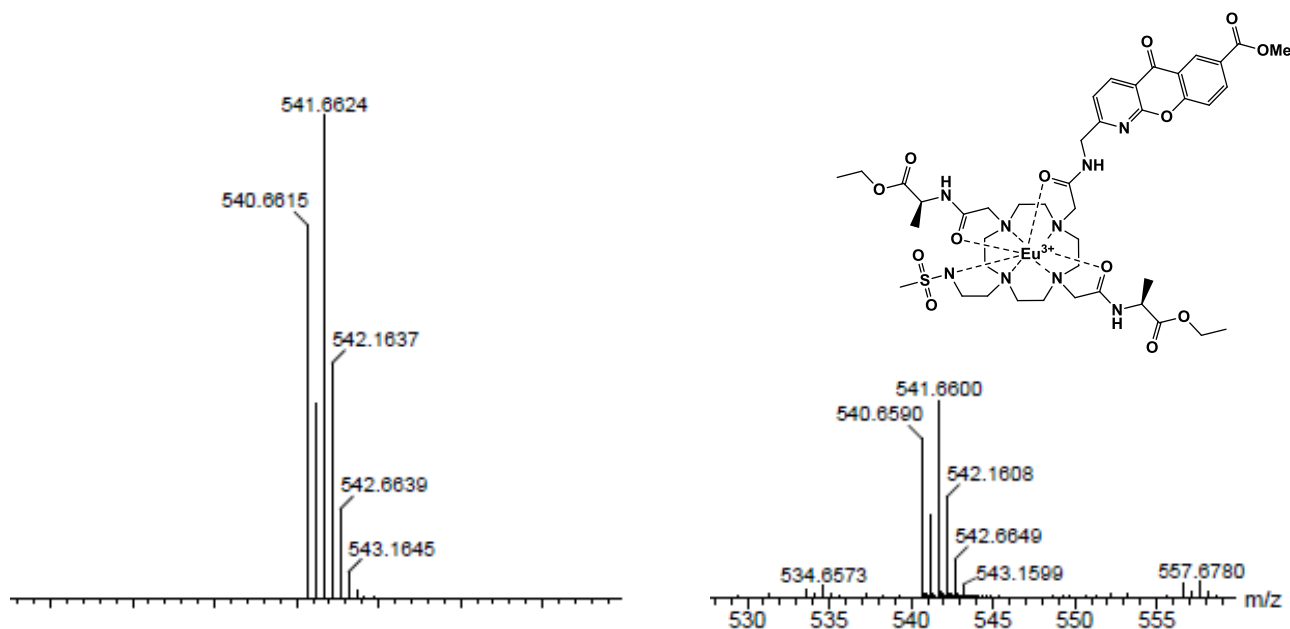
Fig. 20: Calculated (left) and observed (right), accurate mass spectral data for [Eu·L^6]$^{3+}$.

2.4 Photophysical characterisation of the pH-responsive probes

2.4.1 Emission spectral characteristics

Emission spectra for all the pH-responsive complexes are shown below, recording at limiting low and high pH values, for the europium and terbium analogues. For the *para*-trifluoromethyl complexes, the europium and terbium complexes were examined in solution together, and so the spectra here shows a mix of the two ([Eu·**L⁸**]³⁺ and [Tb·**L⁸**]³⁺).

The europium spectra of the methyl-sulfonamide *para*-methoxy-phenylsulfonamide pH responsive complexes are similar in spectral form. The most obvious difference is the drastic reduction in emission intensity for [Eu·**L⁷**]³⁺, by a factor of around 10 at high pH. There is a small change in emission form, most noticeably with a small peak appearing within the $\Delta J = 2$ manifold at 625 nm at higher pH. With the *para*-trifluoromethyl- derivative, [Eu·**L⁸**]³⁺, this $\Delta J = 2$ band is fully resolved into two peaks of roughly equal intensity, but again with an overall decrease in emission intensity. The terbium complexes of the same ligands show contrasting behaviour however. For the methyl-sulfonamide complex, [Tb·**L⁶**]³⁺, there is approximately a doubling in increase in emission intensity at higher pH, and the two main bands around 545 nm ($\Delta J = -1$) are also clearly resolved into two main components at this pH. The *para*-methoxy- and *para*-trifluoromethyl-sulfonamide complexes, [Tb·**L⁷**]³⁺ and [Tb·**L⁸**]³⁺, exhibit an identical form to the methyl- complex, but intriguingly the overall emission intensity decreases, by a factor of around 4.
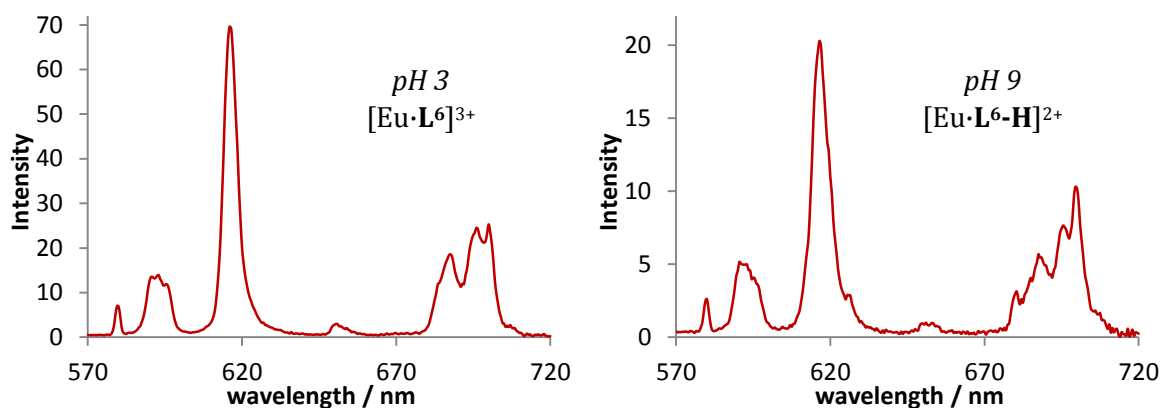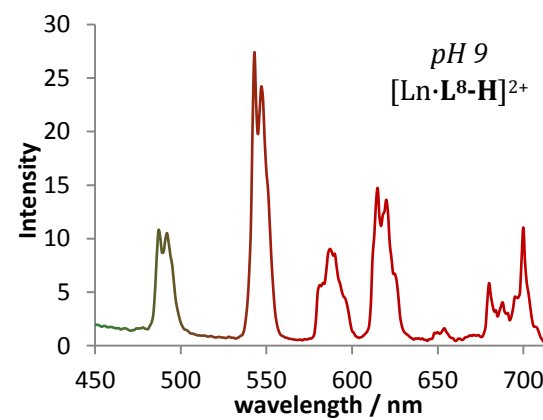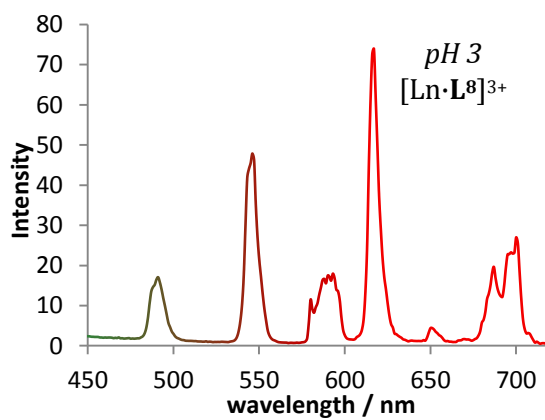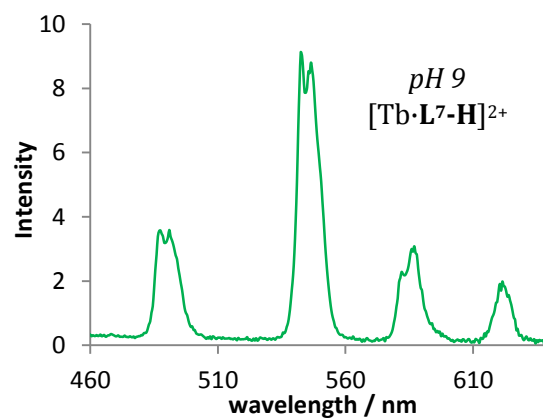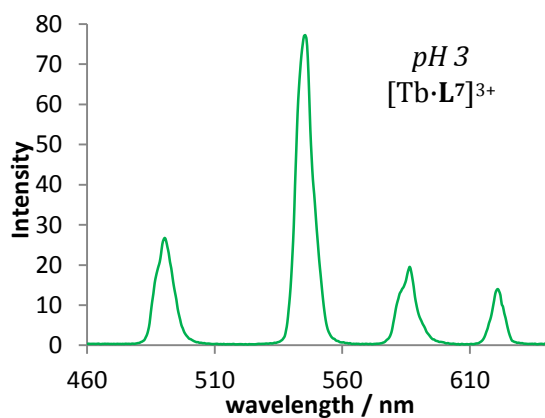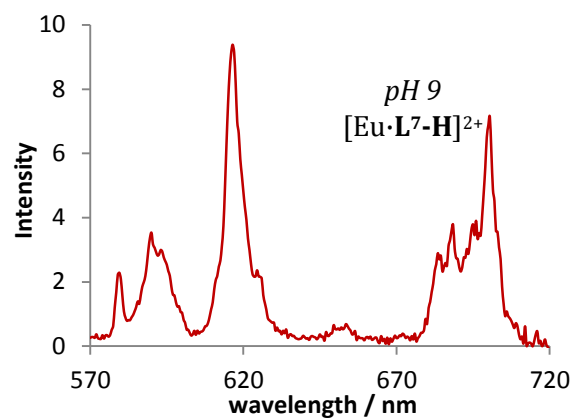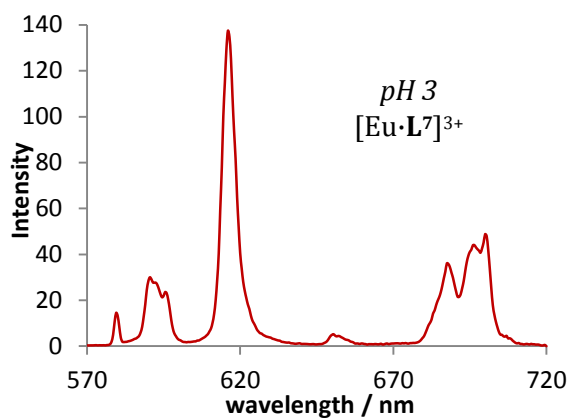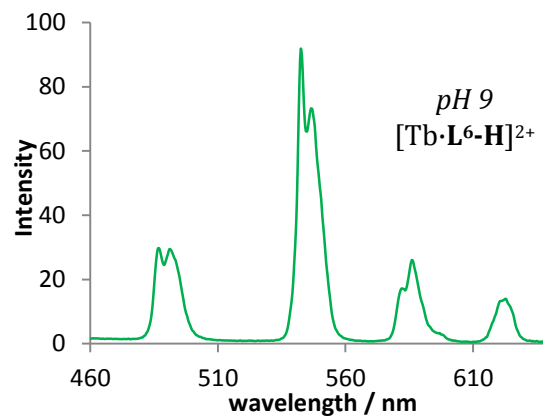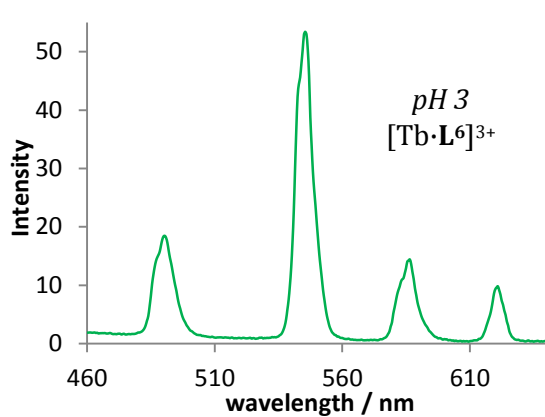
The dpqC sulfonamide $[Eu \cdot \mathbf{L^9}]^{3+}$ exhibits relatively little change in the form of its spectra and the pH extremes. The $\Delta J = 1$ and $\Delta J = 4$ bands were identical in form, with just a small change in the relative intensities of the splitting observed within the $\Delta J = 2$ manifold. It was therefore not examined any further as a pH probe as the pH-dependent emission spectral changes were too small to be of use.
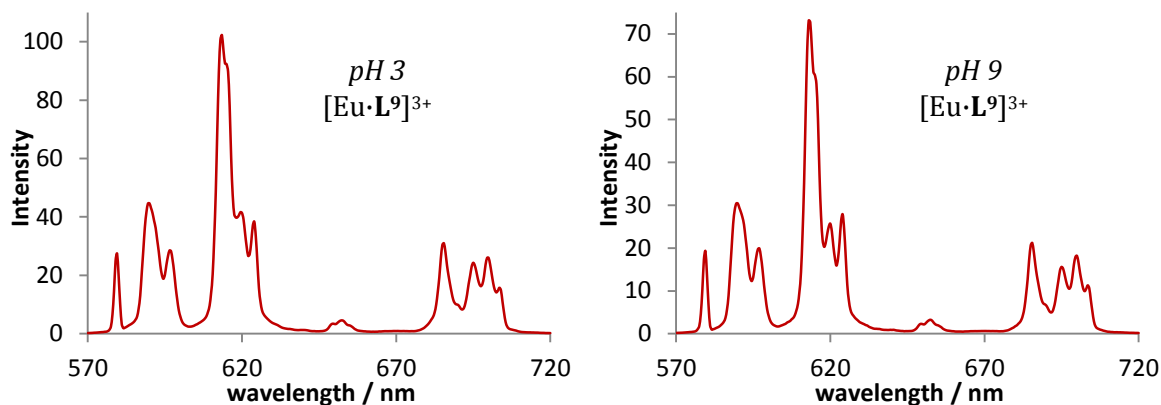
The azaxanthone-methylsulfonamide complex, $[Eu \cdot \mathbf{L^{10}}]^+$ is slightly unusual in that the emission intensity increased and then subsequently decreased upon varying the pH from 3 to 9. The form of the spectra at the two pH limits is markedly different. There is less splitting at high pH, suggesting a higher degree of symmetry in the sulfonamide bound species.
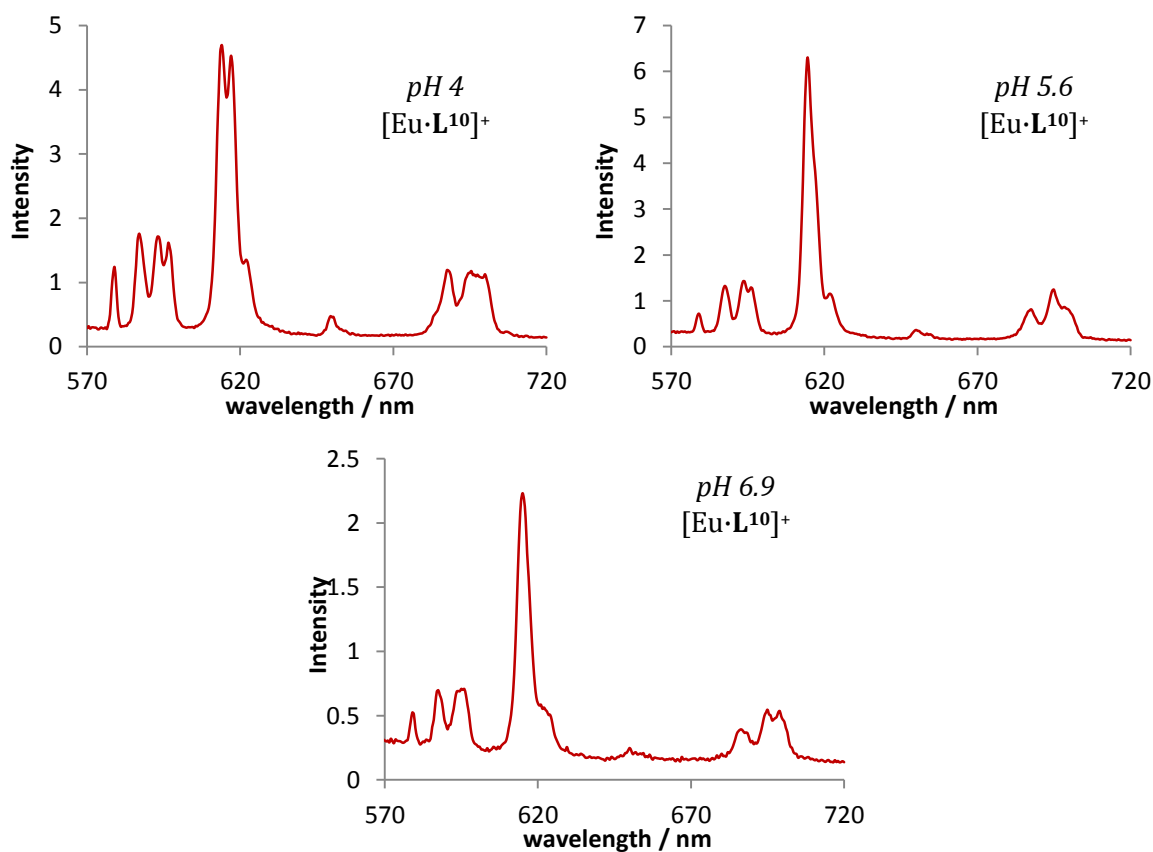
The total emission spectrum of [Eu·L^{11}]$^{3+}$ is dominated by ligand fluorescence at 450 nm. Lanthanide emission was still observed but there appeared to be very little change in the form of emission over the entire pH range. Again, this spectral invariance led to this system not being examined in greater detail.
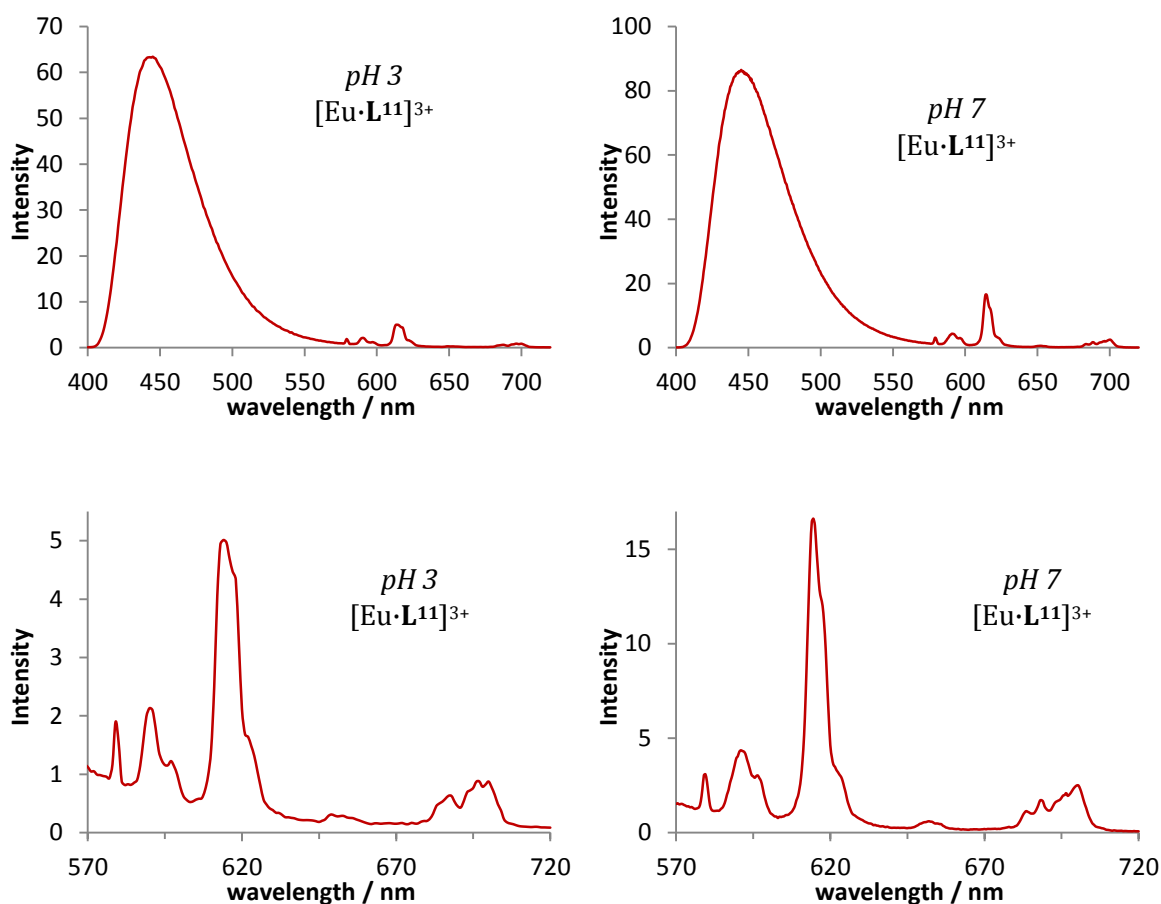
2.4.2 Estimation of complex hydration states, q

Inner sphere hydration numbers for the pH-responsive complexes were calculated by measuring the relevant excited state lifetimes in H_2O and D_2O, at the limiting pH values. The rates of decay, both at low and high pH (Table 6) suggest that within the series [Ln·L^{6-8}]$^{3+}$, the complexes were behaving quite differently from one another. The behaviour of [Ln·L^7]$^{3+}$ is most clear, and shows a switching from one bound water molecule to none upon sulfonamide ligation at higher pH. This correlates with the observations made with the bicarbonate series which had two bound water molecules. Presumably, the steric hindrance associated with the sulfonamide moiety means only a single bound water molecule can be accommodated, rather than two in the unbound form.

Table 6: Radiative decay constants, luminescence lifetimes and calculated q values for the complexes $[\text{Ln}\cdot\textbf{L}^6]^{3+}$ to $[\text{Ln}\cdot\textbf{L}^{11}]^{3+}$.

Complex	pH 3					pH 9				
	k_{H2O} / ms^{-1}	τ / ms	k_{D2O} / ms^{-1}	τ / ms	q	k_{H2O} / ms^{-1}	τ / ms	k_{D2O} / ms^{-1}	τ / ms	q
$[\text{Eu}\cdot\textbf{L}^6]^{3+}$	1.64	0.61	1.03	0.98	0.2	2.15	0.46	1.03	0.96	0.8
$[\text{Tb}\cdot\textbf{L}^6]^{3+}$	0.81	1.24	0.64	1.56	0.5	0.76	1.58	0.63	1.32	0.3
$[\text{Eu}\cdot\textbf{L}^7]^{3+}$	2.09	0.48	0.78	1.28	1.0	1.41	0.71	0.99	1.01	-0.1
$[\text{Tb}\cdot\textbf{L}^7]^{3+}$	0.73	1.37	0.51	1.96	0.8	0.58	1.72	0.53	1.89	-0.1
$[\text{Eu}\cdot\textbf{L}^8]^{3+}$	1.67	0.60	0.72	1.39	0.6	2.06	0.49	1.02	0.98	0.7
$[\text{Tb}\cdot\textbf{L}^8]^{3+}$	0.75	1.34	0.49	2.06	0.9	0.75	1.34	0.55	1.81	0.6
$[\text{Eu}\cdot\textbf{L}^9]^{3+}$	2.96	0.34	1.02	0.98	1.9	1.83	0.55	0.86	1.16	0.7
$[\text{Eu}\cdot\textbf{L}^{10}]^{+}$	2.37	0.42	0.92	1.08	1.4	1.90	0.52	0.75	1.34	0.5
$[\text{Eu}\cdot\textbf{L}^{11}]^{3-}$	1.91	0.52	0.97	1.03	0.8	1.57	0.64	0.92	1.08	0.5

The dpqC *para*-methoxyphenyl sulfonamide complex, $[\text{Eu}\cdot\textbf{L}^9]^{3+}$ showed a clear switching from two bound water molecules at low pH, to one at higher pH. Again this behaviour correlates with a single water molecule being displaced upon sulfonamide ligation at higher pH values.

The other complexes exhibit non-integral q values. This could mean that at a given pH, there exists a mixture of species of differing q value, and so an average value is observed.

3 Bicarbonate Probes for the Mitochondria

3.1   Introduction

Monitoring real-time changes of bicarbonate concentrations within the mitochondrial region of cells is important to gaining an understanding of signalling mechanisms involved in the Krebs cycle and glycolysis.[121]   Syntheses of a range of lanthanide based optical probes, possessing varying steric demand and charge were described in chapter two.

$[Ln \cdot L^2]^{3+}$ R = CO_2Et, R' = OMe
$[Ln \cdot L^3]$ R = CO_2^-, R' = O^-

$[Ln \cdot L^4]^{3+}$ R = CO_2Et, R' = OMe
$[Ln \cdot L^5]$ R = CO_2^-, R' = O^-
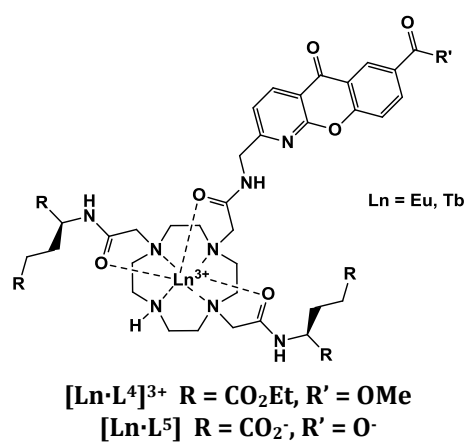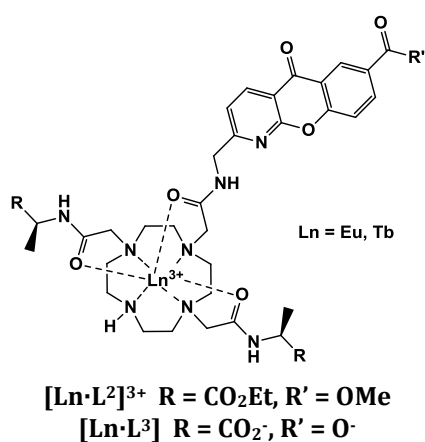
This chapter details work aiming to probe the concentration of bicarbonate by use of either a ratiometric analysis of a pair of emission bands within each spectrum, or use the relative emission intensity between europium and terbium analogues of a common ligand.   The series of probes were evaluated towards relevant bioactive oxy-anions and protein, through a series of spectral titrations, allowing estimates of their binding constants.   Subsequent competition experiments were undertaken to investigate selectivity of the response to bicarbonate in the presence of biologically relevant molecules.   Finally, microscopy experiments examined the localisation of the complexes in the mitochondria and how changes in the emitted light by the probes varied as a function of pCO_2.

3.2   Spectral titrations and calculation of apparent affinity constants

To assess the binding of the complexes towards bicarbonate and various other oxy-anions, a series of spectral titrations was performed. Incremental amounts of the anion, as a concentrated stock solution, were added to a solution of the complex so that the total volume change did not

exceed 5%. A 0.1 M NaCl background was used in order to maintain a constant ionic strength when adding the anions as their sodium salts. This sodium chloride concentration was chosen to mimic that found at a typical extracellular value. The number of data points taken was typically around 15, ensuring that the curved part of the binding plot was well represented. The concentration range spanned from zero, up to the limiting value, where no change appeared to occur either in the emission spectral form or intensity.

The pH of the solution was carefully controlled by adjusting the anion stock solutions to the designated pH, as well as that of the initial complex solution. It was then assumed that small additions of the stock solution at the same pH to the complex solution caused no significant change. Measurements of pH taken at the start and end of the titration indicated this was true, and the pH fluctuated by no more than ± 0.05 units.

A further consideration took account of dissolved bicarbonate that is naturally present through the equilibrium with atmospheric CO_2.[122] To minimise this uncertainty as far as possible, all solutions, with the obvious exception of the bicarbonate stock, were lowered in pH to around 5, bubbled under gentle agitation with argon for ten minutes and then increased back to the desired pH with freshly made concentrated potassium hydroxide solution. Bicarbonate stock solutions were freshly made with distilled, degassed water.

The data obtained was plotted, overlaying each spectrum obtained, so that changes to the form and intensity were easily observed. Ratiometric analysis was performed to allow binding affinities to be calculated. It is possible to take the ratio in a number of ways; by using a pair of individual emission wavelengths (such as 616 nm / 594 nm), by using a pair of emission bands (most commonly the $\Delta J = 2/\Delta J = 1$ ratio comparing the hypersensitive $\Delta J = 2$ band to the relatively insensitive $\Delta J = 1$ band), or alternatively, indicated at the end of the chapter, by using a red/green (or europium/terbium) emission intensity ratio.

The emission spectra for the titration of $[Eu \cdot \mathbf{L^2}]^{3+}$ with sodium bicarbonate (Fig. 21) is representative, adding a bicarbonate concentration up to 30 mM. Note, that at this final bicarbonate concentration, the limiting spectral form has been reached, and the bicarbonate concentration is at or above the level found at typical extracellular levels. In general, every titration was continued until these criteria were met.

A large significant increase in emission intensity was observed across the emission spectrum, particularly within the $\Delta J = 2$ manifold. The maxima of the $\Delta J = 2$ transition shifts very slightly

upon bicarbonate binding from 614 nm to 616 nm. Small changes to the spectral form are evident, most notable within the $\Delta J = 1$ band.
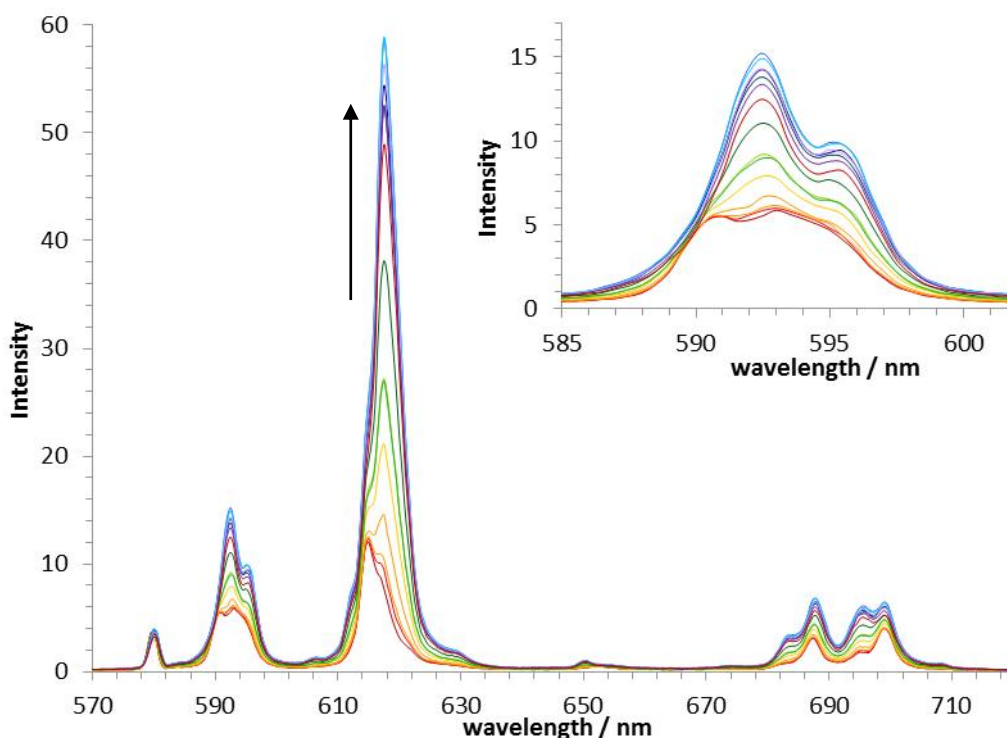
Fig. 21: Variation of the Eu(III) emission spectrum for $[Eu \cdot L^2]^{3+}$, following addition of sodium bicarbonate (H$_2$O, pH = 7.40 ± 0.05, 0 – 30 mM sodium bicarbonate, 40 μM complex, 298 K, I = 0.1 M NaCl, λ_{ex} = 332 nm). Inset shows the magnified $\Delta J = 1$ region, highlighting the change in spectral form and intensity, and the appearance of an apparent isoemissive point at 590 nm.

There are hundreds of possibilities for performing ratiometric analysis on pairs of individual wavelengths. Previous reports have sometimes utilised pairs of wavelengths which are very close to one another (eg 615 nm / 617),[66] but there are potential issues here such as that the emission slits typically being used are 1.5 nm, so there is some overlap if the two wavelengths are only 2 nm apart. Preferentially therefore, wavelengths were selected in different manifolds, and a plot of 617.5 nm / 590 nm is shown in Fig. 18. Fitting this data to a 1:1 binding model, allows an estimation of the apparent binding constant, log K. This was calculated to be 3.80 ± 0.05, using a linear least-squares fitting algorithm, developed in Microsoft Excel. The quoted error is the standard error to the observed data, using the jack-knife procedure.
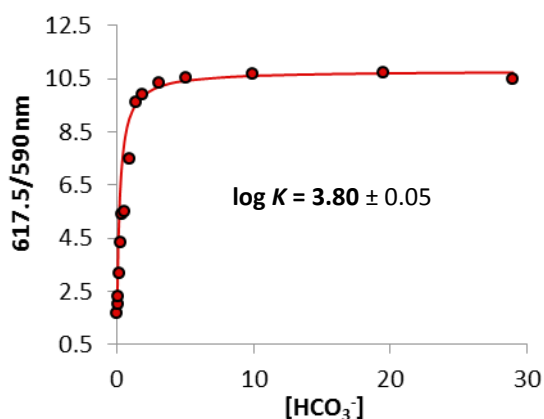
Fig. 22a: Plot of intensity ratio (617.5 nm/590 nm) with [HCO$_3^-$], allowing calculation of the apparent binding constant.
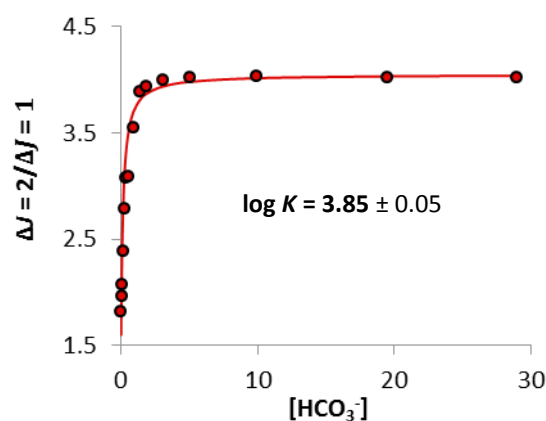
Fig. 22b: Plot of intensity ratio ($\Delta J = 2/\Delta J = 1$) with [HCO$_3^-$], allowing calculation of the apparent binding constant.

Any pair of wavelengths that yield a reasonable binding curve should result in the same value for the binding constant and this is the case here comparing Fig. 22a and Fig. 22b, within the experimental error. When deciding on the ratio to use, a wavelength was often selected that showed the greatest change against another wavelength which remains constant or nearly constant, a so-called isoemissive point. In the example shown above, 617.5 nm is the maxima of the hypersensitive $\Delta J = 2$ band, whilst 590 nm is an isoemissve point within the $\Delta J = 1$ band. The main advantage of calculating affinities using individual wavelengths is that it is possible to take advantage of the very fine structural changes often observed upon anion binding or as a result of a change in the coordination sphere. The overriding disadvantage is that in less emissive samples, the signal-to-noise ratio will be greatly reduced and may lead to larger errors. This will also be the case in microscopy experiments, where using individual wavelengths will simply not be possible. The signal from a 50 μM sample in a 1 ml cuvette will be much stronger then that observable in a cell on a confocal microscope. Furthermore, the resolution of a lambda scan on such equipment is limited to 3 nm and so such high resolution spectra are not possible to obtain.

Calculating integrated area ratios offer a solution. Integrating, and taking a ratio of a pair of whole bands takes account of the decreased intensity in microscopy and allows less emissive or quenched samples to give a more reliable result. In microscopy, it also allows two wider channels to be set up, maximising the signal observed and simplifying the acquisition time and experimental procedure. More details regarding this will follow at the end of the chapter. For europium spectra, it is often best to take a ratio of the $\Delta J = 2/\Delta J = 1$ bands, as the $\Delta J = 2$ band is hypersensitive and should show a large change compared to the magnetic dipole allowed $\Delta J = 1$ band, which shows far less change. Plotting this ratio as a function of bicarbonate concentration

again allows an affinity constant to be estimated. Within the error, this was found to be the same as for that obtained using individual wavelengths.

The change in the observed ratio is another important factor which should be considered. In the integrated area analysis above, the change in intenisty ratio is from approximately 1.75 to 3.75, which is sufficiently large to allows accurate measurements to be made.

3.3   Binding of bicarbonate to the complexes

### 3.3.1   Binding of bicarbonate to the europium complexes

Each of the complexes [Eu·$\mathbf{L}^{1-4}$] was assessed with respect to bicarbonate binding. The form of the limiting emission spectra of the bicarbonate bound adduct in each case was very similar to that for [Eu·$\mathbf{L}^2$]$^{3+}$ in Fig. 16 . The same analysis of the data was performed each time for consistency, i.e. taking the $\Delta J = 2 / \Delta J = 1$ intenisty ratio. The apparent binding constant was calculated, along with the corresponding increase this ratio generated, the intensity increase within the hypersensitive $\Delta J = 2$ band, and the overall increase in europium luminescence are provided in Table 7.

Table 7: Affinity constants of the europium(III) complexes for bicarbonate with the corresponding increase in the $\Delta J = 2/\Delta J = 1$ ratio, increase in $\Delta J = 2$ luminescence and increase in overall europium (III) luminescence (298 K, I = 0.1 M NaCl, pH = 7.40 ± 0.05).

complex	log K	Ratio increase %	$\Delta J = 2$ increase %	Overall intensity increase %
[Eu·$\mathbf{L}^1$]$^{3+}$	3.50 ± 0.05	95	410	265
[Eu·$\mathbf{L}^2$]$^{3+}$	3.85 ± 0.05	120	365	52
[Eu·$\mathbf{L}^3$]	2.75 ± 0.05	120	265	140
[Eu·$\mathbf{L}^4$]$^{3+}$	3.60 ± 0.05	85	255	160

The three triply positively charged complexes all yielded broadly similar binding constants, while the log K value for the zwitterionic complex was approximately one unit lower. This accords with the electrostatic nature of binding. The bicarbonate anion is less inclined to bind to [Eu·$\mathbf{L}^3$], due to the anionic charges on the peripheral arms shielding the lanthanide centre to some extent. The increase in the $\Delta J = 2 / \Delta J = 1$ ratio is approximately the same across the range of complexes. Complex charge appears to have little effect on this, for example, the related [Eu·$\mathbf{L}^2$]$^{3+}$ and [Eu·$\mathbf{L}^3$] having identical increases. It is possible that the size of the pendant arms exerts a limited influence, as the complexes with the sterically more bulky glutamate and

methylphenylalanine arms are those with slightly lower percentage increase. The increase in the $\Delta J = 2$ emission intensity was very high in each case.
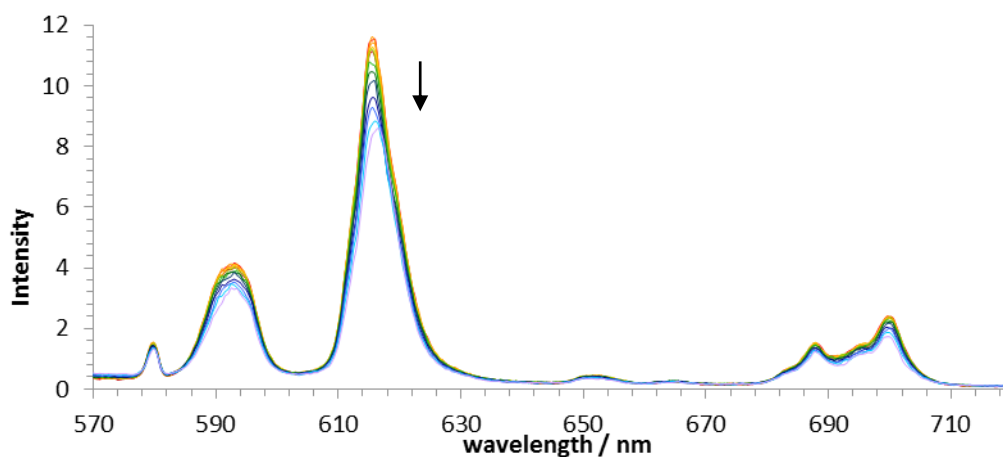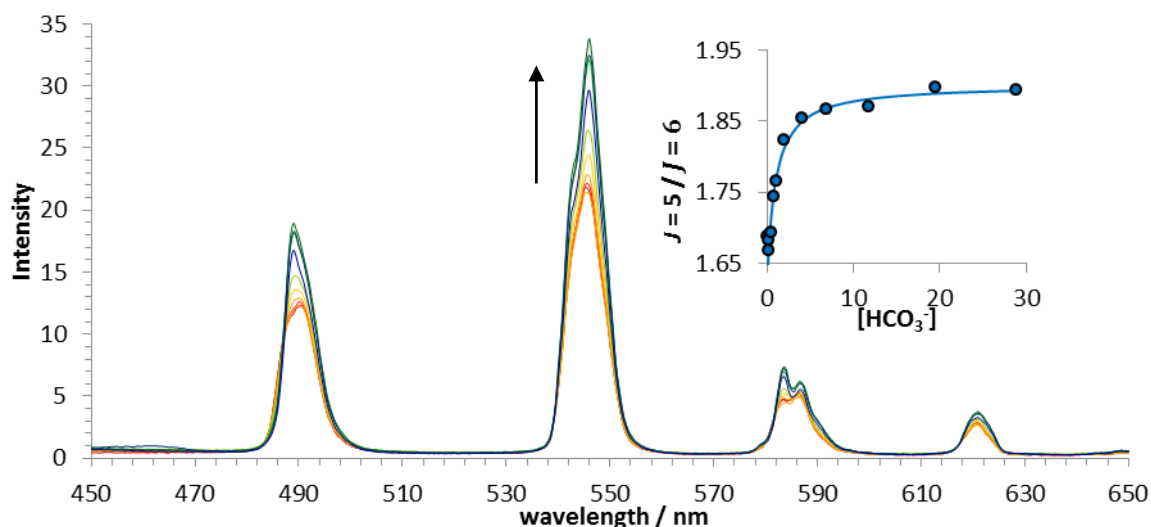

Fig. 23: Variation of the Eu(III) emission spectrum for [Eu·**L⁵**]²⁻, following addition of sodium bicarbonate (H$_2$O, pH = 7.40 ± 0.05, 40 µM complex, 0 – 30 mM sodium bicarbonate, 298 K, I = 0.1 M NaCl, λ_{ex} =332 nm).

For the only overall negatively charged complex, [Eu·**L⁵**]²⁻, a binding constant could not be obtained. Addition of bicarbonate did not lead to the characteristic change in spectral form and intensity observed with the other europium complexes. Conversely, a small decrease or quenching of emission intensity was observed and there was no shift in the $\Delta J = 2$ maxima to 616 nm (Fig. 23). This behaviour suggests that bicarbonate is binding only very weakly to this complex. Presumably, this is due to the complexes negative charge arising from the four bulky carboxylate functionalities that surround the europium centre, protecting it from binding with the anion. It had originally been hoped that by using this dianionic complex, it would be a convenient way to increase the selectivity for monoanionic bicarbonate over trianionic citrate, as the latter which itself has a multiple negative charge at ambient pH. However, it appears that the negative charge is too big, and therefore bicarbonate binding is inhibited as well. This prevented further studies from being undertaken with this complex.

3.3.2   Binding of bicarbonate to the terbium complexes

The bicarbonate titrations were also performed with the terbium analogues, the equivalent data are shown in Fig. 24. The apparent binding affinities follow the same trend as for the europium analogues (Table 8). The most striking feature is that the increases in emission intensities are greatly reduced. Both the increase in the main $\Delta J = -1$ band, and the overall increase are a fraction of what they were for the europium complexes. The general insensitivity of the terbium (III) emission bands to changes in coordination is highlighted here. Whereas for

Fig. 24: Variation of the Tb(III) emission spectrum for [Tb·**L²**]³⁺, following addition of 0 – 30 mM sodium bicarbonate (H₂O, pH = 7.40 ± 0.05, 40 μM complex, 298 K, I = 0.1 M NaCl, λ_{ex} =332 nm).

europium, the hypersensitive ΔJ = 2 band intensity increased much more than the overall luminescence increase (and hence is responsible the large change in the calculated ratio) for terbium there is much less difference between the bands, and consequently a smaller difference in the intensity ratio change. The change in spectral form was similar for each complex examined upon addition of sodium bicarbonate. The ΔJ = -2 and ΔJ = -1 bands showed a modest increase in emission intensity. In each case, the ΔJ = 0 manifold at 680 nm was the only one to show a significant change in form. The relative intensity of the splitting of the two bands within this manifold switched upon the addition of bicarbonate. The ΔJ = +1 manifold at 620 nm was quite weak, and showed relatively little change.

Table 8: Affinity constants of terbium (III) complexes for bicarbonate with the corresponding increase in the ΔJ = -2/ΔJ = -1 ratio, increase in ΔJ = -1 luminescence and increase in overall terbium (III) luminescence (298 K, I = 0.1 M NaCl, pH = 7.40 ± 0.05).

| complex	log K	Ratio increase %	ΔJ = -1 increase %	Overall increase %
[Tb·**L¹**]³⁺	3.75 ± 0.10	18	14	6
[Tb·**L²**]³⁺	3.00 ± 0.05	12	42	34
[Tb·**L³**]	2.52 ± 0.05	17	18	11
[Tb·**L⁴**]³⁺	3.15 ± 0.10	42	27	27

3.3.3 Circularly polarised luminescence of [Ln·L²]³⁺ in response to the addition of sodium bicarbonate

Circularly polarised luminescence spectroscopy can be used to probe the degree of chirality sensed by an electronic transition. Emission dissymmetry factors (g_{em}) can be used to represent this. Conformationally rigid chiral complexes, such as those examined in this series, will therefore exhibit circularly polarised luminescence and can be probed by this technique.
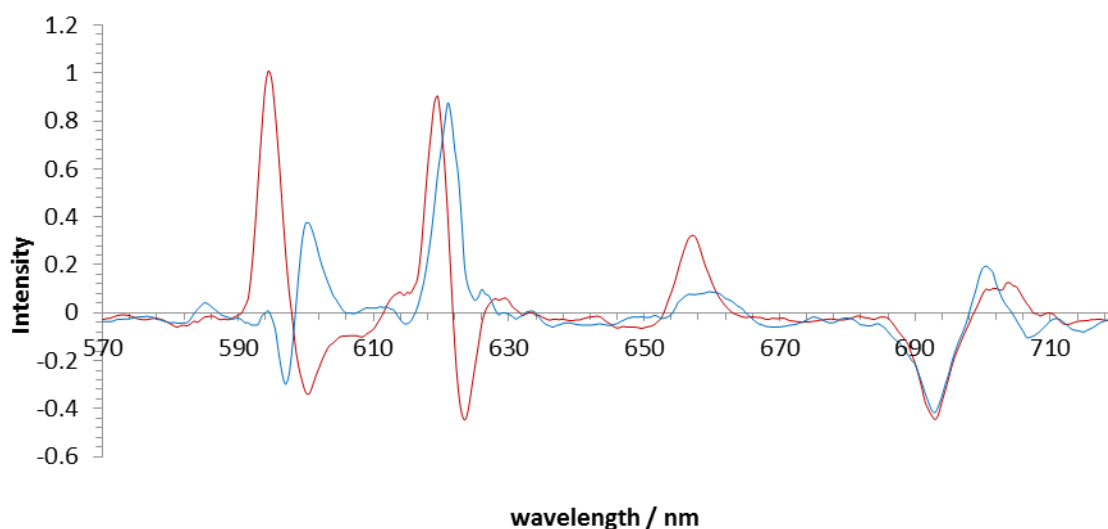
Fig. 25: Circularly polarised luminescence spectra of [Eu·L²]³⁺ (*red*) and of [Eu·L²]³⁺ in the presence of 30 mM sodium bicarbonate (*blue*) (295 K, I = 0.1 M NaCl, pH = 7.40 ± 0.05), showing the large differences in CPL between the aqua and the bicarbonate adduct.

As a representative example from the series, [Eu·L²]³⁺ was chosen for study. Its CPL spectra, shown in red in Fig. 25 reveals a strong CPL signal, as for other complexes of this type. The CPL spectra shows a high degree of similarity in form to that for [Eu·L¹³]³⁺ and [Eu·L⁷⁵]³⁺ (Fig. 26)[19] with a (+-) signal sequence within the ΔJ = 1 band at 590 nm and a (+-) signal sequence also in the ΔJ = 2 band around 616 nm. It is reasonable to suggest then, that this complex adopts the same configuration, namely Δ-($\lambda\lambda\lambda\lambda$). Calculated g_{em} values for [Eu·L²]³⁺ are roughly the same as for [Eu·L¹³]³⁺ (Table 9). This is unsurprising as they are structurally very similar, with an amide linked chromophore and two coordinated amide pendant arms. Values for [Eu·L²]³⁺ were significantly smaller than those observed for [Eu·L⁷⁵]³⁺. This would suggest an increased conformational flexibility on the experimental timescale.
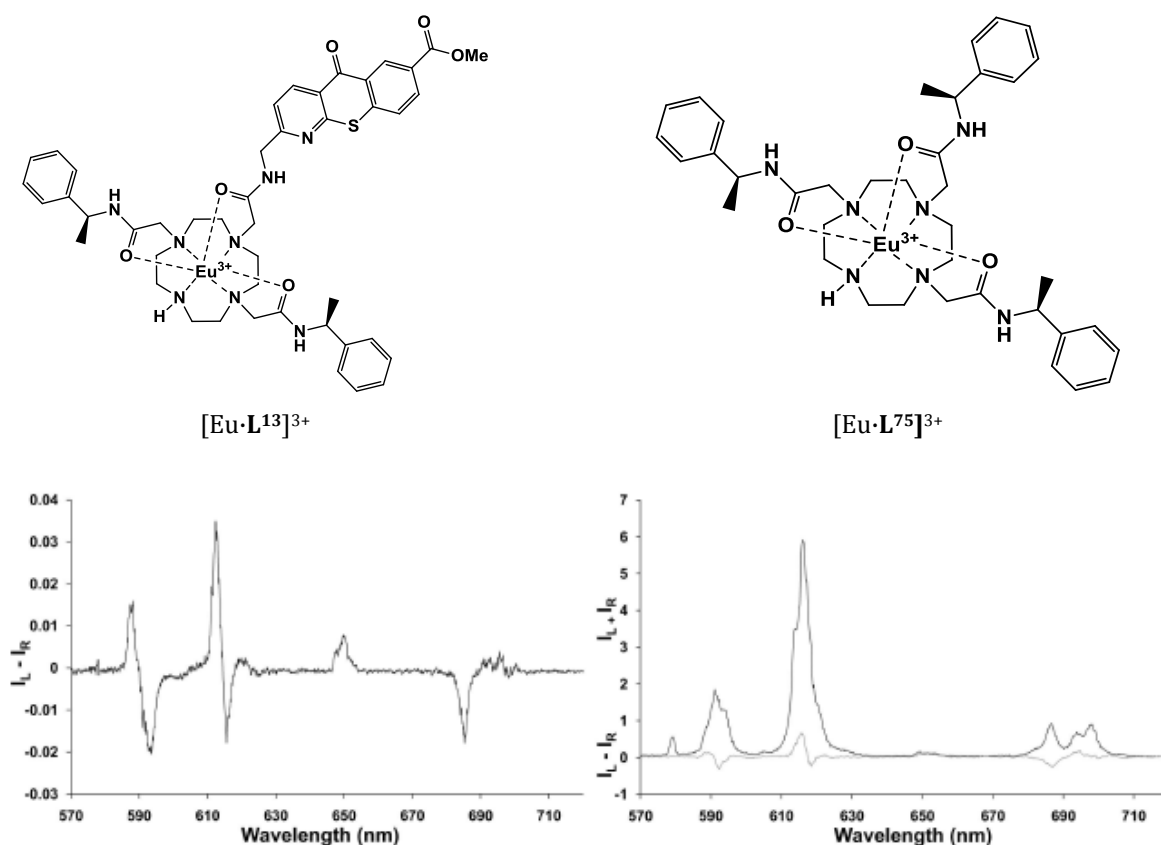
$[Eu \cdot L^{13}]^{3+}$ $[Eu \cdot L^{75}]^{3+}$

Fig. 26: CPL spectra of $[Eu \cdot L^{75}]^{3+}$ (H_2O, 1 mM, 295 K, λ_{ex} = 255 nm) (*left*); total luminescence and CPL spectra (x18) of $[Eu \cdot L^{13}]^{3+}$ (D_2O, 0.05 mM, 295 K, λ_{ex} = 275 nm) (*right*).

Table 9: Emission dissymmetry factors (g_{em}) at specified wavelengths (D_2O, 295 K)

	$\Delta J = 1$	$\Delta J = 2$
$[Eu \cdot L^2]^{3+}$	-0.020 (600 nm)	0.008 (613 nm)
$[Eu \cdot L^{75}]^{3+}$	-0.05 (593 nm)	0.03 (612 nm)
$[Eu \cdot L^{13}]^{3+}$	-0.022 (593 nm)	0.012 (616 nm)

Upon addition of a limiting concentration of sodium bicarbonate (30 mM), the CPL spectra revealed a dramatic and significant change, particularly within the $\Delta J = 1$ manifold (Fig. 25). There is a reversal of sign sequence from (+-) to (-+) and the CPL emission intensity decreases. The $\Delta J = 2$ emission band shifts to 616 nm and accords with the change in the total luminescence. The negative transition at 624 nm disappears. The $\Delta J = 4$ band appears unchanged. Due to the predominantly electronic dipole nature of this transition this is to be expected. Emission dissymmetry factors for the bicarbonate bound adduct, and the aqua complex are shown in Table 10.

Table 10: Emission dissymmetry factors at specified wavelengths (D_2O, 295 K)

λ / nm	$[Eu \cdot L^2]^{3+}$	$[Eu \cdot L^2]^{3+}$ + 30 mM bicarbonate	λ / nm
595.5	0.050	-0.023	597
603	-0.087	0.096	602
624	-0.057	0.013	626.5
657	0.271	0.078	657
694	-0.096	-0.038	692.5

The circularly polarised luminescence of the terbium analogue, $[Tb \cdot L^2]^{3+}$, was also examined. The CPL spectrum of the aqua complex was recorded, and separately in the presence of limiting concentrations of bicarbonate (30 mM) and citrate (2 mM) (Fig. 27). CPL emission was observed in the magnetic dipole allowed ΔJ = -1 and ΔJ = +1 bands for the aqua complex. Addition of citrate caused very little change to the form or intensity of the CPL emission in these bands, but did lead to a switching-on of CPL emission intensity within the ΔJ = -2 band.
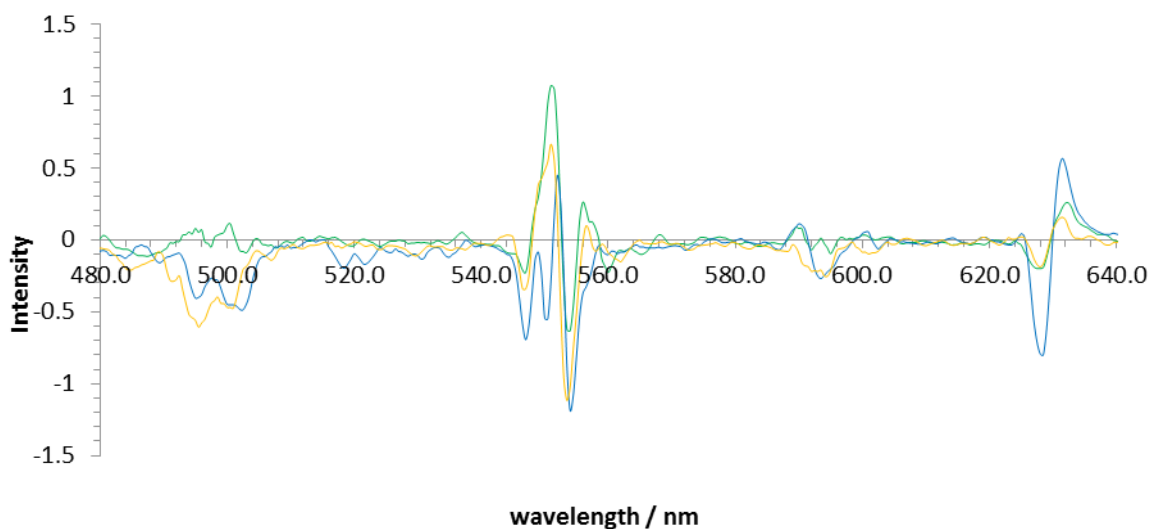
Fig. 27: Circularly polarised luminescence spectra of $[Tb \cdot L^2]^{3+}$ (*green*) and of $[Tb \cdot L^2]^{3+}$ in the presence of 30 mM sodium bicarbonate (*blue*) and of $[Tb \cdot L^2]^{3+}$ in the presence of 2 mM sodium citrate (*orange*) (295 K, I = 0.1 M NaCl, pH = 7.40 ± 0.05).

Addition of bicarbonate to a solution of $[Tb \cdot L^2]^{3+}$ led to a substantial change in the CPL spectrum. The form and intensity of the ΔJ = -1 transitions are particularly different, while the ΔJ = +1 band increased in intensity, but maintained an identical form.

In summary, these experiments show that CPL spectroscopy can be used to signal anion binding, giving profiles that are characteristic of the particular ternary adduct.

3.4 Affinity of the complexes towards other oxy-anions

In any biological medium there exist a number of oxy-anions in addition to bicarbonate which could compete for binding to the lanthanide centre. For example, extracellular fluid composes of approximately 120 mM chloride, 2.3 mM lactate, 0.9 mM phosphate and 0.13 mM citrate. The binding of any of the latter three could potentially cause a change in spectral form or emission intensity competing with that observed for bicarbonate.[2, 123, 124] Within the cellular environment where the probes are to be used, the concentrations of all these anions are constantly changing, and are not accurately known. Therefore, it would be unclear which adducts the emission spectrum actually represents. The probe needs to withstand binding to other oxy-anions as much as possible, and in the context of a competitive background, remain selective for bicarbonate.

The complex, [Eu·**L¹³**]³⁺, which formed the starting point for the novel series discussed in this chapter suffered from this problem of competitive anion binding.[2] The probe exhibited a strong binding to citrate as well as bicarbonate. This meant that, in a biological context, the emission spectrum observed was a mixture of citrate and bicarbonate bound adducts. As such, gaining a meaningful quantification of bicarbonate binding would be difficult, if not impossible. A major aim of this work was to address this issue.

To investigate the aspect of affinity towards other oxy-anions, spectral titrations were performed with individual anions, namely citrate, phosphate and lactate for the range of complexes. Binding constants were calculated in each case, as well as examination of the change of form and intensity of the emission within the spectra.

3.4.1 Binding affinity of the complexes towards citrate

Citrate is perhaps likely to be the species which competes most for coordination to a positively charged metal centre. The three carboxylates have pK_a's of 3.13, 4.76 and 6.40. Thus, at physiological pH, citrate exists as a trianion. This could be expected to have a strong binding affinity for a triply positively charged metal centre, as is found in some of these lanthanide complexes.

Titrations of the europium complexes with citrate, as its trisodium salt, were performed at pH 7.4, as for bicarbonate. The spectral form upon the addition of citrate compared with that

observed for bicarbonate binding is strikingly different. Emission is quenched by citrate, whereas an increase in emission intensity was observed for bicarbonate. For the europium complexes, the change in the $\Delta J = 2 / \Delta J = 1$ ratio was far smaller (20 – 35% change) due to this quenching effect (Table 11). For [Eu·L¹]³⁺ and [Eu·L³], changes in the spectral form were minor. There was only a small change in the form of the $\Delta J = 4$ manifold at 700 nm for the [Eu·L²]³⁺ and [Eu·L⁴]³⁺ pair (Fig. 28).
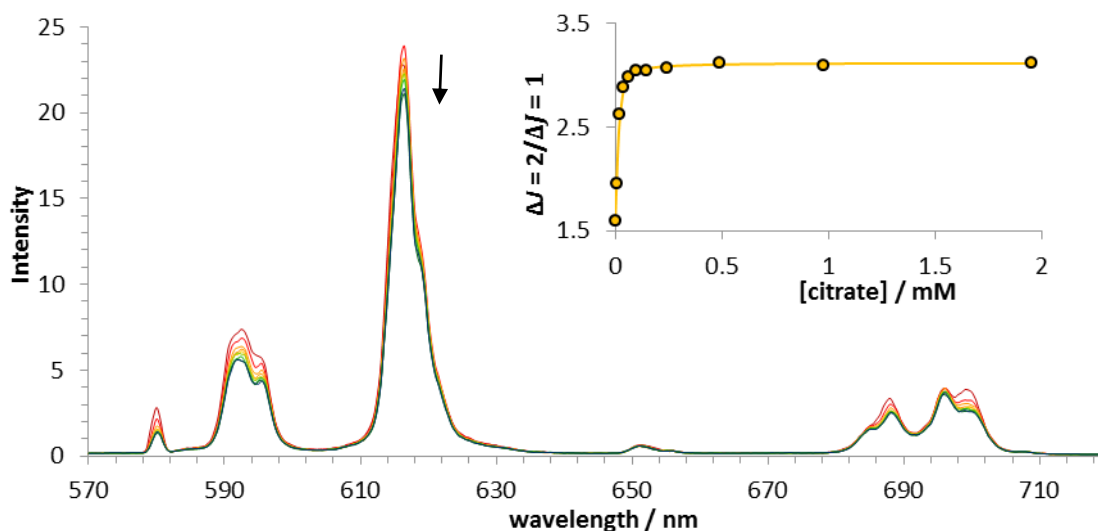
Fig. 28: Variation of the Eu(III) emission spectrum for [Eu·L²]³⁺ following addition of sodium citrate (H_2O, pH = 7.40 ± 0.05, 40 μM complex, 298 K, I = 0.1 M NaCl, λ_{ex} = 332 nm).

The terbium complexes behaved in a very similar way to each other, with considerable quenching observed in all cases (Fig. 29). Spectral modulation was insufficient to allow any
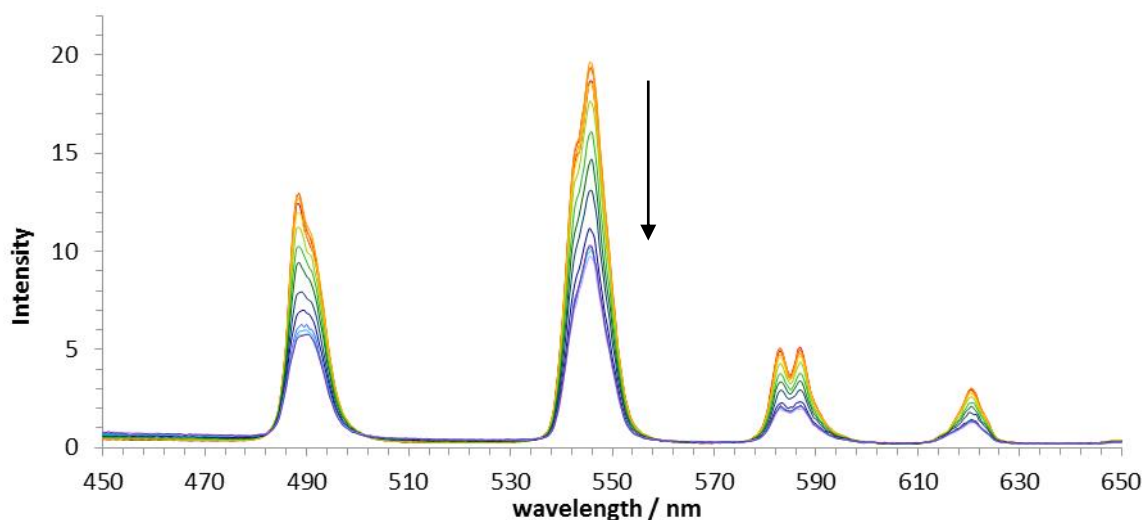
Fig. 29: Variation of the Tb(III) emission spectrum for [Eu·L²]³⁺ following addition of sodium citrate (H_2O, pH = 7.40 ± 0.05, 40 μM complex, 298 K, I = 0.1 M NaCl, λ_{ex} = 332 nm).

ratiometric analysis of the bands. It was observed that the degree of quenching was significantly less for [Tb·L³], the neutral complex, with an overall decrease of just 10%. It appears that the negatively charged pendant arms may inhibit the binding of citrate in accord with the effect of Coulombic repulsion.

Table 11: Affinity constants of europium (III) and terbium (III) complexes for citrate with the corresponding increase in the $J = -1/J = -2$ ratio, increase in $J = -1$ luminescence and increase in overall terbium (III) luminescence (298 K, $I = 0.1$ M NaCl, pH = 7.40 ± 0.05).

complex	log K	Ratio increase %	$\Delta J = 2$ or $\Delta J = -1$ change %	Overall change %
[Eu·L¹]³⁺	4.00 ± 0.05	36	-38	-61
[Eu·L²]³⁺	4.80 ± 0.15	19	-11	-18
[Eu·L³]	3.95 ± 0.05	26	-5	-14
[Eu·L⁴]³⁺	4.40 ± 0.05	19	-	-
[Tb·L¹]³⁺	insufficient spectral		-92	-74
[Tb·L²]³⁺	modulation due to large		-75	-52
[Tb·L³]	degree of quenching		-13	-10

3.4.2 Binding affinity of the complexes towards lactate

Lactate is smaller in size than citrate and possesses just a single negative charge at physiological pH with a pK_a of 3.86. Titrations of sodium lactate with each complex were
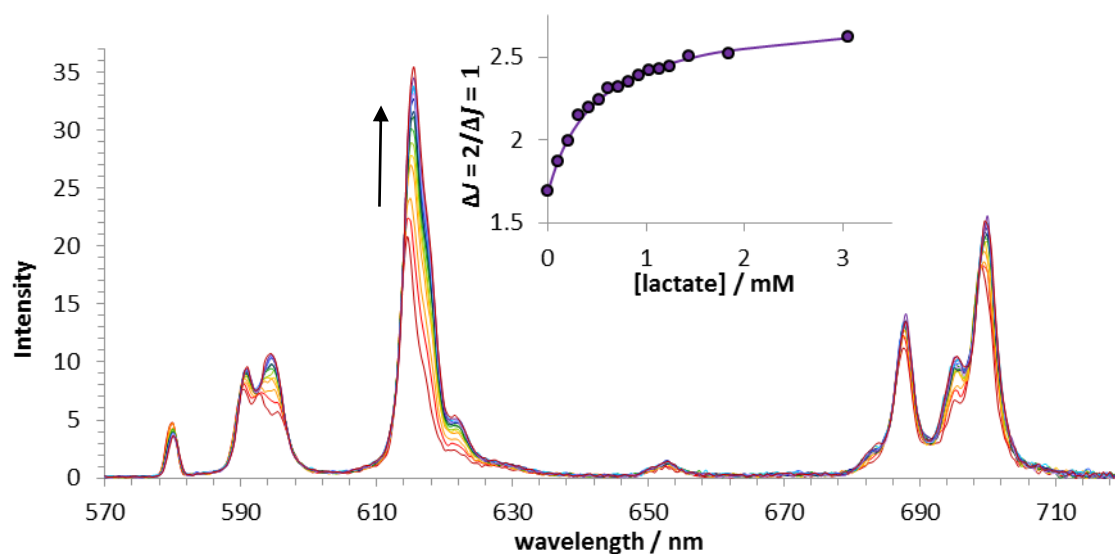
Fig. 30: Variation of the Eu(III) emission spectrum for [Eu·L¹]³⁺, following addition of sodium lactate (H₂O, pH = 7.40 ± 0.05, 40 μM complex, 298 K, $I = 0.1$ M NaCl, λ_{ex} = 332 nm).

performed. The pH for the lactate titrations was at 5.5, as in preliminary work, assessing the pH dependence of the emission in a fixed lactate background, it was shown that this is within a region where pH-modulation of emission was minimal.[123]

Addition of sodium lactate produced a similar response across the series of europium complexes (Fig. 30). There was an overall increase in emission intensity. A characteristic band appears at 594 nm in the ΔJ = 1 manifold, and there is also the appearance of a shoulder in the ΔJ = 2 manifold at 621nm. There was no change in the form of the ΔJ = 4 manifold. The increase in overall emission intensity was again smallest for the neutral complex, indicating that the anionic periphery is inhibiting anion binding (Table 12). Consequently, the binding constant for the neutral complex is once again the lowest.
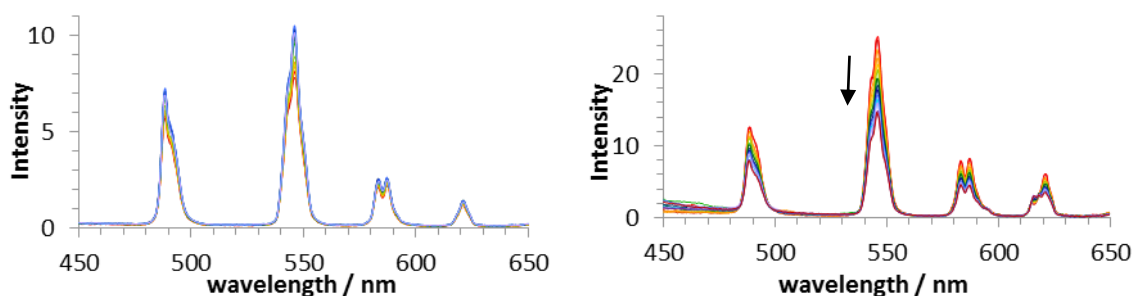
Fig. 31: Variation of the Tb(III) emission spectrum for [Tb·**L¹**]³⁺ (*left*) and [Tb·**L⁴**]³⁺ (*right*) following addition of sodium lactate (H₂O, pH = 5.50 ± 0.05, 40 μM complex, 298 K, *I* = 0.1 M NaCl, λ_ex = 332 nm).

Differing behaviour was observed across the terbium set of complexes, in which [Tb·**L¹**]³⁺ and [Tb·**L²**]³⁺ showed a modest increase in intensity, but with very little change in emission form. In contrast, [Tb·**L³**] and [Tb·**L⁴**]³⁺ exhibited a decrease in emission intensity upon addition of lactate (Fig. 31). For [Tb·**L³**] there was not a sufficient change in form to allow a binding constant to be estimated confidently.

Table 12: Affinity constants of europium (III) and terbium (III) complexes for citrate with the corresponding increase in the calculated ratio, increase in $\Delta J = 2$ or $\Delta J = -1$ luminescence and increase in overall lanthanide (III) luminescence (298 K, $I = 0.1$ M NaCl, pH = 7.40 ± 0.05).

complex	log K	Ratio increase %	$\Delta J = 2$ or $\Delta J = -1$ change %	Overall change %
[Eu·L¹]³⁺	3.30 ± 0.05	55	90	45
[Eu·L²]³⁺	3.05 ± 0.05	25	32	41
[Eu·L³]	2.55 ± 0.05	33	38	18
[Eu·L⁴]³⁺	3.45 ± 0.05	29	52	32
[Tb·L¹]³⁺	3.40 ± 0.05	3	26	23
[Tb·L²]³⁺	3.55 ± 0.05	6	34	32
[Tb·L³]	-	-	-29	-18
[Tb·L⁴]³⁺	2.65 ± 0.10	22	-58	-58

3.4.3 Binding affinity of the complexes towards phosphate

With addition of phosphate, each of the europium complexes behaved slightly differently. The complex [Eu·L¹]³⁺ showed a small decrease in emission intensity with little change to the spectral form. For [Eu·L²]³⁺ there was also little change in the spectral form, but the decrease in intensity was approximately twice as pronounced. The neutral complex, [Eu·L³], was more interesting (Fig. 32). Across the emission spectrum a very small decrease in emission intensity was observed but the distinct appearance of a band at 621 nm was evident, upon the addition of
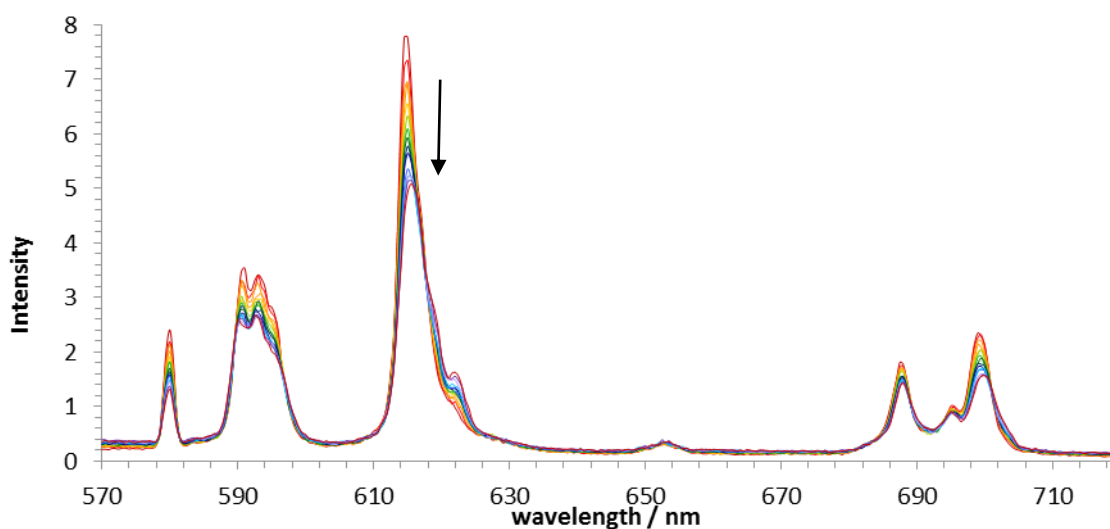
Fig. 32: Variation of the Eu(III) emission spectra for [Eu·L³], following addition of sodium phosphate (H₂O, pH = 5.50 ± 0.05, 40 μM complex, 298 K, $I = 0.1$ M NaCl, λ_{ex} =332 nm).

phosphate. This band appearing as a shoulder, was very similar to that observed with the lactate adducts of the europium complexes. The contrasting behaviour of the emergence of this shoulder, coupled with the overall intensity decrease, meant an estimate of the $\Delta J = 2$ change in intensity became unreliable.

Table 13: Affinity constants for europium (III) and terbium (III) complexes with phosphate defining the corresponding increase in the calculated ratio, increase in $\Delta J = 2$ or $\Delta J = -1$ luminescence and increase in overall lanthanide (III) luminescence (298 K, $I = 0.1$ M NaCl, pH = 7.40 ±0.05).

complex	log K	Ratio increase %	$\Delta J = 2$ or $J = -1$ decrease %	Overall change %
[Eu·**L**^{1}]$^{3+}$	2.90 ± 0.05	19	-29	-25
[Eu·**L**^{2}]$^{3+}$			-62	-52
[Eu·**L**^{3}]	2.00 ± 0.05	8	*	9
[Eu·**L**^{4}]$^{3+}$	3.25 ± 0.05	21	-68	-53
[Tb·**L**^{1}]$^{3+}$	3.05 ± 0.05	11	-132	-105
[Tb·**L**^{2}]$^{3+}$	1.84 ± 0.05	22	-315	-215
[Tb·**L**^{3}]	3.35 ± 0.05	5	-29	-21
[Tb·**L**^{4}]$^{3+}$			-49	-32

3.5   Other factors which may influence the spectral form or intensity

3.5.1 The effect of pH upon the emission spectrum

It is crucial that the bicarbonate responsive probes act independently of pH, and do not exhibit a ratiometric change in response to pH. To assess this, a solution of [Eu·**L**^{2}]$^{3+}$ was taken in a 0.1 M sodium chloride background to maintain a constant ionic strength. Starting at pH 9 and decreasing the pH by approximately 0.5 units each time, a pH titration was undertaken (Fig. 33).

An overall decrease in intensity was apparent from pH 9 to pH 3, with the spectral form remaining constant. Between pH 5 and 8 there was very little change in the intensity of emission, and so the ratio remains constant at physiological pH. The slight increase in intensity and in the $\Delta J = 2/ \Delta J = 1$ ratio above pH 8 may be due to bicarbonate binding, which is difficult to completely inhibit in basic media. Below pH 5, the emission intensity decreases, along with the $\Delta J = 2/ \Delta J = 1$ ratio. This could possibly be ascribed to the protonation of the azaxanthone
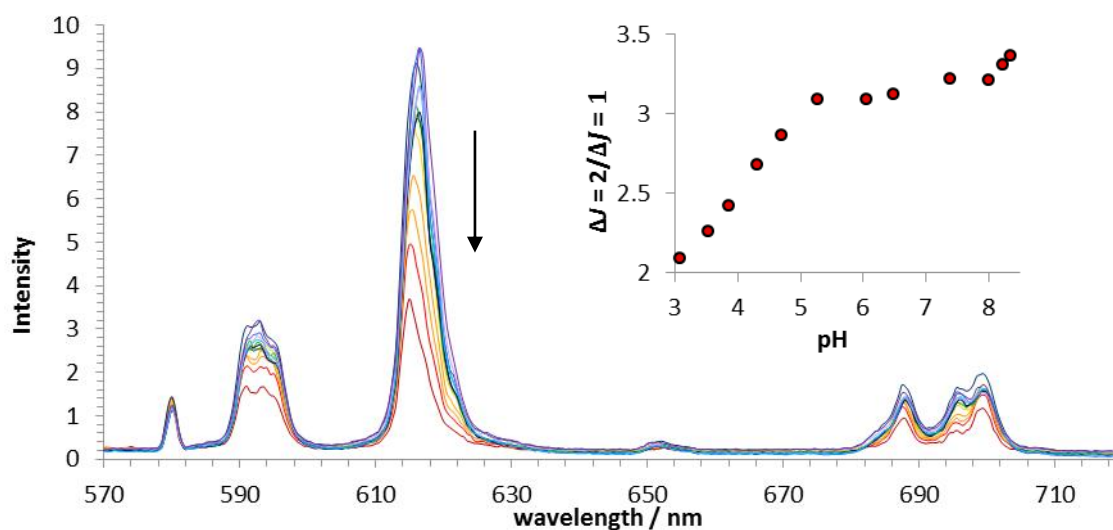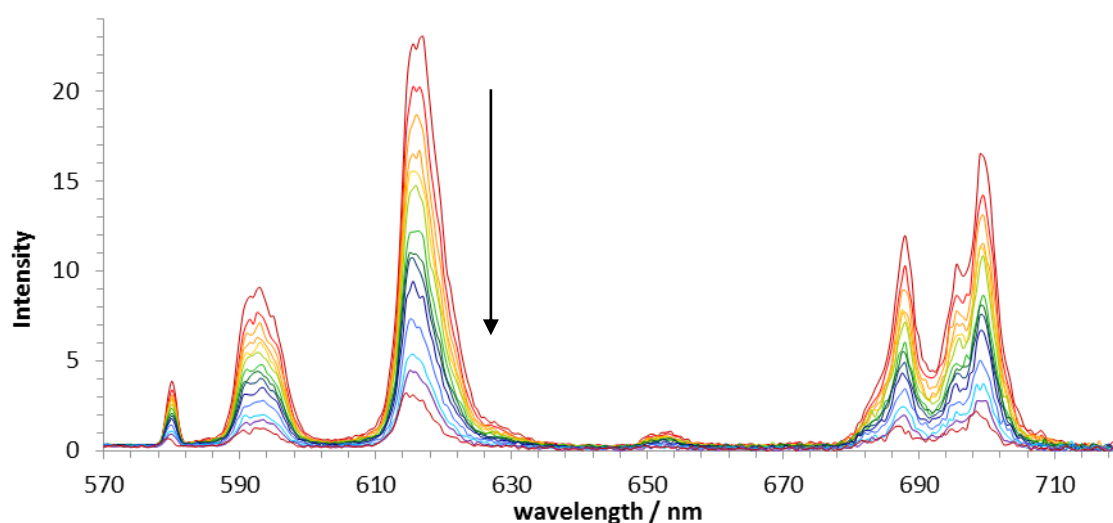
Fig. 33: Variation of the Eu(III) emission spectra for [Eu·**L²**]³⁺, as a function of pH (H₂O, 40 μM complex, 298 K, I = 0.1 M NaCl, λ_{ex} =332 nm).

nitrogen, interfering with hydrogen bonding within the chromophore unit and pushing the sensitiser away from the europium centre. This increased distance would hinder the efficiency of the energy transfer step, leading to a reduction in the emission intensity. Crucially, across the physiologically relevant pH range there is no change in the ΔJ = 2/ ΔJ = 1, or indeed any other ratio.

3.5.2 The effect of ionic strength upon the emission spectrum

All titrations in this thesis were performed in a background of 0.1 M sodium chloride, to maintain a constant ionic strength that mimics the typical extracellular biological salt

Fig. 34: Variation of the Eu(III) emission spectrum for [Eu·**L²**]³⁺, following incremental addition of sodium chloride (H₂O, 40 μM complex, 298 K, I = 0.1 M NaCl, λ_{ex} =332 nm).

concentration. The presence of the chloride anion does quench the intensity of lanthanide emission however via electron transfer quenching of the chromophore singlet excited state. This was investigated through a titration adding incremental amounts of sodium chloride. A quenching of emission was observed that was still evident at the limit of the titration, this was when the chloride concentration was 0.8 M.

By plotting F_0/F versus [Cl$^-$], the Stern-Volmer constant, K_{sv}^{-1}, was assessed to be 100 mM (Fig. 35). This corresponds to the chloride concentration that reduces emission intensity to half of its original values.
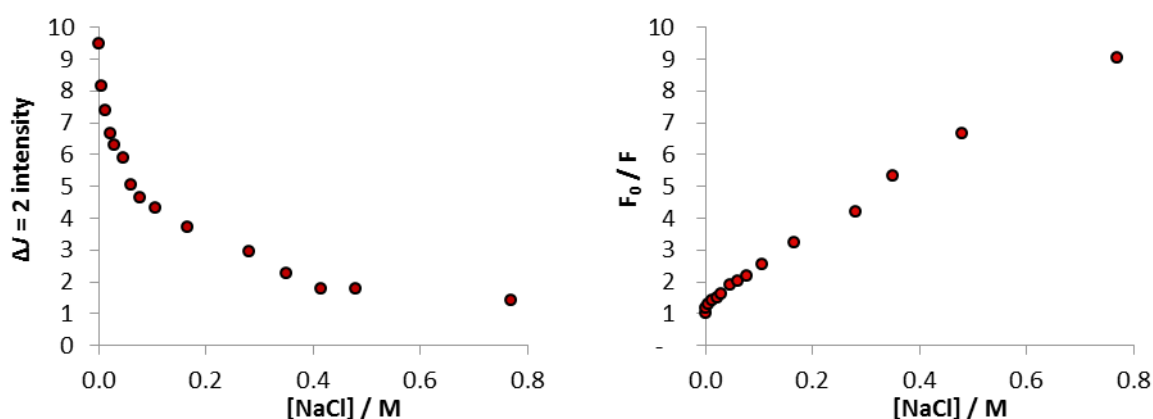
Fig. 35: Decrease in the emission intensity of the ΔJ = 2 band of [Eu·**L**^{4}]$^{3+}$ upon addition of sodium chloride (*left*); Plot of F_0 / F for the emission intensity of the ΔJ = 2 band of [Eu·**L**^{4}]$^{3+}$ upon addition of sodium chloride (*right*).

3.6   The competitive binding between protein and bicarbonate

Anions are not the only class of molecule which could potentially interfere with binding to other lanthanide probes. Binding of the complexes to proteins should also be considered. There exist thousands of proteins within a cell, possessing negatively charged side chain groups on the amino acids, which are capable of competing for binding to the lanthanide metal centres. Many studies have examined protein binding to lanthanide complexes and so it was necessary to investigate the effect protein had upon this series of complexes.[2, 22]   Human serum albumin (HSA) was chosen as a model protein, as it is the most abundant plasma protein.

3.6.1   Binding to human serum albumin

Initially, the binding of HSA with each complex was studied by spectral protein titrations. Incremental amounts of HSA were added as a solid, and the pH carefully adjusted back to 7.40 ±

0.05, if necessary, after each addition. Upon adding increased amounts of HSA, fluorescence originating from the tyrosine and tryptophan residues within the protein was observed.
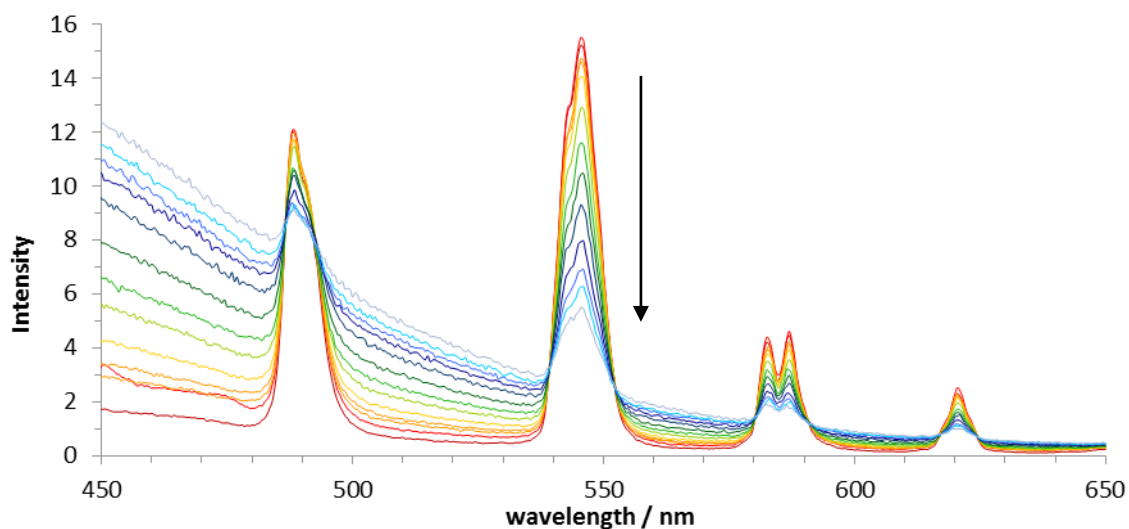
Fig. 36: Variation of the Tb(III) emission spectrum for [Tb·**L³**]³⁺, following the addition of human serum albumin (H_2O, pH = 7.40 ± 0.05, 40 μM complex, 298 K, I = 0.1 M NaCl, λ_{ex} =332 nm).

The protein fluorescence was particularly noticeable in the terbium emission spectra which occur at a lower wavelength (Fig. 36). The maximum of the protein fluorescence was centred at around 440 nm. Adding the protein led to quenching of the lanthanide emission. This was generally more pronounced for europium complexes than for terbium analogues. Changes in the form of the spectra were only really observed for the europium complex and even here they
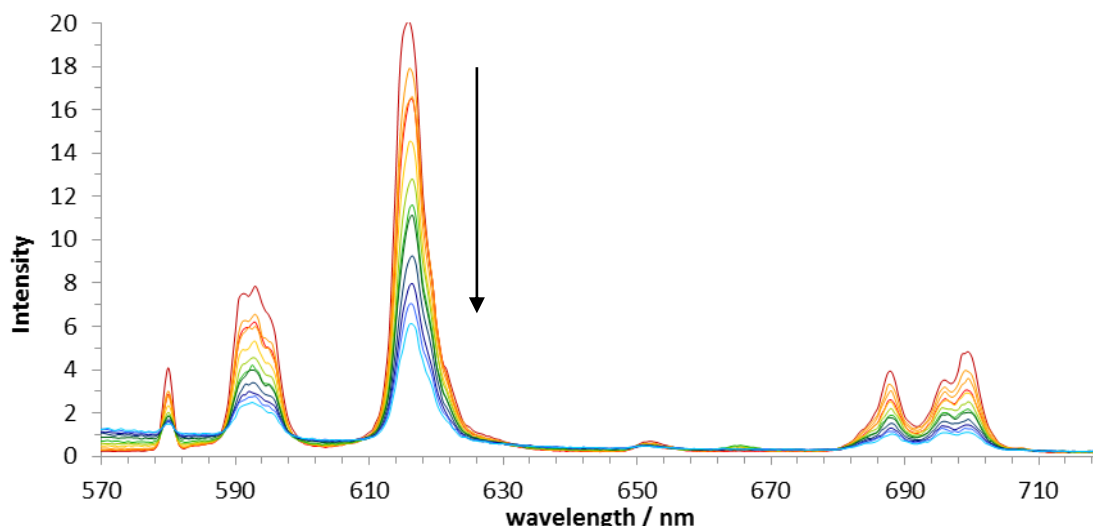
Fig. 37: Variation of the Eu(III) emission spectrum for [Eu·**L²**]³⁺, following the addition of human serum albumin (H_2O, pH = 7.40 ± 0.05, 40 μM complex, 298 K, I = 0.1 M NaCl, λ_{ex} =332 nm).

were relatively minor (Fig. 37). Most noticeable were changes in the relative intensities between the peaks within the hypersensitive $\Delta J = 4$ manifold. The large reduction in emission intensity can be ascribed to quenching of the sensitiser triplet state, inducing a charge transfer process from electron rich residues, such as tyrosine, in the protein.

Ratiometric analyses were performed examining selected bands within the spectrum, as for the characterisation of anion binding. Calculated apparent affinity constants for binding to HSA were similar for all complexes. Values were independent of complex charge and metal ion. For two of the complexes, affinity constants could not be calculated accurately, due to an insufficient change in spectral form.

Table 14: Apparent affinity constants for the binding of human serum albumin to the given complexes (295 K, 50 μM complex, pH = 7.40 ± 0.05).

complex	log K
$[Eu \cdot L^1]^{3+}$	3.20 ± 0.05
$[Eu \cdot L^2]^{3+}$	nd
$[Eu \cdot L^3]$	nd
$[Eu \cdot L^4]^{3+}$	3.30 ± 0.05
$[Tb \cdot L^1]^{3+}$	3.50 ± 0.05
$[Tb \cdot L^2]^{3+}$	3.55 ± 0.05
$[Tb \cdot L^3]$	3.60 ± 0.05
$[Tb \cdot L^4]^{3+}$	3.30 ± 0.05

Measurements of the complex hydration states in the free and protein-bound forms were made through measurement of excited state lifetimes (Table 15). These values are consistent with displacement of coordinated water molecules upon protein binding. Such effects have been established earlier and were ascribed to ligation of Glu or Asp side chain carboxylates.[108]

Table 15: Rate constants, k, (±10%) and lifetimes, (τ), observing the radiative decay of the lanthanide excited states at 616 nm (europium) and 545 nm (terbium) (295 K, 50 μM complex) and derived hydration numbers, q, (±20%) for $[Ln \cdot L^2]^{3+}$, with and without the presence of HSA.

	k_{H2O}	τ_{H2O}	k_{D2O}	τ_{D2O}	q
$[Eu \cdot L^2]^{3+}$	3.85	0.26	1.73	0.58	2.0
$[Eu \cdot L^2]^{3+}$ + HSA	0.90	1.11	0.41	2.40	2.2
$[Tb \cdot L^2]^{3+}$	2.58	0.39	1.63	0.61	0.6
$[Tb \cdot L^2]^{3+}$ + HSA	0.73	1.40	0.55	1.82	0.6

3.6.2 The competitive nature of protein and bicarbonate binding

It had earlier been observed for [Eu·L¹³]³⁺ that there existed a competition between bicarbonate and protein for binding to the metal ion when both species were present in solution. A simple set of experiments was performed with [Eu·L²]³⁺ to examine this aspect.

Firstly, in experiment A, the emission spectrum of the complex alone was recorded in solution. A 30 mM concentration of bicarbonate was added and the spectrum recorded again. The characteristic bicarbonate emission spectrum was observed. To this solution, HSA was added to a concentration of 0.7 mM. This resulted in a lowering of the emission intensity, and the spectrum resembled a mixture of the bicarbonate-bound and unbound complex species. Secondly, this experiment was performed in reverse, experiment B (Fig. 38). After again taking the spectrum of the complex alone under identical conditions, HSA (0.7 mM) was added and the quenched protein bound species was observed, with little change in emission form. Addition of
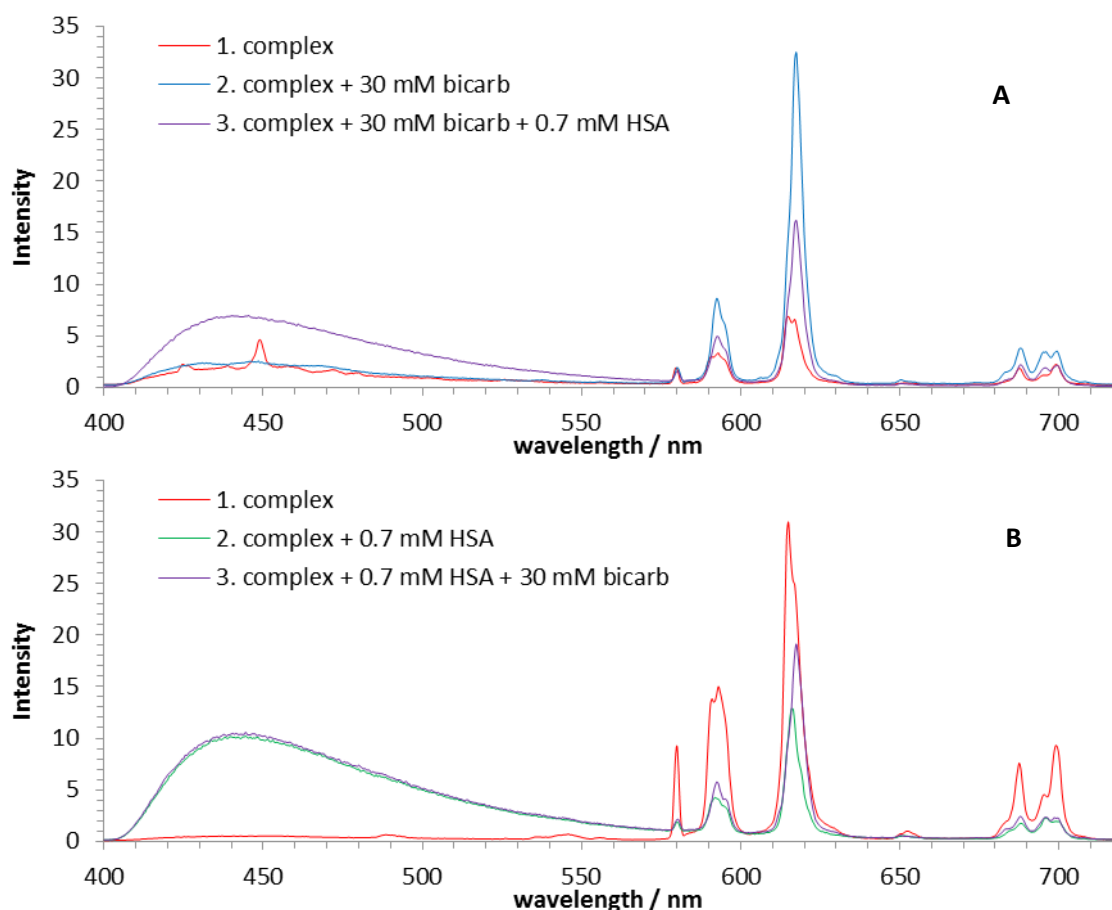
Fig. 38: Variation of the Eu(III) emission spectrum for [Eu·L²]³⁺, followed by the sequential addition of sodium bicarbonate (30 mM) and HSA (0.7 mM) (*top*), and followed by the sequential addition of HSA (0.7 mM) and sodium bicarbonate (30 mM) (*bottom*), (H_2O, pH = 7.40 ± 0.05, 20 μM complex, 298 K, I = 0.1 M NaCl, λ_{ex} =332 nm).

30 mM bicarbonate to this solution gave an identical spectrum to that observed in experiment A. An identical spectrum in terms of form and intensity between the two were observed.

The fact that the same spectrum was observed via either sequence of addition suggests a competition between these two species. The final spectrum in each case is an averaged spectrum for contributions due to bicarbonate bound and protein bound species. This is reflected by the averaged $\Delta J = 2/\Delta J = 1$ ratios observed.

Table 16: $\Delta J = 2/\Delta J = 1$ area ratios corresponding to the data shown in Fig. 38.

	$\Delta J = 2/\Delta J = 1$ ratio		
1. complex	1.8	1.8	1. complex
2. complex + 30 mM bicarb	3.4	2.2	2. complex + 0.7 mM HSA
3. complex + 30 mM bicarb + 0.7 mM HSA	2.7	2.7	3. complex + 0.7 mM HSA + 30 mM bicarb

### 3.6.3 Bicarbonate binding titrations in a background of protein

The effect of a protein background upon bicarbonate binding was examined in further detail. A bicarbonate titration was undertaken in a fixed HSA background, at a concentration of 0.4 mM. Addition of incremental amounts of sodium bicarbonate to the europium complexes [Eu·**L**^{1}]$^{3+}$, [Eu·**L**^{2}]$^{3+}$ and [Eu·**L**^{3}] caused a large increase in spectral intensity and a shift in the $\Delta J = 2$ maxima from 614 to 616 nm, consistent with the behaviour observed when protein was not present (Fig.
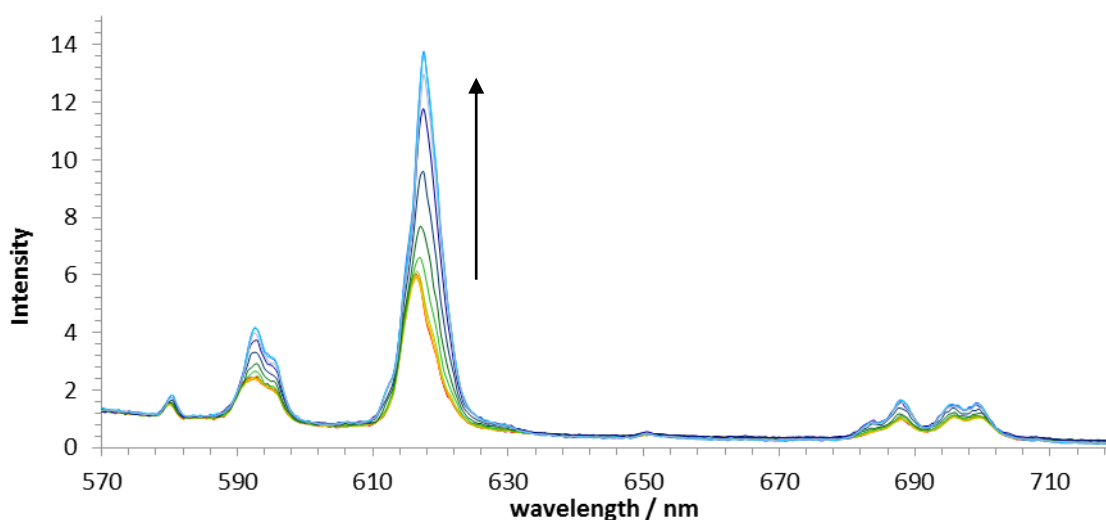
Fig. 39: Variation of the Eu(III) emission spectrum for [Eu·**L**^{2}]$^{3+}$, in a background of 0.7 mM HSA, following addition of up to 30 mM sodium bicarbonate (H_2O, pH = 7.40 ± 0.05, 50 μM complex, 298 K, I = 0.1 M NaCl, λ_{ex} = 332 nm).

39). Adding 5 to 25 mM bicarbonate caused a 250% increase in emission intensity, and up to a 25% increase in the $\Delta J = 2/ \Delta J = 1$ ratio. This is consistent with partial displacement of the bound protein by bicarbonate.

The terbium analogues showed far less change in spectral emission intensity increases upon addition of the same concentrations of bicarbonate (Fig. 40). In each case, the corresponding intensity changes were less than 20%. In a competitive background of protein, it appears that terbium is far less sensitive than europium to the addition of added bicarbonate. This offers the intriguing possibility of using europium to terbium ratios to measure bicarbonate concentrations. In this sense, the terbium complex with its relative insensitivity would be acting as a reference against the strong modulation of the europium analogue.
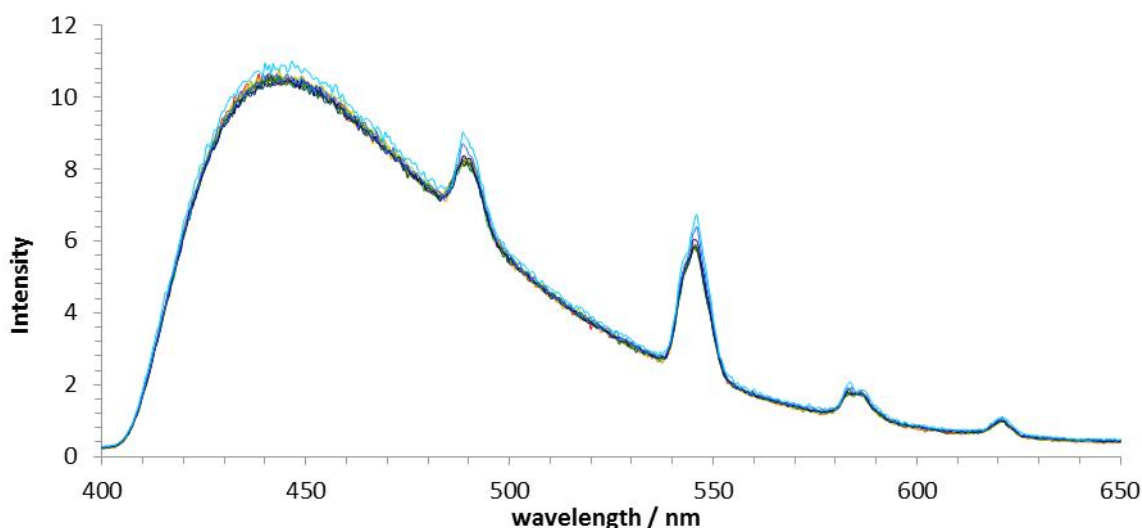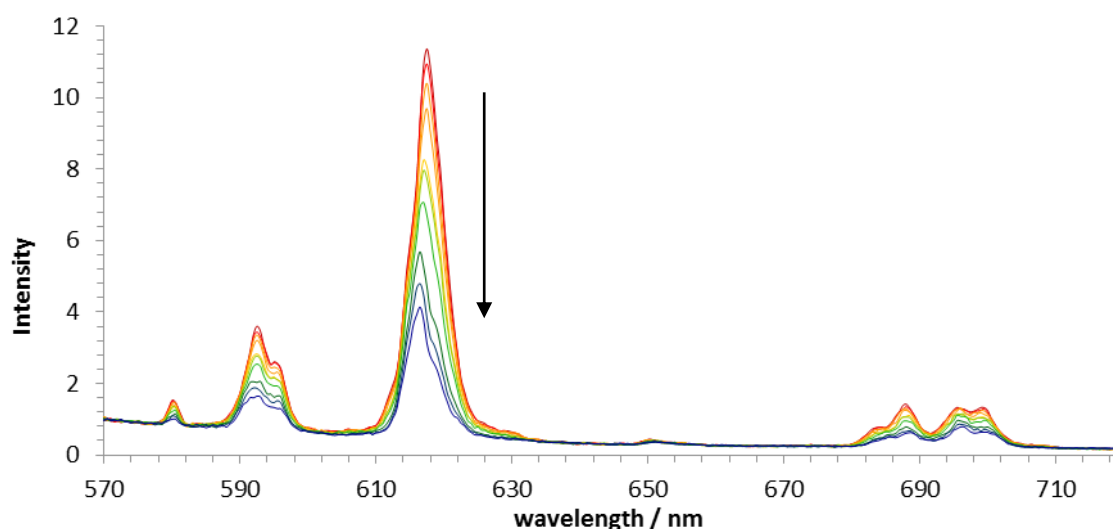

Fig. 40: Variation of the Tb(III) emission spectrum for $[Tb \cdot L^2]^{3+}$, in a background of 0.7 mM HSA, following addition of up to 30 mM sodium bicarbonate (H_2O, pH = 7.40 ± 0.05, 50 μM complex, 298 K, I = 0.1 M NaCl, λ_{ex} = 332 nm).

3.6.4 Competition experiments

Thus far, the effects of lactate, citrate and phosphate on lanthanide emission have been studied individually. Competition experiments were also performed, examining the influence of addition of all these anions to a solution of the complex which contained a fixed background of bicarbonate and protein. The triphosphate ATP was also included in these investigations. This important anion is present at about 0.5 mM concentrations within the mitochondria, and could be capable of binding to the lanthanide complexes, through the terminal phosphate group.

In each case, a fixed background of 0.4 mM human serum albumin and 20 mM bicarbonate was used in experiments with [Eu·**L²**]³⁺.

Addition of phosphate, ATP, citrate and lactate each led to a reduction in emission intensity of the europium complex. However, phosphate and lactate caused very little change, there was less than a 5% decrease in overall emission intensity upon adding up to 2 mM of these anions. Citrate led to a more pronounced decrease in emission intensity (Fig. 41). After adding 2 mM citrate, the emission had decreased by 34%. Addition of citrate continued to have a decreasing effect and at 20 mM citrate, overall emission was reduced by just over 60%. However, at extracellular citrate concentrations of 0.13 mM the decrease was just <5%. ATP caused the most dramatic decrease in emission intensity at similar concentration levels. After addition of 2 mM ATP, the emission had decreased by 85%, and at 0.5 mM by 60%.

Fig. 41: Variation of the Eu(III) emission spectrum for [Eu·**L²**]³⁺, in a background of 0.4 mM HSA and 30 mM sodium bicarbonate, following addition of up to 20 mM sodium citrate (H$_2$O, pH = 7.40 ± 0.05, 50 μM complex, 298 K, I = 0.1 M NaCl, λ_{ex} = 332 nm).

These experiments suggest that the binding of protein and bicarbonate to the europium centre is competitive and that spectral form is not significantly perturbed by concentration changes in phosphate, ATP, citrate or lactate.

3.6.5 Binding to α-acid glycoprotein

As mentioned at the beginning of this section, there exist numerous plasma protein, serum albumin being just one representative example. Another plasma protein, α-acid glycoprotein was therefore also studied in relation to its binding with lanthanide complexes. This protein is typically present in serum at concentrations of around 40 μM, although this concentration is known to rise during inflammation. A titration was carried out using α-AGP with $[Eu·\mathbf{L}^2]^{3+}$, other experimental conditions being identical to that of the analogous titration with HSA. α-AGP was added as very small quantities of a concentrated stock solution rather than as a solid as for HSA, as the concentrations used were far less than for HSA.
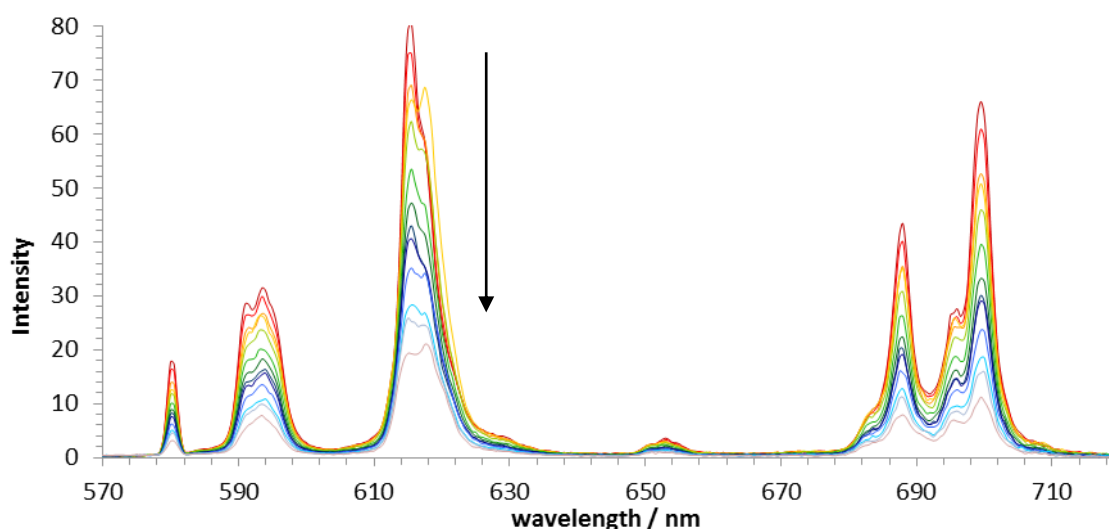
Fig. 42: Variation of the Eu(III) emission spectrum for $[Eu·\mathbf{L}^2]^{3+}$, following addition of α-acid glycoprotein (H$_2$O, pH = 7.40 ± 0.05, 50 μM complex, 298 K, I = 0.1 M NaCl, λ_{ex} = 332 nm).

A clear reduction in lanthanide emission intensity can be observed. Fluorescence from the protein is much weaker here, as the concentration of α-AGP was only 60 μM at the end-point. Spectral form was not modulated sufficiently to allow an accurate binding constant to be calculated.

In summary, the complexes do not show a specific binding to either HSA or α-AGP, both exhibit a decrease in spectral intensity, consistent with quenching of the sensitised triplet state by a charge transfer process.

3.7   Tandem probe methodology using a red : green ratiometric analysis, and time-gated analysis

It is possible that one may think, given the lack of response from the terbium analogue towards bicarbonate binding in a protein background, that the terbium probe offers little in terms of use as a ratiometric probe. However, it is possible that its limited response to great use, by using it in conjunction with the europium probe. Using both probes together, allows the terbium probe to be used an internal calibrant. So, instead of taking a ratio of the $\Delta J = 2/\Delta J = 1$ for europium, or $\Delta J = -1/\Delta J = -2$, for terbium, it is possible to use a pair of europium/terbium emission bands, or a red/green ratio. This is particularly promising for use in cellular applications, where optical microscopy will be used. It allows the use of a wider spectral window maximising the intensity of the emission signal collected and reducing the signal-to-noise ratio. The resolution available on confocal microscopy equipment is also much less than for fluorescence, and so an accurate $\Delta J = 2/\Delta J = 1$ ratio becomes rather difficult to measure. The next stage, therefore, was to assess whether a mixture of europium and terbium complexes of a common ligand could be used to monitor bicarbonate concentrations.

Background media in biological systems contain a huge number of species at varying concentrations. Therefore, the next logical step was to examine the binding of bicarbonate, in a mixed competing background. The anions which were investigated earlier were used at their typical extracellular concentrations, and HSA also at its typical average extracellular concentration of 0.4 mM. The anion ATP is another biological species which is present within the mitochondria, and potentially interfere with bicarbonate binding. It was therefore also included in this background mixture.

Thus, an 80 μM total complex concentration was added to a background solution containing 0.4 mM HSA, 0.13 mM citrate, 1.3 mM lactate, 0.7 mM phosphate and 1 mM ATP. The ratio of the europium to terbium complex concentration used was 3:2. A higher proportion of europium to terbium was required, as terbium has a higher quantum yield, and it is desirable to start at a point where the emission intensity is approximately 1:1. Incremental additions, from a concentrated stock solution of bicarbonate, were made up to a limit of 60 mM. The presence of the competing background lowers the affinity for bicarbonate. Notably, changes to the spectrum occurred over an extended concentration range relative to that for the standard bicarbonate titrations.
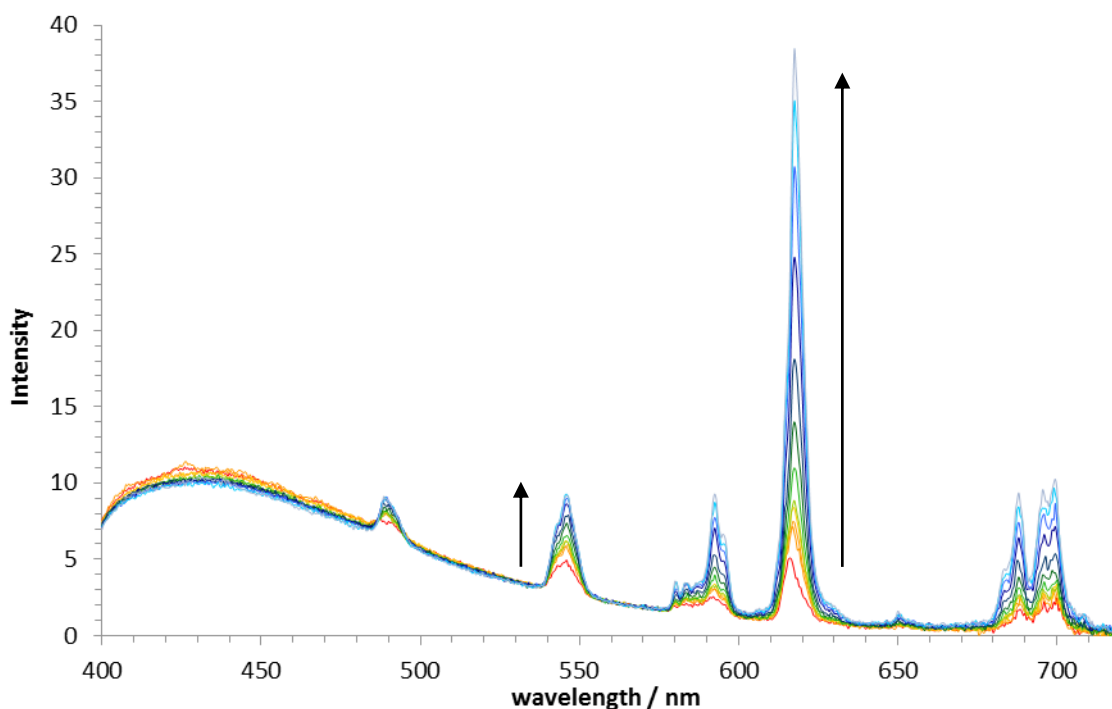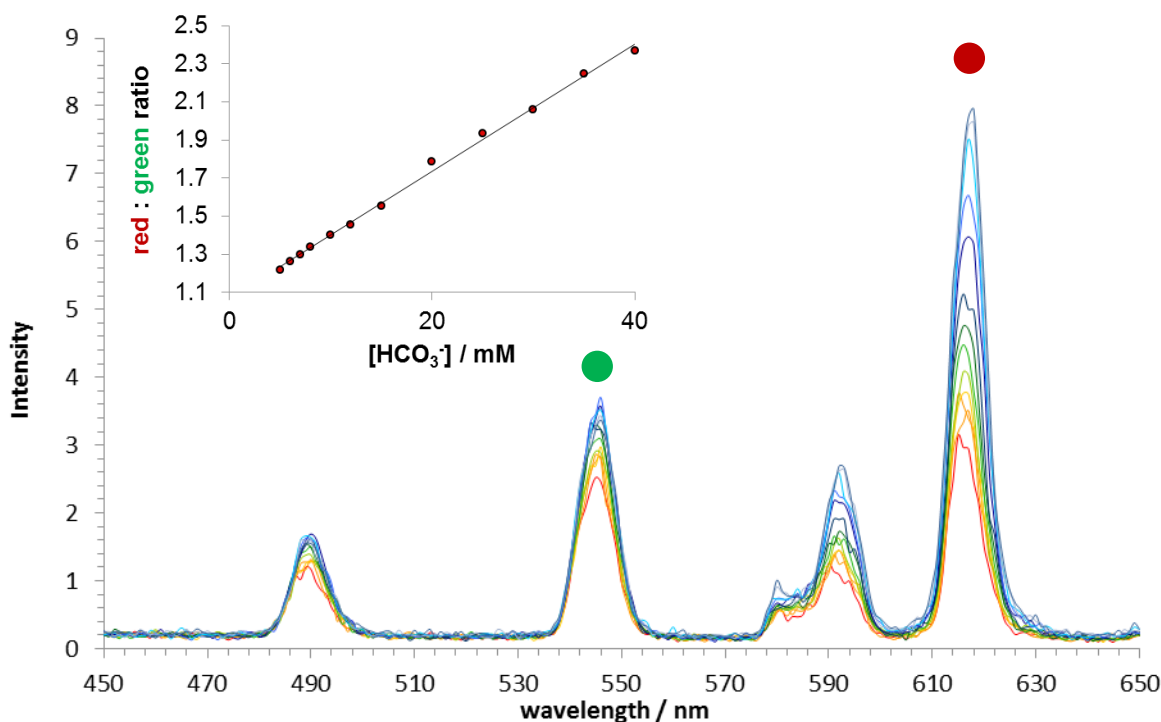
Fig. 43: Variation of the total Ln(III) emission spectrum for $[Tb \cdot \mathbf{L^2}]^{3+}$: $[Eu \cdot \mathbf{L^2}]^{3+}$, 3:2, following addition of up to 60 mM sodium bicarbonate (H_2O, pH = 7.40 ± 0.05, 80 μM total complex, 298 K, I = 0.1 M NaCl, λ_{ex} =332 nm).

An increase in emission intensity for both the europium and terbium band was observed upon addition of sodium bicarbonate (Fig. 43). Observing the maxima for each of the observed bands, the increase was much more substantial for europium than for terbium. It can be seen that the maximum intensity at the start was approximately the same for both europium and terbium, and reached a ratio of about 4:1 at the end of the titration.

Also apparent from the spectral titration is fluorescence emission from the protein at 430 nm, creating the trailing baseline that stretches over the terbium emission spectrum and into the beginning of the europium spectral window. This needs to be mathematically subtracted to allow an accurate europium to terbium ratio to be calculated. However, this can be avoided by taking advantage of the long-lived nature of lanthanide emission and using time-gated data acquisition.

With appropriate instrumentation, time-gated data acquisition is possible. By waiting for a period of 10 μs after the excitation pulse any short-lived fluorescence from protein, the ligand or other species will have decayed to zero. As a consequence, emission solely from the lanthanide ion can be acquired. This removes the trailing baseline which is otherwise observed whenever a spectrum is taken when protein is present within the background medium; it is then easier to take an accurate measurement of the red to green emission intensity ratio.

Fig. 44: Time-gated data showing the variation of the Ln(III) emission spectra for $[Tb\cdot L^2]^{3+}/[Eu\cdot L^2]^{3+}$, following addition of sodium bicarbonate (H_2O, pH = 7.40 ± 0.05, 80 μM total complex, 298 K, I = 0.1 M NaCl, λ_{ex} =365 nm). The inset shows the variation of the red:green ratio, comparingthe integrated emission intensity from 605 – 630 nm (red) against that at 535 – 555 nm (green).

Thus, an integrated ratio of the ΔJ = 2 europium band centred at 616 nm to the ΔJ = -1 terbium band centred at 545 nm was taken and plotted as a function of added bicarbonate. It is pleasing to observe that over the relevant biological range of 10 – 30 mM, a near-linear variation was found. Additionally, the change in the ratio over this range is >40%; suggesting that the use of europium and terbium probes in tandem offers a convenient way of measuring bicarbonate concentrations.

In subsequent microscopy experiments, pCO_2 will be varied between 3% and 5%. The concentration of bicarbonate in solution at 3%, 4% and 5% CO_2 atmospheric concentrations at pH 7.4 can be calculated using the Henderson-Hasselbach equation, *[Eq. 8]*.

$$pH = pK' + \log[HCO_3^-]/spCO_2 \qquad \textbf{[Eq. 8]}$$

The dissolved bicarbonate concentration can be calculated at equilibrium; i.e. at 298 K, 760 mm Hg, pH 7.4. This estimation requires a value of 6.1 to be assumed for the practical coefficient, pK', associated with ionisation of carbonic acid.[125] The calculated values of bicarbonate for 3, 4 and 5% CO_2 are 13.6, 18.1 and 22.7 mM, assuming that the solubility coefficient, s, of CO_2 gas in the medium is 0.0307 mM per mm Hg pCO_2, and the atmospheric pressure is 760 mm Hg. Between 13.6 and 22.7 mM bicarbonate, the europium / terbium emission intensity ratio increased by 45% and 42% respectively for $[Ln·\mathbf{L^1}]^{3+}$ and $[Ln·\mathbf{L^2}]^{3+}$ respectively. This provides sufficient change to be accurately measured.

3.8 Intracellular localisation

A clear, well defined localisation profile is essential for a truly useful cellular probe. Ideally, the probe will localise to just a single cellular compartment, rapidly and efficiently. For the bicarbonate probes discussed here, it is the mitochondria that are the target organelle of interest. The Krebs cycle and glycolysis both produce mitochondrial CO_2 which is converted into bicarbonate for transport. Matching the selective targeting of a probe with its desired analyte function remains a key challenge in general probe design.[20, 68]

To assess the localisation, a number of cell-lines (CHO, NIH-3T3, HeLa, MCF-7, A459) were investigated. These were grown on glass coverslips and the complexes incubated at varying concentrations (10 - 100 µM) and time-points (30 min – 24 h). After the incubation period, the coverslip was removed, washed in phosphate-buffered saline (PBS) and mounted on a glass slide before sealing with nail varnish and visualised using a confocal microscope. Excitation of the azaxanthone chromophore was achieved using a 355 nm UV laser. When examining emission from the complexes alone, a red channel operating over 570 nm – 720 nm was used for europium, and a green channel operating over 450 – 650 nm for terbium.

Localisation was confirmed by co-localising with commercially available cellular stains (Fig. 45). Green emissive probes were used for europium complexes and red emissive probes were used for terbium complexes. At time-points of between 1 and 6 hours, the lanthanide complexes showed a clear co-localisation with the MitoTracker™ probes, confirming a localisation within the mitochondrial region. At time points of around 8 h, the localisation was less distinct, and was probably a combination of localisation within both the mitochondria, and the lysosomes. At further time points (up to 24 h), emission closely matched that of the LysoTracker probes, consistent with dominant lysosomal staining.
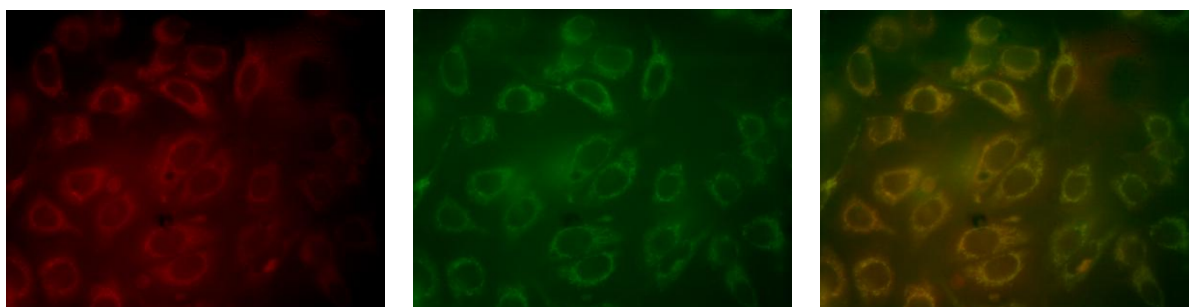
Fig. 45: Microscopy images for [Eu·**L**^{2}]$^{3+}$, 50 μM complex, 4 h incubation, MCF-7 cells, co-staining with MitoTracker Green™: (*left*) Eu(III) complex (570 – 720 nm); (*centre*) MitoTracker Green™; (*right*) overlayed image.

It has been hypothesised that it is the nature of the heterocyclic sensitising unit that is responsible for directing complexes to a particular region within a cell.[22] The complexes in this series correlate well with these observations in that an amide linked azaxanthone unit will lead to a mitochondrial localisation with subsequent shuttling to the lysosomes.

An important point to note is that when examining the terbium complexes and co-localising with MitoTracker red, care needs to be taken to ensure that cross-excitation does not take place. Excitation of MitoTracker red occurs at 579 nm, which happens to lie directly under the $\Delta J = 0$ emission band of terbium. Excitation of the terbium complex may therefore subsequently cause excitation of MitoTracker red. This aspect meant that when observing terbium emission, whilst MitoTracker red is present, emission could not be collected over the range in which MitoTracker red emits, which is from 560 – 700 nm. In practice, this meant that terbium emission was selected over the range 450 – 555 nm conveniently covering the two main emissive bands.

3.9   Cytotoxicity studies

It is imperative when designing cellular probes for reporting upon physiological conditions, that the probe be non-toxic towards the cell. It needs to be shown that the presence of the probe does not induce a toxic effect, or induce stress to the cell perturbing its homeostasis. The concentration used of the probe is an important factor, as it is the toxicity of the probe at the applied concentration which is crucial. Virtually all compounds will be toxic to some degree, if administered at a sufficiently high concentration.

The cytotoxicity of a complex refers to its ability to be toxic to and kill cells, resulting in a number of cellular fates. They may undergo necrosis where they lose membrane integrity and die rapidly. Alternatively, they can undergo a decrease in viability where they stop growing and dividing, or they can activate apoptosis; this is programmed cell death.

Cell viability can be readily assessed by measuring membrane integrity, as this is often compromised by compounds exhibiting cytotoxic effects. Trypan blue is a commonly used dye for this purpose.[37] Normally, it is excluded from the interior of healthy cells, but it can freely cross into the cell and intracellular compartments if the external membrane is compromised, thus providing a qualitative rather than quantitative assessment of cytotoxicity.

An alternative method involves the MTT assay.[67] This was used for the attainment of quantitative cytotoxicity data for the complexes studied in this thesis. The MTT assay measures the reducing potential of a cell using a colorimetric reaction. Mitochondrial reductase enzymes of viable cells reduce MTT into an insoluble purple formazan product. This can be solubilised and its concentration quantified spectrophotometrically. The amount of formazan produced is proportional to the number of viable cells.

Cells were grown overnight to allow them to adhere to the surface in 96-well plates, with approximately 10,000 cells per well initially. Varying concentrations of the complex were then administered in triplicate or quadruplicate, spanning a two-log range typically up to 200 μM, and incubated for a period of 24 h. For the final 4 h, MTT was added to the medium. After this time, the complex medium and MTT were removed, and DMSO added to solubilise the formazan product. The absorbance of this product at 540 nm could then be recorded using a plate reader. Mouse skin fibroblasts (NIH-3T3 cells) were used in the assay as in previous studies they had been shown to possess the best adherence to the base of the wells.[126] This is of importance as the process of removing the medium at the end of the incubation period sometimes can dislodge poorly adhered cells.

To process the results, the percentage viability of a well was calculated from the relative absorbance of the well, compared to a well containing untreated cells. It was found that viability decreased exponentially with increasing concentration of the probe. Conversion to a logarithmic scale allowed for a linear relationship with complex concentration to be observed. This procedure allowed an IC_{50} value to be calculated. This is the concentration of the complex required to inhibit viability by 50%.

In all cases, the IC_{50} values at 24 h for all complexes examined in the series were above 200 μM, which was the upper limit incubated in these studies. Considering that typical dosages are well below these values, typically around 20 – 50 μM and involve time periods of around 2 - 4 hours, it can be assumed that the complexes will not exert a significant cytotoxic effect in the experiments performed.

3.10 Variable CO_2 Microscopy Experiments

Preliminary work utilising $[Eu \cdot L^1]^{3+}$ had previously shown that the emission intensity decreased as the level of atmospheric CO_2, and consequently mitochondrial bicarbonate
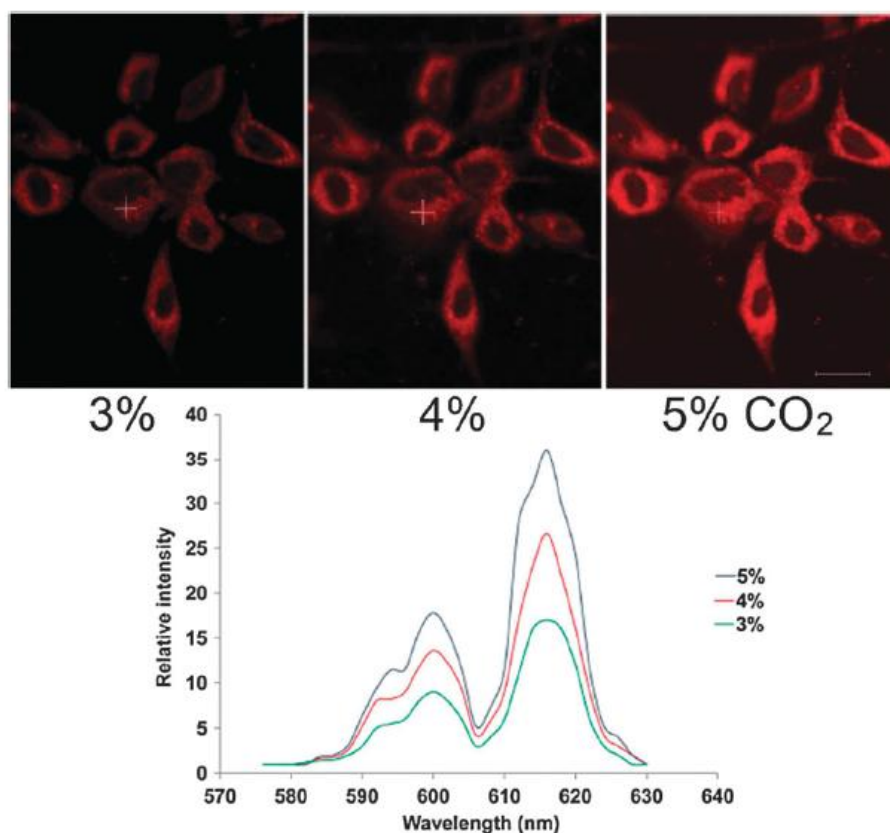
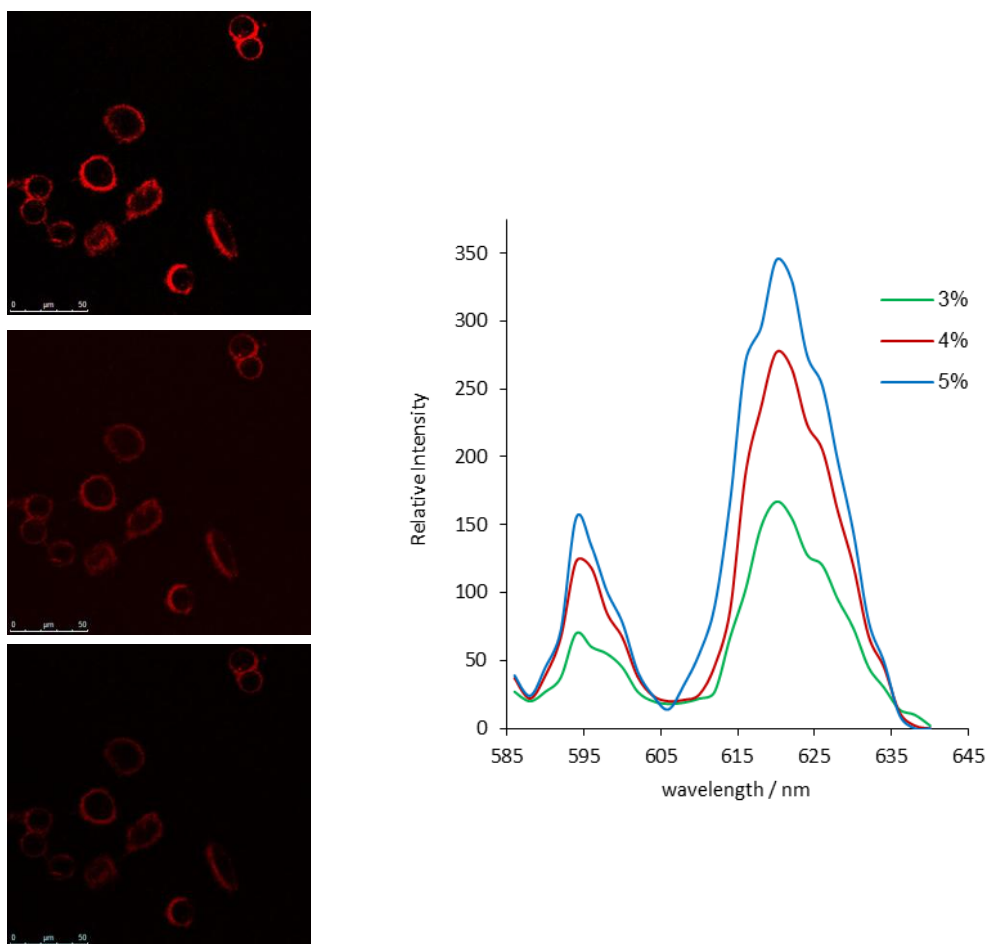**Fig. 46:** Confocal microscopy images for $[Eu \cdot L^1]^{3+}$ 50 μM complex, 2-3.5 h incubation, λ_{ex} = 360 nm) in HeLa cells at 3% (left image), 4%(centre image) and 5% (right image) atmospheric CO_2 (scale bar 20 microns). The graph shows a plot of the relative intensities of complex emission as a function of pCO_2.

concentration was reduced (Fig. 46). When the incubation was performed at a constant atmospheric CO_2 of 5% over the same time period, no significant modulation of intensity was observed. This initial result suggested that the series of probes could find use in relaying spatial concentrations of bicarbonate over the time scale of imaging experiments.

To build upon these initial observations, a number of points needed to be investigated. Firstly, the reversibility of the above process should be examined. When reducing the atmospheric CO_2 concentration and observing the decrease in emission intensity it is necessary to show that when the CO_2 concentration is subsequently increased back to the starting value, that the emission intensity also increases back to its original value. Secondly, an investigation of whether this process can be inhibited in some way is of interest. This may involve either blocking or enhancing bicarbonate production within the mitochondria, and observing any changes in emission which occur. Lastly, investigations with the terbium analogues were to be performed. Given the observed lack of spectral intensity change *in vitro*, if this behaviour is maintained, then it may be expected that it will remain insensitive to changes in atmospheric CO_2 concentrations *in cellulo*.

3.10.1 Reversibility studies and quantification using the europium analogues

Initially, it was established that the observed result could be repeated and that the effect was fully reversible. After repeating the initial experiment where the percentage CO_2 was decreased from 5% to 3%, the CO_2 concentration was then increased stepwise back up to 5%. Emission spectral intensity increased back to the original values. The variation of europium emission intensity from a repeated experiment of this type is shown in Fig. 47. It can be seen to be in good agreement with the original data discussed in the previous section. When examining the percentage increases in emission intensity, the two data sets accorded very well with each other. The $\Delta J = 2$ band intensity increased by 110% in each case from 3% to 5%, whilst the $\Delta J = 2 \, / \, \Delta J = 1$ intensity ratio increased by 14% and 16% respectively.
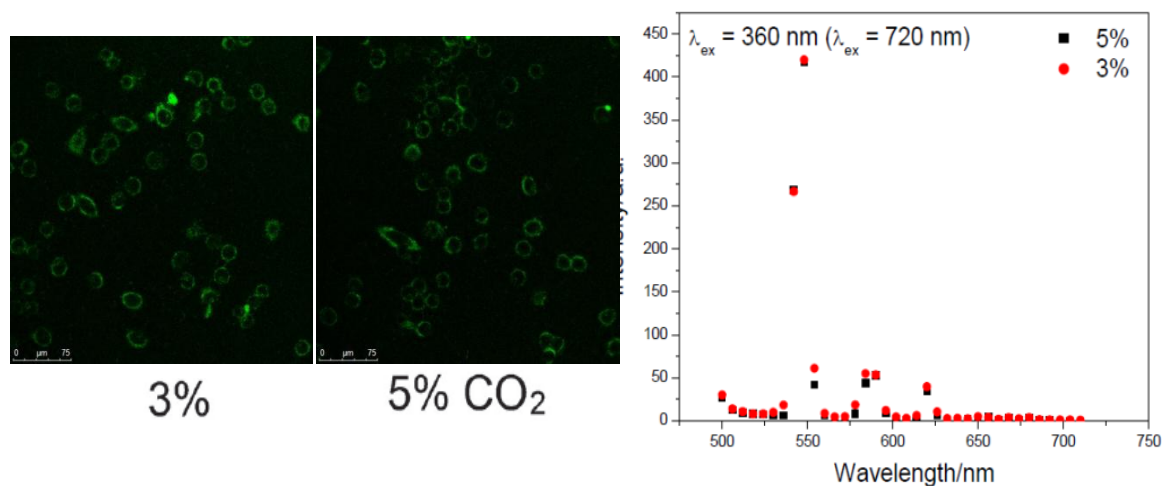
Fig. 47: Confocal microscopy images for [Eu·**L¹**]³⁺ 50 μM complex, 2-3.5 h incubation, λ_{ex} = 360 nm) in HeLa cells at 3% (bottom image), 4% (middle image) and 5% (top image) atmospheric CO_2 (scale bar 20 microns). The graph shows a plot of the relative intensities of complex emission as a function of pCO_2.

3.10.2 Variable pCO_2 using the terbium analogues as a control

In vitro experiments examining the terbium complexes had revealed that they showed little response to addition of bicarbonate in competitive backgrounds, and could therefore be used as a standard to calibrate the europium emission. It was necessary to check whether this behaviour was also observed in cells. The europium complexes had been shown to exhibit a significant change when the atmospheric concentration of CO_2 was varied between 3% and 5%, and so this experiment was repeated for incubations of the terbium analogues.

The complex [Tb·**L²**]³⁺ was incubated for 2 h at a concentration of 50 μM. Upon cycling between 3% and 5% CO_2 no significant modulation of the emission intensity or spectral form was observed (Fig. 48). In independent repeated experiments, the change in emission intensity over this range of 3 - 5% CO_2 was always less than 10%.

Fig. 48: Confocal microscopy images for $[Tb \cdot L^1]^{3+}$ 50 μM complex, 2-3.5 h incubation, λ_{ex} = 360 nm) in HeLa cells at 3 (left image) & and 5% (right image) atmospheric CO_2 (scale bar 20 microns). The graph shows a plot of the relative intensities of complex emission as a function of pCO_2.

The lack of response observed with the terbium analogues *in cellulo* suggested that if used in tandem with the europium probes, that by using a red : green ratiometric analysis, changes in bicarbonate concentrations can be monitored and quantified, as found with the *in vitro* calibration.

3.10.3 pCO₂ calibration using both europium and terbium analogues

A further experiment was performed where both the europium and terbium analogues were incubated with the cells at the same time. Initial experiments indicated that a higher ratio of europium to terbium complex was required than with the *in vitro* studies which used a 3:2 ratio, to gain enough signal from the europium component. Thus, a 3:1 ratio of europium to terbium complex of $[Ln \cdot L^2]^{3+}$ was used. This was incubated with NIH-3T3 cells for one hour at 5% CO_2 to allow complex uptake within the mitochondria. At this point, spectral data were obtained examining two emission channels. The green terbium channel was set from 450 to 570 nm observing emission arising from only the terbium component. The red europium channel collected emission from 600 to 720 nm. Subsequently, the percentage CO_2 within the live cell imaging chamber was adjusted, and a period of 25 minutes allowed to elapse to allow equilibration, before taking the reading at that concentration. This was repeated for integer concentrations of CO_2 between 2 and 7%. The range was extended from the previous experiments of this type which had looked between 3 and 5%, as another aspect we wished to address was the range over which this effect worked. The values of 3 and 5% CO_2 correspond to bicarbonate concentrations of just 13.6 and 22.7 mM bicarbonate, so extending the range is logical.

To extract an intensity value for each image, three small (about 500 pixels) areas representing a mitochondrial part of the cell were taken. The maximum values observed in each case were averaged, giving the lanthanide intensity for that image. An intensity ratio was then calculated using the europium and terbium images to give the red/green ratio. The data from Fig. 49 is plotted in Table 17. Whilst the range of 3-5% is approximately linear, the data fits to a sigmoidal curve over the fuller range of 2-7% CO_2, suggesting that these are the limits which can be probed *in cellulo*.

This experiment shows that a mix of europium and terbium complexes can be used in tandem to monitor changes in bicarbonate concentrations within the mitochondrial region of cells. This is unprecedented.

Table 17: Eu(III) and Tb(III) emission intensities, and the calculated red/green ratio for a range of pCO_2 after incubation in NIH-3T3 cells.

% CO$_2$	Eu(III) intensity	Tb(III) intensity	Red/green ratio
2	56	96	0.58
3	78	128	0.61
4	93	133	0.70
5	118	140	0.84
6	160	147	1.09
7	160	138	1.16
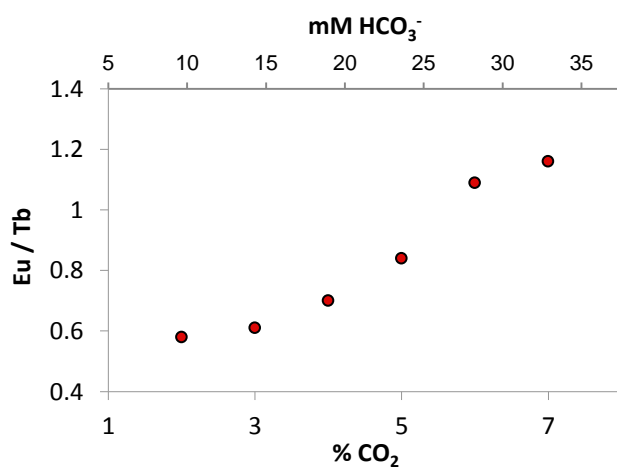
Fig. 49: Plot of Eu(III)/Tb(III) emission intensities as a function of pCO_2. observed in the mitochondria of NIH-3T3 cells.

3.10.4 Using acetazolamide to inhibit modulation of the spectral form

Acetazolamide, **76**, is a broad spectrum carbonic anhydrase inhibitor. It suppresses the activity of carbonic anhydrases which are a family of zinc-containing enzymes that rapidly interconvert carbon dioxide and water to bicarbonate anions and protons. Carbonic anhydrases were the first enzymes discovered to contain zinc, and are now known to be among the most efficient enzymes in biology. As well as maintaining an acid-base balance in the blood, this process helps to transport carbon dioxide out of tissues.[89] This is the case in the mitochondria, where vast quantities of CO_2, produced through glycolysis and the Krebs cycle, need to be removed and transported away.

76
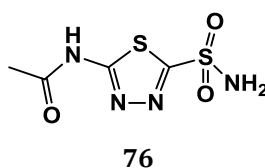
The experiment in which the atmospheric carbon dioxide concentrations were controlled and varied during incubation with the europium complex was performed again, but in the presence of acetazolamide. Acetazolamide concentrations of both 1 and 10 μM were used, for an incubation period of 1 h. Acetazolamide is not toxic, at these concentrations, in the cell lines used, as determined by an independent MTT assay.

Using the same time incubation periods, concentration of complex and experimental conditions as in the previous experiments, no significant modulation in the emission intensity upon adjusting the pCO_2 between 3% and 5% was observed in the presence of acetazolamide (Fig. 50). Furthermore when acetazolamide was present, the spectral intensity was lowered.
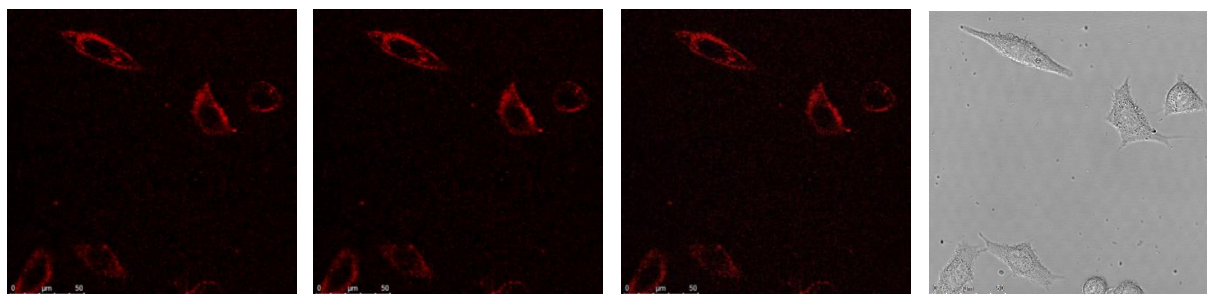
Fig. 50: Confocal microscopy images for [Eu·**L¹**]³⁺ 50 μM complex, 2-3.5 h incubation, λ_{ex} = 360 nm) in HeLa cells at 3% (left image), 4% (centre left image) and 5% (centre right image) atmospheric CO_2 (scale bar 20 microns). Transmission (right image).

Taken together, it appears that acetazolamide is inhibiting the conversion of CO_2 to bicarbonate, and this is being reflected in the emission of the europium probe. It has been shown that the bicarbonate bound complex is more emissive than a protein-bound europium complex. So, in the presence of acetazolamide, bicarbonate concentrations decrease and there is a higher proportion of protein-bound complex that quenches emission.

3.11 Measuring fluctuations of bicarbonate concentrations within marine algae

Certain species of marine algae, called coccolithophores, are unique amongst marine species in that they extrude intricate calcium carbonate shells termed coccoliths on their exterior surface. Coccolithophores are single-celled spherical algae, and are found in vast quantities in the upper layers of the oceans. Coccolithophores are of scientific interest, as they may play a large part in global climate change.[91, 92]

The exact purpose of the calcium carbonate liths remains unknown. The mechanism through which they are formed, and extruded is only partially understood. Current understanding comes largely from studies looking at sections of coccolithophores at various stages of growth, and isolated incompletely formed coccoliths.[95] Coccolith growth initiates with nucleation of an elliptical ring of calcium carbonate crystals and then simultaneously progresses in a number of well-constrained directions. It is hoped that if fluctuations of bicarbonate levels could be monitored within the algae in real time, then further details of this mechanism may be revealed.

Organic pH-responsive fluorescent probes have been observed to be taken up within coccolithophores.[96] However, it appears this is a very inefficient process, as long incubation times were used (2 days). In some cases, it appeared necessary to remove the calcium carbonate shells via incubation in mild acid, in order to allow the probes to enter.

Responsive lanthanide probes of the type discussed in this chapter had previously only been used in applications with mammalian cells. Although the mechanisms of uptake, localisation and fate in such mammalian cell-lines is now fairly well understood, at the outset of this work it was unclear how algae or plant cells would respond to incubations of the lanthanide complexes.

Initially, the same procedure found to be successful with mammalian cells was examined. However, no internal localisation was observed after incubation of the complexes for up to 12 hours at concentrations of 50 μM. Concentrations were increased to 200 μM, and time periods

were studied at up to 3 days, but no convincing evidence was found to show that the probes had entered the cells.

An alternative method involved removal of the calcium carbonate shells, in the hope that this would enable uptake of the probes. To achieve this, the algae were briefly suspended in mild hydrochloric acid (pH 5) for one minute to remove the shells, and then the pH of the seawater solution was restored to its original value of 8.2. The probe was incubated at this stage, and aliquots taken periodically over the next two days and observed by microscopy. Again, no clear definitive uptake of the probe was observed. It was seen by microscopy that acid treatment successfully removed the calcium carbonate shells. After 24 hours they were seen to have partially grown back, and after 48 hours appeared to be fully grown. This suggests that acid treatment is not particularly harmful to the algae, and they continue to grow normally after the event.

As an alternative method for checking whether the probe had localised, emission spectra of the algae were recorded on a fluorimeter. After the time periods above, suspensions of the algae in the complex incubated seawater were taken. An emission spectrum was taken of the suspension at this point, and lanthanide emission could be observed, along with emission from the chloroplasts. Lanthanide emission did appear to be fairly significantly quenched. The algae were then centrifuged, and resuspended in fresh seawater a number of times, in order to remove any complex adhered to the surfaces and present within the seawater incubation. By the third wash, only chlorophyll emission was visible in suspensions of the algae, with the lanthanide emission found only in the seawater washings. This suggests that uptake of the complexes had not occurred.

Arguably, it is possible that the probe does localise within the algae, but is being quenched to such an extent that no lanthanide emission is observable. The intracellular composition of the algae is unknown.[127] Also, if the probe is localising to the mitochondria within the algae, and the algae contain only one mitochondrion then this may not be providing sufficient signal to be observed. Experimental methods should perhaps be extended to include ICP-MS, as this should provide evidence of any quantity of europium present. If detected, this can only come from the probes, so it could be concluded that it is quenching rather than non-uptake of the probes responsible for the lack of observable signal.

3.12 Measurement of bicarbonate levels in serum samples

The probes, [Ln·$\mathbf{L^{1-4}}$], were primarily designed with intracellular purposes in mind but need not necessarily be limited to such applications. Whilst they have been carefully designed to selectively measure concentrations of bicarbonate anions, crucially they function whilst withstanding competing biological backgrounds of other anionic species and proteins. Therefore, they could potentially perform equally well when applied to *in vitro* testing of biological fluids, which also contain such species.

Serum (blood plasma in which the blood cells have been removed) is one possible medium that could be tested. The rapid measurement of bicarbonate levels within serum is crucial in emergency medicine in determining acidosis.[128] There is a need for a new rapid, reliable test for measuring this parameter. Emission spectra can be acquired within a few minutes and so a ratiometric lanthanide based probe may offer a convenient way of achieving this.

The tandem europium/terbium emission method was selected for this application, as it had been highly successful for the *in vitro* calibration discussed previously. A bicarbonate titration was undertaken, using human serum as the background medium. To start, 1 ml of human serum was taken and any bicarbonate naturally present removed by lowering the pH to 5 and bubbling argon gas through for 10 minutes with gentle agitation. The pH was increased back to 7.4, immediately prior to the start of the titration. Sequential additions of a bicarbonate stock solution were added up to a final concentration of 40 mM. It was found that the observed intensity increase upon bicarbonate addition was greatly reduced when undertaken in a background of serum. There was also a reduction in the signal to noise ratio. This may be due in part to the increased turbidity of the serum compared to water, in addition to the higher degree of quenching. However, using a europium/terbium mix, similar to the microscopy experiments, allows a larger spectral window to be used (Fig. 51). Indeed, by calculating a red : green intensity ratio plotted as a function of added bicarbonate, a binding curve was obtained that could be used as a calibration curve thereby allowing values of bicarbonate concentration to be estimated for other serum samples.
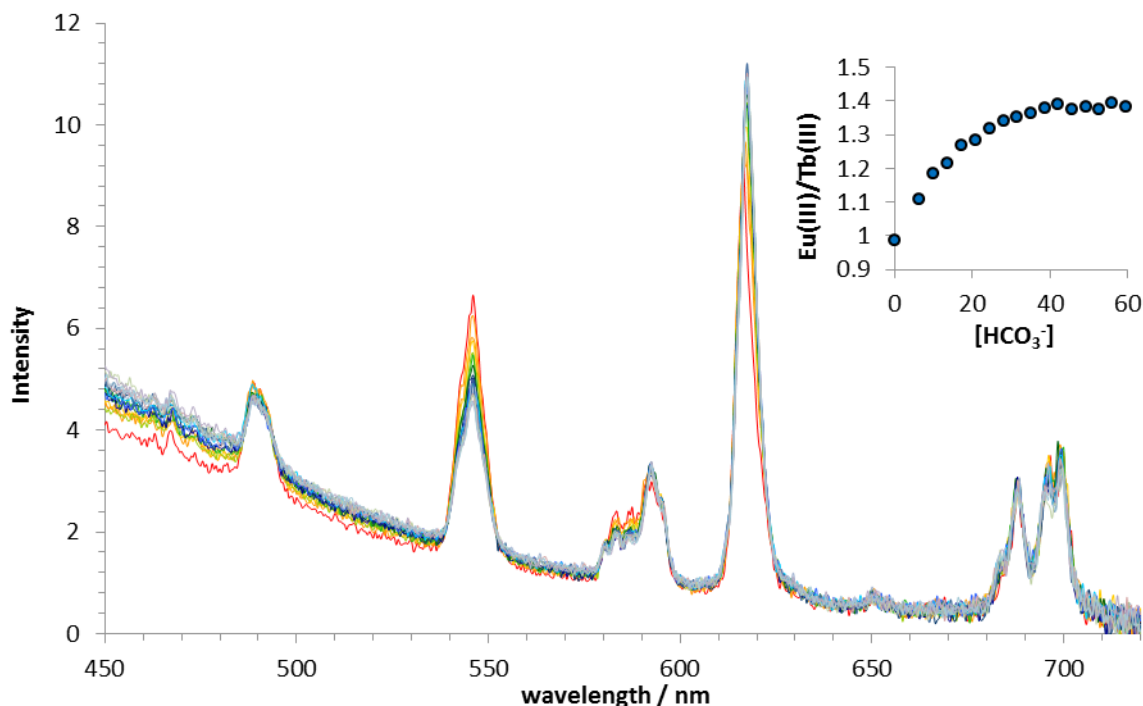
Fig. 51 Variation of the Ln(III) emission spectrum for [Tb·L^2]$^{3+}$: [Eu·L^2]$^{3+}$, following addition of sodium bicarbonate (H$_2$O, pH = 7.40 ± 0.05, 75 μM total complex, 298 K, I = 0.1 M NaCl, λ_{ex} =332 nm). Inset is a plot of the integrated intensity ratio (605 - 630 nm/535 – 555 nm) with [bicarbonate].

3.13 Conclusions

A novel series of lanthanide-based probes has been synthesised. They exhibit a selective binding to bicarbonate anions, as reported through changes in their emission profiles. The complexes are non-toxic to cells, and localise within the cellular mitochondria. Their responsive behaviour is maintained within the mitochondrial region, and has been used to measure the response to variations in external pCO$_2$.

The synthesis of the probes was undertaken via a route that has a number of common intermediates. This allows structurally analogous series to be created relatively easily. Reaction yields for key steps were optimised where appropriate, and this proved crucial, given the long linear sequence needed for the final complexes.

Sensitisation of the coordinated lanthanide ion occurs via an azaxanthone chromophore, which is linked to the macrocycle by an amide linkage. This sensitising moiety appears to be responsible for directing the complex to the mitochondria, behaviour that is consistent with earlier work where this moiety was previously incorporated into related complex structures. Modifications to the pair of *trans* amide arms allow variation of overall complex charge and

steric bulk. In this manner, a range of five ligands with an overall complex charge between +3 and -2 was synthesised.

Apparent binding affinities towards a range of anions were calculated. The change in spectral from was most significant following addition of bicarbonate. Binding of protein and bicarbonate to the europium complex was competitive at physiological values. As the coordination of bicarbonate increases europium emission intensity, whilst protein association leads to an overall quenching of emission, the increase in bicarbonate concentration in the presence of protein is signalled by an increase in overall europium emission intensity. The selective binding towards bicarbonate was maintained in a competitive background of other anions and protein. Particularly when a background of protein was present, the europium analogues exhibited a far greater spectral change than the analogous terbium complexes. This allows a tandem probe methodology to be created, where a mixture of both europium and terbium complexes of a common ligand are used at the same time. This has been used earlier with systems that report urate concentration changes in urine or serum, based on the differential quenching sensitivity of Tb and Eu analogues.[27]

The complexes have been used to monitor changes in the steady-state bicarbonate concentrations within the mitochondrial region of living cells. Upon cycling the pCO_2 between 3% and 5%, the emission spectral intensity of the europium complexes varied proportionally. With the corresponding terbium analogue, the change observed was <10%. Acetazolamide was shown to inhibit the spectral response of the europium probes. By using a mixture of europium and terbium complexes, it is possible to calibrate a red/green ratio, from which changes in bicarbonate concentrations can be monitored.

3.14 Future Work

The behaviour of the complexes within mammalian cells is highly promising. Now that the use of a tandem probe methodology using europium and terbium analogues together has been established, its potential could be further explored. For example, processes known to occur within the mitochondria could be inhibited or stimulated whilst the probes are incubated, and the spectral response measured.

Another experiment could be performed, similar to the inhibition of carbonic anhydrase activity by acetazolamide but using antimycin A. This is a compound which blocks complex III of the electron transport chain,[129] thus bicarbonate production should be halted. Alternatively,

carbonyl cyanide *m*-chlorophenyl hydrazine (CCCP) could also be used to block oxidative phosphorylation, which would also be expected to stop formation of mitochondrial CO_2.[130]

Further studies could be performed using the carbonic anhydrase inhibitor, acetazolamide. This was shown to lead to a reduction in the signal of europium emission, as it greatly slows down the conversion of mitochondrial CO_2 to bicarbonate. Eventually, given a long enough time period however, the signal may return to original values.

Conversely, the mitochondria could be stimulated such that an increase in production of bicarbonate occurs. This could potentially be achieved on whole cells by starving them in a medium deficient in pyruvate, and then feed them pyruvate back. If the cells contain a bicarbonate-responsive lanthanide probe, this may be accompanied by an increase in emission of the europium analogue relative to that of terbium.

Whilst the novel series of probes described in this chapter fulfill all the criteria set out in the introduction section, an improved set of probes could be created, based on the knowledge gained through this work. The area in which an improvement would be most useful is the quantum yield of the complexes. By requiring a more highly emissive probe to be made that also resists photobleaching. Such work is currently being undertaken, investigating alternative sensitising systems. It is hoped that these complexes will exhibit higher quantum yields and extinction coefficients. Key challenges remain however, as any new probe still needs to retain the ideal localisation profile, non-toxicity and selectivity profile for bicarbonate.

The bicarbonate responsive probes described were shown to be insensitive to fluctuations in pH over the range of 5 - 8. The pH changes within the mitochondria are also of interest, however. It would be interesting, and useful, to have a pH responsive probe that localises to the mitochondria and use this to monitor mitochondrial pH. Using these probes, it would be of interest to repeat the experiments described for the bicarbonate-responsive probes, such as examining the variation in response to pCO_2, with the pH-responsive probes and observe changes, if any, in pH during the time-course of the experiment. Together, the two sets of probes would give an increased understanding of the processes occurring.

4   pH Probes For The Lysosomes

4.1   Introduction

Chapter three began with a brief discussion of the importance of matching probe function with probe localisation, and this is an equally important issue here. Within the lysosomal compartments of cells, it is arguably the pH which is the most important parameter to measure. The lysosomes are the waste disposal compartments of cells, containing many different species. Measurement of individual anions is perhaps less important. Indeed, a bicarbonate probe for the lysosomes would be useless as the pH is typically around 4.5 meaning that virtually no bicarbonate would be present at this pH. Although the normal pH of a lysosome is around 4.5 to 6.5, abnormal pH is associated with a number of diseases, and the pH changes through the life-cycle of a lysosome.[131] Therefore, measurement of these values by a pH-dependent probe would be highly useful in assessing mechanisms involved in these diseases. Organic, fluorescent pH-dependent probes that localise to acidic compartments in cells,[78] such as the lysosomes, are available but as discussed in detail in the introductory chapter they are known to have significant drawbacks and are considered to be unreliable.[80, 84] There is a requirement for more efficient, improved pH-responsive probes for the lysosomes.

This chapter details the development of lanthanide-based pH-responsive probes. A number of designs are considered, in relation to meeting the combined aims of lysosomal distribution and a pH-responsive output over the relevant pH range of 4-6. The behaviour of promising candidates is discussed in terms of pH titrations, examining the influence of competing species such as anions and protein, and preliminary cell-based experiments.

4.2   The design of pH-dependent probes with an appropriate pH-dependent range

The final class of pH responsive lysosomal probes, which are described in detail at the end of this chapter, were only reached after examining a number of different types of complexes. These consisted of various chromophores and pH-dependent moieties. Their synthesis, along with a brief rationale explaining their design was given in chapter two. Although they are of limited use as pH probes for the lysosomal region of cells, lessons can be learnt about probe design from their results. It is also possible that they could find use in other applications.
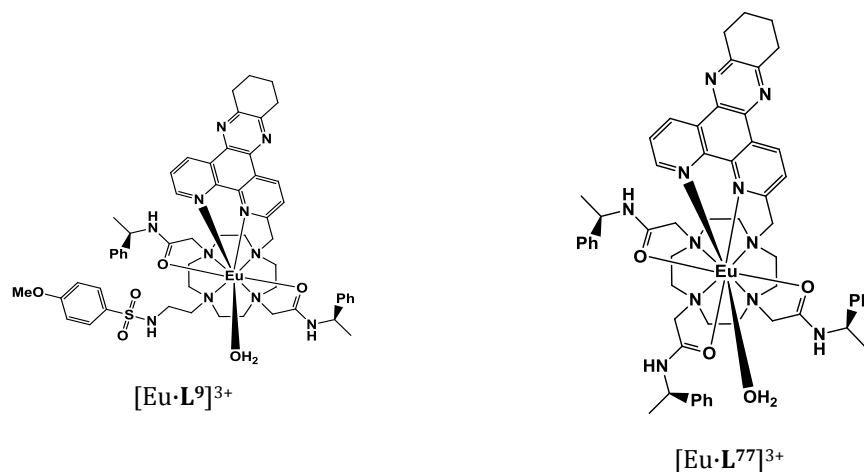
[Eu·**L**⁹]³⁺   [Eu·**L**⁷⁷]³⁺

4.2.1   The importance of the capping ligand

The complex, [Eu·**L**⁹]³⁺, was the first complex to be examined during this work. The structurally related complex, [Eu·**L**⁷⁷]³⁺, has been shown to exhibit a lysosomal distribution.[26] It was hoped that exchange of one of the amide pendant arms for a pH dependent sulfonamide moiety, would not alter this localisation profile. Instead, it was postulated that this would lead to a modulation in the europium spectral form, associated with pH-dependent sulfonamide nitrogen ligation.

The complex was synthesised as outlined in chapter two. The initial europium emission spectra taken at high and low pH appeared to show little change in the form of emission. To investigate this further, a full pH titration was undertaken over the range pH 3 – 9. Outside of these limits, decomplexation of the lanthanide ion may be possible, and it adequately covers the biological range which we are interested in. The titration was performed in a 0.1 M sodium chloride background, to maintain a constant ionic strength when adding small quantities of concentrated hydrochloric acid or sodium hydroxide to change the pH. The pH titration began at pH 9, and decreased by intervals of approximately 0.33 down to pH 3. The pH titrations were performed by acidification as this procedure minimises the risk of bicarbonate formation which may contaminate stock solutions of sodium hydroxide.

The pH titration of [Eu·**L**⁹]³⁺ showed no modulation of spectral form across the entire pH range (Fig. 52). There was a quenching of emission intensity as the pH was increased. Examination of any pair of bands or individual wavelengths gave rise to no change in their intensity ratios.
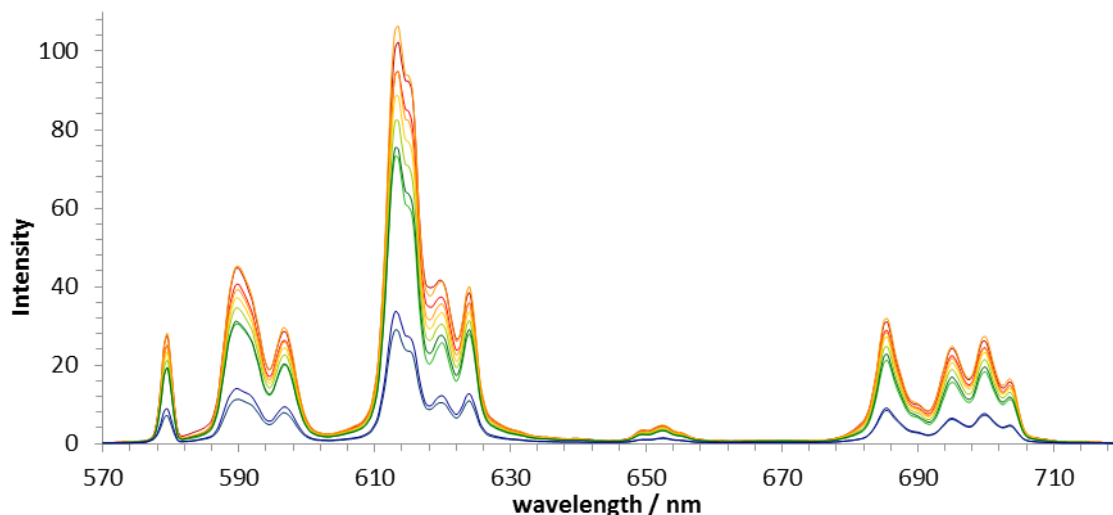
Fig. 52: Variation of the Eu(III) emission spectrum for $[Eu·L^9]^{3+}$ as a function of pH, from pH 4 (red) to 9 (blue). (H_2O, 50 µM complex, 298 K, I = 0.1 M NaCl, λ_{ex} = 340 nm).

It was expected that upon deprotonation of the sulfonamide nitrogen, it would bind to the metal centre causing a change in the spectral form. So, either the sulfonamide is not binding at all, or there is binding, but just not in a manner that causes a change in spectral form. Examination of the lifetimes of the excited states in H_2O and D_2O gave values for the number of coordinated water molecules at the limits of the titration (Section 2.4.2). At pH 3, the hydration state of the europium was 1.9, and at pH 9 this was 0.7. This indicates that upon moving from pH 3 to pH 9, a water molecule is displaced from the coordination sphere, suggesting that binding of the sulfonamide nitrogen is occurring.

It appears that binding of the sulfonamide may be occurring but without a change in spectral form. This is most likely because the sulfonamide is not binding at the capping axial position in the square antiprismatic coordination environment. As described in previous chapters, it is this feature which is the overriding influence upon spectral form for this class of complexes. In the related complex, $[Eu·L^{77}]^{3+}$, it is the pyridyl nitrogen from the chromophore which occupies this site and so this is presumably also true for $[Eu·L^9]^{3+}$. Binding of the sulfonamide presumably occurs in the plane of the amide oxygen donors, displacing a water molecule and causing no change to the spectral form. The decrease in luminescence intensity upon sulfonamide binding may be associated with the steric bulk of the sulfonamide or a π-π interaction between the dpqC chromophore and the phenyl group on the sulfonamide partly quenching the intermediate dpqC excited state.

As no ratiometric output was gained from this probe, it offers no use as an intracellular probe. It does however serve to highlight the importance of this geometric aspect in probe design. Evidently, there is a need to ensure that the reversibly bound donor site occupies an axial position, in this class of complexes.

4.2.2 The importance of relatively simple changes to the emission spectra and ratiometric analysis

The complex [Eu·**L**^{10}]$^+$ has a vacant site free in the axial position, so binding of the methyl sulfonamide is possible at this important position in this case. The anionic arms derived from alanine were incorporated, as they had previously been shown to inhibit interference from anion binding in pH-responsive probes.[69]
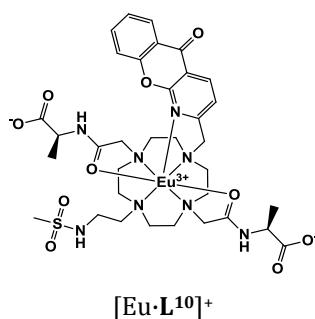
[Eu·**L**^{10}]$^+$

A pH titration of [Eu·**L**^{10}]$^+$ was carried out over the pH range of 9 to 3, in a 0.1 M sodium chloride background (Fig. 53). For simplification, the $\Delta J = 2$ band is shown separately in Fig. 54, as it can be seen that the spectra overlap each other. Upon moving from pH 3 to pH 5 there is an
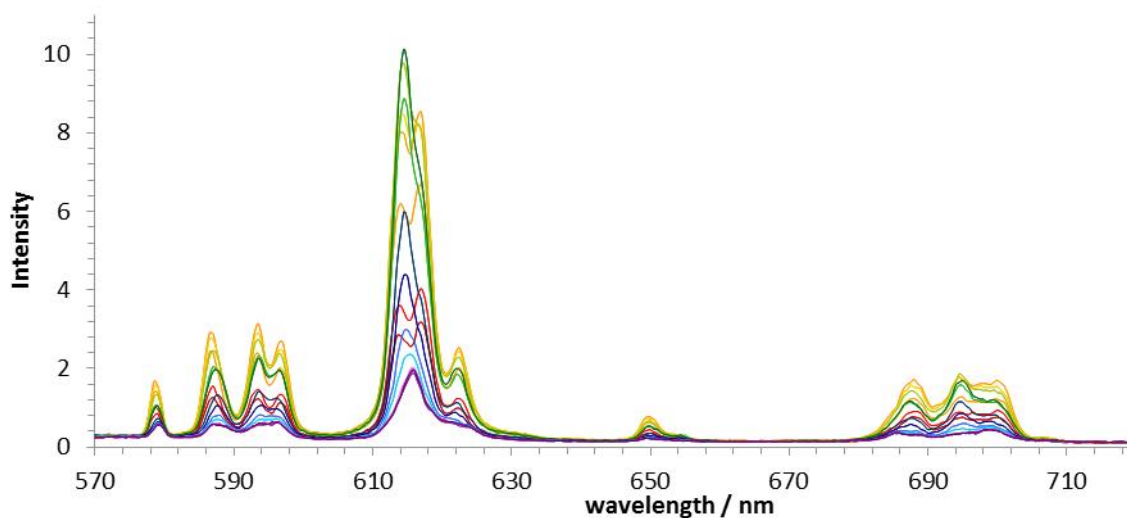
Fig. 53: Variation of the Eu(III) emission spectrum for [Eu·**L**^{10}]$^+$ as a function of pH (H$_2$O, 40 μM complex, 298 K, I = 0.1 M NaCl, λ_{ex} = 340 nm).
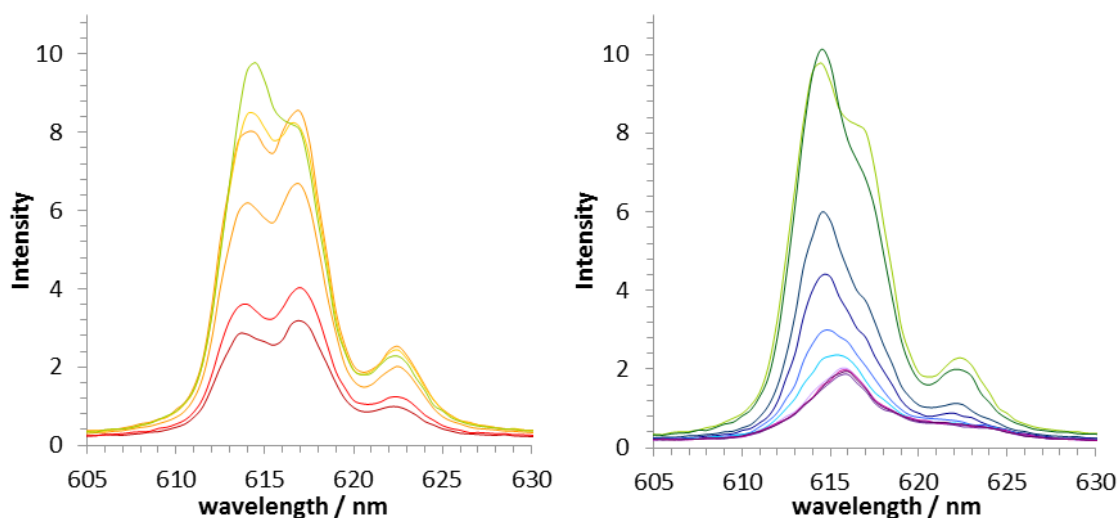
Fig. 54: Variation of the Eu(III) emission spectrum for [Eu·**L^{10}**]$^+$ as a function of pH, (H$_2$O, 40 μM complex, 298 K, I = 0.1 M NaCl, λ_{ex} = 340 nm). (*left*) shows the pH range from pH 3 (red) to pH 5.5 (green), (*right*) shows the pH range from pH 5.5 (green) to pH 9 (blue),

increase in emission intensity, whilst the form of the spectra remains largely constant across this pH range (left, Fig. 50). At pH 5, the form of the spectra changes drastically, and following this point, the emission intensity decreases. The most obvious differences between the two limiting spectral forms are an increased splitting within the bands at low pH. The main band within the ΔJ = 2 manifold centered at 615 nm is split into two, and there is also another band emerging at 622 nm at low pH. This slightly unusual behaviour suggests there may be two processes contributing to the change in spectral form and intensity.

Examination of the excited state lifetimes in H$_2$O and D$_2$O revealed that the number of coordinated water molecules switched from 1.4 to 0.5 upon moving from pH 3 to pH 9, presumably as sulfonamide ligation takes place. This is consistent with displacement of a coordinated water molecule upon binding of the sulfonamide nitrogen. This complex is an improvement on the dpqC-based probe, [Eu·**L^9**]$^{3+}$, in the previous section in that sulfonamide binding causes a change in the spectral form. However, the nature of the increase and then decrease in intensity limits the applicability of the probe through ratiometric analysis, however. A plot of the ΔJ = 2 / ΔJ = 1 ratio highlights this (Fig. 55, left). For a calculated ratio, there are two possible pH values which this could correspond to centered around pH 5. Close examination of the spectral form does allow each case to be distinguished, when this information is available.
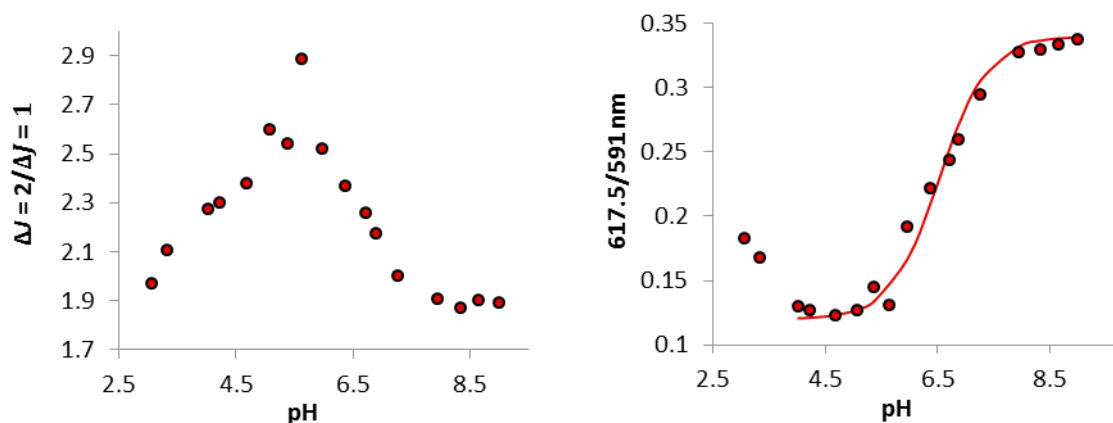
Fig. 55: Plots of ratios as a function of pH for [Eu·**L^{10}**]$^+$. (*left*) the ΔJ = 2 / ΔJ = 1 ratio and (*right*) the 617.5 / 591 nm ratio

The large change in the spectral form makes it likely that binding of the sulfonamide is occurring as required at the axial position. As higher pH values are approached, the sulfonamide binds and effectively locks the pendent arms into a more rigid conformation, leading to a reduced splitting within the spectra at this point. The subsequent decrease in emission intensity could occur because binding of the sulfonamide has an increased steric demand at the metal centre, and might weaken the azaxanthone-lanthanide interaction. If the azaxanthone nitrogen is no longer directly bound, the distance dependent energy transfer step will be less efficient, accounting for the weaker emission observed. Displacement of a coordinated azaxanthone moiety has been reported recently, when HSA bound to a bis-azaxanthone europium complex.[132]

The use of integrated area ratios was shown to be ineffective at constructing pH curves. Taking the emission at a wavelength of 591 nm to that at 617.5 nm does lead to a curve for which a good fit of the data can be found (Fig. 55, right). Differentiation of the curve can abstract a pK_a value for this, which was calculated to be 6.5. This value is perhaps too high for measurement of lysosomal pH which is usually 1 – 2 units lower. It is likely that in competing backgrounds, this pK_a would alter, and so therefore required investigation.

The spectral response of [Eu·**L^{10}**]$^{3+}$ to pH is unaffected by the presence of protein. Performing the pH titration in a background of 0.4 mM HSA, led to a very similar spectral output, in terms of intensity changes and spectral form. The insensitivity of the observed spectra to the presence of protein is a promising attribute, as it suggests that the system may be applicable for biological samples. The effect of added anions was also investigated. Addition of a mixed anion background containing, 30 mM bicarbonate, 2.3 mM lactate, 1.3 mM phosphate, 0.13 mM citrate
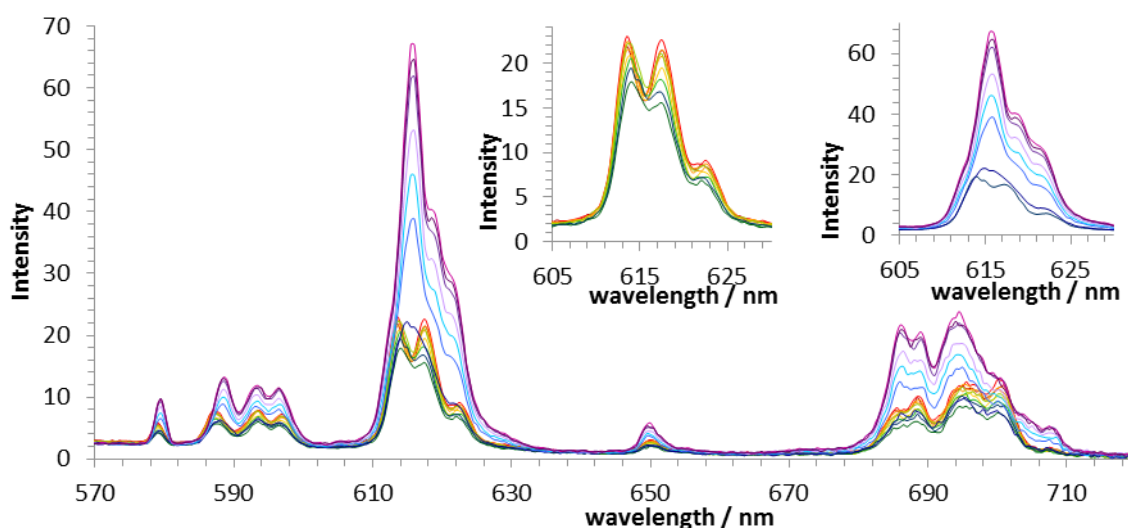
Fig. 56: Variation of the Eu(III) emission spectrum for [Eu·**L^{10}**]$^{3+}$ as a function of pH in a background of protein and 30 mM sodium bicarbonate, 2.3 mM sodium lactate, 1.3 mM sodium phosphate, 0.13 mM sodium citrate and 0.1 M sodium chloride. (H$_2$O, 40 μM complex, 298 K, I = 0.1 M NaCl, λ_{ex} = 340 nm). Inset shows the ΔJ = 2 region highlighted for (*left*) pH 3 to 5, and (*right*) pH 5 to 9.

and 100 mM chloride caused a very different response to pH in terms of the spectral output (Fig. 56). At low pH values the form is very similar to that in a 0.1 M sodium chloride background, although increasing pH leads to a very slight decrease in intensity as opposed to a large increase in intensity. Above pH 6, there is a very large increase in emission intensity across the spectral window, but particularly within the ΔJ = 2 manifold. A plot of the integrated ratio of the ΔJ = 2 band vs. ΔJ = 1 band shows negligible change below pH 6, and a sharp increase in the ratio up to pH 8 at which point it levels out (Fig. 57). The apparent pK$_a$ defining this behaviour is 7.00 (± 0.05) which can be ascribed to bicarbonate binding.

A pH titration in a fixed background of 30 mM sodium bicarbonate confirmed this behaviour (Fig. 59), as the large increase in spectral intensity at high pH was also observed in this case
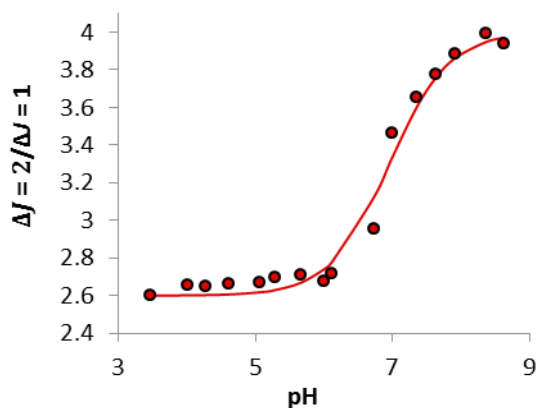
Fig. 57: Plot of the ΔJ = 2 / ΔJ = 1 ratio as a function of pH for [Eu·**L^{10}**]$^{3+}$ in a background of mixed anions and protein. pK$_a$ = 7.0 ± 0.05.
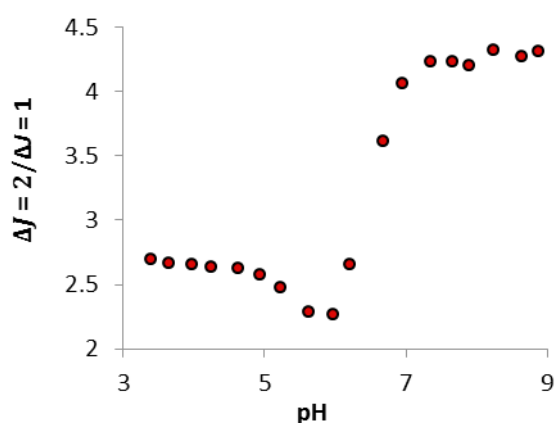
Fig. 58: Plot of the ΔJ = 2 / ΔJ = 1 ratio as a function of pH for [Eu·**L^{10}**]$^{3+}$ in a background of 30 mM sodium bicarbonate.

both in terms of changes in form and relative intensity (compare Fig. 56 and Fig. 59).
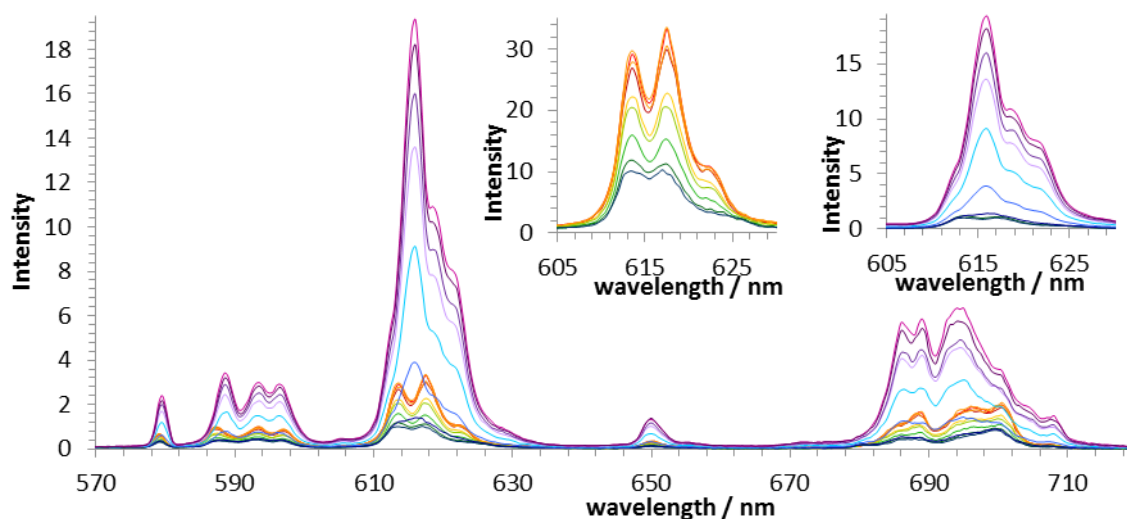
Fig. 59: Variation of the Eu(III) emission spectra for [Eu·**L**^{10}]$^{3+}$ as a function of pH in a background of 30 mM sodium bicarbonate. (H$_2$O, 40 μM complex, 298 K, I = 0.1 M NaCl, λ_{ex} = 340 nm).

Finally, the response to pH was studied by following changes in the circularly polarised luminescence of this complex. Circularly polarised emission spectra were recorded at the two pH limits and also at pH 5.6 which is approximately where the cross-over point is between the two forms (Fig. 60). A background of 0.1 M NaCl was used. Changes in the CPL spectrum were evident between the two pH limits. The ΔJ = 1 manifold changes from a (-+) signal sequence at pH 3 to a (++-) sequence at pH 9 whilst the ΔJ = 2 manifold changes from a (++-) sequence to a (--) sequence. This shows that it is possible to follow the binding of the sulfonamide by changes in the circularly polarised luminescence and that binding of the sulfonamide changes the chirality at the metal centre. This is the first example of signalling a pH change using lanthanide based CPL.

Due to this signigicant change in form of the CPL emission, it may also be possible to use ratiometric analysis to analyse pairs of bands and gain information that is otherwise hidden within the total emission spectra. For example, the ratio of the ΔJ = 2 / ΔJ = 1 bands is approximately 2.0 at both pH 3 and pH 9. If a ratio is taken using data from the corresponding CPL spectra, then the values are substantially different. Thus, by taking a ratio of the ΔJ = 2 / ΔJ = 1 bands a value of +0.2 is found at pH 3 and -8.3 at pH 9, allowing the different pH values to be distinguished clearly.
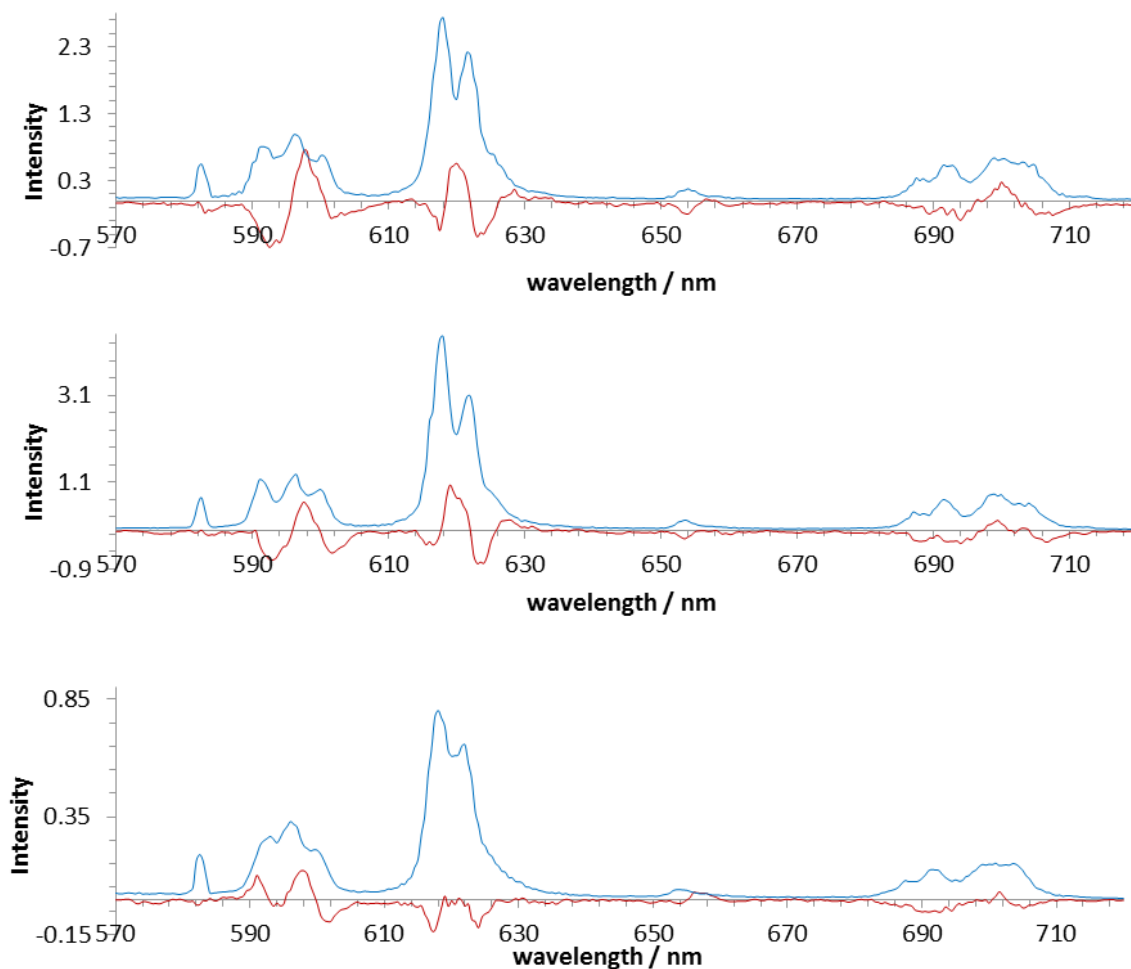
Fig. 60: Circularly polarised luminescence spectra (*red*) and total emission spectra (*blue*) of [Eu·**L**¹⁰]³⁺ at pH 3 (top), pH 5.6 (middle) and pH 9 (bottom). (295 K, I = 0.1 M NaCl)

4.2.3 The importance of pK$_a$ and withstanding a competitive biological background

The europium azathioxanthone complex [Eu·**L**¹¹]³⁻ contains a non-coordinating chromophore. This should mean that the distance between this sensitiser and the europium should remain approximately constant during any reversible binding event. Thus, the decrease in emission intensity associated with binding by the pH-dependent donor group should not be observed .

The emission spectra at both low and high pH were shown in the previous chapter and a large amount of ligand fluorescence was observed, relative to the intensity of the lanthanide emission.

[Eu·L^{11}]$^{3-}$
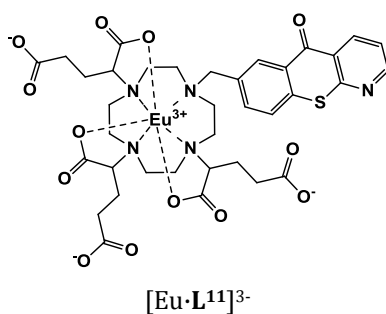
A pH titration was first undertaken in a background of 0.1 M sodium chloride. The lanthanide emission intensity decreased in response to lowering the pH. The fluorescence from the ligand also decreased. The relative form of the lanthanide spectrum showed little change, and as such it was not possible to extract any information from the usual $\Delta J = 2$ / $\Delta J = 1$ ratio analysis. Plotting the ratio of the $\Delta J = 2$ band to ligand fluorescence did however yield some information. There was a gradual increase in this ratio from 3 to 6, possibly associated with binding of the terminal carboxylate which will occur over this region.[115] Between pH 6 and 8 there was no change in this ratio, and then a very small increase from pH 8 to 9, possibly due to the competitive binding of bicarbonate.

The titration of [Eu·L^{11}]$^{3-}$ was then undertaken in a mixed anion background (Fig. 61), in a background of protein (Fig. 62), and with both mixed anions and protein present (Fig. 63). In a background of mixed anions containing chloride, lactate, phosphate, citrate and bicarbonate there was an overall increase in emission intensity (Fig. 61). Ligand fluorescence increased by a
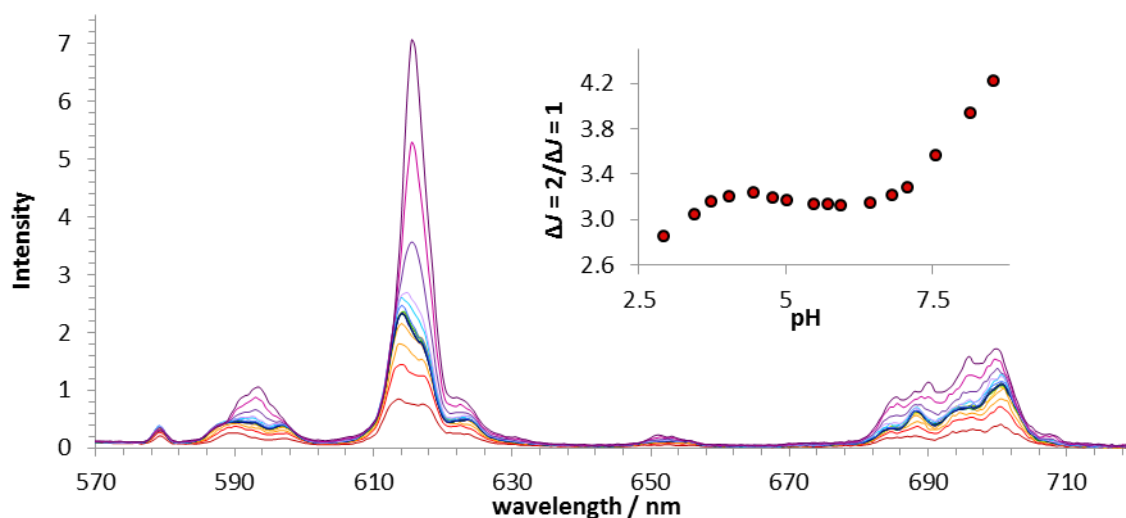
Fig. 61: Variation of the Eu(III) emission spectrum for [Eu·L^{11}]$^{3-}$ as a function of pH in a background of 30 mM sodium bicarbonate, 2.3 mM sodium lactate, 0.13 mM sodium citrate and 0.9 mM sodium phosphate (H$_2$O, 40 μM complex, 298 K, I = 0.1 M NaCl, λ_{ex} = 380 nm).

very small amount as the pH increased. Europium emission intensity increased steadily from pH 3 to pH 4.5. It then remained constant until 7, and there was a strong increase up to pH 9. This second increase was accompanied by a change in spectral form, and is probably due to bicarbonate binding in this pH régime. A plot of the pH dependence of the $\Delta J = 2 \,/\, \Delta J = 1$ ratio for this system is shown in the insert in Fig. 57.

In the presence of protein, the titration of [Eu·**L**^{11}]$^{3-}$, with respect to pH showed an increase in europium emission from pH 3 to around pH 5.8, and then from pH 5.8 till 9 there was a very small decrease in emission intensity (Fig. 62). The $\Delta J = 2 \,/\, \Delta J = 1$ ratio also defined variation of this change .
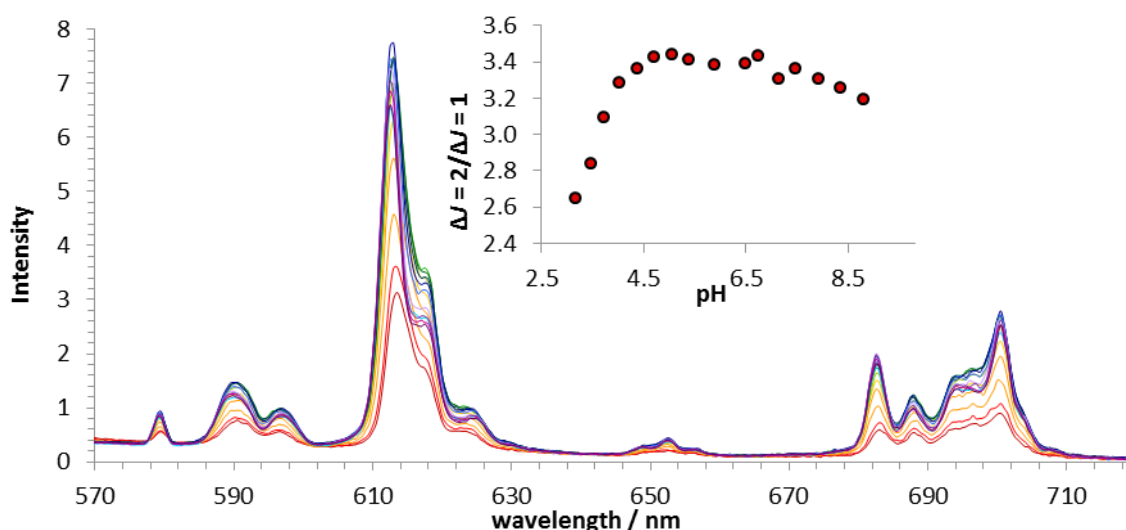
Fig. 62: Variation of the Eu(III) emission spectrum for [Eu·**L**^{11}]$^{3+}$ as a function of pH in a background of protein (H$_2$O, 40 µM complex, 298 K, I = 0.1 M NaCl, λ_{ex} = 380 nm).

When performing the titration in a background containing both the mix of anions and protein that the potential difficulties of using [Eu·**L**^{11}]$^{3-}$ in a biological context were really highlighted. The response of the complex to pH in this background was a large increase in emission intensity from pH 3 to 6, but then a very large substantial decrease from pH 6 to 9 (Fig. 63). Ratiometric analysis using pairs of bands revealed the complexity of the system. Given the vastly different response of the probe to pH in different backgrounds, this particular complex is unlikely to be useful as a probe of pH.
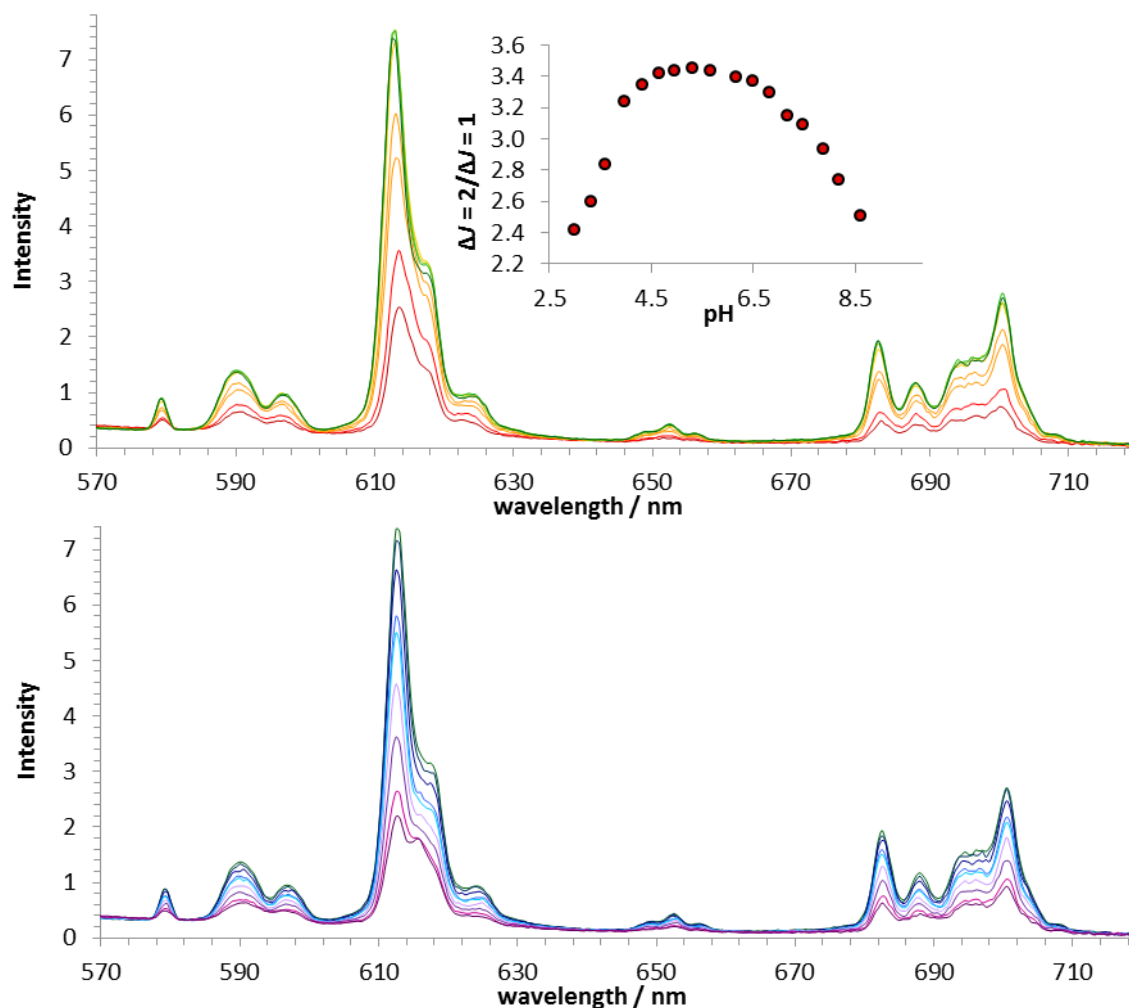
Fig. 63: Variation of the Eu(III) emission spectrum for [Eu·**L**^{11}]$^{3-}$ as a function of pH in a background of mixed anions and protein (H$_2$O, 40 μM complex, 298 K, I = 0.1 M NaCl, λ_{ex} = 380 nm).

4.3   A series of probes for assessing lysosomal pH based upon sulfonamide ligation

The probes described in the previous section suffered from various problems, including a pK$_a$ lying outside the lysosomal pH range, sensitivity to interference from anions and protein, and an unsuitability for simple ratiometric analysis. It had been observed that the bicarbonate series of probes, discussed throughout chapter three, exhibited a lysosomal distribution at extended time-points approaching 24 h. They had been shown to withstand competing backgrounds and were highly successful in providing ratiometric outputs. They also contained a free cyclen NH and so it was postulated that incorporating a pH sensitive moiety onto this position would enable the complexes to be used as pH sensors. This does, of course, assume that lysosomal localisation would still exist and the complexes would remain non-toxic. It was hoped that the

complex would no longer exhibit such a high response to the presence of bicarbonate, as the sulfonamide substituent would increase the steric demand at the metal centre, and binding of bidentate ligands such as bicarbonate would then be disfavoured.

The synthesis of such probes was described in chapter two. The initial work to assess their performance involved a series of spectral titrations, examining the changes in emission intensity and spectral form in response to pH in various background media.
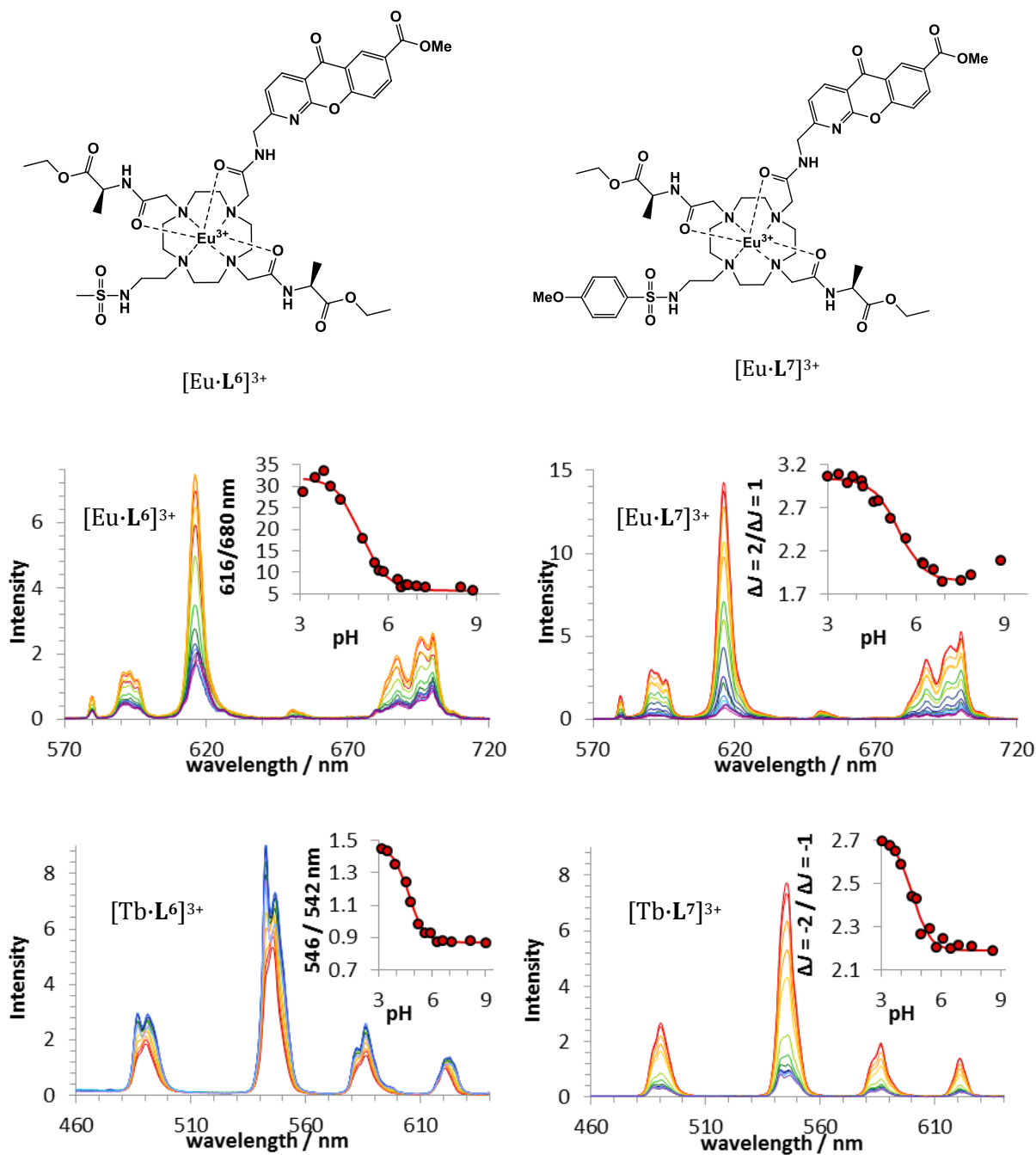
Fig. 64: Variation of the Ln(III) (Ln = Eu, Tb) emission spectrum as a function of pH (H$_2$O, 40 μM complex, 298 K, I = 0.1 M NaCl, λ_{ex} = 332 nm). (*top left*) [Eu·**L^6**]$^{3+}$, (*top right*) [Eu·**L^7**]$^{3+}$, (*bottom left*) [Tb·**L^6**]$^{3+}$ and (*bottom right*) [Tb·**L^7**]$^{3+}$.

Firstly, the spectra were recorded in aqueous salt solution (0.1 M sodium chloride, maintaining a constant ionic strength) (Fig. 64). The complexes $[Eu \cdot L^6]^{3+}$ and $[Eu \cdot L^7]^{3+}$ behaved quite similarly to one another. Each showed a very large increase in emission intensity across the spectral window, as the pH was decreased from 9 to 3. There was no obvious change to the form of the emission, which appeared very similar for each complex. For $[Eu \cdot L^7]^{3+}$, ratiometric analysis comparing the $\Delta J = 2 / \Delta J = 1$ ratio gave a pK_a for sulfonamide binding of 5.4 ± 0.1. The small deviation and increase observable approaching pH 9 is possibly due to the influence of dissolved bicarbonate.

For $[Eu \cdot L^6]^{3+}$, ratiometric analysis of the bands could not yield an appropriate binding curve. Examination of the wavelengths at 616 nm versus 680 nm, where there appeared to be an apparent isoemissive point, did yield an appropriate sigmoidal curve. The pK_a for this complex was slightly lower, at 5.1 ± 0.1.

In contrast, the terbium emission spectra of the same two ligands behaved quite differently to one another. There are some similarities. Both showed a large change in the form of the emission, between low and high pH. At pH 3, the form of the emission was rather featureless, and consisted of four broad bands, corresponding to each of the main emissive transitions. At pH 9, each of the first three bands became quite clearly resolved into two. They differed in that whilst $[Tb \cdot L^6]^{3+}$ exhibited a decrease in emission upon moving from pH 9 to pH 3, $[Tb \cdot L^7]^{3+}$ increased its emission intensity. The increase in the emission intensity behaviour of $[Tb \cdot L^7]^{3+}$ matched that of the europium analogues which also increased, and by approximately the same amount.

It is $[Tb \cdot L^6]^{3+}$ which appears to be the anomaly in this mini-series, although the change in emission is less than that for the others. Using the $\Delta J = 2 / \Delta J = 1$ ratio to analyse the data for $[Tb \cdot L^7]^{3+}$, a pK_a of 4.6 ± 0.1 was obtained. For $[Tb \cdot L^6]^{3+}$ individual wavelengths were required, and a plot of 546 nm / 542 nm gave a pK_a for sulfonamide binding of 4.7 ± 0.1 with this complex.

A larger emission intensity decrease for the complexes of L^7 realtive to L^6 was observed, this may be due to intramolecular charge transfer processes quenching emission to a greater degree between the *para*-methoxy sulfonamide and the azaxanthone, when the sulfonamide is bound to the metal centre and brought into close proximity at high pH.

Comparing the pK_a values of the complexes, each terbium analogue had lower pK_a values than the europium complexes, about 0.5 units lower. Whilst the values for the two terbium

complexes are roughly similar to one another, [Eu·**L**^{7}]$^{3+}$ has a slightly higher value than [Eu·**L**^{6}]$^{3+}$. Terbium (III) is more charge dense, so the Tb-sulfonamide interaction is stronger than the Eu-sulfonamide interaction. Thus, it is harder to protonate the nitrogen in the terbium analogues, leading to the lower pKa observed with terbium compared to europium.

[Tb·**L**^{6}]$^{3+}$ is the anomaly in the series in that it is the only complex where an increase in emission intensity occurs as pH rises. This is tentatively ascribed to the dominating effect of disruption to the intramolecular hydrogen bonding within the chromophore unit. Pertubation to hydrogen bonding at low pH causes modulation of the sensitiser to lanthanide distance, and effects the efficiency of energy transfer leading to a decrease in emission intensity at low pH, observed for the [Tb·**L**^{6}]$^{3+}$ analogue. With [Tb·**L**^{7}]$^{3+}$, the previously mentioned effect of intramolecular charge transfer from the aryl sulfonamide dominates, and so it instead at high pH that a large decrease in emission intensity is observed.

As throughout this thesis, the next stage was to examine the effect of added protein or anions. All four pH titrations were repeated in a fixed salt background containing 0.4 mM human serum
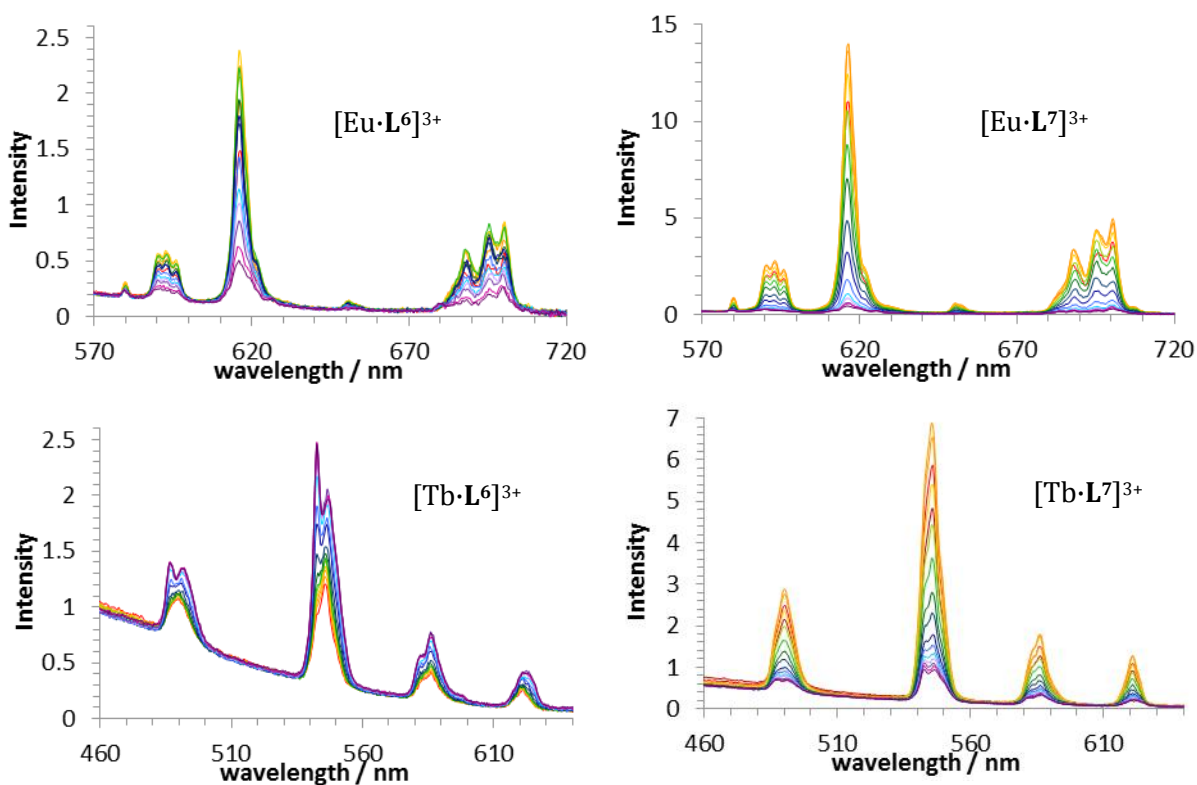
Fig. 65: Variation of the Ln(III) (Ln = Eu, Tb) emission spectrum as a function of pH in a fixed background of 0.4 mM human serum albumin (H$_2$O, 40 μM complex, 298 K, I = 0.1 M NaCl, λ_{ex} = 332 nm). (*top left*) [Eu·**L**^{6}]$^{3+}$, (*top right*) [Eu·**L**^{7}]$^{3+}$,(*bottom left*) [Tb·**L**^{6}]$^{3+}$ and (*bottom right*) [Tb·**L**^{7}]$^{3+}$.

albumin (Fig. 65). The relative form and intensity changes with respect to the changes in pH were very similar to those observed without the background of protein. [Tb·L⁶]³⁺ still exhibited the opposite behaviour to the other three. It is promising that the spectral response appear unaffected by the presence of protein, and suggests that the complex may be useful in biological situations.

Working systematically through these titrations, the final set were performed in a background of both the mixed anions and protein. Changes were more clearly defined for the [Ln·L⁷]³⁺ duo of probes. Ratiometric analysis, examining the integrated area ratios of the two main bands in the spectra gave a pK_a of 5.9 ± 0.05 for both the europium and terbium analogue. For [Ln·L⁶]³⁺ it was not possible to use area ratios to plot accurate pH curves. It was, however, possible to find individual wavelengths which provided this information. The 620 nm / 615.5 nm ratio from the europium spectra yielded a pK_a of 6.8, whilst the 545.5 nm / 542.5 nm ratio from the terbium spectra gave a slightly lower pK_a of 6.5.
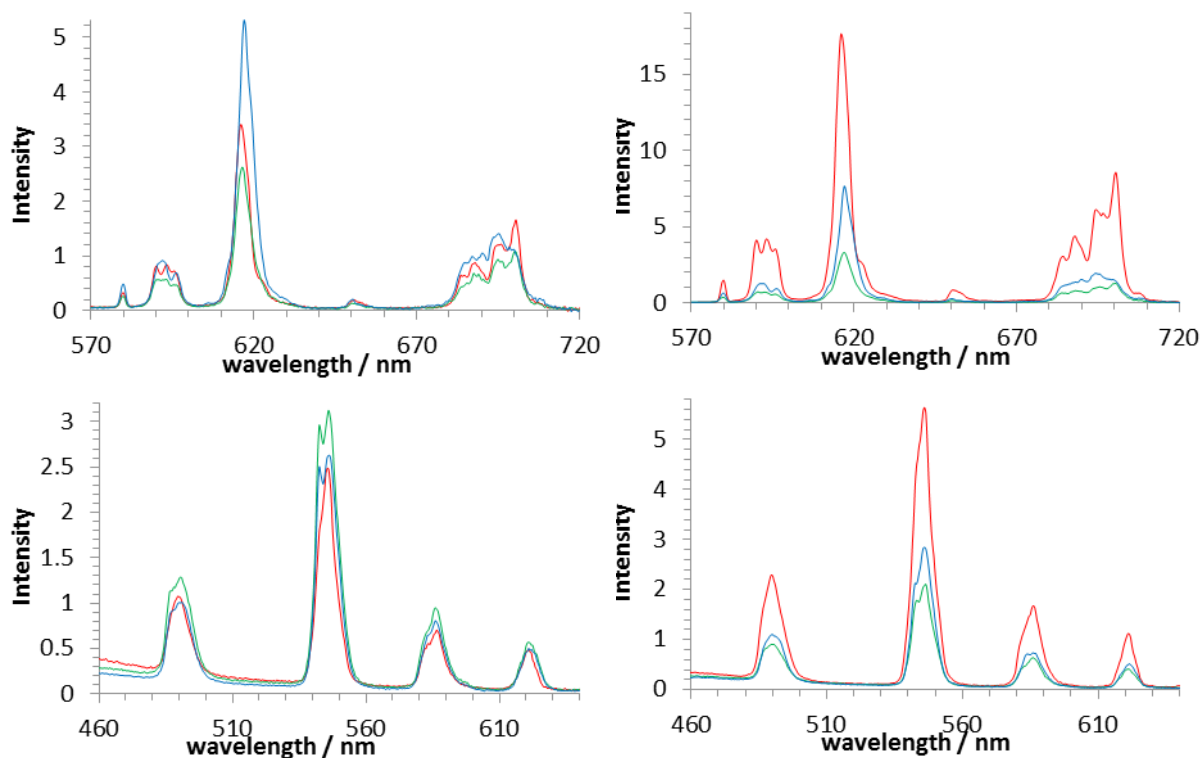
Fig. 66: Variation of the Ln(III) (Ln = Eu, Tb) emission spectrum as a function of pH in a fixed background of 2.3 mM lactate, 0.9 mM phosphate, 0.13 mM citrate and 30 mM bicarbonate (H₂O, 40 µM complex, 298 K, I = 0.1 M NaCl, λ_{ex} = 332 nm). (*top left*) [Eu·L⁶]³⁺, (*top right*) [Eu·L⁷]³⁺,(*bottom left*) [Tb·L⁶]³⁺ and (*bottom right*) [Tb·L⁷]³⁺.

4.4 Using a red : green ratiometric analysis

In chapter three, fluctuations in bicarbonate concentrations were measured, both *in vitro* and *in cellulo,* using a ratio of the europium to terbium emission intensity. This worked particularly successfully when applied to the microscopy experiments and it was hoped to extend this method to the lysosomal pH probes.
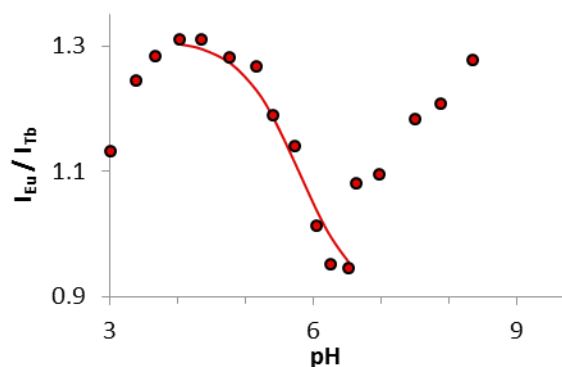
Fig. 67: Ratio of the europium emission versus terbium emission with respect to pH for [Ln·**L⁶**]³⁺

A mixture of the europium and terbium complexes of **L⁶** were taken together and subjected to a pH titration over the range of pH 3 to 9. A ratio of the $\Delta J = 2$ at 605 – 630 nm band of the europium spectrum was taken versus the $\Delta J = -1$ band of terbium at 534 – 550 nm (Fig. 67). At the two extremes of the titration, the data tails off in opposite directions. Over the relevant pH range of interest the usual sigmoidal curve is apparent. This yields a pK_a value of 5.8. This value is higher than that observed when calculating the pK_a using changes within one of the lanthanides only which were 5.4 and 4.7. If greater signal intensity is required, then using europium to terbium intensity ratios in this manner may offer the most simple option. Alternatively, it offers a way of tuning the pK_a of the system. Using the same ligand, **L⁶**, can lead to pK_a's of 4.7, 5.4 or 5.8 depending on whether the lanthanide used is terbium, europium or a mixture of the two, respectively. The difference observed between europium and terbium analogues of a common ligand is again likely to be due to the stronger charge density of terbium making the sulfonamide nitrogen harder to protonate.

4.5 Analysis of the complexes using changes in the circularly polarised luminescence

The complexes are amenable to analysis examining their circularly polarised luminescence. It had been shown for the structurally related bicarbonate series of probes, that binding of anions

induced a change in the chirality at the metal centre. It is likely that binding of the sulfonamide arm may also cause this, in the case of this series of probes.

[Tb·**L⁶**]³⁺ had been shown to be the only complex in the series to demonstrate an increase in emission intensity upon increasing pH. The CPL spectrum of this complex was taken at both low and high pH (Fig. 68). Circularly polarised emission was observed in each case. The most intense emission arose from the ΔJ = -1 band at 545 nm, and this was accompanied by a significant change in the circularly polarised emission depending on pH. This behaviour is consistent with a distortion of the complex geometry (ie. the CPL is at a maximum when the twist angle about the principal axis defining the ring N_4 and oxygen donors is 22.5°) (Section 1.1.4) upon binding by the methyl sulfonamide. Emission dissymmetry values are considerably higher for the complex when taken at pH 9, which corresponds to when the sulfonamide nitrogen is bound (Table 18).
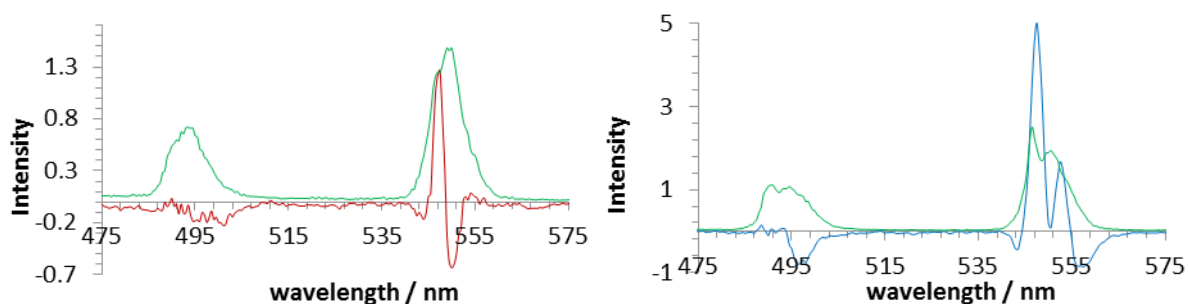
Fig. 68: Total emission spectra (green) and circularly polarised luminescence spectra (red = pH 3, blue = pH 9) of [Tb·**L⁶**]³⁺ at pH 3 (*left*) and pH 9 (*right*). (295 K, I = 0.1 M NaCl).

Table 18: Emission dissymmetry factors (g_{em}) at pH 3 and pH 9 for the maxima/minima of the transitions within the ΔJ = -1 manifold for [Tb·**L⁶**]³⁺.

pH 3	pH 9
(548 nm) +0.051	(548 nm) +0.125
(551 nm) -0.022	(553 nm) +0.057
	(560 nm) -0.213

Given the change in CPL spectra observed upon changing pH, it should be possible to follow a pH titration in terms of the variation of the emission dissymmetry factor. This is shown in Fig. 69 for $[Eu \cdot \mathbf{L^7}]^{3+}$, in which the emission dissymmetry factor, calculated at 632 nm, is examined as a function of pH. Fitting a curve to the data yields a pK_a of 5.5 ± 0.1. This is in good agreement with data calculated using the $\Delta J = 2 / \Delta J = 1$ ratio of the total emission, which estimated the pK_a to be 5.4 ± 0.1. This is the first time that CPL has been used to assess the pK_a of an emissive lanthanide complex.
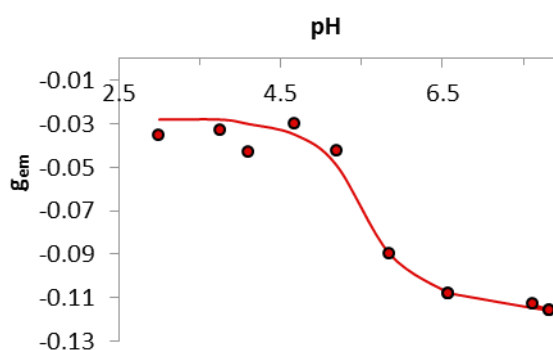
Fig. 69: Variation in the emission dissymmetry factor (632 nm) as a function of pH for $[Eu \cdot \mathbf{L^7}]^{3+}$

4.6 Cellular localisation behaviour

The cellular localisation of the probes needed to be established before further microscopy experiments could be performed. The complexes in this series closely resembled the bicarbonate probes in the previous chapter which showed a mitochondrial distribution, before shuttling to the lysosomes. All previous analogous complexes, in which an azaxanthone sensitiser was linked to the cyclen framework *via* an amide linkage, had shown this distribution pattern.[2]

The localisation experiments were performed in a similar manner to that described in chapter 3. Mouse skin fibroblast cells (NIH-3T3) were incubated with each complex (50 µM) for several different time periods. For the final 5 minutes of incubation, the commercially available LysoTracker™ probes were added, in order to assess when the lysosomal localisation was reached. Each of the complexes in this series behaved in a similar fashion to one another.

The localisation of [Tb·**L⁷**]³⁺ is shown in Fig. 70, along with the emission from LysoTracker Red. Overlaying of the two image channels shows a very high degree of co-localisation, and indicates that the complexes are localising to the lysosomes, at time periods of between one and four hours. This is in contrast to other complexes containing an amide coordinating azaxanthone, which exhibited a mitochondrial distributions at these time periods, and only showing a lysosomal distribution at much longer time-points.
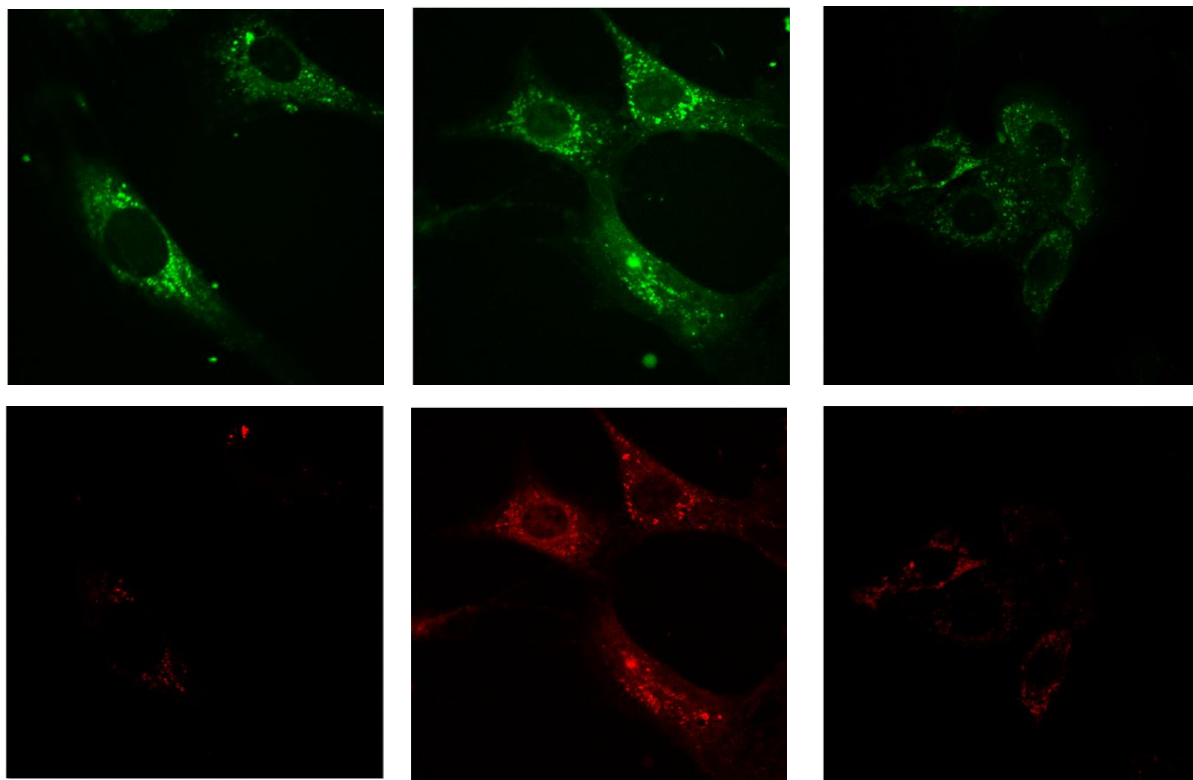
Fig. 70: Confocal microscopy images for [Tb·**L⁷**]³⁺ (*top*), 50 μM complex, (*left*) 1h incubation, (*middle*) 2h incubation, (*right*) 4h incubation. Lower three images show the corresponding LysoTracker Red emission.

The inclusion of a sulfonamide arm has altered the localisation profile. This is however, highly useful for the application in which the probe is intended. It is no longer necessary to wait for at least 10 h for a lysosomal distribution; and instead, the results are achieved within one hour.

4.7 Cytotoxicity studies

The pH-responsive complexes [Ln·**L⁶⁻⁸**]³⁺ were assessed for their cytotoxicity. The MTT assay, described in chapter three was performed, looking at incubations of up to 200 μM for 24 hours using mouse skin fibroblast (NIH-3T3) cells. As found for the related bicarbonate probe series,

no significant toxicity was observed under these conditions. Calculated IC_{50} values were found to be greater than 200 μM in each case.

4.8 Conclusions

Modification to the structure of the bicarbonate probes described in chapter three by incorporating a variety of sulfonamides into the macrocyclic ligand has led to a series of pH-responsive complexes. Tuning of the pH-responsive range of the complex, or the pK_a of sulfonamide binding was achieved by variation of the sulfonamide.

The pH-response of sulfonamide binding was not prevented in competing backgrounds, examining the influence of added anions and protein. Differing backgrounds did adjust the pK_a of binding, however, with the pK_a shifting to slightly higher values if protein or anions were present. This is likely to mean that a system monitoring pH with these probes may need to be calibrated independently for each individual system.

Changes within the circularly polarised luminescence emission spectra could be monitored as a function of pH. Binding of the sulfonamide causes a change in the local helicity at the metal centre, and this is reflected in changes in the CPL emission. The largest changes to the CPL spectrum occurred with the terbium analogues. Nevertheless, it was still possible to analyse data for each europium analogue, monitoring the pH dependence of the emission dissymmetry factor. The pK_a value calculated using this method, matched that found by examining data from changes in the total emission spectrum.

The complexes described were non-toxic to cells, and localised preferentially to the lysosomes within one hour. This localisation profile remained constant for a number of hours, which should allow experiments examining pH changes in the lysosomes within this time period.

The work described is promising, as it suggests the probes potential to be used *in cellulo* to monitor changes in pH within the lysosomes.

4.9 Future Work

There is plenty of scope to extend the work presented in this chapter. Most of it focuses on the application of the probes in cell-based work, and then examination by confocal microscopy.

There are one or two minor structural changes which could be made to the probes, however. To address the issues associated with the small effects of a change in pK_a upon background

composition, it may be beneficial to use complexes with a lower overall charge. The work in chapter three showed that by using neutral or anionic complexes, affinities for anions was reduced. Thus, using the neutral analogues of the complexes in this chapter, anion interference may be suppressed further.

The immediate cellular work in this area to be undertaken involves establishment of a reliable calibration. This involves incubating the cells in high potassium salt buffered solutions of differing pH, together with the ionophores monensin and nigericin.[133] A tandem probe approach would be used, and the ratio of europium/terbium emission calculated at each pH. This should allow a calibration curve to be constructed for that system. The selection of buffers needs careful thought as a citrate or phosphate buffer is likely to quench the emission of the complexes.

Further cell work should also focus on ways of deliberately perturbing the system, and monitoring any spectral changes that occur. Administration of chloroquine is known to cause an elevation of pH within the lysosomes. A series of experiments could be devised to observe these changes via variation in the europium/terbium ratio. The effect of chloroquine concentration on intralysosomal pH could be examined as a function of time.

One last option for further work is to combine the ideas presented and discussed throughout this thesis and create pH probes for the mitochondria. Addition of the pH-responsive sulfonamide altered the localisation away from the mitochondria. It remains a challenge to incorporate a pH responsive moiety whilst retaining a mitochondrial localisation.

5 Experimental

5.1   General Procedures

5.1.1   Reagents and Solvents

All commercially available reagents were used as received from their respective suppliers. Water and H_2O refer to high purity water obtained from the "PuriteSTILL Plus" purification system, with conductivity of <0.04 μS cm^{-1}. Reactions requiring anhydrous conditions were carried out using Schlenk-line techniques, under an atmosphere of dry argon. All solvents used were laboratory grade, and where required were dried using an appropriate drying agent.

5.1.2   Chromatography

Thin-layer chromatography was performed using silica plates (Merck 5554) or neutral aluminium oxide plates (Merck 5550), each visualised using UV irradiation or by staining with iodine or Dragendorff's reagent, as appropriate.

Preparative column chromatography was carried out using silica (Merck Silica Gel 60, 230-400 mesh) or neutral aluminium oxide (Merck Aluminium Oxide 90, 70-230 mesh), pre-soaked in ethyl acetate.

5.1.3   Exchange of complex counter-anions

Exchange of complex counter-anions was performed using 'DOWEX® 1x2-200' ion exchange resin (Sigma-Aldrich). Typically, the resin (1 g) was prepared by boiling in MeOH (50 ml) overnight followed by washing with H_2O (500 ml). The resin was then loaded into a pipette and $HCl_{(aq)}$ passed through (1 M, 25 ml), this was then washed with H_2O until the washings were pH 7.

5.1.4   Spectroscopy

^{1}H and ^{13}C-NMR spectra were recorded on a Varian Mercury-400 (^{1}H at 399.96 MHz), Bruker Avance-400 (^{1}H at 400.13 MHz, ^{13}C at 100.61 MHz), Varian Inova-500 (^{1}H at 499.78 MHz, ^{13}C at 125.67 MHz), or a Varian VNMRS-700 (^{1}H at 699.73 MHz, ^{13}C at 175.95 MHz) spectrometer. All spectra were internally referenced to the solvent residual proton signals. All chemical shifts are

given in ppm, with coupling constants in Hz. Splitting patterns are described as singlet (s), doublet (d), triplet (t), quartet (q) or multiplet (m).

5.1.5 Optical Spectroscopy

UV/Vis absorbance spectra were recored on a Perkin Elmer Lambda 900 UV/Vis/NIR spectrometer using FL Winlab software). Emission spectra were recorded on a ISA Joblin-Yvon Spex Fluorolog-3 luminescent spectrometer using DataMax v2.20 software). Lifetimes were measured on a Perkin Elmer LS55 luminescence spectrometer using FL Winlab Molecular Spectroscopy Version 4.00.02 software. Each sample was contained in quartz cuvettes with a pathlength of 1cm. Measurements were recorded at 298 K. Generally, an integration time of 0.5 seconds, increment of 0.5 nm and excitation and emission slits of 2.5 and 1.5 nm respectively were used. Circularly polarized luminescence measurements were made using a home-built CPL spectrophotometer, based on a Spex Fluoromax-2-spectrofluorimeter at the University of Glasgow with the assistance of Dr R. D. Peacock. Measurements were undertaken in D_2O using indirect excitation at 332 nm. Absorbance measurements of 96-well plates were made on an Analytik Jena FLASHScan 530 using WinFLASH version 1.5 software.

5.1.6 pH measurements

pH measurements were undertaken using a Jenway 3020 or a Jenway 3320 pH meter attached to an Aldrich Chemical Company micro-pH combination electrode. Calibration of the pH meter was conducted daily using a three point calibration: pH =4.00, pH = 7.00 and pH = 7.00 buffer solutions (Aldrich). For measurements in D_2O, the pD was calculated using the actual pH meter reading and *[Eq. 9]*.

$$pD = pH \text{ (meter reading)} + 0.41 \qquad \textbf{\textit{[Eq. 9]}}$$

5.1.7 Luminescent titrations

Luminescent titrations were carried out, examining the effect of a number of different anions and protein upon the emission spectra of the complexes. Protein was added as a solid, and pH adjustments were made, if necessary, after each addition. Anions were added as a small volume from a concentrated stock solution. Volume additions at each point were typically only 0.1% of

the original solution. A correction for this small dilution effect was nevertheless made for each Ln(III) spectrum.

5.1.8 Determination of binding constants

The apparent binding constants were calculated from the data obtained following these luminescent titrations. *[Eq. 10]* was fitted to the data, using a non-linear least squares fitting algorithm in Microsoft Excel 2010, using the solver add-in.

$$[X] = \frac{f/K + [EuL]*f - [EuL]*f^2}{1 - f}$$

[Eq. 10]

Where
$$f = \frac{F - F_0}{F_1 - F_0}$$

And [X] is the concentration of the anion or selected added species in solution

K is the binding constant

F is the ratio or intensity of the selected peak

F_0 is the ratio or intensity of the selected peak at the beginning of the titration

F_1 is the final ratio or intensity of the selected peak

[Ln·L] is the total concentration of the Ln(III) complex in solution

5.1.9 Lifetime measurements

Lifetimes of Eu(III) and Tb(III) complexes were measured by excitation (332 nm) of the sample using a short pulse of light followed by monitoring the integrated intensity of light (616 nm for Eu(III), 545 nm for Tb(III)) emitted during a fixed gate time, t_g, after a delay time, t_d. At least 20 delay times were used covering at least 3 lifetimes. A gate time of 0.1 ms was used, and the excitation and emission slits were set to 10 nm and 5 nm band-pass respectively. The obtained exponential decay curves were plotted in Microsoft Excel and *[Eq. 11]* fitted to the data:

$$I = A_0 + A_1 e^{-kt}$$

[Eq. 11]

where: *I* is the intensity at time *t* after the flash

A$_0$ is the intensity after the decay has finished

A$_1$ is the pre-exponential factor

k is the rate constant for the decay of the excited state

The excited state lifetime, τ, is the inverse of the rate constant, *k*.

5.1.10 Inner Sphere Hydration Number (*q'*) Determination

The rate constant for the depopulation of the lanthanide excited state in water may be represented as the sum of a number of different contributing factors. In *[Eq. 5.2]*, these are the natural radiative rate constant (k_r), the global rate constant for non-radiative quenching mechanisms (k_{nr}) and the rate constant associated with energy transfer to nearby XH matched oscillators, respectively.

$$k_{H_2O} = k_r + k_{nr} + \sum k_{XH}$$

[Eq. 12]

It is assumed that in D_2O, all exchangeable XH oscillators have zero contribution to the quenching, so the equation simplifies to:

$$k_{D_2O} = k_r + k_{nr}$$

[Eq. 13]

The difference between the rate constants is therefore given by the sum of the rate constants for the non-radiatve decay to nearby XH oscillators.

$$k_{H_2O} - k_{D_2O} = \Delta k = \sum k_{XH}$$

[Eq. 14]

Assuming that OH oscillators are the major contributor to the Σk_{XH} term, then this equation can be modified to relate the number of inner sphere water bound molecules to the difference in the rate of quenching between H_2O and D_2O.

$$q' = A(\Delta k - x - y)$$

[Eq. 15]

A is a proportionality constant, representing the sensitivity of a particular lanthanide ion to vibronic quenching by XH oscillators. It takes a value of 1.2 ms^{-1} for europium and 5 ms^{-1} for terbium. *x* is a correction factor, allowing for the effect of closely diffusing OH oscillators. *x* takes a value of 0.25 ms^{-1} for europium and 0.06 ms^{-1} for terbium complexes. The final correction needed, *y*, relates to the particular case of close proximity amide NH oscillators, such as the carbonyl bound amide groups common in most of the complexes presented in this thesis. This takes a value of 0.075n ms^{-1} for europium complexes and 0.01n ms^{-1} for terbium complexes, where n is the number of such bound amides.

$$q'_{Eu} = 1.2\left(\Delta k - 0.25 - 0.075n\right)$$ **[Eq. 16]**

$$q'_{Tb} = 5\left(\Delta k - 0.06 - 0.01n\right)$$ **[Eq. 17]**

5.1.11 Mammalian Cell Culture

Three cell lines were selected for cellular studies: CHO (Chinese Hamster Ovary), NIH-3T3 (mouse skin fibroblast) and HeLa (human endothelial carcinoma cells). Cells were maintained in exponential growth as monolayers in F-12 (Ham) medium for CHO cells or DMEM (Dulbecco's Modified Eagle Medium) for NIH and HeLa cell lines. For each cell line, the medium was supplemented with 10% foetal bovine serum (FBS) and 1% penicillin and streptomycin. Cells were incubated at 37 °C, 20% average humidity and 5% (v/v) CO_2.

5.1.12 Marine Cell Culture

Six algeal cell lines were selected for study: three coccolithophores; *Geophyrocapsa oceanica*, *Calcidiscus leptoporus* and *Emiliania huxleyi* and three diatoms; *Ditylum brightwelli*, *Rhizoselenia setigera* and *Stephanodiscus hantzschii*.

5.1.13 Cytotoxicity measurements

IC_{50} values were determined using the MTT assay. Approximately 1 x 10^4 NIH 3T3 cells in 100 µl DMEM were seeded into each well of flat-bottomed 96-well plates and allowed to attach overnight. Complex solutions were added to triplicate wells to give final concentrations over a 2-log range. After 20 h incubation, MTT (1.0 mM) was added to each well and the plated incubated for a further 4 h. The culture medium was removed, and DMSO (150 µl) was added. The plate was shaken for 20 seconds and the absorbance measured at 520 - 560 nm in a microplate reader against a blank of DMSO.

5.1.14 Fluorescence Microscopy

Epifluorescence images were taken on a Zeiss Axiovert 200M epifluorescence microscope equipped with an Axiocam CCD camera and 63x/1.40 oil DIC and 40x/1.40 oil DIC objectives. G365 filters (Zeiss) were used for excitation of the complexes, with 546±12 and 570LP filters used for emission of Tb and Eu respectively.

5.1.15 HPLC Analysis

Reverse phase HPLC traces were recorded at 298 K using a Perkin Elmer system using a 4.6 x 150 mm 4μm Phenomenex Synergi Fusion RP 80Å analytical column. A gradient elution with a solvent system composed of H_2O + 0.1% HCOOH/ MeCN + 0.1% HCOOH was used for a total run time of 22.4 min. In each case, a single major product was observed in >95% purity using a diode array UV-Vis detector operating at 332 nm. A fluorescence detector was also connected, monitoring eluent from the column at 545 or 616 nm, emission was seen for each of the peaks observed before suggesting that each peak corresponds to a lanthanide bound chromophore.

Time (min)	Solvent A (%)	Solvent B (%)	Curvature
0	95	5	0
2.4	95	5	0
15.4	0	100	1
17.4	0	100	0
19.4	95	5	1
22.4	95	5	0

5.1.16 Confocal Microscopy

Confocal microscopy images were taken using a Leica SP5 II equipped with a 355 nm coherent CW UV laser and HeNe and Argon lasers operating at 458, 476, 488, 514 and 633 nm, running LAS AF software.

The detection system could be altered between 400 – 800 nm using a PMT-based tri-imaging system, also equipped with a GaAr HiD dectotor system operating in bright red mode. Scanning speed could be adjusted between 10 – 8000 Hz (using a resonance galvonemetric scanner). The pinhole was calculated automatically using the Airy disc size and the lowest wavelength number.

The microscope has an environmental chamber attached for temperature and CO_2 enrichment (Life Imaging Services Brick, Life Imagining Services Cube), standard operating conditions were 37 °C and 5% CO_2, humidity was controlled by a bubble humidifier.

5.1.17 Flow Cytometry

Flow cytometric analysis and sorting was conducted using a DakoCytomation Inc. MoFlo multi-laser flow cytometer (Fort Collins, CO, USA) operating at 60 psi with a 70 μM nozzle. Samples were interrogated with a 100mW 488 nm solid state laser. Fluorescence signals were

detected through interference filters (FL1 530/40, FL2 670/30 nm) and were collected in the logarithmic mode. Data were analysed using Summit v4.3 software (Dakocytomation).

For flow cytometry, cells were grown to confluence in 6-well plates. Medium was replaced and cells were treated with complex. Cells were detached from the plastic surface with 0.25% (v/v) trypsin solution for five minutes at 37 °C. The resulting cell suspension was pelleted by centrifugation. Immediately prior to flow cytometric analysis, cell suspensions were filtered through a 40 μm filter.

5.2   Synthesis

5.2.1   Azaxanthone Chromophore

2-[4-(Methoxycarbonyl)phenoxy]-6-methylnicotinic acid[2]
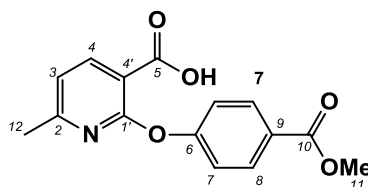
Sodium metal (0.94 g, 40.8 mmol) was carefully added to dry methanol (15 ml) under argon. Methyl-4-hydroxybenzoate (12.6 g, 82.8 mmol) was then added, forming a viscous light yellow solution. Solvent was removed from the solution under reduced pressure to leave a glassy pale yellow solid. 2-Chloro-6-methylnicotinic acid (2.50 g, 14.6 mmol) was added and the mixture heated at 155 °C for 15 hours with stirring under argon. The mixture was cooled to room temperature and 100 ml of cold water added. The resulting suspension was extracted with diethyl ether (5 x 50 ml) and the aqueous phase acidified with glacial acetic acid to pH 4, yielding a white precipitate. This was collected by Buchner filtration, washed thoroughly with water and dried under vacuum (3.73 g, 12.9 mmol, 88%).

R_F = 0.31 (DCM : 5% MeOH); m.p. 121 – 123 °C (Lit. 118 – 120 °C); ^{1}H-NMR (CDCl$_3$, 700 MHz) δ 8.41 (1H, d, J = 8.0, H^4), 8.12 (2H, d, J = 9.0, H^8), 7.24 (2H, d, J = 9.0, H^7), 7.06 (1H, d, J = 8.0, H^3), 3.94 (3H, s, H^{11}), 2.42 (3H, s, H^{12}); ^{13}C-NMR (CDCl$_3$, 175 MHz) δ 166.5 (C^5), 166.5 (C^{10}), 163.4 (C^2), 160.0 (C$^{1'}$), 156.4 (C^6), 143.8 (C^4), 131.5 (C^8), 127.5 (C^9), 121.6 (C^7), 119.9 (C^3), 110.6 (C$^{4'}$), 52.7 (C^{11}), 24.3 (C^{12}); HRMS (ES-) (m/z): [M - H]$^-$ calculated for C$_{15}$H$_{12}$NO$_5$ 286.0715, found 286.0710.

7-Methoxycarbonyl-2-methyl-1-azaxanthone[2]
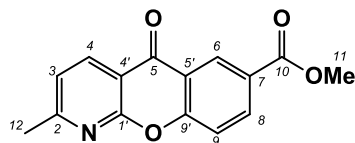
Polyphosphoric acid (70 g) and 2-[4-(methoxycarbonyl)phenoxy]-6-methylnicotinic acid (3.43 g, 12.0 mmol) were heated together for 18 h, at 120 °C under argon. The resulting brown solution was cooled to 0 °C and methanol (100 ml) was added with vigorous stirring. Conc. $KOH_{(aq)}$ was added at 0 °C, until pH 7 was reached. The mixture was extracted with DCM (4 x 100 ml) and solvent removed to yield the desired product as a yellow solid (1.44 g, 5.34 mmol, 45%).

R_F = 0.26 (hexane : EtOAc, 50 : 50); m.p. 197 – 199 °C (Lit. 194 – 196 °C); ^{1}H-NMR (CDCl$_3$, 400 MHz) δ 8.98 (1H d, J = 2.5, H^6), 8.59 (1H, d, J = 8.0, H^4), 8.40 (1H, dd, J = 8.0, 2.5, H^8), 7.64 (1H, d, J = 8.0, H^9), 7.33 (1H, d, J = 8.0, H^3), 3.98 (3H, s, H^{11}), 2.72 (3H, s, H^{12}); ^{13}C-NMR (CDCl$_3$, 101 MHz) δ 176.8 (C^5), 165.7 (C^{10}), 165.6 (C^2), 159.3 (C^1), 158.2 (C^9'), 137.5 (C^4), 135.9 (C^8), 129.1 (C^6), 126.8 (C^7), 121.7 (C^3), 121.4 (C^5'), 118.9 (C^9), 114.3 (C^4'), 52.5 (C^{11}), 25.1 (C^{12}); MS (ES+) m/z 291.9 [M + Na]$^+$; HRMS (ES+) (m/z): [M + H]$^+$ calculated for $C_{15}H_{12}NO_4$ 270.0766, found 270.0767.

7-Methoxycarbonyl-2-dibromomethyl-1-azaxanthone
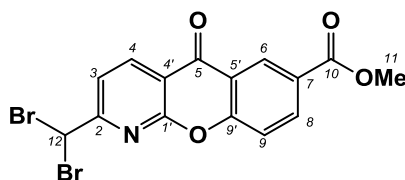
7-Methoxycarbonyl-2-methyl-1-azaxanthone (564 mg, 2.09 mmol) was dissolved in CCl$_4$ (15 ml) and stirred under argon, under irradiation using a 100 W tungsten filament lamp. After 5 minutes, NBS (820 mg, 4.65 mmol) and dibenzoyl peroxide (25 mg) was added. After 18 h the solution was hot filtered and the solvent removed under reduced pressure. The residue was dissolved in DCM (50 ml), washed with water (3 x 50 ml) and the organic phase dried over MgSO$_4$. The solvent was removed under reduced pressure and the product used directly in the next step without further purification (794 mg, 1.86 mmol, 89%).

R_F = 0.38 (hexane : EtOAc, 50 : 50); ^{1}H-NMR (CDCl$_3$, 400 MHz) δ 9.00 (1H, d, J = 2.5, H^6), 8.81 (1H, d, J = 8.0, H^4), 8.44 (1H, dd, J = 8.0, 2.5, H^8), 7.93 (1H, d, J = 8.0, H^3), 7.68 (1H, d, J = 8.0, H^9), 6.68 (1H, s, H^{12}), 3.99 (3H, s, H^{11}).

7-Methoxycarbonyl-2-bromomethyl-1-azaxanthone
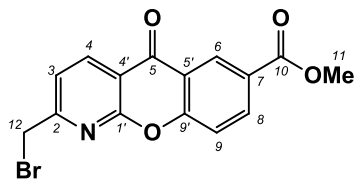
Diethylphosphite (1.19 ml, 9.25 mmol) and diisopropylamine (1.51 ml, 10.8 mmol) were added at 0 °C to a stirred solution of 7-methoxycarbonyl-2-dibromomethyl-1-azaxanthone (0.835 g, 1.96 mmol) in dry THF (30 ml) under argon. After ten minutes the reaction was halted and poured onto iced water (50 ml), then extracted with $CHCl_3$ (3 x 50 ml). This was backwashed with sat. $NaHCO_{3(aq)}$ (50 ml) followed by water (50 ml). The organic phase was dried over $MgSO_4$, and the solvent removed under reduced pressure. The desired product was purified by column chromatography (silica, DCM → 3% MeOH) as a fine white powder (0.532 g, 1.53 mmol, 78%).

R_F = 0.42 (hexane : EtOAc, 50 : 50); m.p. 166 – 168 °C (Lit. 156 – 158 °C); ^{1}H-NMR (CDCl$_3$, 700 MHz) δ 9.00 (1H, d, J = 2.0, H^6), 8.73 (1H, d, J = 8.0, H^4), 8.44 (1H, dd, J = 9.0, 2.0, H^8), 7.67 (1H, d, J = 9.0, H^9), 7.62 (1H, d, J = 8.0, H^3), 4.62 (2H, s, H^{12}), 3.99 (3H, s, H^{11}); ^{13}C-NMR (CDCl$_3$, 176 MHz) δ 176.6 (C^5), 165.7 (C^{10}), 162.6 (C^2), 159.8 (C$^{1'}$), 158.4 (C$^{9'}$), 139.0 (C^4), 136.5 (C^8), 129.4 (C^6), 127.2 (C^7), 121.5 (C^3), 121.5 (C$^{5'}$), 119.1 (C^9), 116.1 (C$^{4'}$), 52.7 (C^{11}), 32.1 (C^{12}); MS (ES+) m/z 371.2 [M + Na]$^+$.

7-Methoxycarbonyl-2-pththalimidomethyl-1-azaxanthone[2]
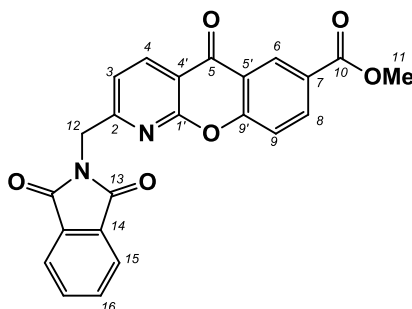
7-Methoxycarbonyl-2-bromomethyl-1-azaxanthone (0.216 g, 0.598 mmol) and potassium pththalimide (0.443 g, 2.39 mmol) were stirred in DMF (12 ml), under argon for 1 h at room temperature. Solvent was then removed under reduced pressure and the desired product purified by column chromatography (silica, DCM → 5% MeOH) to yield the product as a bright yellow powder (0.155 g, 0.374 mmol, 63%).

m.p. >250 ℃ (Lit. >250 ℃); ^{1}H-NMR (CDCl$_3$, 700 MHz) δ 8.97 (1H, s, H^6), 8.68 (1H, d, J = 8.0, H^4), 8.39 (1H, dd, J = 9.0, 2.0, H^8), 7.93 (2H, dd, J = 5.5, 3.0, H^{15}), 7.79 (2H, dd, J = 5.5, 3.0, H^{16}), 7.60 (1H, d, J = 9.0, H^9), 7.41 (1H, d, J = 8.0, H^3), 5.14 (2H, s, H^{12}), 3.70 (3H, s, H^{11}); ^{13}C-NMR (CDCl$_3$, 176 MHz) δ 177.0 (C^5), 168.2 (C^{13}), 165.6 (C^{10}), 162.2 (C^2), 160.0 (C$^{1'}$), 158. 7 (C$^{9'}$), 138.6 (C^4), 136.4 (C^8), 134.5 (C^{16}), 132.5 (C^{14}), 129.8(C^6), 127.4 (C^7), 124.0 (C^{15}), 121.4 (C$^{5'}$), 119.5 (C^3), 119.3 (C$^{9'}$), 116.0 (C$^{4'}$), 52.8 (C^{11}), 43.1 (C^{12}); MS (ES+) m/z 437.3 [M + H]$^+$.

7-Methoxycarbonyl-2-aminomethyl-1-azaxanthone[2]
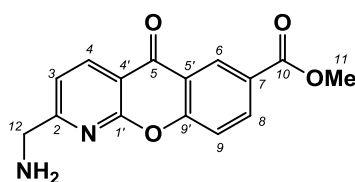
7-Methoxycarbonyl-2-phthtalimidomethyl-1-azaxanthone (0.128 g, 0.308 mmol) was dissolved in DCM : MeOH (50 : 50, 10 ml) and stirred under argon at room temperature. H$_2$NNH$_2$.H$_2$O (30 µl, 0.620 mmol) was added and the temperature increased to 50 °C. After 4 h the reaction was halted, allowed to cool to room temperature and the pH adjusted to 2 by the addition of conc. HCl. The resulting mixture was heated at 50 °C for 1 h. The reaction was then cooled in a fridge for 2 h and the product obtained as its hydrochloride salt by centrifugation (55 mg, 0.193 mmol, 63%).

m.p. >250 ℃ (Lit. >250 ℃); ^{1}H-NMR (CDCl$_3$, 400 MHz) δ 8.74 (1H, s, H^6), 8.66 (1H, d, J = 8.0, H^4), 8.38 (1H, d, J = 8.5, H^8), 7.70 (1H, d, J = 8.5, H^9), 7.58 (1H, d, J = 8.0, H^3), 4.70 (2H, s, H^{12}), 3.92 (3H, s, H^{11}); ^{13}C-NMR (CDCl$_3$, 101 MHz) δ 177.3 (C^5), 169.4 (C^2), 165.7 (C^{10}), 160.1 (C$^{1'}$), 158.7 (C$^{9'}$), 138.4 (C^4), 136.3 (C^8), 129.5 (C^6), 126.8 (C^7), 121.5 (C$^{5'}$), 119.3 (C^3), 118.9 (C$^{9'}$), 115.5 (C$^{4'}$), 52.5 (C^{11}), 44.8 (C^{12}); MS (ES+) m/z 285.1 [M + H]$^+$.

2,5-Dioxopyrrolidin-1-yl-2-chloroacetate[33]
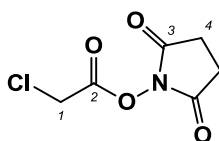
Chloroacetic acid (4.00 g, 42.6 mmol), EDC (8.10 g, 42.3 mmol) and N-hydroxysuccinimide (4.86 g, 42.3 mmol) were stirred in dry DCM (200 ml) for 18 h under argon. The solvents were

removed under reduced pressure and the remaining residue redissolved in DCM (50 ml). The organic phase was washed with water (75 ml), dried over $MgSO_4$ and the solvent removed under reduced pressure to yield the product as a white solid (4.61 g, 24.1 mmol, 57%).

R_F = 0.51 (silica, EtOAc); m.p. 102 – 104 °C; ^{1}H-NMR ($CDCl_3$, 400 MHz) δ 4.39 (2H, s, H[1]), 2.89 (4H, s, H[4]); ^{13}C-NMR ($CDCl_3$, 101 MHz) δ 168.5 (C[3]), 163.6 (C[2]), 38.2 (C[1]), 25.9 (C[4]).

7-Methoxycarbonyl-2-chloromethylcarbonylaminomethyl-1-azaxanthone
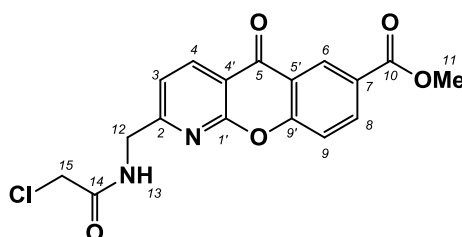
7-Methoxycarbonyl-2-aminomethyl-1-azaxanthone (147 mg, 0.459 mmol), 2,5-dioxopyrrolidin-1-yl-2-chloroacetate (175 mg, 0.917 mmol) and triethylamine (160 μl, 1.15 mmol) were stirred in dry THF (20 ml) under argon for 18 h at room temperature. DCM (20 ml) was added and the mixture was washed repeatedly with H_2O (5 x 20 ml). The solvent was removed under reduced pressure to leave the desired product as a light yellow powder (101 mg, 0.282 mmol, 61%).

^{1}H-NMR ($CDCl_3$, 700 MHz) δ 8.99 (1H, d, J = 2.0, H[6]), 8.70 (1H, d, J = 8.0, H[4]), 8.43 (1H, dd, J = 8.5, 2.0, H[8]), 7.67 (1H, d, J = 8.5, H[9]), 7.66 (1H, br s, H[13]), 7.45 (1H, d, J = 8.0, H[3]), 4.76 (2H, d, J = 5.5, H[12]), 4.17 (2H, s, H[15]), 3.98 (3H, s, H[11]); ^{13}C-NMR ($CDCl_3$, 176 MHz) δ 176.7 (C[5]), 166.5 (C[14]), 165.7 (C[10]), 162.4 (C[2]), 160.0 (C[1']), 158.3 (C[9']), 138.6 (C[4]), 136.4 (C[8]), 129.3 (C[6]), 127.2 (C[7]), 121.5 (C[5']), 119.9 (C[3]), 119.1 (C[9]), 115.8 (C[4']), 52.7 (C[11]), 45.0 (C[12]), 42.7 (C[15]); MS (ES+) m/z 361.1 [M + H]+; HRMS (ES+) (m/z): [M + Na]+ calculated for $C_{17}H_{13}ClNaN_2O_5$ 383.0419, found 383.0411.

5.2.2 Pendant arms

(*S*)-Alanine ethyl ester hydrochloride
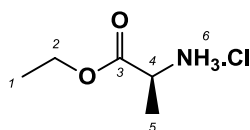
(*S*)-Alanine (1.00 g, 11.2 mmol) was suspended in dry ethanol (40 ml). Dry HCl (produced by dropping conc. H_2SO_4 onto NaCl and passing through conc. H_2SO_4) was bubbled through the

solution for 3 h, while refluxing under argon. The mixture was boiled under reflux for a further 12 h, and the solvent removed under reduced pressure to yield a white solid (1.71 g, 11.2 mmol, >99 %).

m.p. 82 – 83°C; ^{1}H-NMR (CD$_3$OD, 400 MHz) δ 4.27 (q, 2H, J = 7.0, H^2), 4.02 (1H, q, J = 7.0, H^4), 1.53 (d, 3H, J = 7.0, H^5), 1.29 (t, 3H, J = 7.0, H^1); ^{13}C-NMR (CDCl$_3$, 175 MHz) δ 170.0 (C^3), 62.4 (C^2), 49.3 (C^4), 16.1 (C^5), 14.0 (C^1); HRMS (ES+) (*m/z*): [M + H]$^+$ calculated for C$_5$H$_{12}$O$_2$N 118.0863, found 118.0863.

N-Bromoacetyl-(*S*)-alanine ethyl ester
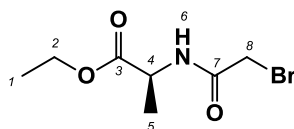
(*S*)-Alanine ethyl ester hydrochloride (1.71 g, 11.2 mmol) was stirred under argon at -20 °C in dry CHCl$_3$ (10 ml). Triethylamine (2.3 ml, 32.0 mmol) and bromoacetyl bromide (1.6 ml, 17.9 mmol) were added and the mixture stirred at -20 °C for 2 h before being allowed to gradually warm to room temperature and stirred for a further 12 h. The reaction was then halted and washed with HCl$_{(aq)}$ (6 M, 30 ml) and then H$_2$O (4 x 25 ml). The organic phase was dried and the product recrystallised from DCM / pet. ether as white crystals (1.88 g, 7.95 mmol, 71 %).

m.p. 33 – 34 °C; ^{1}H-NMR (CDCl$_3$, 400 MHz) δ 7.03 (1H, br s, H^6), 4.45-4.65 (1H, m, H^4), 4.23 (1H, q, J = 7.0, H^2), 3.88 (2H, s, H^8), 1.45 (3H, d, J = 7.0, H^5), 1.28 (3H, t, J = 7.0, H^1); ^{13}C-NMR (CDCl$_3$, 125 MHz) δ 172.5 (C^7), 165.6 (C^3), 62.1 (C^2), 48.8 (C^4), 42.3 (C^8), 18.0 (C^5), 14.0 (C^1); MS (ES+) *m/z* 260.1 [M + Na]$^+$; HRMS (ES+) (*m/z*): [M + Na]$^+$ calculated for C$_7$H$_{12}$NO$_3$BrNa 259.9893, found 259.9895.

N-Bromoacetyl-(*S*)-glutamic acid diethyl ester
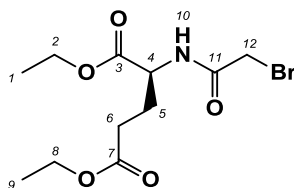
(*S*)-Glutamic acid diethyl ester hydrochloride (2.40 g, 10.0 mmol) was stirred under argon at -20 °C in dry CHCl3 (10 ml). Triethylamine (3.0 ml, 20.0 mmol) and bromoacetylbromide (1.13 ml,

12.5 mmol) were added and the mixture stirred at -20 °C for 2 h before being allowed to warm to room temperature and stirred for a further 12 h. The reaction was then halted and washed with $HCl_{(aq)}$ (6 M, 30 ml) and then H_2O (4 x 20 ml). The organic phase was dried and the solvent removed under reduced pressure to yield the product (2.08 g, 6.38 mmol, 64%).

^1H-NMR (CDCl$_3$, 400 MHz) δ 7.16 (1H, br s, H[10]), 4.48-4.66 (1H, br m, H[4]), 4.20 (2H, q, J = 7.0, H[2]), 4.12 (2H, q, J = 7.0, H[8]), 3.86 (2H, s, H[12]), 2.32-2.42 (2H, m, H[6]), 2.22 (1H, m5-2.29, H[5]), 2.00-2.10 (1H, m, H[5']), 1.28 (3H, t, J = 7.0, H[9]), 1.24 (3H, t, J = 7.0, H[1]); ^{13}C-NMR (CDCl$_3$, 101 MHz) δ 172.7 (C[11]), 171.2 (C[7]), 165.8 (C[3]), 62.0 (C[2]), 60.9 (C[8]), 52.3 (C[12]), 30.1 (C[4]), 28.5 (C[6]), 26.0 (C[5]), 14.1 (C[1]), 14.0 (C[9]); MS (ES+) m/z 346.1 and 348.1 [M + Na]$^+$. HRMS (ES+) (m/z): [M + Na]$^+$ calculated for $C_{11}H_{19}NO5_3Br$ 323.0368, found 323.0358.

(S)-2-Bromopentanedioic acid 5-benzyl ester 1-*tert*-butyl ester
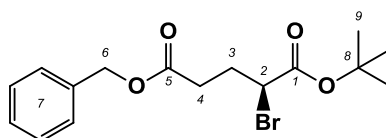
A solution of (S)-2-bromo-pentanedioic acid-5-benzyl ester (1.00g, 3.43 mmol) in *tert*-butyl acetate (15 ml) and $HClO_4$ in H_2O (70%, 0.20 mmol) was stirred at rt. After 16 h, H_2O was added to the reaction mixture, and the organic phase separated. The organic phase was washed successively with H_2O (2 x 25 ml) and 5% aq. Na_2CO_3 solution (2 x 25 ml) The solvent was removed under reduced pressure to yield a pale yellow oil (0.923 g, 2.58 mmol, 81%).

^1H-NMR (CDCl$_3$, 400 MHz) δ 7.30-7.41 (5H, m, H[7]), 5.11 (2H, s, H[6]), 4.30 (1H, dd, J = 6.0, 2.0, H[2]), 2.56-2.64 (2H, m, H[4]), 2.33-2.41 (1H, m, H[3]), 1.47 (9H, s, H[9]); ^{13}C-NMR (CDCl$_3$, 126 MHz) δ 173.1 (C[5]), 169.5 (C[1]), 136.2 (C[7(q)]), 128.9 (C[7]), 128.8 (C[7]), 128.3 (C[7]), 82.8 (C[8]), 66.9 (C[6]), 47.1 (C[2]), 31.8 (C[4]), 30.0 (C[3]), 27.8 (C[9]); HRMS (ES+) m/z: [M + H]$^+$ calculated for $C_{21}H_{16}BrO_4$ 379.0334, found 379.0345.

(S)-2-Bromopentanedioic dimethyl ester
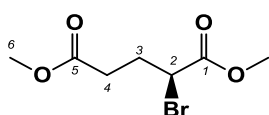
Sodium nitrite (5.50 g, 80.1 mmol) dissolved in H_2O (50 ml) was added dropwise to a stirred solution of sodium bromide (16.0 g, 156 mmol) and S-glutaric acid 5 methyl ester (6.41 g, 39.8 mmol) in 1M HBr (250 ml), cooled at -5 °C. After 20 h, conc. H_2SO_4 (1 ml) was added dropwise to

the reaction mixture, which was subsequently extracted with diethyl ether (2 x 250 ml). The combined organic extracts were washed with brine (2 x 200 ml), dried over MgSO$_4$, filtered and the solvent removed under reduced pressure. The crude material was dissolved in anhydrous MeOH (50 ml) and conc. H$_2$SO$_4$ (0.5 ml) was added. The solution was stirred at 50 ℃ under argon for 4 h. After cooling, the solvent was removed under reduced pressure and the crude material purified by column chromatography (silica, 100% toluene → 25% DCM) to yield a colourless oil (6.19 g, 25.9 mmol, 65%).

^{1}H-NMR (CDCl$_3$, 400 MHz) δ 4.35 (1H, t, J = 8.0, H^2), 3.76 (3H, s, H^7), 3.66 (3H, s, H^6), 2.41.2.49 (2H, m, H^4), 2.28-2.44 (1H, m, H^3), 2.19-2.31 (1H, m, H$^{3'}$); ^{13}C-NMR (CDCl$_3$, 101 MHz) δ 172.5 (C^5), 169.8 (C^1), 53.1 (C^7), 51.9 (C^6), 44.6 (C^2), 31.3 (C^4), 29.8 (C^3); HRMS (ES+) m/z [M + H]$^+$ calcualted for C$_7$H$_{11}$O$_4$Na^{79}Br 260.9738, found 260.9740.

5.2.3   [Ln·L^1]$^{3+}$

1,7-Bis(benzyloxycarbonyl)-1,4,7,10-tetraazacyclododecane[119]
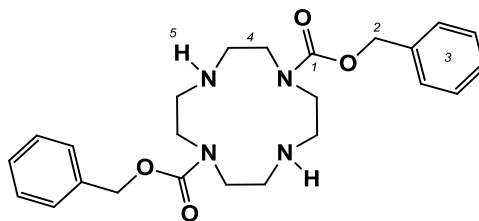
Disodium hydrogen phosphate (14.0 g, 98.6 mmol) was added to a solution of 1,4,7,10-tetraazacyclododecane (5.00 g, 29.0 mmol) in purite water : dioxane (5 : 2, 70 ml). The pH was adjusted to 2.5 by the addition of conc. HCl. Benzyl chloroformate (10.0 ml, 70.1 mmol) was dissolved in dioxane (20 ml) and added dropwise to the mixture over 2 h at room temperature, followed by stirring for a further 18 h. A colourless solution was formed containing a white precipitate. Solvent was removed under reduced pressure leaving a viscous white residue. This was extracted with diethyl ether (3 x 50 ml), removing side products. The aqueous phase was further extracted with DCM (3 x 50 ml). The organic phase was dried under reduced pressure to yield a colourless viscous oil. The oil was redissolved in DCM (5 ml) followed by precipitation via the addition of diethyl ether (60 ml) and sonication. The product was obtained by filtration as a coarse white powder (9.68 g, 22.0 mmol, 76%).

^{1}H-NMR (CDCl$_3$, 400 MHz) δ 7.32 – 7.39 (10H, m, H^3), 5.17 (4H, s, H^2), 2.85 – 3.90 (16H, br, H^4), 1.66 (2H, br, s, H^5); ^{13}C-NMR (CDCl$_3$, 100 MHz) 156.3 (C^1), 136.0 (C^{3q}), 128.9 (C^{3q}), 129.0 (C^3), 1289 (C^3), 128.7 (C^3), 128.6 (C^3), 128.4(C^3), 128.3(C^3), 68.0(C^4), 67.9(C^4), 50.8(C^4), 50.6(C^4),

50.4(C^4), 50.0(C^4), 49.8(C^4), 49.3(C^4), 49.2(C^4); HRMS (ES+) (*m/z*): [M + H]+ calculated for $C_{24}H_{33}N_4O_4$ 441.2502, found 441.2504.

4,10-Bis-[((*S*)-1-phenyl-ethylcarbamoyl)-methyl]-1,4,7,10-tetraazacyclododecane-1,7-dicarboxylic acid dibenzyl ester[134]
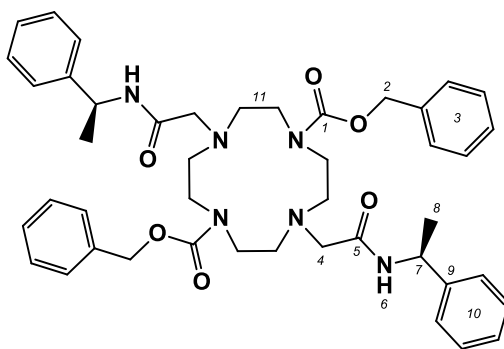
1,7-Bis(benzyloxycarbonyl)-1,4,7,10-tetraazacyclododecane (1.82 g, 4.14 mmol) was dissolved in dry MeCN (30 ml) and 2-chloro-*N*-[(*S*)-1phenylethyl]ethanamide (2.39 g, 12.1 mmol) added. Cs_2CO_3 (2.17 g, 6.66 mmol) was added and the mixture stirred at 70 °C under argon for 24 h. The reaction was allowed to cool to room temperature and the solvent removed under reduced pressure. DCM (25 ml) was added and the mixture washed with water (3 x 25 ml). The solvent was again removed under reduced pressure. The residue was sonicated in diethyl ether (2 x 25 ml) and the resulting solution centrifuged. The precipitated solid was isolated by column chromatography on silica gel (DCM → 6% MeOH), as a brown glassy oil (2.40 g, 3.14 mmol, 71%).

1H-NMR (CDCl3, 400 MHz) δ 7.65 (2H, s br, H6), 7.15 - 7.40 (20H, m, H3,10), 4.99-5.19 (2H, m, H7), 4.97 (4H, s br, H2), 3.28 – 3.61 (8H, br m, H11), 3.08 (4H, s, H4), 2.56 – 2.71 (8H, br m, H11), 1.35-1.45 (6H, m, H8); 13C-NMR (CDCl3, 101 MHz) δ 170.0 (C5), 156.7 (C1), 143.5 (C9q), 136.5 (C3q), 128.7(C3,10), 128.3(C3,10), 128.3(C3,10), 127.4(C3,10), 127.3(C3,10), 126.2 (C3,10), 67.4 (C2), 59.1 (C4), 54.4 - 56.3 (C11), 48.7 (C7), 47.7 - 48.9 (C11), 22.0 (C8); MS (ES+) *m/z* 763.6 [M + H]+; HRMS (ES+) (*m/z*): [M + Na]+ calculated for $C_{44}H_{54}O_6N_6Na$ 785.4003, found 785.3975.

N-((S)-1-Phenyl-ethyl)-2-(7-[((S)-1-phenyl-ethylcarbamoyl)-methyl]-1,4,7,10-tetraaza-cyclododec-1-yl)-acetamide[134]
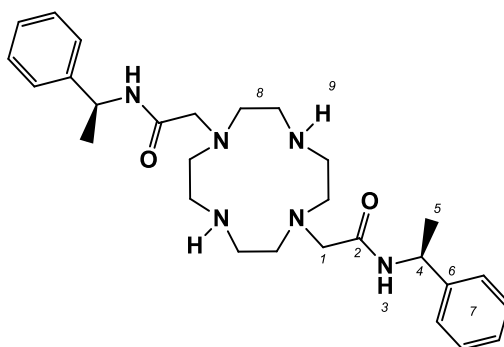
4,10-Bis-[((S)-1-phenyl-ethylcarbamoyl)-methyl]-1,4,7,10-tetraazacyclododecane-1,7-dicarboxylic acid dibenzyl ester (2.35 g, 3.08 mmol) was dissolved in EtOH (40 ml) and Pd/C (50 mg) and ammonium formate (1.20 g, 19.0 mmol) were added. The mixture was heated under reflux for 18 h and then allowed to cool to room temperature. Solvent was removed under reduced pressure and the residue dissolved in DCM (100 ml). This was washed repeatedly with water, dried over $MgSO_4$ and the solvent removed under educed pressure to leave a glassy white solid (1.15 g, 2.32 mmol, 75%).

^{1}H-NMR (CD$_3$OD, 500 MHz) δ 7.20 - 7.36 (10H, m, H^7), 4.99-5.11 (2H, m, H^4), 3.38-3.46 (4H, br m, H^1), 2.83 - 3.22 (16H, br, H^8), 1.46 (6H, d, J = 7.0, H^5); ^{13}C-NMR (CD$_3$OD, 126 MHz) δ 172.5 (C^2), 145.7 (C^7), 130.7(C^7), 128.9(C^7), 127.9 (C^7), 57.0 (C^1), 52.4 (C^4), 51.0 (C^8), 50.6 (C^8), 45.0 (C^8), 23.5 (C^5); MS (ES+) m/z 495.3 [M + H]$^+$; HRMS (+m/z): [M + H]$^+$ calculated for $C_{28}H_{43}O_2N_6$ 495.3442, found 495.3449.

4,10-Bis[((S)-1-phenyl-ethylcarbamoyl)-methyl]-1,4,7,10-tetraazacyclododecane-1-carboxylic acid *tert*-butyl ester[134]
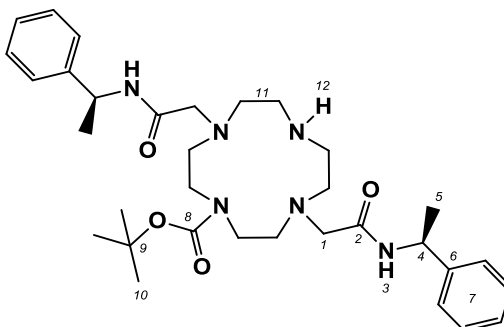
N-((*S*)-1-Phenyl-ethyl)-2-(7-[((*S*)-1-phenyl-ethylcarbamoyl)-methyl]-1,4,7,10-tetraaza-cyclododec-1-yl)-acetomide (0.812 g, 1.67 mmol) and di-*tert*-butyl dicarbonate (0.363 mg, 1.67 mmol) were stirred, under argon, in $CHCl_3$ at 30 °C for 18 h. Solvent was then removed under reduced pressure and the product purified by column chromatography on silica gel (DCM → 3% MeOH) to yield a viscous oil (239 mg, 0.407 mmol, 24%).

^{1}H-NMR ($CDCl_3$, 500 MHz) δ 7.81 (1H, br s, H^{12}), 7.15 - 7.35 (10H, m, H^7), 5.01-5.15 (2H, m, H^4), 2.91-2.13 (4H, m, H^1), 2.50 - 3.40 (16H, br m, H^{11}), 1.57 (6H, d, *J* = 7.0, H^5), 1.38-1.41 (9H, m, H^{10}); ^{13}C-NMR ($CDCl_3$, 126 MHz) δ 170.4 (C^2), 156.6 (C^8), 143.7 (C^{7q}), 128.8 (C^7), 127.4 (C^7), 126.6 (C^7), 80.3 (C^{10}), 59.4 (C^1), 49.0 – 54.1 (C^{11}), 48.8 (C^4), 28.6 (C^{10}), 21.9 (C^5); MS (ES+) +*m/z* 595.4 [M + H]$^+$; HRMS (ES+) (*m/z*): [M + H]$^+$ calculated for $C_{33}H_{51}O_4N_6$ 595.3966, found 595.3962.

2-[(2-(7-*tert*-Butoxycarbonyl-4,10-bis-[((*S*)-1-phenyl-ethylcarbamoyl)-methyl]-1,4,7,10-tetraaza-cyclododec-1-yl)-acetylamino)-methyl]-10-oxo-10*H*-9-oxa-1-aza-anthracene-6-carboxylic acid methyl ester[2]
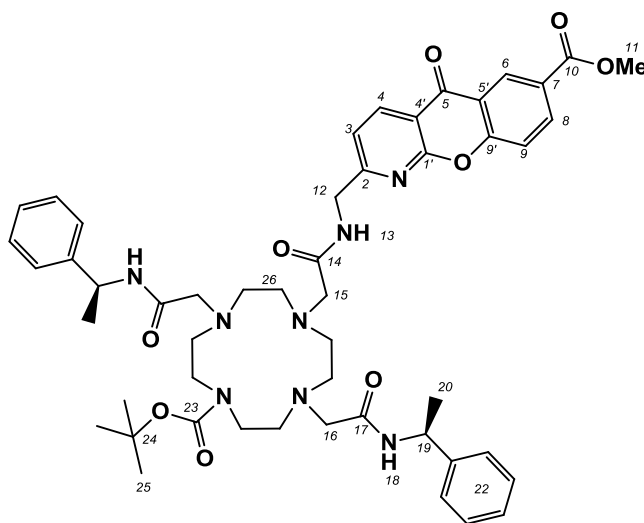
4,10-Bis[((*S*)-1-phenyl-ethylcarbamoyl)-methyl]-1,4,7,10-tetraazacyclododecane-1-carboxylic acid *tert*-butyl ester (90 mg, 0.150 mmol) was combined with 7-methoxycarbonyl-2-chloromethylcarbonylaminomethyl-1-azaxanthone (54 mg, 0.150 mmol) and DIPEA (53 μl, 0.300 mmol) in dry MeCN (10 ml) under argon. The mixture was stirred at 60 °C for 24 h. A further addition of DIPEA (25 μl, 0.150 mmol) was made at this time-point and the mixture stirred for a further 18 h. Solvent was removed under reduced pressure and the residue purified by column chromatography (silica, DCM → 5% MeOH) to yield a glassy orange solid (91 mg, 99 μmol, 66%).

^{1}H-NMR (CDCl$_3$, 500 MHz) δ 8.95 (1H, d, *J* = 2.5, H^6), 8.62 (1H, d, *J* = 8.0, H^4), 8.41 (1H, dd, *J* = 8.5, 2.0, H^8), 8.23 (1H, br s, H^{13}), 7.58 (1H, d, *J* = 8.5, H^9), 7.39 (1H, d, *J* = 8.0, H^3), 7.18 - 7.27 (10H, m, H^{22}), 5.03-5.15 (2H, m, H^{19}), 4.54 (2H, d, *J* = 5.0, H^{12}), 3.97 (3H, s, H^{11}), 2.40 - 3.16 (22H, br m, H^{15,16,26}), 1.41 (6H, d, *J* = 6.5, H^{20}), 1.39 (9H, s, H^{25}); ^{13}C-NMR (CDCl$_3$, 126 MHz,) δ 176.8 (C^5), 171.3 (C^{14}), 170.4 (C^{17}), 165.8 (C^{10}), 163.9 (C^2), 160.0 (C$^{1'}$), 158.3 (C$^{9'}$), 156.3 (C^{23}), 143.6, 143.1 (C^{21}), 138.2 (C^4), 136.4 (C^8), 129.3 (C^6), 126.4 – 129.0 (C^{22}), 127.2 (C^7), 121.6 (C$^{5'}$), 120.0 (C^3), 119.0 (C^9), 115.5 (C$^{4'}$), 80.1 (C^{24}), 60.0 (C^{26}), 59.3 (C^{26}), 54.4 (C^{26}), 53.3 (C^{26}), 52.8 (C^{11}), 48.6 (C^{19}), 47.7 (C^{15,16}), 44.7 (C^{12}), 28.6 (C^4), 21.6 (C^{25}), 21.4 (C^{20}); MS(ES+) *m/z* 919.7 [M + H]$^+$; HRMS (ES+) *m/z*: [M + H]$^+$ found 919.4720 C$_{50}$H$_{63}$O$_9$N$_8$ requires 919.4713.

2-[(2-(4,10-Bis-[((S)-1-phenyl-ethylcarbamoyl)-methyl]-1,4,7,10-tetraazacyclododec-1-yl)acetylamino)-methyl]-10-oxo-10*H*-9-oxa-1-aza-anthracene-6-carboxylic acid methyl ester, (L^1)[2]
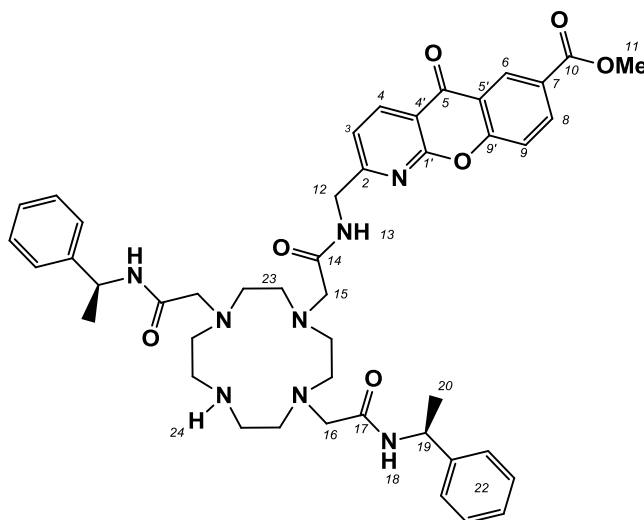
2-[(2-(7-*tert*-Butoxycarbonyl-4,10-bis-[((*S*)-1-phenyl-ethylcarbamoyl)-methyl]-1,4,7,10-tetraaza-cyclododec-1-yl)-acetylamino)-methyl]-10-oxo-10*H*-9-oxa-1-aza-anthracene-6-carboxylic acid methyl ester (85.0 mg,) in DCM : TFA (50 : 50, 2 ml) was stirred in a sealed flask for 12 h yielding a yellow solution. Solvent was then removed under reduced pressure to yield the a glassy yellow solid in quantitative yield which was used immediately in the next step, having confirmed removal of the Boc-protecting group by mass spectrometry and ^{1}H-NMR spectroscopy.

^{1}H-NMR (CDCl$_3$, 400 MHz) δ 9.31 (1H, s, H^{13}), 8.91 (1H, d, *J* = 1.5, H^6), 8.58 (1H, d, *J* = 8.0, H^4), 8.39 (1H, dd, *J* = 8.5, 1.5, H^8), 8.10 (2H, br s, H^{18}), 7.57 (1H, d, *J* = 8.5, H^9), 7.38 (1H, d, *J* = 8.0, H^3), 7.15 -

7.23 (10H, m, H^{22}), 4.90 (2H, br m, H^{19}), 4.55 (2H, br m, H^{12}), 3.96 (3H, s, H^{11}), 2.85 - 3.65 (22H, br m, C^{16,26}), 1.40 (6H, s, J = 6.5 H^{20}); MS (ES+) m/z 819 .5 [M + H]$^+$.

[Eu·L^1]Cl$_3$
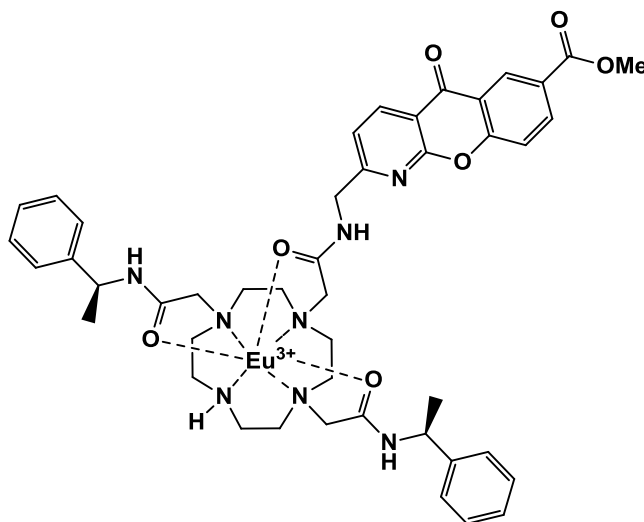
2-[(2-(4,10-Bis-[((*S*)-1-phenyl-ethylcarbamoyl)-methyl]-1,4,7,10-tetraazacyclododec-1-yl)acetylamino)-methyl]-10-oxo-10*H*-9-oxa-1-aza-anthracene-6-carboxylic acid methyl ester (20.1 mg, 22.6 μmol) was added to Eu(OTf)$_3$ (16.5 mg, 27.8 μmol) and dissolved in MeCN (1 ml). The reaction stirred for 48 h at 75 ℃. The reaction was cooled to room temperature and the solvents removed under reduced pressure. The remaining residue was dissolved in dry MeCN (0.1 ml) and the mixture dropped onto anhydrous Et$_2$O (5 ml) which resulted in the precipitation of the title compound as a triflate salt. The precipitate was centrifuged and dissolved in aqueous MeOH : H$_2$O (50 : 50, 3 ml). The pH was then adjusted carefully to 10 by addition of conc. NaOH solution to remove the excess Eu as Eu(OH)$_3$ resulting in a white precipitate, which was removed by centrifugation. The pH was adjusted back to neutral and the mixture lyophlised to give a bright yellow solid which was loaded onto a DOWEX 1-X8(Cl) anion exchange resin. The column was eluted with water → 10% NH$_4$OH. The fractions were combined and lyophilized to yield the Eu-complex as its chloride salt as a light yellow glassy solid (10.8 mg, 11.1 μmol, 49%).

λ_{abs}(H$_2$O): 332 nm; HRMS (ES+) m/z: [M + 2Na]$^+$ found 1017.3122 C$_{45}$H$_{55}$^{151}EuN$_8$O$_7$Na$_2$ requires 1017.3107.; t_R = 10.0 min; τ_{H2O} = 0.26 ms, τ_{D2O} = 0.64 ms, q =2.2 .

[Tb·L¹]Cl₃

The complex was prepared using an analogous method as for [Eu·L¹]Cl₃ using L¹ (20.1 mg, 22.6 μmol) and Tb(OTf)₃ (16.9 mg, 27.8 μmol) to yield the terbium complex as its chloride salt (16.6 mg, 17.0 μmol, 75%).

λ_{abs}(H₂O): 332 nm; HRMS (ES+) *m/z*: [M + 2Na]⁺ found 1023.3179 C₄₅H₅₅TbN₈O₇Na₂ requires 1023.3164.; t_R = 10.0 min; τ_{H2O} = 1.15 ms, τ_{D2O} = 2.50 ms, *q* =2.1 .

5.2.4 [Ln·L²]³⁺ and [Ln·L³]

(*SS*)-1,7-Bis(benzyloxycarbonyl)-4,10-bis(ethyl-*N*-acetyl-*S*-alanine)-1,4,7,10-tetraazacyclododecane
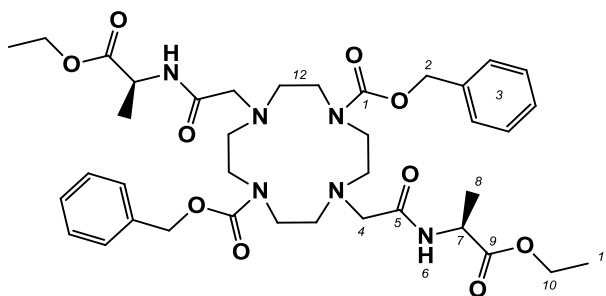
1,7-Bis(benzyloxycarbonyl)-1,4,7,10-tetraazacyclododecane (1.82 g, 4.13 mmol) was dissolved in dry MeCN (20 ml) and bromoacetyl-(*S*)-alanine ethyl ester (2.07 g, 8.69 mmol) was added. K₂CO₃ (1.4 g, 10.2 mmol) was added and the mixture stirred at 60 °C under argon for 2 days. The reaction was allowed to cool to room temperature and filtered. Solvent was removed under reduced pressure. The product was isolated by column chromatography (silica, DCM → 4% MeOH), as a light orange glassy oil (2.92 g, 3.87 mmol, 94%).

¹H-NMR (CDCl₃, 700 MHz) δ 7.50 – 7.61 (2H, br s, H⁶), 7.27 7.37 (10H, br m, H³), 5.05 (4H, s, H²), 4.31-4.52 (2H, br m, H⁷), 4.09 (4H, q, *J* = 7.0, H¹⁰), 2.76 – 3.47 (16H, br, H⁴,¹²), 1.21-1.41 (3H, br m, H⁸), 1.21 (6H, t, *J* = 7.0, H¹¹); ¹³C-NMR (CDCl₃, 176 MHz) δ 173.9 (C⁹), 170.9 (C⁵), 157.0 (C¹), 136.7 (C³), 128.8 (C³), 128.4 (C³), 67.6 (C¹⁰), 61.5 (C⁴), 55.9 (C¹²), 54.9 (C¹²), 48.1 (C⁷), 18.1 (C⁸), 14.4 (C¹⁰); MS (ES+) *m/z* 755.4 [M + H]⁺; HRMS (ES+) (*m/z*): [M + H]⁺ calculated for C₃₈H₅₅N₆O₁₀ 755.3980, found 755.3967.

(*SS*)-1,7-Bis(ethyl-*N*-acetyl-*S*-alanine)-1,4,7,10-tetraazacyclododecane
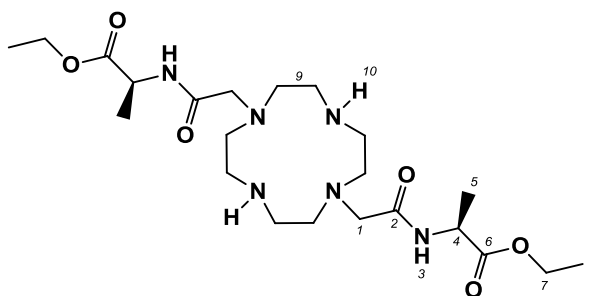
(*SS*)-1,7-Bis(benzyloxycarbonyl)-4,10-bis(ethyl-*N*-acetyl-*S*-alanine)-1,4,7,10-tetraazacyclododecane (0.973 g, 1.35 mmol) was dissolved in MeOH (20 ml) and Pd(OH)$_2$/C (Pd content 10%) (75 mg) added. The mixture was shaken in a Parr hydrogenator flask at 40 psi H$_2$ for 3 days. The resulting mixture was filtered through celite leaving a clear solution which was dried under reduced pressure to yield a yellow viscous oil (0.400 g, 0.823 mmol, 61%).

^{1}H-NMR (CDCl$_3$, 400 MHz) δ 7.61-7.80 (2H, br m, H^{10}), 7.44.7.60 (2H, br m, H^3), 4.50-4.58 (2H, m, H^4), 4.11-4.22 (4H, m, H^7), 3.13-3.33 (4H, m, H^1), 2.60 - 2.85 (16H, br, H^9), 1.35-1.39 (6H, m, H^8), 1.21-1.30 (6H, m, H^5); ^{13}C-NMR (CDCl$_3$, 101 MHz) δ 173.1 (C^6), 171.0 (C^2), 62.1 (C^7), 61.4 (C^1), 53.4 (C^9), 52.5 (C^9), 48.2 (C^4), 18.5 (C^6), 14.4 (C^8); MS (ES+) *m/z* 487.4 [M + H]$^+$; HRMS (ES+) (*m/z*): [M + H]$^+$ calculated for C$_{22}$H$_{43}$O$_6$N$_6$ 487.3239, found 487.3248.

(*SS*)-1,7-Bis(ethyl-*N*-acetyl-*S*-alanine)-4-carboxylic   acid-*tert*-butyl-ester-1,4,7,10-tetraazacyclododecane
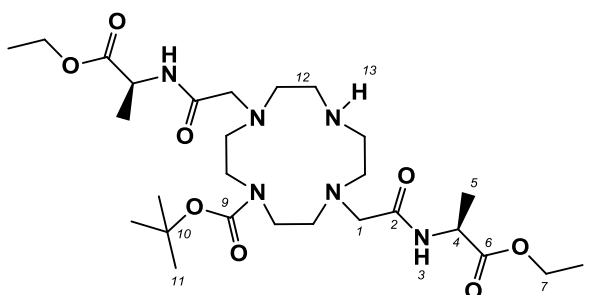
(*SS*)-1,7-Bis(ethyl-*N*-acetyl-*S*-alanine)-1,4,7,10-tetraazacyclododecane (0.812 g, 1.67 mmol) and di-*tert*-butyl dicarbonate (0.363 mg, 1.67 mmol) were stirred, under argon, in CHCl$_3$ at 30 °C for 18 h. Solvent was then removed under reduced pressure and the product purified by column chromatography (alumina, DCM → 3% MeOH) to yield a light yellow glassy oil (239 mg, 0.407 mmol, 24%).

R_F = 0.23 (alumina, DCM : 8% MeOH); ^{1}H-NMR (CDCl$_3$, 700 MHz) δ 7.47 (2H, br s, H^3), 4.58 (2H, q, J = 7.5, H^4), 4.16 (4H, q, J = 7.5, H^7), 3.16-3.39 (4H, m, H^1), 2.80 - 3.40 (16H, br, H^{12}), 1.42 (9H, s, H^{11}), 1.40 (6H, t, J = 7.5, H^5), 1.24 (6H, t, J = 7.5, H^8); ^{13}C-NMR (CDCl$_3$, 126 MHz) δ 173.2 (C^6), 170.5 (C^2), 156.5 (C^9), 80.4 (C^{10}), 61.9 (C^7), 59.7 (C^1), 55.3 (C^{12}), 48.2 (C^{12}), 48.0 (C^4), 28.9 (C^{11}), 18.3 (C^5), 14.5 (C^8); MS (ES+) m/z 587.5 [M + H]$^+$; HRMS (ES+) (m/z): [M + H]$^+$ calculated for C$_{27}$H$_{51}$N$_6$O$_8$ 587.3758, found 587.3768.

Tert-butyl 4,10-bis([(2S)-1-ethoxy-1-oxopropan-2-yl]carbamoyl)methyl)-7-[([7-(methoxycarbonyl)-5-oxo-5H-chromeno[2,3-b]pyridin-2-yl]methyl)carbamoyl)methyl]-1,4,7,10-tetraazacyclododecane-1-carboxylate
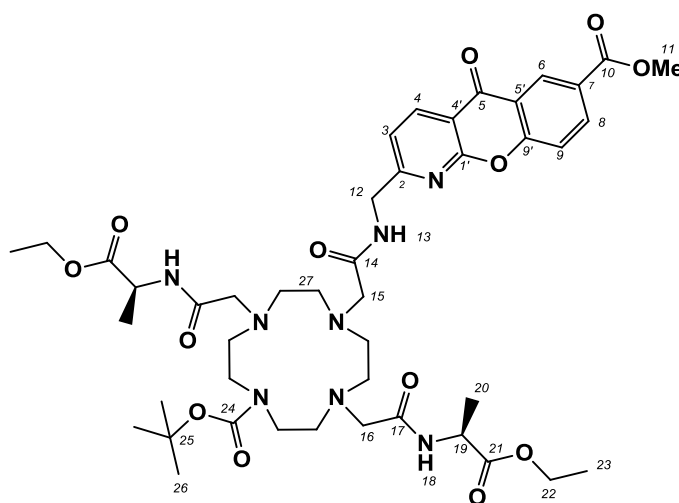
(*SS*)-1,7-Bis(ethyl-*N*-acetyl-*S*-alanine)-4-carboxylic acid *tert*-butyl ester-1,4,7,10-tetraazacyclododecane (98.7 mg, 0.168 mmol) was combined with 7-methoxycarbonyl-2-chloromethylcarbonylaminomethyl-1-azaxanthone (16.8 mg, 46.6 μmol) and DIPEA (40 μl, 0.230 mmol) in dry MeCN under argon. The mixture was stirred at 60 °C for 24 h. A further addition of 7-methoxycarbonyl-2-chloromethylcarbonylaminomethyl-1-azaxanthone (19.0 mg, 52.7 μmol) and DIPEA (50 μl, 0.287 mmol) was made at this time-point and the mixture stirred for a further 18 h. Solvent was then removed under reduced pressure and the residue purified by column chromatography (silica, DCM → 7% MeOH) to yield a glassy orange solid (63.9 mg, 70.2 μmol, 71%).

^{1}H-NMR (CDCl$_3$, 500 MHz) δ 11.21 (2H, br s, H^{18}), 8.96 (1H, d, J = 2.5, H^6), 8.64 (1H, d, J = 8.0, H^4), 8.41 (1H, dd, J = 9.0, 2.5, H^8), 7.60 (1H, d, J = 9.0, H^9), 7.43 (1H, d, J = 8.0, H^3), 4.71 (2H, d, J = 5.0, H^{12}), 4.50 (2H, p, J = 7.0, H^{19}), 4.12 (4H, q, J = 7.0, H^{22}), 3.96 (3H, s, H^{11}), 3.55 - 2.60 (22H, br. m, H^{15,16,27}), 1.53 (6H, t, J = 7.5, H^{20}), 1.39 (9H, s, H^{26}), 1.37 (6H, t, J = 7.0, H^{23}); ^{13}C-NMR (CDCl$_3$, 126 MHz) δ 176.8 (C^5), 173.1 (C^{14}), 165.7 (C^{17}), 160.0 (C$^{1'}$), 158.2 (C$^{9'}$), 155.8 (C^{24}), 138.2 (C^4), 136.3 (C^8), 129.3 (C^6), 127.0 (C^7), 121.5 (C$^{5'}$), 119.7 (C^3), 118.9 (C^9), 115.4 (C$^{4'}$), 61.6 (C^{22}), 53.7 (C^{27}),

52.7 (C^{11}), 47.4 (C^{16}), 46.7 (C^{27}), 44.8 (C^{12}), 42.0 (C^{19}), 28.6 (C^{25}), 18.8 (C^{26}), 14.3 (C^{23}), 12.2 (C^{20}); HRMS (ES+) (*m/z*): [M + H]+ calculated for $C_{44}H_{63}N_8O_{13}$ 911.4515, found 911.4518.

(*SS*)-1,7-Bis(ethyl-*N*-acetyl-*S*-alanine)-4-[7-methoxycarbonyl-2-chloromethylcarbonylmethyl-1-azaxanthone]-1,4,7,10-tetraazacyclododecane, (L²)
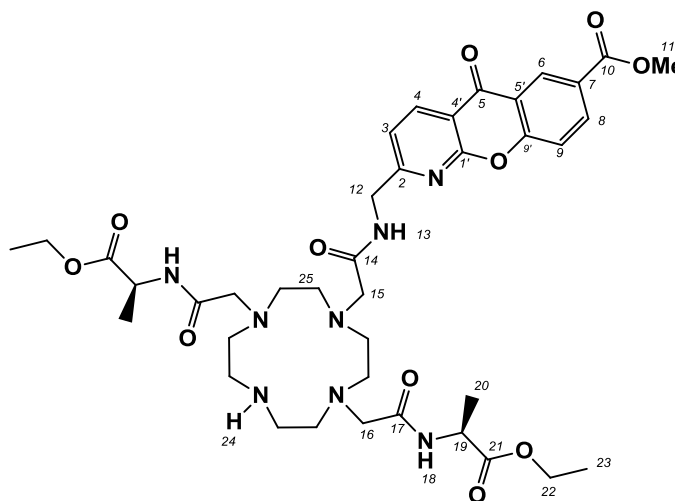
Tert-butyl 4,10-bis([(2*S*)-1-ethoxy-1-oxopropan-2-yl]carbamoyl}methyl)-7-[([7-(methoxycarbonyl)-5-oxo-5H-chromeno[2,3-b]pyridin-2-yl]methyl}carbamoyl)methyl]-1,4,7,10-tetraazacyclododecane-1-carboxylate (98.7 mg, 0.168 mmol) in DCM : TFA (50 : 50, 2 ml) was stirred in a sealed flask for 12 h yielding a yellow solution. Solvent was then removed under reduced pressure to yield a glassy yellow solid which was used immediately in the next step, after verifying removal of the Boc-protecting group by mass spectrometry. MS (ES+) *m/z* 811.4 [M + H]+.

[Eu·L²]Cl₃,
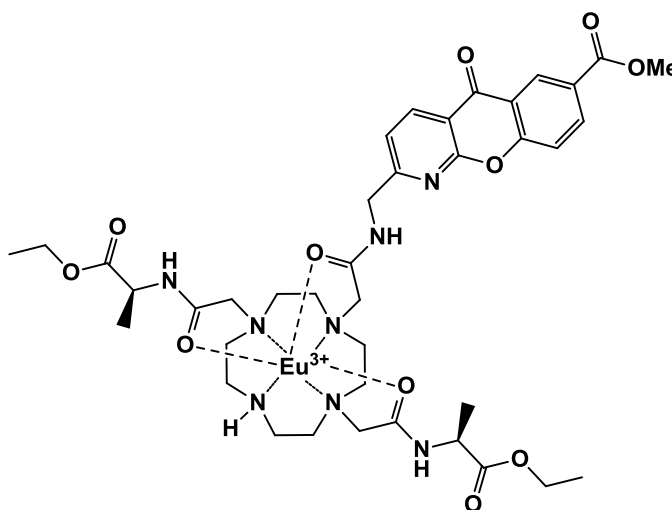
(*SS*)-1,7-Bis(ethyl-*N*-acetyl-*S*-alanine)-4-[7-methoxycarbonyl-2-chloromethylcarbonylmethyl-1-azaxanthone]-1,4,7,10-tetraazacyclododecane (22.4 mg, 23.3 μmol) was added to Eu(OTf)₃ (19 mg, 31.9 μmol) and dissolved in MeCN (1 ml). The reaction was stirred for 48 h at 75 ℃. The reaction was cooled to room temperature and the solvents removed under reduced pressure. The remaining residue was dissolved in dry MeCN (0.1 ml) and the mixture dropped onto anhydrous Et₂O (5 ml) which resulted in the precipitation of the triflate salt. The precipitate was centrifuged and dissolved in aqueous MeOH : H₂O (50 : 50, 3 ml). The pH was then adjusted carefully to 10 by addition of conc. NaOH solution to remove any excess Eu as Eu(OH)₃, resulting in a white precipitate which was removed by centrifugation. The pH was adjusted back to neutral and the mixture lyophilised to give a bright yellow solid which was loaded onto a DOWEX 1-X8(Cl) anion exchange resin. The column was eluted with water → 10% NH₄OH. The fractions were combined and lyophilized to yield the chloride salt as a light yellow glassy solid (14.0 mg, 14.5 μmol, 62%).

HRMS (ES+) (*m/z*): [M + HCO₂⁻]²⁺ calculated for $C_{40}H_{57}^{153}EuN_8O_{13}$ 504.1550 found 504.1538; t_R = 9.4 min; τ_{H2O} = 0.26 ms, τ_{D2O} = 0.58 ms; q = 2.0.

[Tb·L²]Cl₃,

The complex was prepared by an analogous method as for [Eu.L²]Cl₃, using L² (11.2 mg, 11.7 μmol) and Tb(OTf)₃ (8.3 mg, 14.0 μmol) to yield the Tb-complex as its chloride salt (9.0 mg, 9.3 μmol, 79%).

HRMS (ES+) (*m/z*): [M + 2Na]$^{2+}$ calculated for $C_{40}H_{57}TbNa_2N_8O_{13}$ 507.1571 found, 507.1540; t_R = 9.5 min; τ_{H2O} = 1.11 ms, τ_{D2O} = 2.44 ms; q = 2.2.

2- [[2-(4- [(1-Carboxyethyl)carbamoyl]methyl]-10[[(carboxymethyl)carbamoyl]methyl]-1,4,7,10-tetraazacyclododecan-1-yl)acetamido]methyl}-5-oxo-5H-chromeno[2,3-b]pyridine-7-carboxylic acid, (H$_3$L^3)
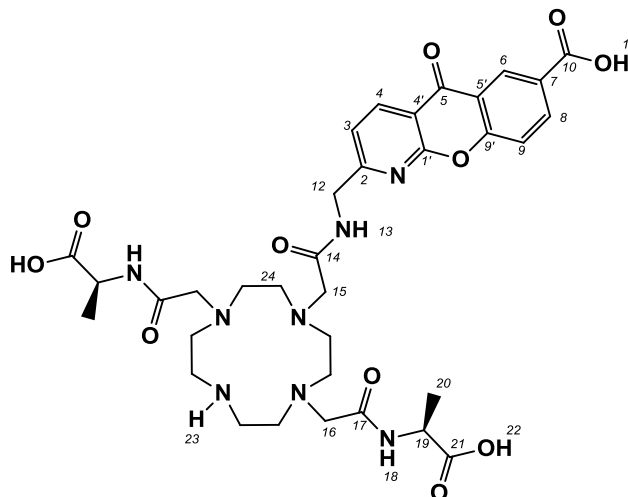
Aqueous KOD solution (1 ml, 0.1 M) was added to (*SS*)-1,7-bis(ethyl-*N*-acetyl-*S*-alanine)-4-[7-methoxycarbonyl-2-chloromethylcarbonylmethyl-1-azaxanthone]-1,4,7,10-tetraazacyclododecane (30 mg, 40.0 μmol). The reaction mixture was stirred under argon at room temperature and progress monitored by ^{1}H-NMR, observing the formation of ethanol and methanol solvent peaks, with the corresponding elimination of the methyl- and ethyl-ester peaks. After 3 h, the pH of the mixture was decreased to pH 6.5 with conc. HCl$_{(aq)}$ and the solution loaded onto a DOWEX 50X4-100 strong cation exchange resin. The column was eluted with 10% NH$_4$OH and the fractions containing product lyophilized to yield the title compound as a orange glassy solid which was immediately used in the complexation reactions (16.1 mg, 21.6 μmol, 54%).

^{1}H-NMR (D$_2$O, 400 MHz) δ [signals all quite broad], 8.71-8.94 (1H, br m, H^6), 8.48-8.64 (1H, br d, H^4), 8.28-8.41 (1H, br m, H^8), 7.55-7.85 (1H,br m, H^9), 7.32-7.45 (1H,br m, H^3), 4.50-4.70 (2H, br m, H^{12}), 4.32-4.44 (2H, br m, H^{19}), 3.55 - 2.60 (22H, br m, H^{15,16,24}), 1.53 (6H, br t, *J* = 7.5, H^{20}).

[Eu·L³]
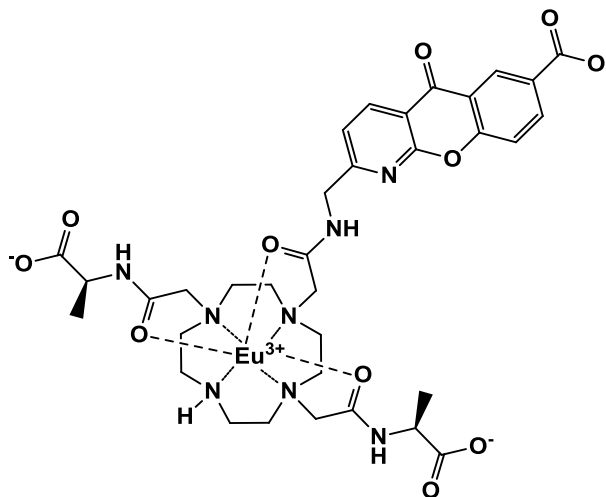
2- [[2-(4- [(1-Carboxyethyl)carbamoyl]methyl]-10[[(carboxymethyl)carbamoyl]methyl]-1,4,7,10-tetraazacyclododecan-1-yl)acetamido]methyl)-5-oxo-5H-chromeno[2,3-b]pyridine-7-carboxylic acid (12.1 mg, 16.0 μmol) was added to Eu(OAc)₃ (1.2 eq, 19.2 μmol) and dissolved in 3 ml H_2O : MeOH (7 : 1). The pH was carefully adjusted to 5 by the addition of acetic acid and the reaction stirred for 48 h at 75 ℃. The reaction was cooled to room temperature and the pH carefully adjusted to 10 by the addition of conc. NaOH solution, to precipitate excess europium as Eu(OH)₃ which was removed by centrifugation. The pH was adjusted back to 6.5 with acetic acid and the sample lyophilized to yield the product (2.5 mg, 2.8 μmol, 18%).

HRMS (ES+) (*m/z*): [M + H]⁺ calculated for $C_{34}H_{42}{}^{151}EuN_8O_{11}$ 891.2185 found, 891.2205; t_R = 8.8 min; τ_{H2O} = 0.26 ms, τ_{D2O} = 0.67 ms; q = 2.3.

[Tb.L³]

The complex was prepared using an analogous method as for [Eu.L³]Cl₃ using L³ (4.0 mg, 5.4 μmol) and Tb(OAc)₃ (2.3 mg, 6.5 μmol) to yield the Tb-complex as its chloride salt (1.0 mg, 1.1 μmol, 20%)

HRMS (ES+) (*m/z*): [M + H]⁺ calculated for $C_{34}H_{42}TbN_8O_{11}$ 896.2227, found 896.2270; t_R = 8.8 min; τ_{H2O} = 1.11 ms, τ_{D2O} = 2.55 ms; q = 2.3.

5.2.5 [Ln·L⁴]³⁺ and [Ln·L⁴]⁻

(SS)-1,7-Bis(benzyloxycarbonyl)-4,10-bis(diethyl-N-acetyl-S-glutamate)-1,4,7,10-tetraazacyclododecane
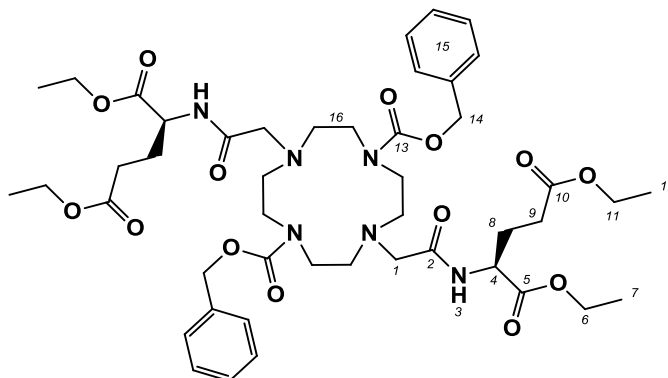
1,7-Bis(benzyloxycarbonyl)-1,4,7,10-tetraazacyclododecane (1.35 g, 3.00 mmol) was dissolved in dry MeCN (50 ml) and *N*-bromoacetyl-(*S*)-glutamic acid diethyl ester (2.08 g, 6.38 mmol) was added. K_2CO_3 (2.50 g, 18.0 mmol) was added and the mixture stirred at 60 °C under argon for 3 days. The reaction was allowed to cool to room temperature and filtered. Solvent was removed under reduced pressure. The desired product was isolated by column chromatography (silica, DCM → 3% MeOH) as a glassy orange solid (1.08 g, 1.55 mmol, 81%).

^{1}H-NMR (CDCl₃, 400 MHz) δ 7.63 (2H, br s, H³), 7.27 – 7.36 (10H, m, H¹⁵), 5.10 (4H, q, *J* = 7.0, H¹⁴), 4.53 (2H, br s, H⁴), 4.15 (4H, q, *J* = 7.0, H⁶), 4.09 (4H, q, *J* = 7.0, H¹¹), 3.30 – 3.56 (8H, br, H¹⁶), 2.73 – 3.29 (4H, br, H¹), 2.72 – 2.96 (8H, br, H¹⁶), 2.40 (4H, br, H⁹), 2.19 (2H, br, H⁸), 2.03 (2H, br, H⁸'), 1.25 (6H, t, *J* = 7.0, H¹²), 1.22 (6H, t, *J* = 7.0, H⁷); ^{13}C-NMR (CDCl₃, 101 MHz) δ 172.9 (C¹⁰), 172.8 (C⁵), 172.0 (C²), 157.0 (C¹³), 136.7 (C¹⁵q), 128.7 (C¹⁵), 128.3 (C¹⁵), 128.3 (C¹⁵), 67.5 (C¹⁴) 61.7 (C⁶), 60.8 (C¹¹), 55.1 (C¹⁶), 55.2 (C¹), 51.7 (C⁴), 47.9 (C¹⁶), 30.7 (C⁹), 27.3 (C⁸), 14.3 (C⁷), 14.3 (C¹¹); MS (ES+) *m/z* 927.9 [M + H]⁺; HRMS (ES+) (*m/z*): [M + H]⁺ calculated for $C_{46}H_{67}N_6O_{14}$ 927.4715, found 927.4710.

(*SS*)-1,7-Bis(diethyl-*N*-acetyl-*S*-glutamate)-1,4,7,10-tetraazacyclododecane
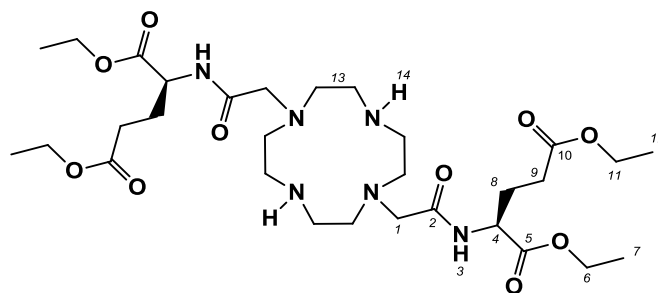
(*SS*)-1,7-Bis(benzyloxycarbonyl)-4,10-bis(ethyl-*N*-acetyl-*S*-glutamate)-1,4,7,10-tetraazacyclododecane (1.72 g, 1.92 mmol) was dissolved in MeOH (20 ml) and Pd(OH)$_2$/C (Pd content 10%) (75 mg) added. The mixture was shaken in a Parr hydrogenator flask at 40 psi H$_2$ for 3 days. The resulting mixture was filtered through celite leaving a clear solution which was dried under reduced pressure to a light yellow oil (1.08 g, 1.55 mmol, 81%).

^{1}H-NMR (CDCl$_3$, 500 MHz) δ 8.65 (2H, br s, H^{14}), 7.88 (2H, br d, H^3), 4.57 (2H, m, H^4), 4.15 (4H, m, H^6), 4.09 (4H, q, *J* = 7.0, H^{11}), 3.34 (2H, d, *J* = 16.0 H^1), 3.26 (2H, d, *J* = 16.0 H$^{1'}$), 2.70 - 3.00 (16H, br m, H^{13}), 2.40 (4H, m, H^9), 2.19 (2H, m, H^8), 1.99 (2H, m, H$^{8'}$), 1.24 (6H, t, *J* = 7.5, H^{12}), 1.22 (6H, t, *J* = 7.5, H^7); ^{13}C-NMR (CDCl$_3$, 126 MHz) δ 172.9 (C^{10}), 172.2 (C^5), 171.7 (C^2), 61.7 (C^6), 60.5 (C^{11}), 58.3 (C^1), 51.2 – 53.4 (C^{13}), 52.0 (C^4), 30.5 (C^9), 26.9 (C^8), 14.1 (C^7), 14.0 (C^{12}); HRMS (ES+) (*m/z*): [M + H]$^+$ calculated for C$_{30}$H$_{55}$N$_6$O$_{10}$ 659.3980, found 659.3984.

(*SS*)-1,7-Bis(ethyl-*N*-acetyl-*S*-glutamate)-4-carboxylic   acid-*tert*-butyl-ester-1,4,7,10-tetraazacyclododecane
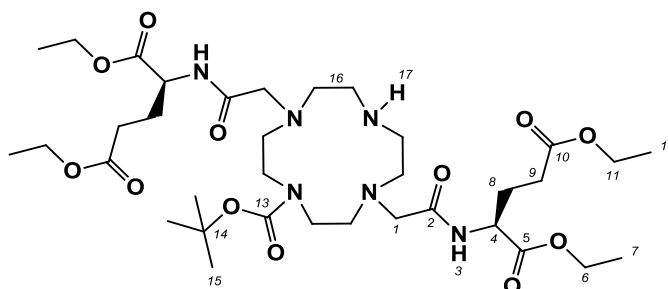
(*SS*)-1,7-Bis(ethyl-*N*-acetyl-*S*-glutamate)-1,4,7,10-tetraazacyclododecane (0.483 g, 0.694 mmol) and di-*tert*-butyl dicarbonate (0.150 mg, 0.687 mmol) were stirred, under argon, in CHCl$_3$ at 30 °C for 18 h. Solvent was removed under reduced pressure and the product purified by column chromatography (alumina, DCM → 1% MeOH) to yield a glassy orange solid. (224 mg, 0.295 mmol, 43%).

R_F = 0.28 (alumina, DCM : 3% MeOH); ^{1}H-NMR (CDCl$_3$, 500 MHz) δ 7.75 (1H, br s, H^{17}), 7.63 (2H, br d, H^3), 4.58 (2H, m, H^4), 4.17 (4H, m, H^6), 4.12 (4H, q, J = 7.0, H^{11}), 3.51 (2H, d, J = 15.5 H^1), 3.28 (2H, d, J = 15.5 H$^{1'}$), 2.80 - 3.40 (16H, br m, H^{16}), 2.45 (4H, t, J = 7.5, H^9), 2.22 (2H, m, H^8), 2.01 (2H, m, H$^{8'}$), 1.46 (9H, s, H^{15}), 1.27 (6H, t, J = 7.5, H^7), 1.25 (6H, t, J = 7.5, H^{12}); ^{13}C-NMR (CDCl$_3$, 126 MHz) δ 173.3 (C^{10}), 172.2 (C^5), 171.0 (C^2), 155.0 (C^{13}), 80.7 (C^{14}), 61.9 (C^6), 60.8 (C^{11}), 58.6 (C^1), 55.4 (C^{16}), 52.9 (C^{16}), 52.0 (C^4), 51.2 (C^{16}), 30.9 (C^9), 28.7 (C^{15}), 26.9 (C^8), 14.4 (C^7), 14.3 (C^{11}); HRMS (ES+) m/z: [M + H]$^+$ calculated for C$_{35}$H$_{63}$N$_6$O$_{12}$ 759.4504, found 759.4517.

Tert-butyl 4,10-bis([(2_S_)-1-ethoxy-1-oxopropan-2-yl]carbamoyl}methyl)-7-[([7-(methoxycarbonyl)-5-oxo-5H-chromeno[2,3-b]pyridin-2-yl]methyl)carbamoyl)methyl]-1,4,7,10-tetraazacyclododecane-1-carboxylate, (38)
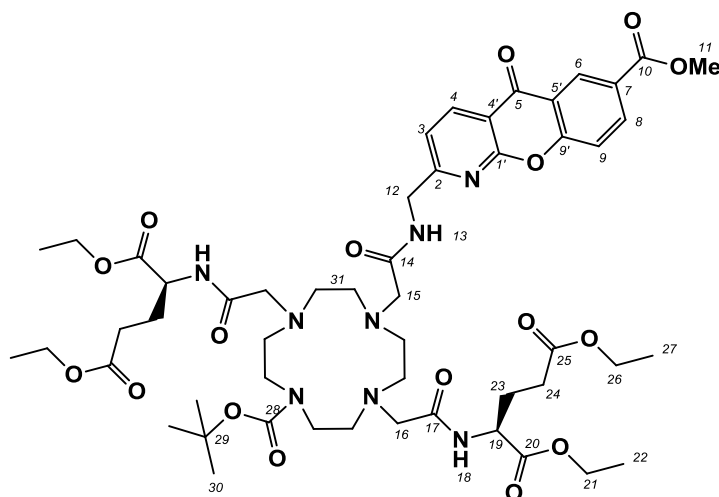
(_SS_)-1,7-Bis(ethyl-_N_-acetyl-_S_-glutamate)-4-carboxylic acid _tert_-butyl ester-1,4,7,10-tetraazacyclododecane (38.0 mg, 50.0 μmol) was combined with 7-methoxycarbonyl-2-chloromethylcarbonylaminomethyl-1-azaxanthone (18.0 mg, 49.9 μmol) and DIPEA (40 μl, 0.230 mmol) in dry MeCN under argon. The mixture was stirred at 60 °C for 24 h. Solvent was removed under reduced pressure and the residue purified by column chromatography (silica, DCM → 7 % MeOH) to yield a glassy orange solid (63.9 mg, 70.2 μmol, 71%).

^{1}H-NMR (CDCl$_3$, 500 MHz) δ 11.21 (2H, br s, H^{13}), 9.08 (1H, br s, H^{13}), 8.96 (1H, d, J = 2.5, H^6), 8.64 (1H, d, J = 8.0, H^4), 8.41 (1H, dd, J = 9.0, 2.5, H^8), 7.60 (1H, d, J = 9.0, H^9), 7.43 (1H, d, J = 8.0, H^3), 4.71 (2H, d, J = 5.0, H^{12}), 4.50 (2H, p, J = 7.0, H^{19}), 4.17 (4H, m, H^{21}), 4.12 (4H, q, J = 7.0, H^{26}), 3.96 (3H, s, H^{11}), 3.55 - 2.60 (22H, br. m, H^{15,16,31}), 2.41 (4H, t, J = 7.0, H^{24}), 2.21 (2H, m, H^{23}), 2.04 (2H, m, H^{23}), 1.39 (9H, s, H^{30}), 1.29 (6H, t, J = 7.0, H^{22}), 1.27 (6H, t, J = 7.0, H^{27}); ^{13}C-NMR (CDCl$_3$, 126 MHz) δ 176.8 (C^5), 173.1 (C^{25}), 172.4 (C^{14}), 170.8 (C^{17}), 160.0 (C$^{1'}$), 158.3 (C$^{9'}$), 156.0 (C^{28}),

138.2 (C[4]), 136.3 (C[8]), 129.3 (C[6]), 127.1 (C[7]), 121.6 (C[5']), 119.9 (C[5']), 119.0 (C[9]), 115.5 (C[4']), 80.5 (C[25]), 61.8 (C[22]), 60.7 (C[26]), 60.3 (C[31]), 59.5 (C[31]), 54.4 (C[31]), 53.1 (C[31]), 52.8 (C[11]), 52.0 (C[19]), 47.6 (C[16]), 44.8 (C[12]), 30.7 (C[24]), 28.6 (C[29]), 26.9 (C[23]), 20.5 (C[30]), 14.1 (C[27]); MS (ES+) *m/z* 1083.5 [M + H]+; HRMS (ES+) (*m/z*): [M + H]+ calculated for $C_{52}H_{75}N_8O_{17}$ 1083.5250, found 1083.5261.

(*SS*)-1,7-Bis(ethyl-*N*-acetyl-*S*-glutamate)-4-[7-methoxycarbonyl-2-chloromethylcarbonylmethyl-1-azaxanthone]-1,4,7,10-tetraazacyclododecane, (L[4])
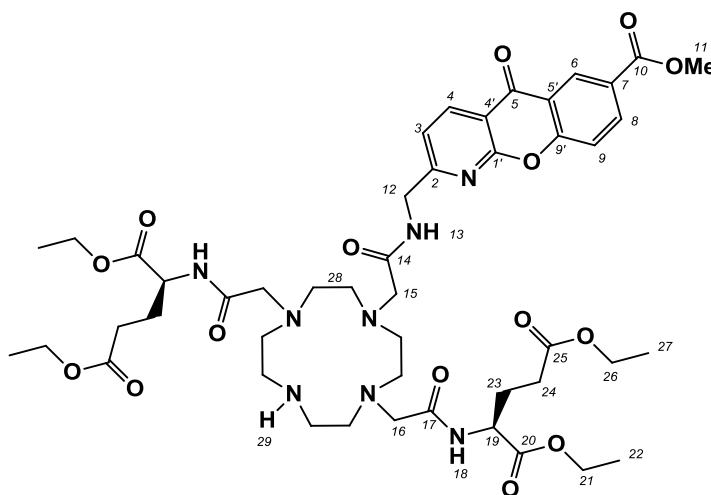
Tert-butyl 4,10-bis([(2*S*)-1-ethoxy-1-oxopropan-2-yl]carbamoyl}methyl)-7-[([7-(methoxycarbonyl)-5-oxo-5H-chromeno[2,3-b]pyridin-2-yl]methyl}carbamoyl)methyl]-1,4,7,10-tetraazacyclododecane-1-carboxylate (52.0 mg, 0.048 mmol) in DCM : TFA (50 : 50, 2 ml) was stirred in a sealed flask for 12 h yielding a yellow solution. Solvent was removed under reduced pressure to yield a glassy yellow solid in quantitative yield.

^{1}H-NMR (CDCl₃, 700 MHz) δ 8.65 (1H, d, *J* = 7.5, H[4]), 8.47 (1H, s, br, H[11]), 8.30 (1H, d, *J* = 8.0, H[6]), 7.85 (2H, s, br, H[16]), 7.78 (1H, t, *J* = 8.0, H[7]), 7.59 (1H, d, *J* = 8.0, H[9]), 7.48 (1H, d, *J* = 7.5, H[3]), 7.43 (1H, t, *J* = 8.0, H[8]), 4.71 (2H, d, *J* = 5.5, H[12]), 4.49 (2H, q, *J* = 7.0, H[19]), 4.13 (4H, q, *J* = 7.0, H[21]), 4.07 (4H, q, *J* = 7.0, H[26]), 2.40 (4H, t, *J* = 7.0, H[24]), 2.20 (2H, m, H[23]), 2.08 (2H, m, H[23']), 1.24 (6H, t, *J* = 7.0, H[25]), 1.21 (6H, t, *J* = 7.0, H[22]). ^{13}C-NMR (CDCl₃), 176 MHz) δ 177.4 (C[5]), 163.7 (C[2]), 160.2 (C[4']), 155.8 (C[9']), 138.2 (C[4]), 135.9 (C[7]), 127.0 (C[6]), 125.0 (C[8]), 121.9 (C[5']), 119.4 (C[3]), 118.6 (C[9]), 115.6 (C[1']), 61.9 (C[24]), 60.9 (C[21]), 52.2 (C[17]), 45.0 (C[10]), 30.9 (C[19]), 26.7 (C[18]), 14.4 (C[25]), 14.3 (C[22]); MS (ES+) *m/z* 984.0; HRMS (ES+) (*m/z*): [M + H]+ calculated for $C_{47}H_{67}N_8O_{15}$ 983.4726, found 983.4716.

[Eu·L⁴]Cl₃
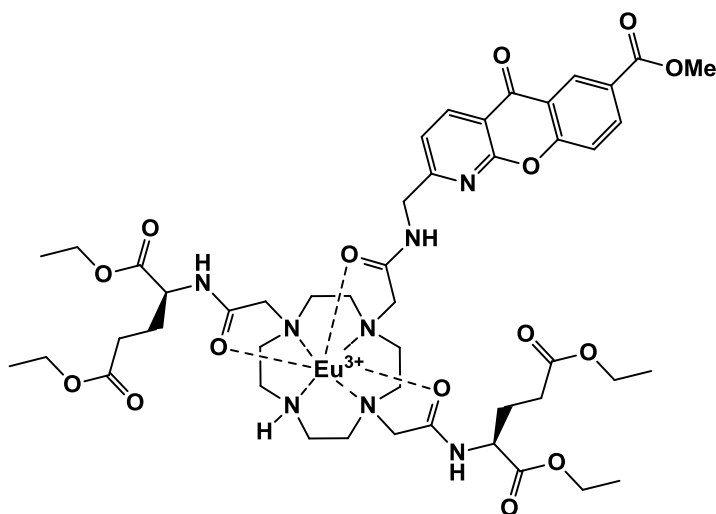
(*SS*)-1,7-Bis(ethyl-*N*-acetyl-*S*-glutamate)-4-[7-methoxycarbonyl-2-chloromethylcarbonylmethyl-1-azaxanthone]-1,4,7,10-tetraazacyclododecane (23.4 mg, 23.8 μmol) was added to Eu(OTf)₃ (15.6 mg, 26.2 μmol) and dissolved in MeCN (1 ml). The reaction was stirred for 72 h at 60 ℃. The reaction was then cooled to room temperature and the solvents removed under reduced pressure. The remaining residue was dissolved in dry MeCN (0.1 ml) and the mixture dropped onto anhydrous Et₂O (5 ml) which resulted in the precipitation of the title compound as a triflate salt. The precipitate was centrifuged and dissolved in aqueous MeOH : H₂O (50 : 50, 3 ml). The pH was then adjusted carefully to 10 by addition of conc. NaOH solution to remove the excess Eu as Eu(OH)₃ resulting in a white precipitate which was removed by centrifugation. The pH was adjusted back to neutral and the mixture lyophlised to give a bright yellow solid which was loaded onto a DOWEX 1-X8(Cl) anion exchange resin. The column was eluted with water → 10% NH₄OH. The fractions were combined and lyophilized to yield the Eu-complex as its chloride salt as a light yellow glassy solid (12.0 mg, 10.2 μmol, 43%).

HRMS (ES+) (*m/z*): $[M]^{3+}$ calculated for $C_{47}H_{66}{}^{151}EuN_8O_{15}$ 378.4615 found, 378.4612; t_R = 10.3 min; τ_{H2O} = 0.48 ms, τ_{D2O} = 1.14 ms; q = 0.9.

[Tb·L⁴]Cl₃

The complex was prepared by an analogous method as for [Eu.L⁴]Cl₃ using L⁴ (23.4 mg, 23.8 μmol) and Tb(OTf)₃ (15.9 mg, 26.2 μmol) to yield the Tb-complex as its chloride salt (26.3 mg, 22.2 μmol, 93%).

HRMS (ES+) (*m/z*): [M]$^{3+}$ calculated for $C_{47}H_{66}TbN_8O_{15}$ 380.4628 found, 380.4634; t_R = 10.4 min; τ_{H2O} = 1.24 ms, τ_{D2O} = 1.96 ms; q = 10.4

(2*S*)-2-[2-(4-([[((7-Carboxy-5-oxo-5H-chromeno[2,3-b]pyridin-2-yl)methyl)carbamoyl]methyl)-7-((([(1*S*)-1,3-dicarboxypropyl]carbamoyl)methyl)1,4,7,10-tetraazacyclododecan-1-yl)acetamido]pentane dioic acid, (L^5)
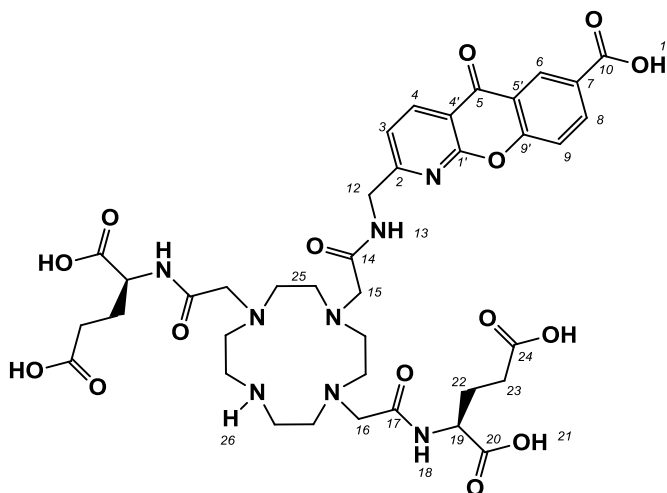
Aqueous KOD solution (1 ml, 0.1 M) was added to (*SS*)-1,7-Bis(ethyl-*N*-acetyl-*S*-glutamate)-4-[7-methoxycarbonyl-2-chloromethylcarbonylmethyl-1-azaxanthone]-1,4,7,10-tetraazacyclododecane (39.8 mg, 40.5 µmol). The reaction mixture was stirred under argon at room temperature and progress monitored by ^{1}H-NMR spectroscopy, observing the formation of ethanol and methanol solvent peaks, with the corresponding elimination of the methyl- and ethyl-ester peaks. After 3 h the pH of the mixture was decreased to pH 6.5 with conc. HCl$_{(aq)}$ and the solution loaded onto a DOWEX 50X4-100 strong cation exchange resin. The column was eluted with 10% NH$_4$OH and the fractions containing the desired product lyophilized to yield a orange glassy solid which was immediately used in the complexation reactions.

^{1}H-NMR (CDCl$_3$, 400 MHz) [all signals quite broad] δ 8.85 (1H, br m, H^6), 8.54 (1H, br d, H^4), 8.36 (1H, br m, H^8), 7.65 (1H, br m, H^9), 7.39 (1H, br m, H^3), 4.62 (2H, br m, H^{12}), 4.39 (2H, br m, H^{19}), 2.37 -3.54 (22H, br m, H^{15,16}), 2.39 (4H, br m, H^{34}), 2.10 (4H, br m, H^{23}).

Na₂[Eu·L⁵]
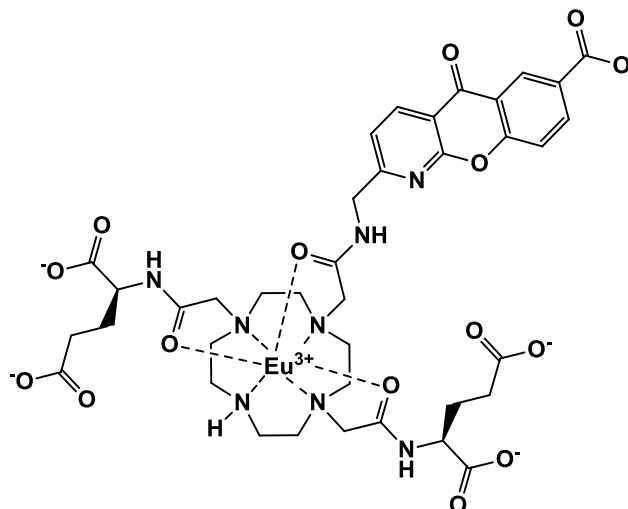
2-   [[2-(4-   [(1-Carboxyethyl)carbamoyl]methyl]-10[[(carboxymethyl)carbamoyl]methyl]-1,4,7,10-tetraazacyclododecan-1-yl)acetamido]methyl}-5-oxo-5H-chromeno[2,3-b]pyridine-7-carboxylic acid (14.2 mg, 16.7 μmol) was added to Eu(OAc)₃ (6.5 mg, 18.4 μmol) and dissolved in 3 ml H₂O : MeOH (7 : 1). The pH was carefully adjusted to 5 by the addition of acetic acid and the reaction stirred for 48 h at 75 ℃. The reaction was cooled to room temperature and the pH carefully adjusted to 10 by the addition of conc. NaOH solution, to precipitate excess europium as Eu(OH)₃ which was removed by centrifugation. The pH was adjusted back to 6.5 with acetic acid and the sample lyophilized to yield a colourless solid (3.2 mg).

HRMS (ES-) (m/z): $[M]^{2-}$ calculated for $C_{38}H_{45}{}^{151}EuN_8O_{15}$ 502.1035 found, 502.1042; t_R = 8.6 min; τ_{H2O} = 0.37 ms, τ_{D2O} = 0.75 ms; q = 1.1.

Na₂[Tb·L⁵]

The complex was prepared by an analogous method as for Na₂[Eu.L⁵] using L⁵ (14.2 mg, 16.7 μmol) and Tb(OAc)₃ (6.6 mg, 18.4 μmol) to yield the Tb-complex as its chloride salt (5.8 mg)

HRMS (ES-) (m/z): $[M]^{2-}$ calculated for $C_{38}H_{45}TbN_8O_{15}$ 505.1056 found, 505.1046; t_R = 9.4 min; τ_{H2O} = 1.21 ms, τ_{D2O} = 2.39 ms; q = 1.5.

5.2.6 Ligands and complexes of L[6-9]

(*SS*)-1,7-Bis(ethyl-*N*-acetyl-*S*-alanine)-4-[7-methoxycarbonyl-2-chloromethylcarbonylmethyl-1-azaxanthone]-10-[2'-(methylsulfonylamino)ethyl]-1,4,7,10-tetraazacyclododecane, (L[6])
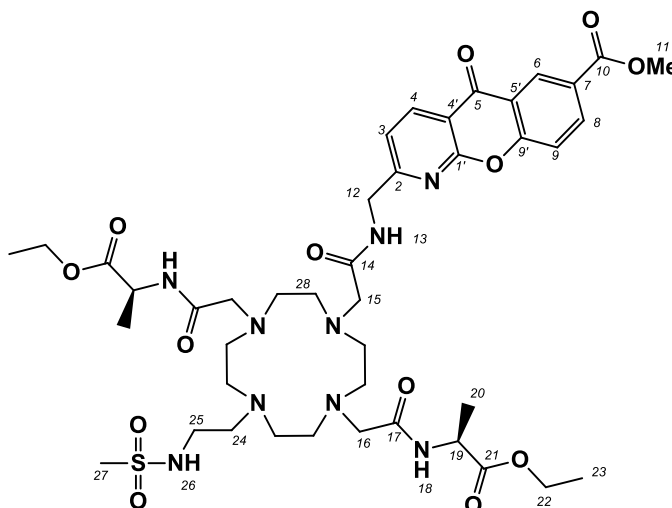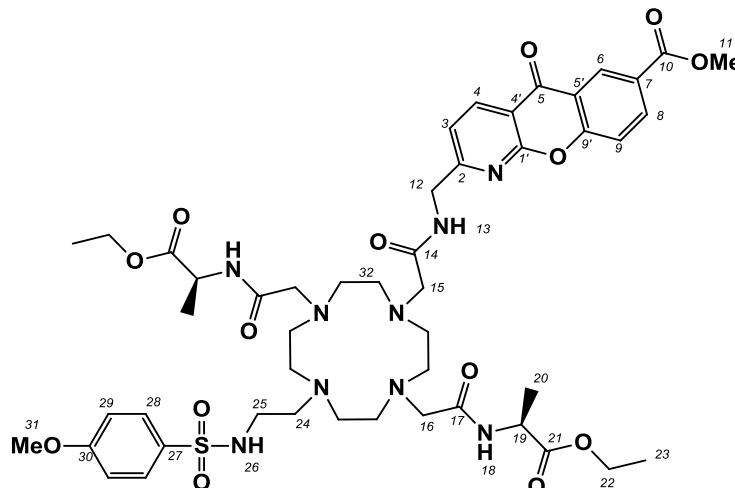

(*SS*)-1,7-Bis(ethyl-*N*-acetyl-*S*-alanine)-4-[7-methoxycarbonyl-2-chloromethylcarbonylmethyl-1-azaxanthone]-1,4,7,10-tetraazacyclododecane (100mg, 123 μmol), methylsulfonate-*N*-methanesulfonylethylamine (28 mg, 129 μmol) and K_2CO_3 (18 mg, 129 μmol) were stirred in MeCN (3 ml), under argon, at 65 °C for 24 h. Solvent was removed under reduced pressure and the residue dissolved in DCM (5 ml) allowing the insoluble salts to be removed by centrifugation. Solvent was again removed under reduced pressure before purification by column chromatography on silica gel (DCM → 10% MeOH) yielded an orange glassy solid (76 mg, 74.0 μmol, 60%).

^{1}H-NMR (CDCl$_3$, 700 MHz) δ 8.93 (1H, d, J = 1.5, H^6), 8.65 (1H, d, J = 8.0, H^4), 8.36 (1H, dd, J = 9.0, 1.5, H^8), 7.62 (1H, d, J = 9.0, H^9), 7.59 (1H, d, J = 8.0, H^3), 4.63-4.71 (2H, m, H^{12}), 4.41-4.49 (1H, m, H^{19}), 4.38-4.44 (1H, m, H^{19}), 4.12-4.18 (4H, m, H^{22}), 4.03.4.11 (2H, m, H^{25}), 3.97 (3H, s, H^{11}), 3.85 (3H, s, H^{31}), 1.85–3.45 (24H, br, H^{15,16,24,32}), 1.40-1.49 (6H, m, H^{20}), 1.14 (6H, t, J = 7.0, H^{23}); ^{13}C-NMR (CDCl$_3$, 126 MHz) δ 176.8 (C^5), 173.2 (C^{14}), 172.4 (C^{21}), 171.1 (C^x), 165.8 (C^{10}), 165.2 (C^{17}), 163.0 (C^2), 159.7 (C$^{1'}$), 158.3 (C$^{9'}$), 138.3 (C^4), 136.0 (C^8), 129.4 (C^{29}), 129.2 (C^6), 126.8 (C^7), 121.5 (C$^{5'}$), 120.3 (C^3), 118.9 (C^9), 115.3 (C$^{4'}$), 114.4 (C^{28}), 61.7 (C^{22}), 61.5 (C^{22}), 57.5 (C^{24}), 55.8 (C^{31}), 55.4 (C^{11}), 52.6 (C^{11}), 49.9 (C^{16}), 48.8 (C^{19}), 48.5 (C^{15}), 45.1 (C^{12}), 41.8 (C^{27}), 40.4 (C^{19}), 17.7 (C^{20}), 14.3 (C^{23}), 14.2 (C^{23}); HRMS (ES+) (*m/z*): [M+H]$^+$ calculated for $C_{42}H_{62}N_9O_{13}S$ 933.4188 found, 933.4181.
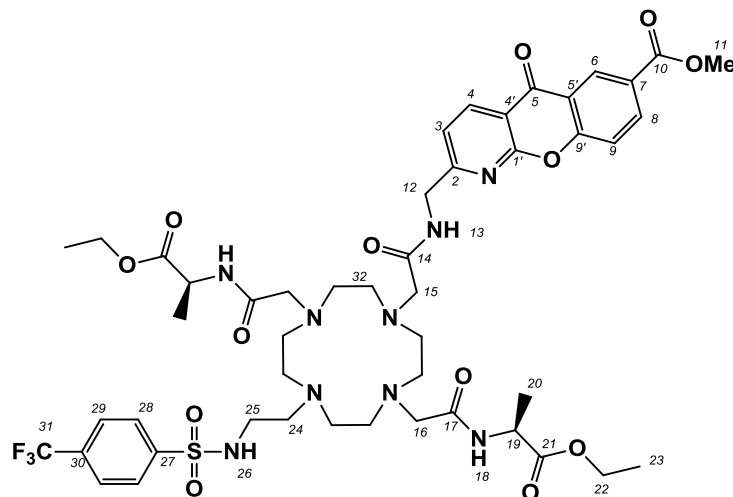
(*SS*)-1,7-Bis(ethyl-*N*-acetyl-*S*-alanine)-4-[7-methoxycarbonyl-2-chloromethylcarbonylmethyl-1-azaxanthone]-10-[2'-(4-Methoxyphenylsulfonylamino)ethyl]-1,4,7,10-tetraazacyclododecane, (L[7])

(*SS*)-1,7-Bis(ethyl-*N*-acetyl-*S*-alanine)-4-[7-methoxycarbonyl-2-chloromethylcarbonylmethyl-1-azaxanthone]-1,4,7,10-tetraazacyclododecane (100 mg, 123 μmol), 2-paramethoxyphenylsulfonate-*N*-methanesulfonylethylamine (50 mg, 125 μmol) and K_2CO_3 (18 mg, 129 μmol) were stirred in MeCN (3 ml), under argon, at 65 °C for 24 h. Solvent was removed under reduced pressure and the residue dissolved in DCM (5 ml) allowing the insoluble salts to be removed by centrifugation. Solvent was again removed under reduced pressure before purification by column chromatography on silica gel (DCM → 10% MeOH) to yield an orange glassy solid (40 mg, 39 μmol, 31%).

^{1}H-NMR (CDCl$_3$, 700 MHz) δ 8.93 (1H, d, *J* = 1.5, H^6), 8.65 (1H, d, *J* = 8.0, H^4), 8.36 (1H, dd, *J* = 9.0, 1.5, H^8), 7.75 (2H, d, *J* = 9.0, H^{29}), 7.62 (1H, d, *J* = 9.0, H^9), 7.59 (1H, d, *J* = 8.0, H^3), 6.95 (2H, d, *J* = 9.0, H^{28}), 4.63-4.72 (2H, m, H^{12}), 4.42-4.50 (1H, m, H^{19}), 4.37-4.43 (1H, m, H^{19}), 4.02-4.11 (2H, m, H^{25}), 3.97 (3H, s, H^{11}), 3.85 (3H, s, H^{31}), 1.85 – 3.45 (24H, br, H^{15,16,24,32}), 1.38-1.42 (3H, m, H^{20}), 1.33-1.37 (3H, m, H^{20}), 1.14 (3H, t, *J* = 7.0, H^{23}), 1.12 (3H, t, *J* = 7.0, H^{23}); ^{13}C-NMR (CDCl$_3$, 126 MHz) δ 176.8 (C^5), 173.2 (C^{14}), 172.4 (C^{21}), 165.8 (C^{10}), 165.2 (C^{17}), 163.0 (C^2), 159.7 (C$^{1'}$), 158.3 (C$^{9'}$), 138.3 (C^4), 136.0 (C^8), 129.4 (C^{29}), 129.2 (C^6), 126.8 (C^7), 121.5 (C$^{5'}$), 120.3 (C^3), 118.9 (C^9), 115.3 (C$^{4'}$), 114.4 (C^{28}), 61.7 (C^{22}), 61.5 (C^{22}), 57.5 (C^{24}), 55.8 (C^{31}), 55.4 (C^{11}), 52.6 (C^{11}), 49.9 (C^{16}), 48.8 (C^{19}), 48.5 (C^{15}), 45.1 (C^{12}), 40.4 (C^{19}), 17.7 (C^{20}), 14.3 (C^{23}), 14.2 (C^{23}); HRMS (ES+) *m/z*: [M + H]$^+$ calculated for $C_{48}H_{66}N_9O_{14}S$ 1024.445 found 1024.459.

(*SS*)-1,7-Bis(ethyl-*N*-acetyl-*S*-alanine)-4-[7-methoxycarbonyl-2-chloromethylcarbonylmethyl-1-azaxanthone]-10-[2'-(4-trifluoromethylphenylsulfonylamino)ethyl]-1,4,7,10-tetraazacyclododecane, (L[8])

(*SS*)-1,7-Bis(ethyl-*N*-acetyl-*S*-alanine)-4-[7-methoxycarbonyl-2-chloromethylcarbonylmethyl-1-azaxanthone]-1,4,7,10-tetraazacyclododecane (68 mg, 84 μmol), 2-paramethoxyphenylsulfonate-*N*-methanesulfonylethylamine (60 mg, 126 μmol) and K_2CO_3 (13 mg, 92.4 μmol) were stirred in MeCN (3 ml), under argon, at 65 °C for 24 h. Solvent was removed under reduced pressure and the residue dissolved in DCM (5 ml) allowing the insoluble salts to be removed by centrifugation. Solvent was again removed under reduced pressure before purification by column chromatography on silica gel (DCM → 10% MeOH) to yield a pale orange glassy solid (23 mg, 22 μmol, 26%).

^{1}H-NMR (CDCl$_3$, 700 MHz) δ 8.93 (1H, d, *J* = 1.5, H[6]), 8.65 (1H, d, *J* = 8.0, H[4]), 8.36 (1H, dd, *J* = 9.0, 1.5, H[8]), 7.75 (2H, d, *J* = 9.0, H[29]), 7.62 (1H, d, *J* = 9.0, H[9]), 7.59 (1H, d, *J* = 8.0, H[3]), 6.95 (2H, d, *J* = 9.0, H[28]), 4.65-4.70 (2H, m, H[12]), 4.43-4.49 (1H, m, H[19]), 4.38-4.42 (1H, m, H[19]), 4.02-4.10 (2H, m, H[25]), 3.97 (3H, s, H[11]), 3.85 (3H, s, H[31]), 1.85 – 3.45 (24H, br, H[15,16,24,32]), 1.14 (3H, t, *J* = 7.0, H[23]), 1.12 (3H, t, *J* = 7.0, H[23]); ^{13}C-NMR (CDCl$_3$, 126 MHz) δ 176.8 (C[5]), 173.2 (C[14]), 172.4 (C[21]), 165.8 (C[10]), 165.2 (C[17]), 163.0 (C[2]), 159.7 (C[1']), 158.3 (C[9']), 138.3 (C[4]), 136.0 (C[8]), 129.4 (C[29]), 129.2 (C[6]), 126.8 (C[7]), 121.5 (C[5']), 120.3 (C[3]), 118.9 (C[9]), 115.3 (C[4']), 114.4 (C[28]), 61.7 (C[22]), 61.5 (C[22]), 57.5 (C[24]), 55.8 (C[31]), 55.4 (C[11]), 52.6 (C[11]), 49.9 (C[16]), 48.8 (C[19]), 48.5 (C[15]), 45.1 (C[12]), 40.4 (C[19]), 17.7 (C[20]), 14.3 (C[23]), 14.2 (C[23]); HRMS (ES+) (*m/z*): [M+H]+ calculated for $C_{48}H_{63}F_3N_9O_{13}S$ 1062.4218 found, 1062.4231.

[Eu·L⁶]Cl₃
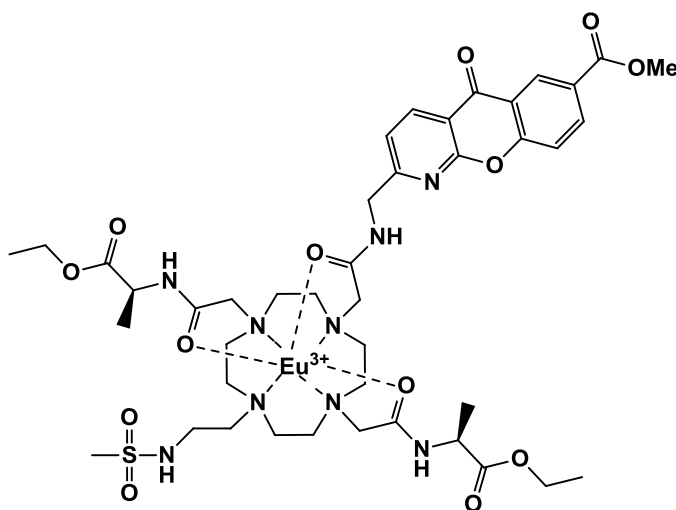
(*SS*)-1,7-Bis(ethyl-*N*-acetyl-*S*-alanine)-4-[7-methoxycarbonyl-2-chloromethylcarbonylmethyl-1-azaxanthone]-10-[2'-(methylsulfonylamino)ethyl]-1,4,7,10-tetraazacyclododecane (18.1 mg,. 17.6 μmol) was added to Eu(OTf)₃ (11.9 mg, 20.0 μmol) and dissolved in MeCN (1 ml). The reaction was stirred for 48 h at 80 ℃. The reaction was then cooled to room temperature and the solvents removed under reduced pressure. The remaining residue was dissolved in dry MeCN (0.1 ml) and the mixture dropped onto anhydrous Et₂O (5 ml) which resulted in the precipitation of the title compound as a triflate salt. The precipitate was centrifuged and dissolved in aqueous MeOH : H₂O (50 : 50, 3 ml). The pH was then adjusted carefully to 10 by addition of conc. NaOH solution to remove the excess Eu as Eu(OH)₃, in a white precipitate which was removed by centrifugation. The pH was adjusted back to neutral and the mixture lyophlised to give a bright yellow solid which was loaded onto a DOWEX 1-X8(Cl) anion exchange resin. The column was eluted with water and the fractions combined and lyophilized to yield the Eu-complex as its chloride salt, as a light yellow glassy solid (7.8 mg, 7.2 μmol, 41%).

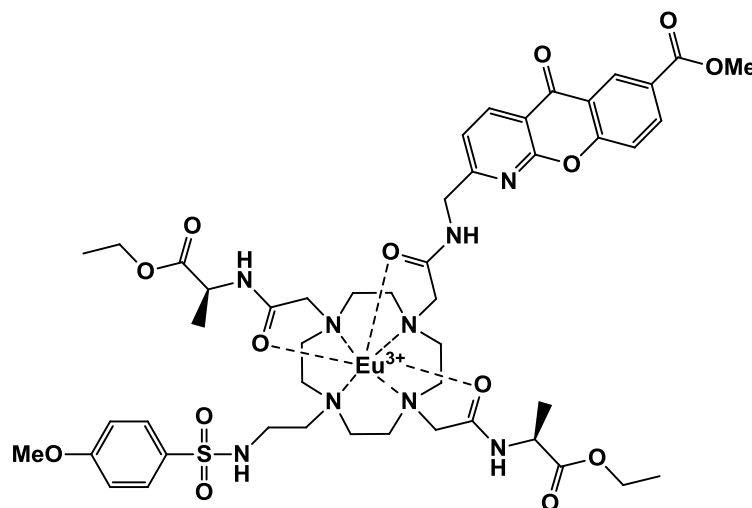HRMS (ES+) *m/z*: [M-H]²⁺ calculated for $^{151}\text{EuC}_{42}\text{H}_{61}\text{N}_9\text{O}_{13}\text{S}$ 540.6615 found, 540.6590; τ_{H2O} (pH 3) = 0.61 ms, τ_{D2O} (pH 3) = 0.98 ms, τ_{H2O} (pH 9) = 0.46 ms, τ_{H2O} (pH 9) 0.96 ms; q_{pH3} = 0.2, q_{pH9} = 0.8.

[Tb·L⁶]Cl₃

The complex was prepared by an analogous method as for [Eu.L⁶]Cl₃ using L⁶ (18.1 mg,. 17.6 μmol) and Tb(OTf)₃ (11.9 mg, 20.0 μmol) to yield the Tb-complex as its chloride salt (8.9 mg, 8.2 μmol, 47%).

HRMS (ES+) (+m/z): [M - H]$^{2+}$ calculated for TbC$_{42}$H$_{61}$N$_9$O$_{13}$S 544.6642 found, 544.6635; τ_{H2O} (pH 3) = 1.24 ms, τ_{D2O} (pH 3) = 1.56 ms, τ_{H2O} (pH 9) = 1.58 ms, τ_{H2O} (pH 9) 1.32 ms; q_{pH3} = 0.5, q_{pH9} = 0.3.
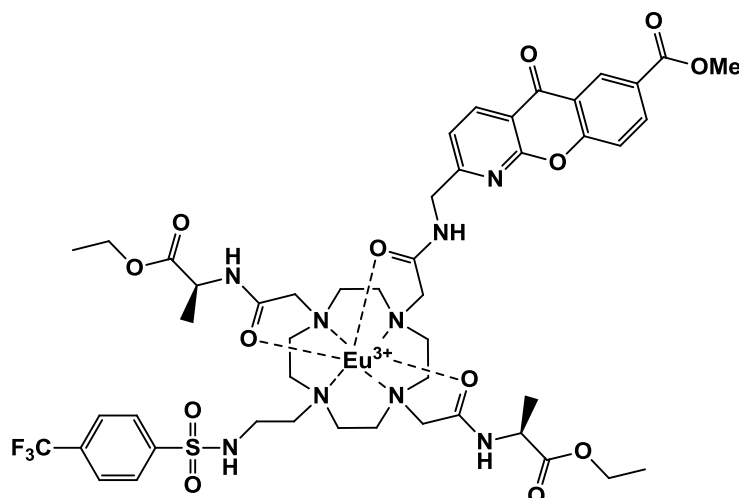
[Eu·L⁷]Cl₃

The complex was prepared by an analogous method as for [Eu.L⁶]Cl₃ using L⁷ (18.5 mg, 18.0μmol) and Eu(OTf)₃ (11.9 mg, 20.0 μmol) to yield the Eu-complex as its chloride salt (10.8 mg, 9.1 μmol, 52%)

HRMS (ES+) m/z: [M - H]$^{2+}$ calculated for ^{151}EuC$_{48}$H$_{65}$N$_9$O$_{13}$S 587.6748 found, 587.6750; τ_{H2O} (pH 3) = 0.48 ms, τ_{D2O} (pH 3) = 1.28 ms, τ_{H2O} (pH 9) = 1.37 ms, τ_{H2O} (pH 9) 1.96 ms; q_{pH3} = 1.0, q_{pH9} = -0.1.

[Tb·L⁷]Cl₃

The complex was prepared by an analogous method as for [Eu.L⁶]Cl₃ using L⁷ (10.4 mg, 9.9 μmol) and Tb(OTf)₃ (11.9 mg, 20.0 μmol) to yield the Tb-complex as its chloride salt (6.7 mg, 5.6 μmol, 57%)

HRMS (ES+) m/z: [M - H]$^{2+}$ calculated for TbC$_{48}$H$_{65}$N$_9$O$_{13}$S 590.6774 found, 590.6763; τ_{H2O} (pH 3) = 1.37 ms, τ_{D2O} (pH 3) = 1.96 ms, τ_{H2O} (pH 9) = 1.72 ms, τ_{H2O} (pH 9) 1.89 ms; q_{pH3} = 0.8, q_{pH9} = -0.1.

[Eu·L^8]Cl$_3$

The complex was prepared by an analogous method as for [Eu.L^6]Cl$_3$ using L^8 (10.4 mg, 9.9 µmol) and Eu(OTf)$_3$ (6.0 mg, 10.0 µmol) to yield the Eu-complex as its chloride salt (3.2 mg, 2.7 µmol, 27%)

HRMS (ES+) *m/z*: [M - H]$^{2+}$ calculated for ^{151}EuC$_{48}$H$_{61}$F$_3$N$_9$O$_{13}$S 606.6632 found, 606.6641; τ_{H2O} (pH 3) = 0.49 ms, τ_{D2O} (pH 3) = 0.98 ms, τ_{H2O} (pH 9) = 0.49 ms, τ_{H2O} (pH 9) 0.98 ms; q_{pH3} = 0.6, q_{pH9} = 0.7.

[Tb·L^8]Cl$_3$

The complex was prepared by an analogous method as for [Eu.L^6]Cl$_3$ using L^8 (10.4 mg, 9.9 µmol) and Tb(OTf)$_3$ (6.0 mg, 10.0 µmol) to yield the Tb-complex as its chloride salt (2.8 mg, 2.3 µmol, 23%)

HRMS (ES+) *m/z*: [M - H]$^{2+}$ calculated for TbC$_{48}$H$_{61}$F$_3$N$_9$O$_{13}$S 609.6652 found, 609.6648; τ_{H2O} (pH 3) = 1.34 ms, τ_{D2O} (pH 3) = 2.06 ms, τ_{H2O} (pH 9) = 1.34 ms, τ_{H2O} (pH 9) 1.81 ms; q_{pH3} = 0.7 q_{pH9} = -0.6.
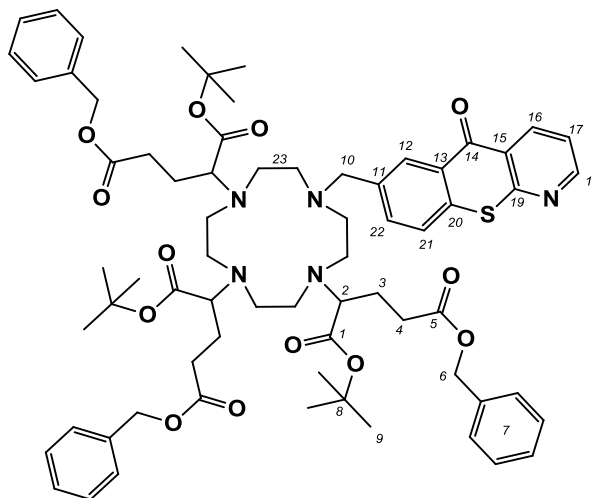
5-Benzyl 1-*tert*-butyl 2-4,7-bis[5-(benzyloxy)-1-(*tert*-butoxy)-1,5-dioxopentan-2-yl]-1,4,7,10-tetraazacyclododecan-1-yl}pentanedioate
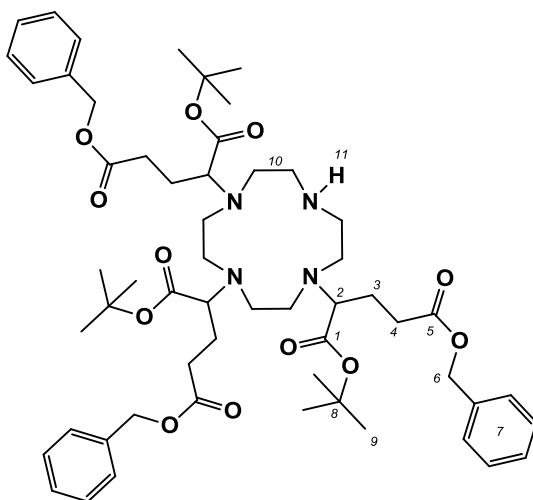
5-Benzyl 1-*tert*-butyl 2-bromopentanedioate (511 mg, 1.41 mmol), 1,4,7,10-tetraazacyclododecane (81 mg, 0.470 mmol) and K_2CO_3 (99 mg, 0.716 mmol) were stirred together in dry MeCN under argon for 24 h at 60 °C. The reaction was halted and solvents removed under reduced pressure. The residue was redissolved in DCM (10 ml) and filtered to remove potassium salts, the solvent was again removed under reduced pressure. The brown residue was purified by column chromatography (silica, DCM → 7 % MeOH) to yield a glassy pale orange solid (343 mg, 0.343 mmol, 73%).

^{1}H-NMR (CDCl$_3$, 700 MHz) δ 9.61 (1H, s, br, H^{11}), 7.28-7.38 (15H, m, H^7), 5.02 - 5.16 (6H, m, H^6), 2.62 – 3.32 (16H, br m, H^{10}), 2.26 – 2.59 (9H, br m, H^{2,4}), 1.80 – 2.16 (6H, br m, H^3), 1.44 (27H, s, H^9); ^{13}H-NMR (CDCl$_3$, 176 MHz) δ 172.6 (C^5), 172.5 (C^5), 172.3 (C^5), 171.3 (C^1), 177.1 (C^1), 170.7 (C^1), 135.6 (C^{7q}), 135.8 (C^{7q}), 128.5 (C^7), 128.5 (C^7), 128.5 (C^7), 128.5 (C^7), 82.0 (C^8), 66.4 (C^6), 66.3 (C^6), 66.3 (C^6), 60.1 (C^2), 45.8 – 52.3 (C^{10}), 30.5 (C^4), 28.4 (C^9), 24.7 (C^3); MS (ES+) *m/z* 1002.0 [M + H]$^+$; HRMS (ES+) *m/z*: $C_{56}H_{81}N_4O_{12}$ requires 1001.5851, found 1001.5842.

5-Benzyl 1-*tert*-butyl 2-4,7-bis[5-(benzyloxy)-1-(tert-butoxy)-1,5-dioxopentan-2-yl]-10-(5-oxo-5H-thiochromeno[2,3-b]pyridin-7yl)methyl)-1,4,7,10-tetraazacyclododecan-1-yl}pentanedioate

5-Benzyl 1-*tert*-butyl 2-4,7-bis[5-(benzyloxy)-1-(tert-butoxy)-1,5-dioxopentan-2-yl]-1,4,7,10-tetraazacyclododecan-1-yl)pentanedioate (237 mg, 0.237 mmol), 7-bromomethyl-1-azathioxanthone (100 mg, 0.327 mmol) and K_2CO_3 (50 mg, 0.368 mmol) were stirred together in dry MeCN (5 ml) under argon for 24 h at 70 °C. The reaction was halted and solvents removed under reduced pressure. The residue was redissolved in DCM (10 ml) and filtered to remove salts, the solvent was again removed. The brown residue was purified by column chromatography (silica, DCM → 7 % MeOH) to a glassy orange solid (81 mg, 0.066 mmol, 58%).

^{1}H-NMR (CDCl$_3$, 400 MHz) δ 8.82 (1H, s, br, H[14]), 8.77-8.81 (1H, m, H[18]), 8.51 (1H, s, H[20]), 7.80-7.85 (1H, m, H[23]), 7.49-7.53 (1H, m, H[24]), 7.41-7.48 (1H, m, H[19]), 7.28-7.38 (15H, m, H[6-9]), 5.02-5.17 (6H, m, H[5]), 1.75-3.51 (33H, m, H[1,2,3,13]), 1.44 (27H, s, H[12]); MS (ES+) *m/z* 1226.7 [M + H]$^+$; HRMS (ES+) *m/z* [M + H]$^+$ C$_{69}$H$_{88}$O$_{13}$N$_5$S requires 1226.6094, found 1226.6114.

7-(1,4,7,10-Tetraazacyclododecan-1-ylnethyl)-5H-thiochromeno[2,3-bi]pyridine-5-one
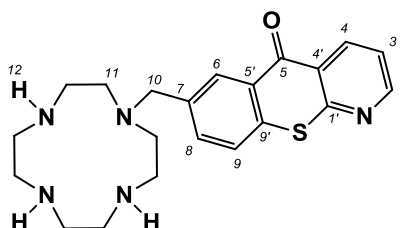
7-Bromomethyl-1-azathioxanthone (0.206 g, 0.673 mmol) was added to a stirred solution of 1,4,7,10-tetraazacyclododecane (1.12 g, 6.53 mmol) and K_2CO_3 (93 mg, 0.673 mmol) in dry MeCN (10 ml) at 55 °C under argon. After 20 h, the solvent was removed under reduced pressure and the residue dissolved in DCM (20 ml). The solution was repeatedly washed with H_2O (5 x 20 ml), dried over $MgSO_4$, and the solvent removed under reduced pressure to yield the title compound as a light yellow oil (0.179 mg, 0.195 mmol, 29%).

^{1}H-NMR (CDCl$_3$, 700 MHz) δ 8.80 (1H, dd, J = 8.5, 2.0, H^5), 8.77 (1H, dd, J = 4.5, 2.0, H^7), 8.48 (1H, d, J = 2.0, H^1), 7.70 (1H, dd, J = 8.5, 2.0, H^{11}), 7.60 (1H, d, J = 8.5, H^{10}), 7.41 (1H, dd, J = 8.5, 4.5, H^6), 3.73 (1H, dd, J = 8.5, 6.0, H^{13}), 2.81 (1H, br s, H^{17}), 2.68 (1H, t, J = 5.0, H^{15}), 2.61 (1H, br s, H^{14}), 2.56 (1H, t, J = 5.0, H^{16}); ^{13}C-NMR (CDCl$_3$, 176 MHz) δ 180.7 (C^3), 158.9 (C^4), 153.3 (C^7), 138.6 (C^{12}), 137.8 (C^5), 136.4 (C^2), 133.9 (C^{11}), 130.0 (C^1), 128.7 (C^9), 126.9 (C^{10}), 126.5 (C^8), 121.6 (C^6), 58.9 (C^{13}), 51.6 (C^{14}), 47.5 (C^{16}), 46.5 (C^{17}), 45.4 (C^{15}); MS (ES+) m/z 398.3 [M + H]$^+$; HRMS (ES+) m/z found 397.1943 [M + H]$^+$ C$_{21}$H$_{27}$ON$_5$S requires 397.1936.

(*SS*)-1,7-Bis(ethyl-*N*-acetyl-*S*-alanine)-4-[1-azaxanthone)-2-methyl]-10-[methylsulfonylaminoethyl]-1,4,7,10-tetraazacyclododecane
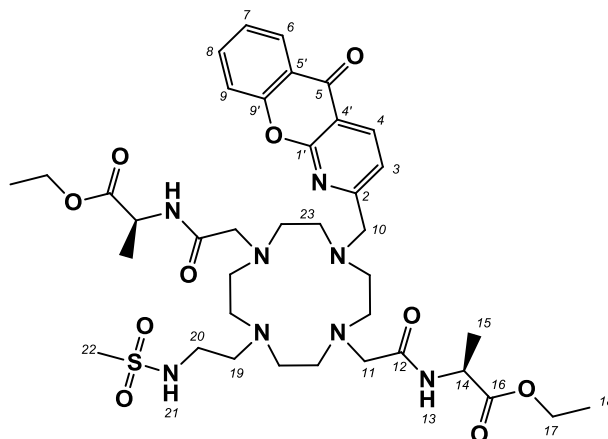

2-Methanesulfonate-*N*-methanesulfonylethylamine (12.8 mg, 58.7 μmol) and K_2CO_3 (8.1 mg, 58.7 μmol) were stirred in dry MeCN (1 ml) at room temperature under argon. (*SS*)-1,7-bis(ethoxycarbonyl-2-ethylcarbamoylmethyl)-4-[(1-azaxanthone)-2-methyl]-1,4,7,10-tetraazacylcododecane (34 mg, 49 μmol) was added after 10 min and the solution heated at 50 °C. After 24 hr, a further addition of 2-methanesulfonate-*N*-methanesulfonylethylamine (3.2 mg, 14.7 μmol) and K_2CO_3 (2.0 mg, 14.7 μmol) was made and the temperature increased to 60 °C. The reaction was stopped after 4 days and the solvent removed under reduced pressure. The resulting solid dissolved in a small amount of DCM (2 ml) and the potassium salts removed by

filtration. The crude mixture was purified by column chromatography (alumina, DCM : 2.5% MeOH); to yield a light yellow glassy solid (24.0 mg, 28.0 μmol, 57%).

^{1}H-NMR (CDCl$_3$, 400 MHz) δ 8.68 (1H, d, J = 8.0, H[6]), 8.24 (1H, d, J = 8.0, H[4]), 8.22 (2H, br s, H[13]), 7.79 (1H, t, J = 8.0, H[7]), 7.60 (1H, d, J = 8.0, H[9]), 7.33-7.46 (2H, m, H[3,8]), 4.31-4.37 (2H, m, H[14]), 4.09-4.13 (4H, m, H[17]), 3.81-4.03 (6H, m, br, H[10, 19, 20]), 2.90-3.30 (16H, br, H[23]), 3.03 (3H, s, H[22]), 1.44 (6H, d, J = 7.0, H[15]), 1.20 (6H, t, J = 7.0, H[18]); ^{13}C-NMR (CDCl$_3$), 101 MHz) δ 177.3 (C[5]), 175.5 (C[16]), 172.6 (C[12]), 163.3 (C[2]), 160.1 (C[1']), 138.2 (C[4]), 135.7 (C[4']), 126.8 (C[9]), 124.9 (C[6]), 121.7 (C[6']), 121.1 (C[5']), 118.5 (C[8]), 115.8 (C[9']), 61.2 (C[17]), 55.8 (C[23]), 55.0 (C[23]), 54.5 (C[23]), 53.2 (C[10]), 49.8 (C[19]), 48.5 (C[14]), 39.0 (C[22]), 21.3 (C[20]), 20.0 (C[15]), 14.1 (C[18]); MS (ES+) m/z 817.5 [M + H]$^+$; HRMS (ES+) m/z found 817.3922 [M + H]$^+$ C$_{38}$H$_{57}$O$_{10}$N$_8$S requires 817.3918.

(*SS*)-1,7-Bis-(*N*-acetyl-*S*-alanine)-4-[1-azaxanthone)-2-methyl]-10-[methylsulfonylaminoethyl]-1,4,7,10-tetraazacyclododecane
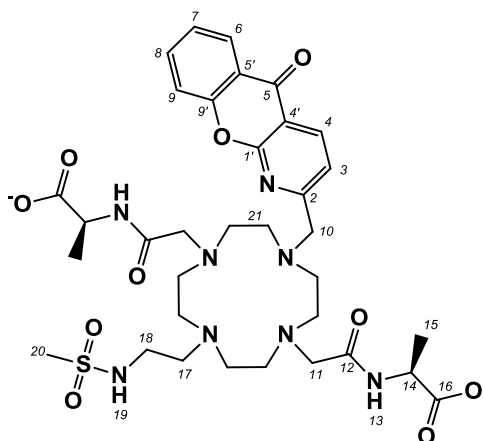
Freshly made aqueous KOD solution (0.6 ml, 0.1 M) was added to (*SS*)-1,7-bis(ethyl-*N*-acetyl-*S*-alanine)-4-[2-chloromethylcarbonylmethyl-1-azaxanthone]-1,4,7,10-tetraazacyclododecane (24 mg, 29.4 μmol). Progress was monitored by NMR. After 1 h, no ethyl group signals were observed in the ^{1}H-NMR spectrum. The pH of the mixture was increased (pH ~ 6) with conc. HCl and the solution loaded onto a DOWEX 50X4-100 strong cation exchange resin. The column was eluted with water → 10% NH$_4$OH. The fractions were combined and lyophilized to yield the title compound as a red oil (17.9 mg, 21.9 μmol, 75%) which was used immediately in the complexation reaction.

^{1}H-NMR (D$_2$O, 400 MHz) δ 8.30 (1H, br, H[6]), 7.81 (1H, br, H[4]), 7.63 (1H, br, H[7]), 7.38 (1H, br, H[9]), 7.31 (1H, br, H[3]), 7.24 (1H, br, H[8]), 3.96 (2H, m, H[10]), 2.90 (6H, br, H[17, 18, 20]), 2.50-2.90 (16H, br, H[22]), 2.58 (3H, br, H[22]), 1.17 (6H, br, H[15]).

N-((S)-1-Phenyl-ethyl-2-[7-[((S)-1-phenyl-ethylcarbomyl)-methyl]-4-(10,11,12,13-tetrahydro-4,5,9,14-tetraaza-benzo[b]triphenylen-6-ylmethyl)-10-[methylsulfonylaminoethyl]-1,4,7,10-tetraaza-cyclododec-1-yl]-acetamide
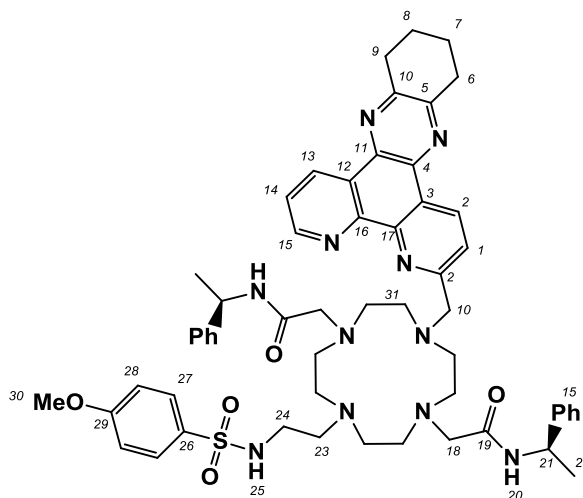
2-(4-Methoxybenzenesulfonate)-*N*-methoxyphenylsulfonylethylamine (49 mg, 0.121 mmol) and Na$_2$CO$_3$ (17 mg, 0.152 mmol) were stirred in dry MeCN (5 ml) under argon). (*N*-((*S*)-1-Phenyl-ethyl)-2-[7-[((*S*)-1-phenyl-ethylcarbamoyl)-methyl]-4-(10,11,12,13-tetrahydro-4,5,9,14-tetraaz-benzo[b]triphenylen-6-ylmethyl)-10-[methylsulfonylaminoethyl]-1,4,7,10-tetraazacyclododec-1-yl]-acetamide (80 mg, 0.101 mmol) was added and the solution heated to 60 °C. The reaction was stopped after 3 days. The solvent was removed under reduced pressure and the resulting solid was dissolved in a small volume of DCM (5 ml) and the potassium salts removed by filtration. The crude mixture was purified by column chromatography (alumina, DCM → 2.5% MeOH, 2.5% NEt$_3$). The residue was washed with water (3 x 10 ml) and the solid dried under reduced pressure to yield a glassy orange solid (43 mg, 43 μmol, 43%).

^{1}H-NMR (CDCl$_3$, 400 MHz) δ 9.47 (1H, d, *J* = 8.0, H^{15}), 9.39 (1H, d, *J* = 8.0, H^1), 9.21 (1H, s, H^{13}), 7.85 (1H, m, H^{14}), 7.71-7.73 (2H, m, H^{27}), 7.51 (1H, d, *J* = 8.0, H^2), 7.20 - 7.30 (10H, br m, H^{25}), 5.13-5.21 (2H, m, H^{24}), 3.78 (3H, s, H^{30}), 3.24 (8H, br, H^{10,18,23}), 2.20 - 2.80 (16H, br, H^{31}), 4.10-4.21 (4H, m, H$^{7, 8}$), 3.77-3.82 (4H, m, H^{6,9}), 1.07 (6H, q, H^{22}). HRMS (ES+) *m/z* found 1006.5113 [M + H]$^+$ C$_{56}$H$_{68}$O$_5$N$_{11}$S requires 1006.5126.

[Eu·L⁹]Cl₃
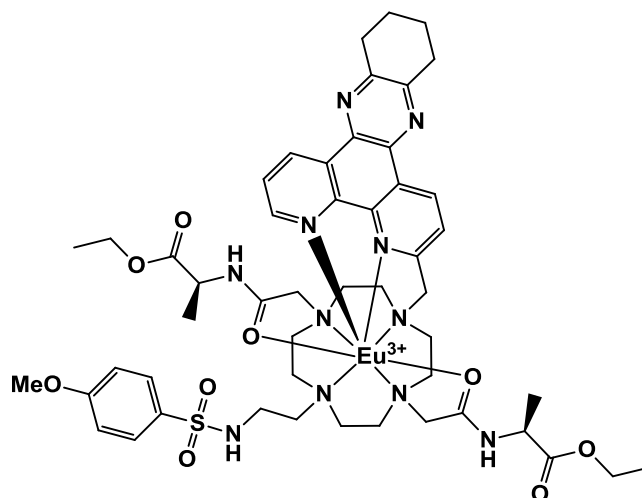
N-((*S*)-1-Phenyl-ethyl-2-[7-[((*S*)-1-phenyl-ethylcarbomyl)-methyl]-4-(10,11,12,13-tetrahydro-4,5,9,14-tetraaza-benzo[b]triphenylen-6-ykmethyl)-10-[methylsulfonylaminoethyl]-1,4,7,10-tetraaza-cyclododec-1-yl]-acetamide (43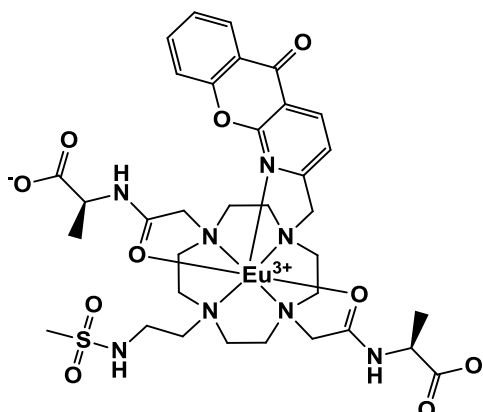 mg, 43 μmol) was added to $Eu(CF_3SO_3)_3$ (31 mg, 52 μmol) and the solids dissolved in dry MeCN (1 ml) and the reaction left to stir at 80 °C for 76 h. After the reaction was cooled to room temperature, the solvents were removed under reduced pressure and the remaining residue was dissolved in dry MeCN (0.1 ml) and the mixture dropped onto anhydrous Et_2O (5 ml) resulting in the precipitation of the title compound as a triflate salt. The precipitate was centrifuged and dissolved in aqueous $MeOH:H_2O$ (50 : 50, 3 ml). The pH was adjusted carefully to 10 by addition of conc. NaOH solution and the resultant precipitate removed by centrifugation. The pH was adjusted back to neutral and the mixture lyophilised to give a bright yellow solid which was loaded onto a DOWEX 1-X8(Cl) anion exchange resin. The column was eluted with water $\rightarrow$ 10% NH_4OH. The fractions were combined and lyophilised to yield a colourless glassy solid (30 mg, 24 μmol, 55%).

HRMS (ES+) *m/z*: $[M - H]^{2+}$ calculated for $^{151}EuC_{50}H_{66}N_{11}O_9S$ 574.6984 found, 574.6992; τ_{H2O} (pH 3) = 0.49 ms, τ_{D2O} (pH 3) = 0.98 ms, τ_{H2O} (pH 9) = 0.49 ms, τ_{H2O} (pH 9) 0.98 ms; q_{pH3} = 0.6, q_{pH9} = 0.7.

[Eu·L¹⁰]Cl₃

(*SS*)-1,7-Bis(carboxy-2-ethylcarbamoylmethyl)-4-[(1-azathioxanthone)-2-methyl]-1,4,7,10-tetraazacyclododecane (17.9 mg, 21.9 μmol) was added to Eu(OAc)₃.4H₂O (10.8 mg, 1.2 eq.) and the solids dissolved in 1 ml H₂O. The pH was carefully adjusted to 6 by the addition of acetic acid and the reaction left to stir at 75°C for 60 h. After the reaction was cooled to room temperature, the pH was then adjusted carefully to 10 by addition of conc. NaOH solution resulting in a white precipitate that was removed by centrifugation. The pH was adjusted back to neutral with acetic acid and the sample lyophilised to yield a light red glassy solid (15.8 mg, 11.8 μmol, 54%).

HRMS (ES+) *m/z*: [M - H]²⁺ calculated for $^{151}EuC_{34}H_{45}N_8O_{10}S$ 910.2186 found, 910.2181; τ_{H2O} (pH 3) = 0.42 ms, τ_{D2O} (pH 3) = 1.08 ms, τ_{H2O} (pH 9) = 1.4 ms, τ_{H2O} (pH 9) 0.52 ms; q_{pH3} = 1.34, q_{pH9} = 0.5.

1. A. Thibon and V. Pierre, *Anal. Bioanal. Chem.*, 2009, **394**, 107-120.

2. B. S. Murray, E. J. New, R. Pal and D. Parker, *Org. Biomol. Chem.*, 2008, **6**, 2085-2094.

3. J. C. G. Bunzli, *Chem. Lett.*, 2009, **38**, 104-109.

4. C. Piguet and J.-C. G. Bunzli, *Chem. Soc. Rev.*, 1999, **28**, 347.

5. N. N. Greenwood and A. Earnshaw, Elsevier, 1998.

6. D. Parker, R. S. Dickins, H. Puschmann, C. Crossland and J. A. K. Howard, *Chem. Rev.*, 2002, **102**, 1977-2010.

7. J.-C. G. Bunzli and C. Piguet, *Chem. Soc. Rev.*, 2005, **34**, 1048-1077.

8. E. G. Moore, A. P. S. Samuel and K. N. Raymond, *Acc. Chem. Res.*, 2009, **42**, 542-552.

9. D. Parker and J. A. G. Williams, *Metal Ions In Biological Systems - The Lanthanides and Their Interrelations with Biosystems*, 2003.

10. R. S. Dickins, D. Parker, J. I. Bruce and D. J. Tozer, *Dalton Trans.* 2003, 1264-1271.

11. S. A. Cotton, John Wiley & Sons, 1991.

12. N. Sabbatini, M. Guardigli and J.-M. Lehn, *Coord. Chem. Rev.*, 1993, **123**, 201-228.

13. C. M. G. dos Santos, A. J. Harte, S. J. Quinn and T. Gunnlaugsson, *Coord. Chem. Rev.*, 2008, **252**, 2512-2527.

14. A. Døssing, *Eur. J. Inorg. Chem.*, 2005, **2005**, 1425-1434.

15. L. Porrès, A. Holland, L.-O. Pålsson, A. Monkman, C. Kemp and A. Beeby, *J. Fluoresc.*, 2006, **16**, 267-273.

16. J.-C. G. Bünzli, S. Comby, A.-S. Chauvin and C. D. B. Vandevyver, *J. Rare Earth*, 2007, **25**, 257-274.

17. J. P. Riehl and F. S. Richardson, *Chem. Rev.*, 1986, **86**, 1-16.

18. F. S. Richardson and J. P. Riehl, *Chem. Rev.*, 1977, **77**, 773-792.

19. J. I. Bruce, D. Parker, S. Lopinski and R. D. Peacock, *Chirality*, 2002, **14**, 562-567.

20. C. P. Montgomery, B. S. Murray, E. J. New, R. Pal and D. Parker, *Acc. Chem. Res.*, 2009, **42**, 925-937.

21. F. S. Richardson and T. R. Faulkner, *J. Chem. Phys.*, 1982, **76**, 1595-1606.

22. F. Kielar, G.-L. Law, E. J. New and D. Parker, *Org.Biomol. Chem.*, 2008, **6**, 2256-2258.

23. D. Parker, *Coord. Chem. Rev.*, 2000, **205**, 109-130.

24. G.-L. Law, R. Pal, L. O. Palsson, D. Parker and K.-L. Wong, *Chem. Commun.*, 2009, 7321-7323.

25. G.-L. Law, D. Parker, S. L. Richardson and K.-L. Wong, *Dalton Trans.,* 2009, 8481-8484.

26. E. J. New, D. Parker and R. D. Peacock, *Dalton Trans.*, 2009, 672-679.

27. R. A. Poole, F. Kielar, S. L. Richardson, P. A. Stenson and D. Parker, *Chem. Commun.*, 2006, 4084-4086.

28.   F. Kielar, C. P. Montgomery, E. J. New, D. Parker, R. A. Poole, S. L. Richardson and P. A. Stenson, *Org. Biomol. Chem.*, 2007, **5**, 2975-2982.

29.   R. S. Dickins, D. Parker, A. S. de Sousa and J. A. G. Williams, *Chem. Commun.*, 1996, 697-698.

30.   S. Ghose, E. Trinquet, M. Laget, H. Bazin and G. Mathis, *J. Alloys Compd.*, 2008, **451**, 35-37.

31.   Y. Haas and G. Stein, *J. Phys. Chem.*, 1972, **76**, 1093-1099.

32.   W. D. Horrocks and D. R. Sudnick, *J. Am. Chem. Soc.*, 1979, **101**, 334-340.

33.   A. Beeby, I. M. Clarkson, R. S. Dickins, S. Faulkner, D. Parker, L. Royle, A. S. de Sousa, J. A. G. Williams and M. Woods, *J. Chem.Soc., Perk. T. 2*, 1999, 493-504.

34.   D. Parker, *Chem. Soc. Rev.*, 2004, **33**, 156-165.

35.   P. Atkinson, K. S. Findlay, F. Kielar, R. Pal, D. Parker, R. A. Poole, H. Puschmann, S. L. Richardson, P. A. Stenson, A. L. Thompson and J. Yu, *Org. Biomol. Chem.*, 2006, **4**, 1707-1722.

36.   Y. Bretonniere, M. J. Cann, D. Parker and R. Slater, *Chem. Commun.*, 2002, 1930-1931.

37.   Y. Bretonniere, M. J. Cann, D. Parker and R. Slater, *Org. Biomol.Chem.*, 2004, **2**, 1624-1632.

38.   M. P. Oude Wolbers, F. C. J. M. van Veggel, B. H. M. Snellink-Ruel, J. W. Hofstraat, F. A. J. Geurts and D. N. Reinhoudt, *J.Chem. Soc., Perk. T. 2*, 1998, 2141-2150.

39.   S. Quici, G. Marzanni, M. Cavazzini, P. L. Anelli, M. Botta, E. Gianolio, G. Accorsi, N. Armaroli and F. Barigelletti, *Inorg. Chem.*, 2002, **41**, 2777-2784.

40.   Pope. S. J. A., *Polyhedron*, 2007, **26**, 4818-4824.

41.   D. Parker and J. H. Yu, *Chem. Commun.*, 2005, 3141-3143.

42.   J. H. Yu and D. Parker, *Eur. J. Org. Chem.*, 2005, 4249-4252.

43.   R. S. Dickens, J. A. K. Howard, C. L. Maupin, J. M. Moloney, D. Parker, R. D. Peacock, J. P. Riehl and G. Siligardi, *New J. Chem.*, 1998, **22**, 891-899.

44.   J. Han, A. Loudet, R. Barhoumi, R. C. Burghardt and K. Burgess, *J. Am. Chem. Soc.*, 2009, **131**, 1642-1643.

45.   T. Doussineau, S. Trupp and G. J. Mohr, *J. Colloid Interface Sci.*, 2009, **339**, 266-270.

46.   B. M. Myers, P. S. Tietz, J. E. Tarara and N. F. Larusso, *Hepatology*, 1995, **22**, 1519-1526.

47.   J. Ji, N. Rosenzweig, C. Griffin and Z. Rosenzweig, *Anal. Chem.*, 2000, **72**, 3497-3503.

48.   T. Jin, A. Sasaki, M. Kinjo and J. Miyazaki, *Chem. Commun.*, 2010, **46**, 2408-2410.

49.   O. Kotova, S. Comby and T. Gunnlaugsson, *Chem. Commun.*, 2011, **47**, 6810-6812.

50.   S. J. A. Pope and R. H. Laye, *Dalton Trans.*, 2006, 3108-3113.

51.   A. Thibon and V. r. C. Pierre, *J. Am. Chem. Soc.*, 2008, **131**, 434-435.

52.   A. R. Lippert, T. Gschneidtner and C. J. Chang, *Chem. Commun.*, 2010, **46**, 7510-7512.

53.   D. Parker, *Aust. J. Chem.*, 2011, **64**, 239-243.

54.   L. Sherwood, *Human physiology: from cells to systems*, Brooks/Cole, Cengage Learning, 2008.

55.   I. Mellman and G. Warren, *Cell*, 2000, **100**, 99-112.

56.   *Microbiology*, McGraw-Hill Companies, The, 1993.

57.   L. Stryer, *Biochemistry*, W.H. Freeman, 1995.

58.   L. Pelkmans and A. Helenius, *Traffic*, 2002, **3**, 311-320.

59.   C. Mineo and R. Anderson, *Histochem. Cell Biol.*, 2001, **116**, 109-118.

60.   S. B. Sieczkarski and G. R. Whittaker, *J. Gen. Virol.*, 2002, **83**, 1535-1545.

61.   E. J. New, A. Congreve and D. Parker, *Chem. Sci.*, 2010, **1**, 111-118.

62.   S. Kessner, A. Krause, U. Rothe and G. Bendas, *BBA Biomembranes*, 2001, **1514**, 177-190.

63.   C. A. Lipinski, F. Lombardo, B. W. Dominy and P. J. Feeney, *Adv. Drug Del. Rev.*, 1997, **23**, 3-25.

64.   E. J. New and D. Parker, *Org. Biomol. Chem.*, 2009, **7**, 851-855.

65.   C. P. Montgomery, E. J. New, L. O. Palsson, D. Parker, A. S. Batsanov and L. Lamarque, *Helv. Chim. Acta*, 2009, **92**, 2186-2213.

66.   R. Pal and D. Parker, *Org. Biomol.Chem.*, 2008, **6**, 1020-1033.

67.   J. Carmichael, W. G. DeGraff, A. F. Gazdar, J. D. Minna and J. B. Mitchell, *Cancer Res.*, 1987, **47**, 936-942.

68.   E. J. New, D. Parker, D. G. Smith and J. W. Walton, *Curr. Opin. Chem. Biol.*, 2010, **14**, 238-246.

69.   R. Pal and D. Parker, *Chem. Commun.*, 2007, 474-476.

70.   C. A. Puckett and J. K. Barton, *J. Am. Chem. Soc.*, 2009, **131**, 8738-8739.

71.   S. Orrenius, B. Zhivotovsky and P. Nicotera, *Nat. Rev. Mol. Cell*, 2003, **4**, 552-565.

72.   S. A. Susin, N. Zamzami and G. Kroemer, *BBA-Bioenergetics*, 1998, **1366**, 151-165.

73.   R. K. Emaus, R. Grunwald and J. J. Lemasters, *BBA - Bioenergetics*, 1986, **850**, 436-448.

74.   D. G. Nicholls, *Aging Cell*, 2004, **3**, 35-40.

75.   M. P. Murphy and R. A. J. Smith, *Annu. Rev. Pharmacool. Toxicol.*, 2007, **47**, 629-656.

76.   Helena M. Cochemé, C. Quin, Stephen J. McQuaker, F. Cabreiro, A. Logan, Tracy A. Prime, I. Abakumova, Jigna V. Patel, Ian M. Fearnley, Andrew M. James, Carolyn M. Porteous, Robin A. J. Smith, S. Saeed, Jane E. Carré, M. Singer, D. Gems, Richard C. Hartley, L. Partridge and Michael P. Murphy, *Cell Met.*, 2011, **13**, 340-350.

77.   H.-K. Woo, E. P. Go, L. Hoang, S. A. Trauger, B. Bowen, G. Siuzdak and T. R. Northen, *Rapid Commun. Mass Spectrom.*, 2009, **23**, 1849-1855.

78.   S. Ohkuma and B. Poole, *PNAS* 1978, **75**, 3327-3331.

79.   V. Teichgraber, M. Ulrich, N. Endlich, J. Riethmuller, B. Wilker, C. C. De Oliveira-Munding, A. M. van Heeckeren, M. L. Barr, G. von Kurthy, K. W. Schmid, M. Weller,

B. Tummler, F. Lang, H. Grassme, G. Doring and E. Gulbins, *Nat. Med.*, 2008, **14**, 382-391.

80. P. M. Haggie and A. S. Verkman, *J. Biol. Chem.*, 2009, **284**, 7681-7686.

81. T. Fukuda, L. Ewan, M. Bauer, R. J. Mattaliano, K. Zaal, E. Ralston, P. H. Plotz and N. Raben, *Ann. Neurol.*, 2006, **59**, 700-708.

82. F. M. Platt and R. H. Lachmann, *BBA - Molecular Cell Research*, 2009, **1793**, 737-745.

83. L. W. Jiang, V. M. Maher, J. J. McCormick and M. Schindler, *J. Biol. Chem.*, 1990, **265**, 4775-4777.

84. Y. Urano, D. Asanuma, Y. Hama, Y. Koyama, T. Barrett, M. Kamiya, T. Nagano, T. Watanabe, A. Hasegawa, P. L. Choyke and H. Kobayashi, *Nat. Med.*, 2009, **15**, 104-109.

85. M. Schindler, S. Grabski, E. Hoff and S. M. Simon, *Biochemistry (Mosc).* 1996, **35**, 2811-2817.

86. J. M. Holopainen, J. Saarikoski, P. K. J. Kinnunen and I. Järvelä, *Eur. J. Biochem.*, 2001, **268**, 5851-5856.

87. W. N. Lipscomb and N. Sträter, *Chem. Rev.*, 1996, **96**, 2375-2434.

88. R. Acin-Perez, E. Salazar, M. Kamenetsky, J. Buck, L. R. Levin and G. Manfredi, *Cell Met.*, 2009, **9**, 265-276.

89. C. A. Wagner, J. Kovacikova, P. A. Stehberger, C. Winter, C. Benabbas and N. Mohebbi, *Neph. Phys.*, 2006, **103**, p1-p6.

90. V. Menon, H. Tighiouart, N. S. Vaughn, G. J. Beck, J. W. Kusek, A. J. Collins, T. Greene and M. J. Sarnak, *Am. J .Kidney. Dis.*, 2010, **56**, 907-914.

91. S. C. Doney, V. J. Fabry, R. A. Feely and J. A. Kleypas, *Ann. Rev. Mar. Sci.*, 2009, **1**, 169-192.

92. V. J. Fabry, *Science*, 2008, **320**, 1020-1022.

93. U. Riebesell, I. Zondervan, B. Rost, P. D. Tortell, R. E. Zeebe and F. M. M. Morel, *Nature*, 2000, **407**, 364-367.

94. L. J. de Nooijer, T. Toyofuku and H. Kitazato, *PNAS*, 2009, **106**, 15374-15378.

95. L. Berry, A. R. Taylor, U. Lucken, K. P. Ryan and C. Brownlee, *Funct. Plant Biol.*, 2002, **29**, 289-299.

96. G. K. Dixon, C. Brownlee and M. J. Merrett, *Planta*, 1989, **178**, 443-449.

97. J. L. Sessler, S. Camiolo and P. A. Gale, *Coord. Chem. Rev.*, 2003, **240**, 17-55.

98. W. W. H. Wong, M. S. Vickers, A. R. Cowley, R. L. Paul and P. D. Beer, *Org. Biomol. Chem.*, 2005, **3**, 4201-4208.

99. S. K. Kim, J. H. Bok, R. A. Bartsch, J. Y. Lee and J. S. Kim, *Org. Lett.*, 2005, **7**, 4839-4842.

100. M. Boiocchi, L. Del Boca, D. E. Gómez, L. Fabbrizzi, M. Licchelli and E. Monzani, *J. Am. Chem. Soc.*, 2004, **126**, 16507-16514.

101. F. M. Pfeffer, T. Gunnlaugsson, P. Jensen and P. E. Kruger, *Org. Lett.*, 2005, **7**, 5357-5360.
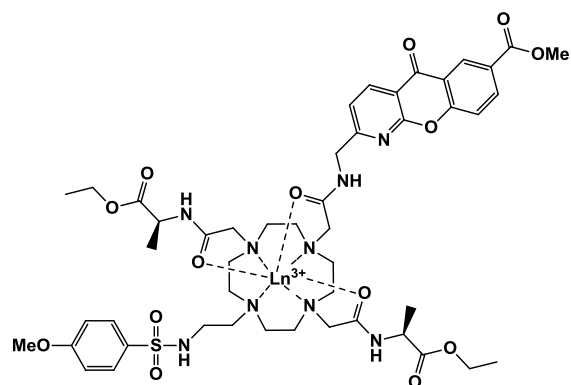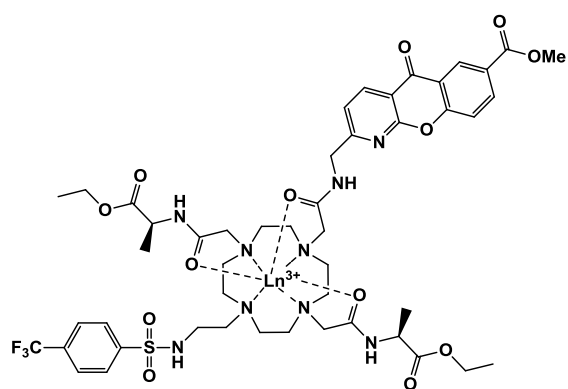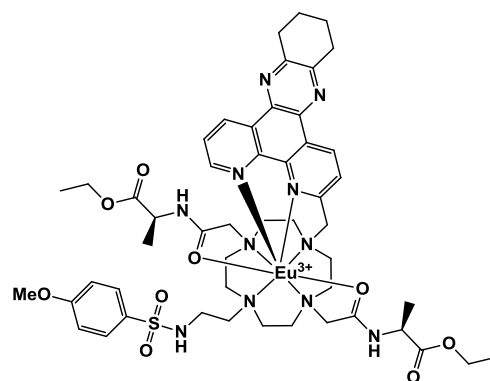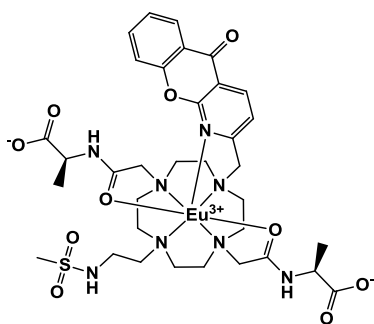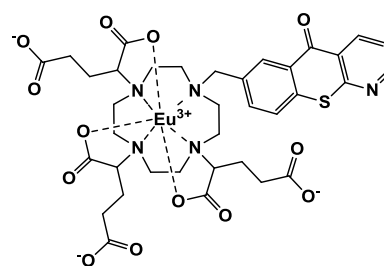
102. J. R. Hiscock, C. Caltagirone, M. E. Light, M. B. Hursthouse and P. A. Gale, *Org. Biomol.Chem.*, 2009, **7**, 1781-1783.

103. H. Yan and H. Li, *Sensors Actuators B: Chem.*, 2010, **148**, 81-86.

104. Z. Liu, C. Zhang, W. He, F. Qian, X. Yang, X. Gao and Z. Guo, *New J. Chem.*, 2010, **34**, 656-660.

105. S. Wu, Z. Li, J. Han and S. Han, *Chem. Commun.*, 2011, **47**, 11276-11278.

106. M. Baruah, W. Qin, N. Basarić, W. M. De Borggraeve and N. Boens, *J. Org. Chem.*, 2005, **70**, 4152-4157.

107. L.-Q. Ying and B. P. Branchaud, *Bioorganic. Med. Chem. Lett.*, 2011, **21**, 3546-3549.

108. J. I. Bruce, R. S. Dickins, L. J. Govenlock, T. Gunnlaugsson, S. Lopinski, M. P. Lowe, D. Parker, R. D. Peacock, J. J. B. Perry, S. Aime and M. Botta, *J. Am. Chem. Soc.*, 2000, **122**, 9674-9684.

109. A. P. de Silva, H. Q. N. Gunaratne, T. Gunnlaugsson, A. J. M. Huxley, C. P. McCoy, J. T. Rademacher and T. E. Rice, *Chem. Rev.*, 1997, **97**, 1515-1566.

110. D. Parker, K. Senanayake and J. A. Gareth Williams, *Chem. Commun.*, 1997, 1777-1778.

111. D. Parker, *Chem. Commun.*, 1998, 245-246.

112. S. Blair, M. P. Lowe, C. E. Mathieu, D. Parker, P. K. Senanayake and R. Kataky, *Inorg. Chem.*, 2001, **40**, 5860-5867.

113. M. P. Lowe and D. Parker, *Inorg. Chim. Acta*, 2001, **317**, 163-173.

114. T. Gunnlaugsson, D. A. Mac Dónaill and D. Parker, *J. Am. Chem. Soc.*, 2001, **123**, 12866-12876.

115. M. P. Lowe, D. Parker, O. Reany, S. Aime, M. Botta, G. Castellano, E. Gianolio and R. Pagliarin, *J. Am. Chem. Soc.*, 2001, **123**, 7601-7609.

116. B. S. Murray, PhD thesis, 2008.

117. F. Kielar, University of Durham, PhD thesis, 2008.

118. J. C. Sheehan and W. A. Bolhofer, *J. Am. Chem. Soc.*, 1950, **72**, 2786-2788.

119. Z. Kovacs and A. D. Sherry, *Tetrahedron Lett.*, 1995, **36**, 9269-9272.

120. S. Aime, A. Barge, M. Botta, J. A. K. Howard, R. Kataky, M. P. Lowe, J. M. Moloney, D. Parker and A. S. de Sousa, *Chem. Commun.*, 1999, 1047-1048.

121. S. Poitry, C. Poitry-Yamate, J. Ueberfeld, P. R. MacLeish and M. Tsacopoulos, *J. Neurosci.*, 2000, **20**, 1809-1821.

122. A. Mills, Q. Chang and N. McMurray, *Anal. Chem.*, 1992, **64**, 1383-1389.

123. R. Pal, D. Parker and L. C. Costello, *Org. Biomol. Chem.*, 2009, **7**, 1525-1528.

124. R. S. Dickins, S. Aime, A. S. Batsanov, A. Beeby, M. Botta, J. Bruce, J. A. K. Howard, C. S. Love, D. Parker, R. D. Peacock and H. Puschmann, *J. Am. Chem. Soc.*, 2002, **124**, 12697-12705.

125. C. T. Flear, S. W. Roberts, S. Hayes, J. C. Stoddart and A. K. Covington, *Clin. Chem.*, 1987, **33**, 13-20.

126. E. J. New, PhD thesis, 2009.

127. M. E. Marsh, *Protoplasma*, 1994, **177**, 108-122.

128. M. J. Martin, E. FitzSullivan, A. Salim, T. V. Berne and S. Towfigh, *Arch. Surg.*, 2005, **140**, 745-751.

129. Y. Hatefi, *Annu. Rev. Biochem*, 1985, **54**, 1015-1069.

130. H. Peter G, in *Methods Enzymol.*, ed. L. P. Sidney Fleischer, Academic Press, 1979, vol. Volume 55, pp. 462-472.

131. J. E. DiCiccio and B. E. Steinberg, *J.Gen.Physiol.*, 2011, **137**, 385-390.

132. G.-L. Law, C. Man, D. Parker and J. W. Walton, *Chem. Commun.*, 2010, **46**, 2391-2393.

133. P. Franck, N. Petitipain, M. Cherlet, M. Dardennes, F. Maachi, B. Schutz, L. Poisson and P. Nabet, *J. Biotechnol.*, 1996, **46**, 187-195.

134. L.-O. Palsson, R. Pal, B. S. Murray, D. Parker and A. Beeby, *Dalton Trans.*, 2007, 5726-5734.

List of Complexes
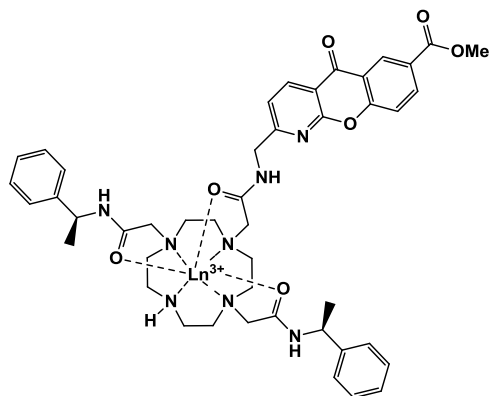
$[Ln \cdot \mathbf{L^1}]^{3+}$
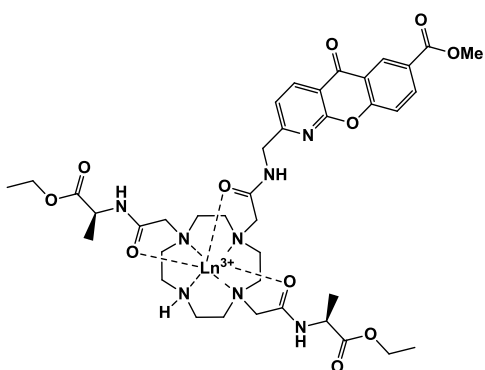
$[Ln \cdot \mathbf{L^2}]^{3+}$
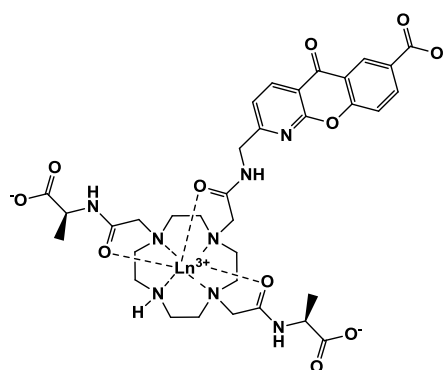
$[Ln \cdot \mathbf{L^3}]$
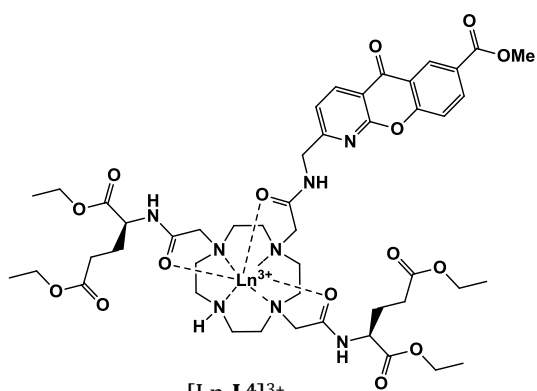
$[Ln \cdot \mathbf{L^4}]^{3+}$
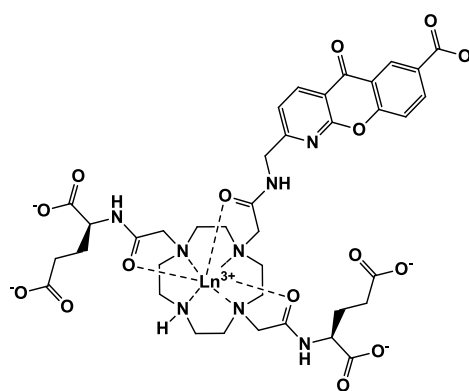
$[Ln \cdot \mathbf{L^5}]^{2-}$

List of Complexes
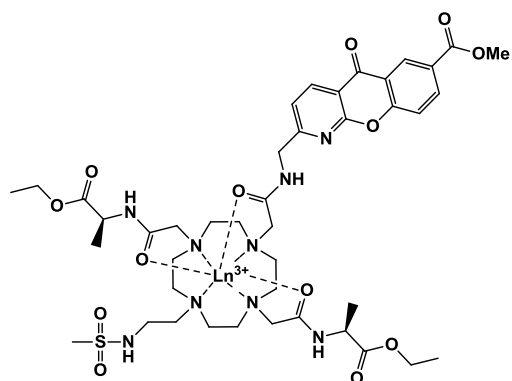
$[Ln \cdot \mathbf{L^6}]^{3+}$

$[Ln \cdot \mathbf{L^7}]^{3+}$

$[Ln \cdot \mathbf{L^8}]^{3+}$

$[Eu \cdot \mathbf{L^9}]^{3+}$

$[Eu \cdot \mathbf{L^{10}}]^{+}$

$[Eu \cdot \mathbf{L^{11}}]^{3-}$